STUDIES ON NEW RUTHENIUM COMPLEXES AND THEIR REACTIVITIES

Ph.D. THESIS

by

MANJU BALA

DEPARTMENT OF CHEMISTRY
INDIAN INSTITUTE OF TECHNOLOGY ROORKEE
ROORKEE-247667 (INDIA)
NOVEMBER, 2018

STUDIES ON NEW RUTHENIUM COMPLEXES AND THEIR REACTIVITIES

A THESIS

Submitted in partial fulfilment of the requirements for the award of the degree

of

DOCTOR OF PHILOSOPHY

in

CHEMISTRY

by

MANJU BALA

DEPARTMENT OF CHEMISTRY
INDIAN INSTITUTE OF TECHNOLOGY ROORKEE
ROORKEE-247667 (INDIA)
NOVEMBER, 2018

INDIAN INSTITUTE OF TECHNOLOGY ROORKEE
ROORKEE

CANDIDATE'S DECLARATION

I hereby certify that the work which is being presented in this thesis entitled "**STUDIES ON NEW RUTHENIUM COMPLEXES AND THEIR REACTIVITIES"** in partial fulfilment of the requirements for the award of the Degree of Doctor of Philosophy and submitted in the Department of Chemistry of the Indian Institute of Technology Roorkee, Roorkee is an authentic record of my own work carried out during a period from July, 2013 to November, 2018 under the supervision of Dr. Kaushik Ghosh, Associate Professor, Department of Chemistry, Indian Institute of Technology, Roorkee.

The matter presented in this thesis has not been submitted by me for the award of any other degree of this or any other Institution.

(**MANJU BALA**)

This is to certify that the above statement made by the candidate is correct to the best of my knowledge.

(Kaushik Ghosh)
Supervisor

The Ph.D. Viva-Voce examination of **Manju Bala**, Research Scholar, has been held on **08th February 2019**.

Chairman, SRC **Signature of External Examiner**

This is to certify that the student has made all the corrections in the thesis.

Signature of Supervisor (s) **Head of the Department**

Dated:

Dedicated
to
My Grand Parents

ACKNOWLEDGEMENTS

This thesis is a result of five years of work through inspiration and perspiration, whereby I have been accompanied and supported by many people to successfully trail the path of research. It is pleasant aspect that I now have the opportunity to express my gratitude to all of them. First and foremost, I would like to thank God Almighty for giving me the strength, knowledge, ability and grace bestowed upon me during my entire life. Without His blessings, this achievement would not have been possible.

I take pride in acknowledging my supervisor Dr. Kaushik Ghosh, Associate Professor, Department of Chemistry, IIT Roorkee, for his valuable guidance and advices. He has given me all the freedom to pursue my research and I shall eternally be grateful to him for his assistance. I pay my heartily gratitude to his wife Rupa Ghosh who supported and encouraged me every time in every aspect of life.

I am highly grateful to Prof. M. R. Maurya, Head of the Department of Chemistry, for providing necessary facilities and support to carry out my work. I take the opportunity to express my gratitude to my Student Research Committee (SRC) members Prof. U. P. Singh, Dr. R. K. Peddinti, Department of Chemistry and Dr. A. K. Sharma, Department of Biotechnology, IIT Roorkee for extending me all possible help and offering valuable suggestions during the entire course. I am thankful to Mr. Charan Singh, Mr. S. P. Singh, Mr. Madan Pal, Mr. Tiwari and other staff members, Department of Chemistry, for giving a helping hand to me on all occasions.

My special thanks are due for the Institute Instrumentation Centre, IIT Roorkee. I am thankful to Prof. U. P. Singh, Neetu Singh, Pankaj, Aurobindo for the help of XRD analysis.

The financial assistance by Council of Scientific and Industrial Research (CSIR), New Delhi is gratefully acknowledged.

I would like to thank my seniors and labmates Dr. Varun Mohan, Dr. Rajan, Dr. Sweety Rathi, Dr. Ashish Kumar Dhara, Dr. Ovender Singh, Dr. Anand, Kiran, Kapil, Ankur, Anshu, Sheela, Sain Singh, Virender who in one way or another contributed in the completion of this thesis..

I would like to gratefully thank my friends Manju yadav, Sudesh yadav, Sudhir yadav, Varsha yadav, Pooja yadav, Dinesh kumar, Pawan, Aarti dalal, Neetu, Neha kamboj, Iram parveen, Surinder, Kavita yadav, Anjlika yadav, Danish, Neha and all my batch mates with whom I have shared the best time of my life and who were always there in the hour of need.

I would also like to thank all the wonderful people met during conference in Italy. Unforgettable memories of that period will be always with me.

My family, pillar of strength for me, deserves special mention for their unflagging love and support in my life. This thesis is heartily dedicated to my grandfather Sh. Gheesa Ram and my grandmother Smt. Phoolvati Devi. I feel most blessed person of the world to have both of them in my life. I am indebted to my beloved mother Smt. Bimla Devi and father Sh. Jitender for their love, affection, constant inspiration, unconditional support throughout my life. I am also indebted to my all family members for their love and encouragement. My special gratitude to my elder brother Ajit Singh, brother-in-law Joginder Singh and elder sister Mithlesh for their unconditional support and inspiration. Love, affection and all the sweet memories with younger brothers Tapesh, Nikhil, Sachin and younger sisters Pinki, Priyanka, Jyoti, Sapna, Mahima will be always with me. I love my cute and charming nephew Divit, Devansh and beautiful niece Tanishka.

At the end, I am thankful to all those people, whose names have been mistakenly left, thank you very much for your support. Finally, I want to heartily apologize to each one of you, if knowingly or unknowingly I have ever hurt you.

Manju Bala

ABSTRACT

Coordination chemistry deals with the study of complexes having a central atom (a metal ion) bound to a set of ligand(s). The properties of metal complexes are manifestation of the nature, coordination number as well as oxidation state of metal ion and the donating properties of the bound ligands. Unlike the organic compounds, different ligands bind to metal ion in different coordination modes. Hence, coordination complexes are found to possess different coordination numbers, coordination geometries, and redox properties. On the other hand, a particular coordinated ligand stabilizes the metal ion in a particular oxidation state or may be in more than one oxidation states.

The thesis entitled "***Studies on new ruthenium complexes and their reactivities***" is divided into six chapters.

In the present report, we have synthesized different ligands having various groups such as diazo (–N=N–), azomethine (–CH=N–) and carboxamide (–CONH–)groups. These ligands were treated with different precursor ruthenium complexes to afford corresponding ruthenium complexes. These ruthenium complexes were characterized by various spectroscopic techniques like IR, UV-Vis spectroscopy, EPR, ^{1}H as well as ^{31}P NMR spectral studies. Some ruthenium complexes were also treated with *in situ* generated nitric oxide (NO) from acidified sodium nitrite ($NaNO_2$) solution (pH ~ 2-3) to produce ruthenium nitrosyl complexes. Nitrosyl complexes were characterized by IR, UV-Vis spectroscopy, ^{1}H as well as ^{31}P NMR spectral studies. Molecular structures of complexes were authenticated using X-ray crystallography. The redox properties of the ligand as well as metal center in the ruthenium complexes with non innocent ligands were investigated using cyclic voltammetry.

Theoretical calculations were also performed on the structure of the complexes to better understand the electronic properties.

In chapter one, literature on the redox, photophysical and photochemical properties of several ruthenium complexes along with brief introduction about coordination complexes and general properties of ruthenium will be reviewed. Role of ruthenium complexes as potential catalysts in organic and organometallic syntheses, transfer hydrogenation along with the importance of these complexes in different fields of bioinorganic chemistry will be scrutinized. Along with nitric oxide releasing molecules (photoNORMs), CO releasing molecules (photoCORMs) will also be described in brief. Various chemical methods and equipments used were comprehensively summarized.

In chapter two, organometallic ruthenium(III) complexes $[Ru(L^1)(PPh_3)_2Cl_2]$ (**1**) (where L^1H_2 =(E)-4-chloro-N-(2-(phenyldiazenyl)phenyl)benzamide and H = dissociable proton) and $[Ru(L^2)(PPh_3)_2Cl]$(**2**)(where L^2H_2 = (E)-2-((4-(dimethylamino)phenyl)diazenyl)-N-(p-tolyl)benzamide and H = dissociable protons) were synthesized through C-H bond activation. Complexes **1** and **2** were treated with acidified nitrite solution to afford organometallic ruthenium nitrosyl complexes $[Ru(L^1)(PPh_3)_2(NO)Cl](ClO_4)$(**3**) and $[Ru(L^2_{NO2})(PPh_3)_2(NO)Cl](PF_6)$(**4**). All the complexes were characterized by UV-vis, IR, ESI-MS, NMR spectroscopic studies. Molecular structures of complexes **3** and **4** were authenticated using X-ray crystallographic studies. Coordinated NO in ruthenium nitrosyls **3** and **4** was found to be photolabile under visible light and photo released NO was transferred to reduced myoglobin. Cytotoxic effects of complexes as well as photo-released NO were investigated. Gene expression studies were performed to understand the different stages of apoptotic cell death.

In chapter three, novel ruthenium(II) coordinated stable aminyl radical complex $[Ru(L^{5\cdot})(PPh_3)_2Cl_2]$ (**5**), was synthesized using ligands L^{3-5}. Cleavage of most stable amide bond and simultaneous production of nitrogen centred radical took place during the reaction course. Complex **5** was characterized by IR, UV-vis and EPR spectroscopic studies. Molecular structure of **5** was authenticated using single crystal X-ray crystallography. Along with spectroscopic characterization, theoretical calculations completely supported the nitrogen centred radical. The interaction of NO with the complex **5** afforded nitrosyl complex $[Ru(L^{5'})(PPh_3)_2(NO)Cl](ClO_4)$ (**6**). Molecular structure of the resultant nitrosyl complex **6** was authenticated by single crystal X–ray diffraction study. The photolability of coordinated NO was examined by using electronic absorption spectral studies under illumination of UV light.

In chapter four, organometallic ruthenium(II) complex $[Ru(L^6C\hat{}N\hat{}N)(PPh_3)_2(CO)]$ (**7**) [where L^6H_2 is (E)-N-((1H-pyrrol-2-yl)methylene)naphthalen-1-amine] [H represents dissociable proton] was synthesized via C-H bond activation using different synthetic strategies. Ruthenium hydrido carbonyl complexes $[Ru(L^6N\hat{}N)(PPh_3)_2(CO)H]$ (**8**) [where L^6H_2 is (E)-N-((1H-pyrrol-2-yl)methylene)naphthalen-1-amine] and $[Ru(L^7N\hat{}N)(PPh_3)_2(CO)H]$ (**9**) [where L^7H_2 is (E)-N-((1H-pyrrol-2-yl)methylene)-1-phenylmethanamine] were isolated. All the complexes were characterized by UV-Vis, IR and NMR spectral studies. Molecular structures of complexes **7**, **8** and **9** were authenticated using X-ray crystallography. Geometry optimization of the complexes **7**–**9** have been performed using Density Functional Theory (DFT) studies. Time-dependent DFT calculations were performed to better understand the electronic properties of complexes **7**–**9**. Complex **7** was utilized as catalyst in transfer hydrogenation of ketones. On the basis of literature study, the

plausible mechanisms were proposed for hydride formation and catalytic transfer hydrogenation. Coordinated CO in organometallic ruthenium carbonyl complex **7** was found to be photolabile upon visible light illumination.

In chapter five, reaction of (E)-4-((2-nitrophenyl)diazenyl)phenol (L^8H, H = dissociable proton) with $Ru(PPh_3)_3Cl_2$ afforded novel organometallic anion radical complex $[Ru(L_A^{8-\cdot})(Cl)(PPh_3)_2]$ (**10**). During the synthesis of complex **10**, nitro group in ligand converted to nitroso group through oxygen atom transfer to labile triphenylphosphine. One electron reduced nitroso group was coordinated to ruthenium in η^1(N) mode. Complex **10** was treated with acidified nitrite to afford nitrosyl complex $[Ru(L_B^{8-\cdot})(PPh_3)_2(NO)](ClO_4)$(**11**) and it is a rare example of an organometallic ruthenium complex having azo anion radical as well as two different noninnocent ligands coordinated to one metal. Both the complexes were characterized by UV-vis, IR, NMR spectroscopic studies. Redox properties of complex **10** were investigated using cyclic voltammetry. Molecular structures of complexes **10** and **11** were authenticated using X-ray crystallographic studies. DFT calculations were performed to better understand the electronic properties of complex **10**.

In chapter six, half sandwich ruthenium complexes $[(p\text{-cym})Ru^{II}(L^{9-12})Cl]PF_6$(**12-15**) containing N^N chelating schiff base ligand were successfully designed and synthesized. All the synthesized complexes were characterized by UV-vis, IR, ESI-MS, NMR spectroscopic studies. Molecular structures of **12** and **15** were authenticated using X-ray crystallography. Complexes **12-15** were utilized to investigate the anti-cancer activity studies on MCF-7, MDA-MB-435s and HEK-293 cell lines. Among all the complexes, complex **15** was found to be more potent against MCF-7 and MDA-MB-435s cancer cells as compared to complexes

12-14. However, all the complexes exhibited less cytotoxicity or almost inactivity towards HEK-293 normal cells.

LIST OF PUBLICATIONS

Journal Publications

1. Kaushik Ghosh*****, Rajan Kumar, Sushil Kumar, **Manju Bala**, Udai P. Singh "Orthometallation in bidentate Schiff base ligands via C-H activation: synthesis of ruthenium(III) organometallic complexes" *Transition Met. Chem.* **2015**, *40*, 831–837.
2. Rajan Kumar, Sushil Kumar, **Manju Bala**, Anand Ratnam, Udai P. Singh, Kaushik Ghosh***** "Site-specific orthometallation *via* C–H bond activation and syntheses of ruthenium (III) organometallics: studies on nitric oxide (NO) reactivity and photorelease of coordinated NO" *RSC Adv*. **2016**, *6*, 72096–72106.
3. Rajan Kumar, Anjlika Yadav, Anand Ratnam, Sushil Kumar, **Manju Bala**, Debpali Sur, Shikha Narang ,Udai P. Singh, Prabhat K. Mandal,***** Kaushik Ghosh***** "Organometallic ruthenium nitrosyl obtained by C–H bond activation – Photoinduced delivery of nitric oxide and NO-mediated antiproliferation activity studies" *Eur. J. Inorg. Chem.* **2017**, 5334–5343.
4. Anand Ratnam, **Manju Bala**, Rajan Kumar, U.P. Singh, Kaushik Ghosh***** "Design and syntheses of a new family of palladium complexes derived from tridentate ligands and their application as catalysts for Suzuki-Miyaura cross-coupling reactions" *J. Organomet. Chem.* **2018**, *856*, 41-49.
5. Rajan Kumar, Sushil Kumar, **Manju Bala**, Anand Ratnam, Udai P. Singh, Kaushik Ghosh***** "Unprecedented oxidation of aldimine to carboxamido function during reactivity studies on ruthenium complex with acidified nitrite solution: Synthesis of ruthenium nitrosyl complex having $\{RuNO\}^6$ moiety and photorelease of coordinated

NO" *J. Organomet. Chem.* **2018**, *863*, 77-83.

6. **Manju Bala**, Anand Ratnam, Rajan Kumar, Kaushik Ghosh* "Naphthyl C8-H hydrogen activation and synthesis of organometallic ruthenium complex: Crystal structure of hydride intermediates and catalytic transfer hydrogenation" *J. Organomet. Chem.* **2019**, *880*, 91-97.
7. **Manju Bala**, Anand Ratnam, Rajan Kumar, Udai P. Singh, Kaushik Ghosh* "Remarkable effect of position of carboxamido nitrogen in bidentate ligands to synthesize organometallic ruthenium(III) complexes via C-H activation: Organometallic ruthenium nitrosyl complexes and anticancer activity studies" (Manuscript prepared).
8. **Manju Bala**, Anand Ratnam, Rajan Kumar, Udai P. Singh, Kaushik Ghosh* "Unprecedented cleavage of amide bond and spontaneous generation of stable aminyl radical coordinated to ruthenium: Spectroscopic characterization, X-ray crystal structure and theoretical calculations" (Manuscript prepared).
9. **Manju Bala**, Anand Ratnam, Rajan Kumar, Udai P. Singh, Kaushik Ghosh* "In-situ ligand modification to generate anion radical in organometallic ruthenium complex: A rare example of isolation of organometallic azo anion radical during nitric oxide reactivity" (Manuscript prepared).
10. **Manju Bala**, Anand Ratnam, Rajan Kumar, Udai P. Singh, Kaushik Ghosh* "Anticancer Properties of Half-Sandwich Ruthenium(II) Schiff Base Complexes" (Manuscript prepared).

Conference Publications

1. Participated in '***15th national symposium on Modern Trends in Inorganic Chemistry (MTIC-XV), IIT Roorkee, Dec. 13-16, 2013'.***
2. Synthesis and characterization of nitrosyl complexes: Controlled delivery of nitric oxide (NO),'***Indo-French Seminar on Bio-inorganic Approaches to Current Health Problems***', Kaushik Ghosh, Rajan Kumar, Sushil Kumar, **Manju Bala**, Anand Ratnam, in Pondicherry University, Pondicherry, during 24-28 March, **2014**.
3. Participated in GIAN programme on '***Crystal structure determination: principle and application***' organized by Department of Chemistry, IIT Kanpur during Nov.29-Dec.9 **2017**.
4. Poster presentation at '***17th national symposium on Modern Trends in Inorganic Chemistry (MTIC-XVII), NCL Pune, Dec. 11-14, 2017'*** entitled "Unprecedented cleavage of amide bond and spontaneous generation of stable aminyl radical coordinated to ruthenium: Spectroscopic characterization, X-ray crystal structure, and theoretical calculations " **Manju Bala**, Kaushik Ghosh*.
5. Poster presentation at '***22nd CRSI National Symposium in Chemistry February 2 - 4, 2018 and 12th CRSI-RSC Symposium in Chemistry February 1, 2018***', Pt. Ravishankar Shukla University, Raipur (Chhattisgarh) entitled "Remarkable effect of position of carboxamido nitrogen to synthesize organometallic ruthenium (III) complexes via C-H activation: Ruthenium nitrosyl complexes and application in photodynamic therapy" **Manju Bala**, Anand Ratnam, Kaushik Ghosh*. (**Best poster awarded by American Chemical Society, ACS**)
6. Poster presentation in the workshop '***ACS on Campus, February 7, 2018***' at IIT

Roorkee, entitled "Characterization of ruthenium hydrido carbonyl complex as an intermediate during the synthesis of organometallic ruthenium(II) complex: Spectroscopic studies, X-ray crystal structures, catalytic transfer hydrogenation" **Manju Bala**, Kaushik Ghosh*.

7. Poster presentation at '**28th International Conference on Organometallic Chemistry (ICOMC-2018), Florence, Italy, 15-20 July, 2018**' entitled "In-situ ligand modification to generate anion radical in organometallic ruthenium complex: A rare example of isolation of organometallic azo anion radical during nitric oxide reactivity" **Manju Bala**, Kaushik Ghosh*.

TABLE OF CONTENTS

LIST OF FIGURES

LIST OF TABLES AND SCHEMES

General introduction of ruthenium chemistry along with applications

Chapter 1

Abstract

Literature on the redox, photophysical and photochemical properties of several ruthenium complexes along with brief introduction about coordination complexes and general properties of ruthenium will be reviewed in this chapter. Role of ruthenium complexes as potential catalysts in organic and organometallic syntheses, transfer hydrogenation along with the importance of these complexes in different fields of bioinorganic chemistry will be scrutinized. Along with nitric oxide releasing molecules (photoNORMs), CO releasing molecules (photoCORMs) will also be described in brief. Various chemical methods and equipments used were comprehensively summarized.

1.1. Introduction

Coordination chemistry deals with the study of complexes having a central atom (a metal ion) bound to a set of ligand(s). The properties of metal complexes are manifestation of the nature, coordination number as well as oxidation state of metal ion and the donating properties of the bound ligands. Unlike the organic compounds, different ligands bind to metal ion in different coordination modes. Hence, coordination complexes are found to possess different coordination numbers, coordination geometries, and redox properties. On the other hand, a particular coordinated ligand stabilizes the metal ion in a particular oxidation state or may be in more than one oxidation states.[1–3]

From investigation of literature on coordination complexes it was found that ligands having hard donors like carboxamido nitrogen, carboxylate and phenolato oxygen donor center(s) stabilize the metal ion in the higher oxidation state(s). However, ligands having soft donors like pyridine nitrogen, imidazole nitrogen, thiol and thioether donor center(s) stabilize the metal ion in the lower oxidation state(s).[2,4] Hence, the rational designing of new ligands which can stabilize the metal in one or more than one oxidation state(s) is of huge interest in the area of chemical research.

Literature survey on the coordination complexes completely revealed that several interesting properties, for example, tunable redox properties,[5–8] photophysical and photochemical properties[9–12] have been shown by the ruthenium complexes and such properties are very significant for their applications in chemical as well as biological research. Hence, coordination chemistry of ruthenium with different ligands has received considerable current attention.

1.2. Chemistry of ruthenium: General comments

Ruthenium is an element, having symbol Ru and atomic number 44 (Table 1.1) with the electronic configuration $[Kr]4d^7 5s^1$ in Group VIII and Period V of the periodic table. It was first discovered by a Russian scientist Karl Ernst Claus in 1844. It was isolated from the crude platinum part and belongs to the platinum group of metals.[1,13,14] Ruthenium is generally found in ores with the other platinum group metals but small quantities are also found in *pentlandite* extracted from Sudbury, Canada and in *pyroxenite* deposits in South Africa.

Table 1.1 Some properties of ruthenium.[14]

Properties	Value
Atomic symbol	Ru
Group/Period	$8^{th}/5^{th}$
Atomic number	44
Atomic weight ($gmol^{-1}$)	101.07(2)
Electronic configuration	$[Kr]4d^7 5s^1$
Natural abundance/ppm	0.0001
Density (20°C)/gcm^{-3}	12.37
Melting point/°C	2282 (± 20)
Boiling point/°C	4050 (± 100)
Electronegativity (Pouling scale)	2.2
Number of naturally occurring isotopes	7
Metal radius (12-coordinate)/pm	134
Most common oxidation states	2+ and 3+

Generally, ruthenium contains variable number of the oxidation states from 0 to 8 and –2. But 2+ and 3+ are the most stable oxidation states of this element. In general, the geometries of the ruthenium complexes are octahedral for coordination number VI, trigonal bipyramidal for V and tetrahedral for IV coordination number.[1,14] Ruthenium complexes in 3+ oxidation state are low-spin octahedral and paramagnetic with d^5 electronic configuration containing one unpaired electron.[14] Ruthenium complexes in 2+ oxidation state are low-spin octahedral and diamagnetic with d^6 electronic configuration.

1.3. Applications of ruthenium complexes

1.3.1. Water oxidation by ruthenium complexes

The oxidation of water to molecular oxygen ($2H_2O \rightarrow O_2 + 4H^+ + 4e^-$) is well known photosystem-II (PS-II) reaction involved in natural photosynthesis.[15,16,17] Protons and electrons required to store solar energy in chemical bonds are provided by the oxidation of water to oxygen.[18] For a long time, scientists have tried to imitate the photosynthesis owing to increased demands imposed by worldwide energy consumption. To reach this goal, the development of more efficient water oxidation catalysts has become a challenging area of chemical research.

In the 1982, Meyer and coworkers[19] reported the dinuclear ruthenium(III) complex $[(bpy)_2(H_2O)Ru^{III}(\mu\text{-}O)Ru^{III}(H_2O)(bpy)_2]^{4+}$ (where bpy = 2,2′-bipyridine) having an oxo-bridged ligand as a water oxidation catalyst with a turn over number (TON) of 13.2, also known as ‘blue dimer’ due to its characteristic color. Mechanism of the water oxidation by this blue dimer using an excess amount of Ce(IV) as a chemical oxidant (shown in Scheme 1.1) was proposed the Meyer’s group.[20,21]

Llobet and co-workers[22] were reported the first well-characterized dinuclear Ru complex $[Ru_2^{II}(bpp)(terpy)_2(H_2O)_2]^{3+}$ (Hbpp=2,2′-(1H-pyrazole-3, 5-diyl)bis(pyridine) bridged through the terpy-Ru-bpp motif. It was found to be more active than the blue dimer for homogeneous oxygen evolution due to the absence of the μ-oxo bridge.

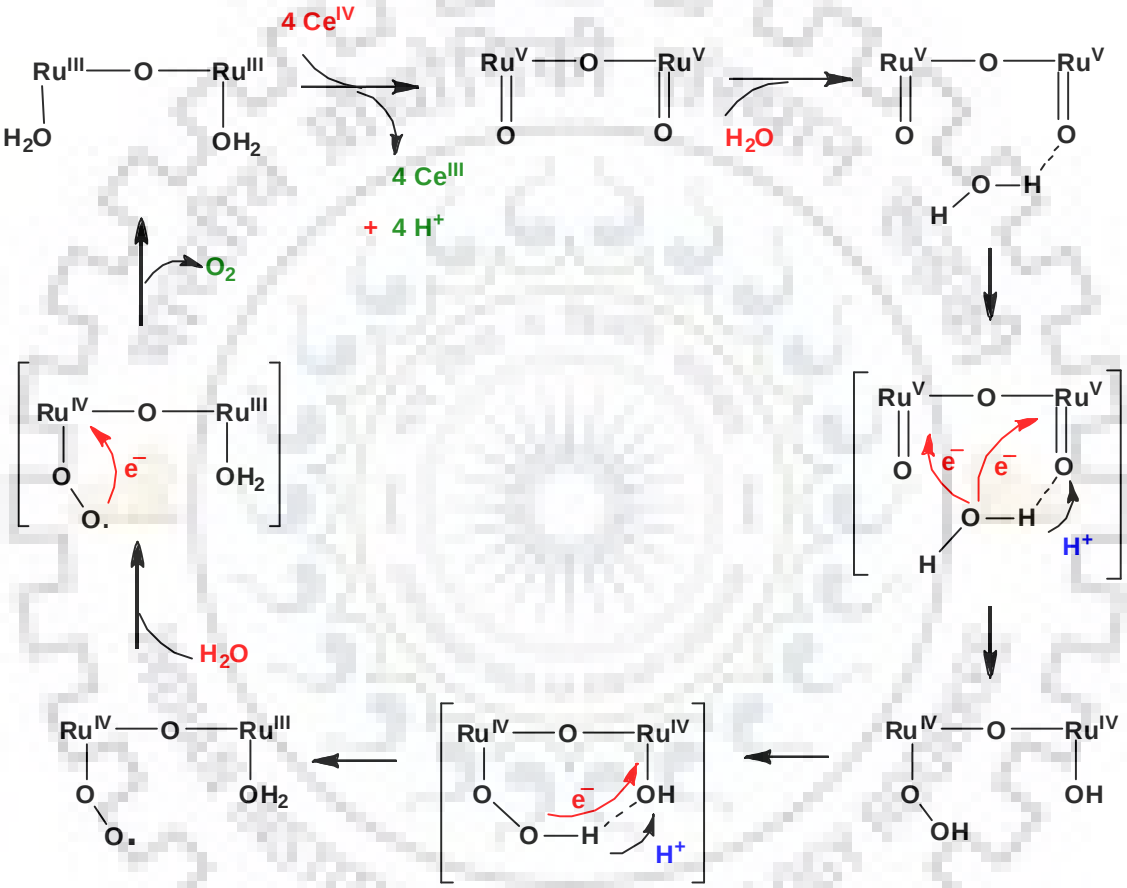

Scheme 1.1 The proposed mechanism of water oxidation using blue dimer catalyst.

Several groups Llobet's[23,24] and Hurst's group[25–27] have used dinuclear and mononuclear ruthenium complexes (Fig. 1.1) catalyst for the oxidation of water into molecular oxygen which contain at least one aqua molecule as a ligand and they have proposed the mechanism of water oxidation into molecular oxygen.

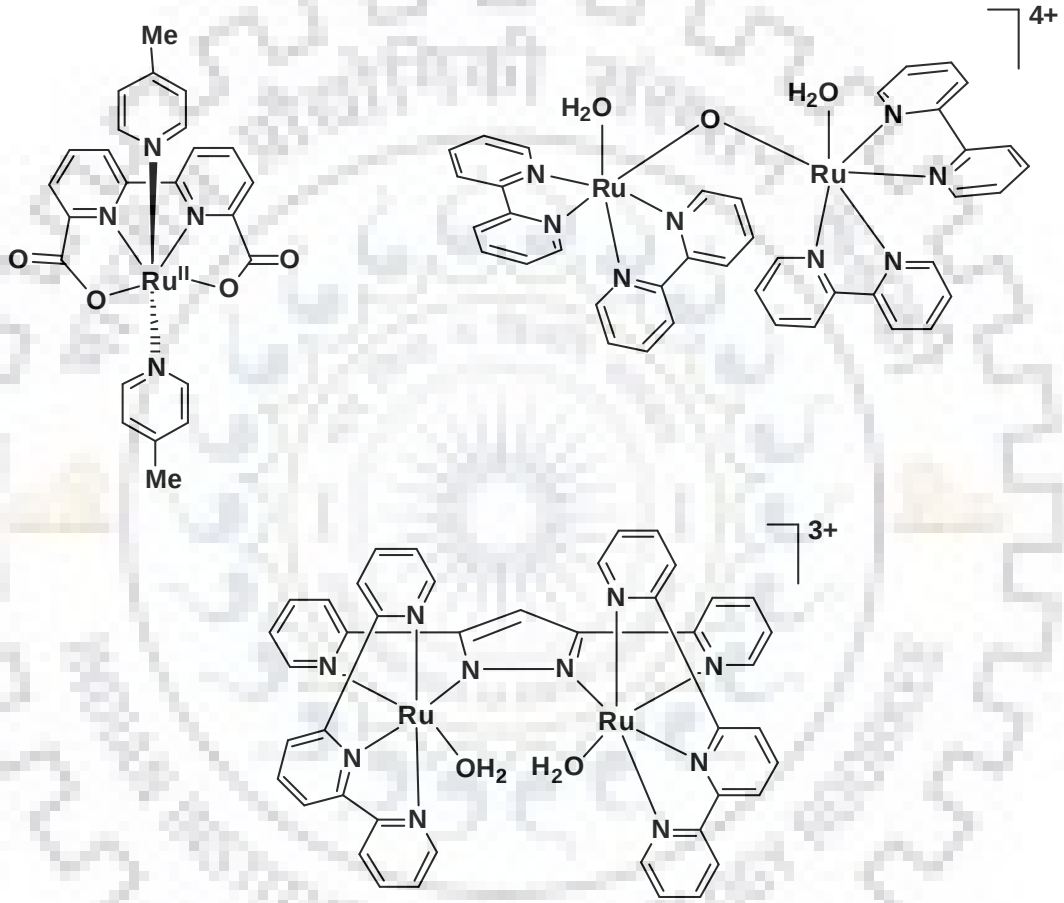

Fig. 1.1 Mononuclear and dinuclear ruthenium complexes used for water oxidation.

On the other hand, Thummel and coworkers[28–30] have also synthesized some non-aqua mononuclear as well as dinuclear ruthenium complexes for water oxidation. In the water oxidation process, Thummel[30] and Meyer[31] and their coworkers were observed a seven coordinated ruthenium intermediate in the catalytic cycle. In the recent past, Duan et al.[32] were isolated a very uncommon seven-coordinated Ru(IV) dimeric complex μ-(HOHOH)-$[Ru^{IV}(L)(pic)_2]_2(PF_6)_3 \cdot 2H_2O$ which was obtained as an intermediate in the water oxidation reaction catalyzed by complex $[Ru^{II}L(pic)_2]$. Recently, Llobet and coworkers[33] also synthesized the seven-coordinated mononuclear Ru(IV) complex, $[Ru^{IV}(OH)(tda\text{-}\kappa\text{-}N^3O)(py)_2]^+$ with high turnover frequencies of 8000−50000s^{-1} depending on pH.

1.3.2. In organic and organometallic syntheses

Cyclometalation, one of the most convenient methods for syntheses of organometallic entities, has gained significant current interest probably because of mildest route followed for activation of strong C-H bonds. The chemistry of organometallic compounds has become fast grown area in the field of chemical research because of vast applications of these complexes in catalysis, organic transformation , bioorganometallic chemistry, photophysical devices etc.[34] Because of versatile chemistry of ruthenium, its complexes were found to have significant contribution in organic[35–48] and organometallic syntheses.[49–61]

Catalytic reactions involving the cleavage of a sp^3 C–H bond adjacent to a nitrogen atom in *N*-2-pyridynyl alkylamines were described by Murai and coworkers.[39] Reaction of α,β-unsaturated imines with CO and alkenes to obtain α,α-disubstituted β,γ-unsaturated γ-butyrolactams in the presence of $Ru_3(CO)_{12}$ as a catalyst were also explained.[41]

The proposed mechanism for ortho-alkylation *via* C-H bond activation by ruthenium complex $RuH_2(CO)(PPh_3)_3$ is shown in Scheme 1.2.[38,45] In this reaction, first, chelation of the carbonyl oxygen to ruthenium initiates cleavage of the C-H bond at the ortho position to generate a metallacycle intermediate. Next, a metal alkyl intermediate is formed during olefin coordination and subsequent migratory insertion. Lastly, during the reductive elimination, ortho alkylated product is obtained with simultaneous regeneration of the initial catalyst, completing the catalytic cycle.

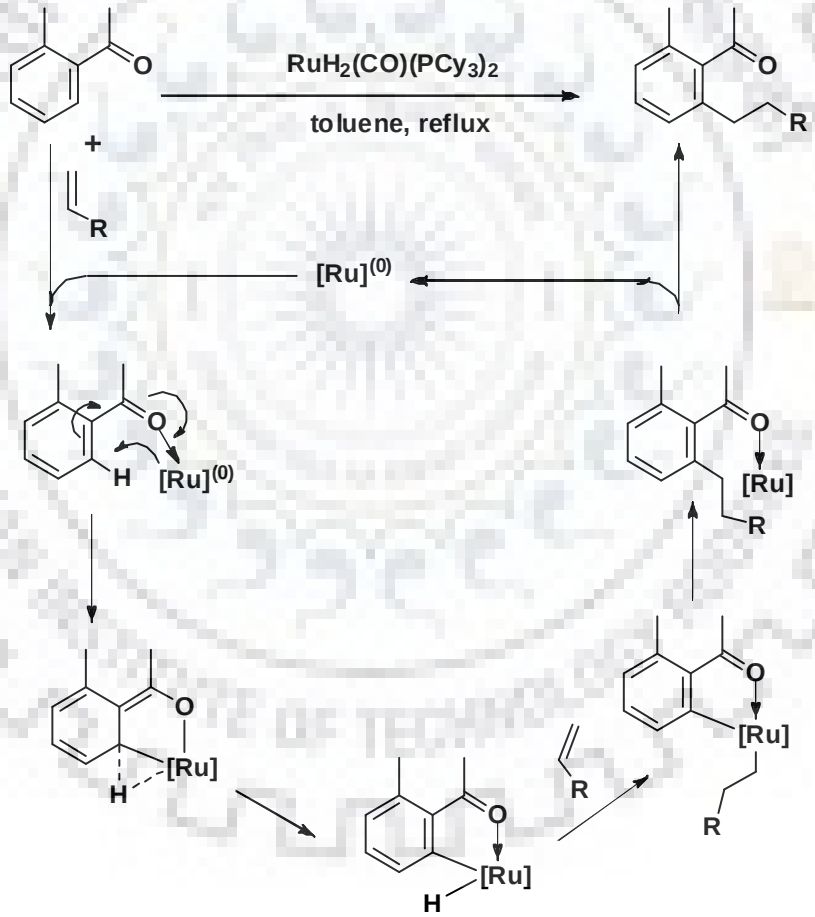

Scheme 1.2 The proposed mechanism for C–H bond activation in Murai's reaction.

Chatani and coworkers[44] have also utilized the ruthenium complexes as catalysts for organic transformations via C–H bond activation. Aromatic amides were used as bidentate N,N chelating directing groups. The functionalization of ortho C–H bonds was observed during the reaction of aryl halides with aromatic amides in the presence of ruthenium catalysts. Substituent effects on aryl bromides as well as aromatic amides were also investigated during the reaction (Scheme 1.3).

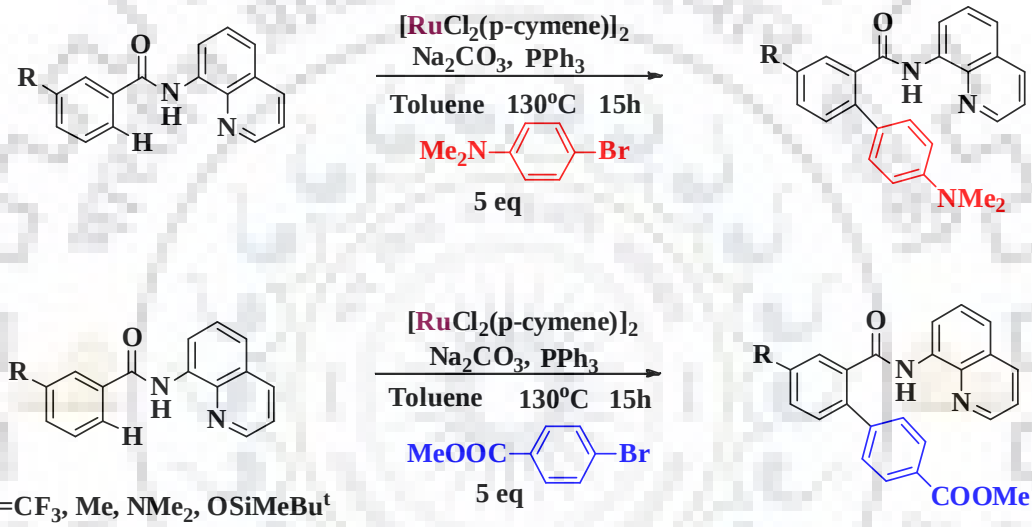

Scheme 1.3 Functionalization of ortho C–H bonds in the presence of ruthenium catalyst.

1.3.2.1 Olefin metathesis and Grubbs' catalysts

The olefin metathesis is a fundamental chemical transformation that involves formation of carbon-carbon double bonds (Scheme 1.4). It proceeds *via* a series of the alternating [2 + 2] cycloadditions and cycloreversions and the generation of metallacyclobutane intermediates during the coordination of the olefin(s) to a metal alkylidene. It can be applied in various synthetically advantageous permutations, such as ring-closing and ring-opening metathesis, cross metathesis (CM), olefinic polymerization.

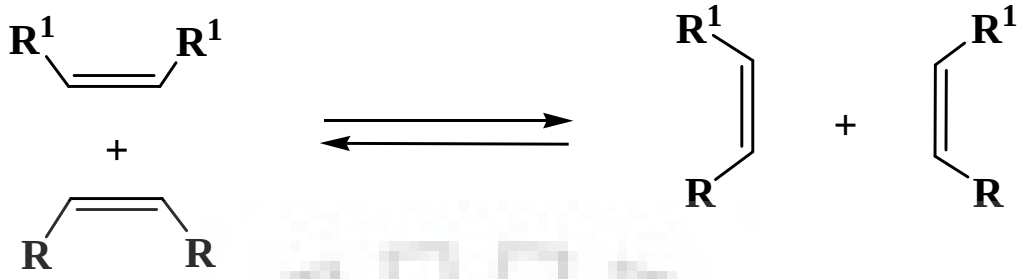

Scheme 1.4 Generalized scheme for olefin metathesis.

Ruthenium-carbene complexes also called as Grubbs' catalysts, named after an American chemist Robert H. Grubbs who first synthesized them, used as catalysts for olefin metathesis.[62-64] In year 2005, the Nobel Prize in chemistry was awarded jointly to Robert H. Grubbs, Yves Chauvin and Richard R. Schrock for the development of the metathesis method in organic synthesis. In Grubbs' catalyst, the geometry around ruthenium centre is found to be distorted square pyramidal as found to be surrounded by five ligands.[64] Because of their low sensitivity to air, moisture and a significant tolerance to different functional groups such as esters, amides, ketones, aldehydes and even for protic functionalities like alcohols, water and acids, Grubbs' catalysts have gained considerable current interest.[64,65] The catalytic activity of Grubbs' catalysts depends on phosphine group as well as on the carbene moiety and the less lability of carbene ligand over phosphine makes these more stable in terms of oxidative and thermal in comparison to corresponding organometallic complexes.[66]

The first well-defined ruthenium-based olefin metathesis catalyst known as Grubbs 1st generation catalyst was reported by Grubbs and co-workers (Fig. 1.2).[64,67]

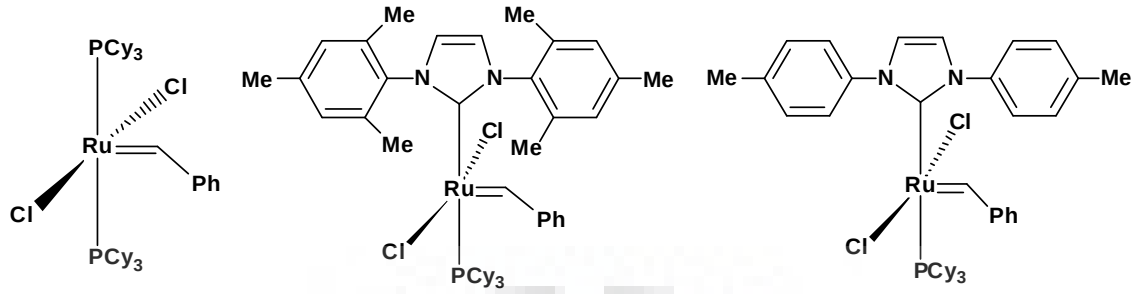

$[(PCy_3)_2Cl_2Ru{=}CHPh]$ $[(PCy_3)(IMes)Cl_2Ru{=}CHPh]$ $[(PCy_3)(ITol)Cl_2Ru{=}CHPh]$

Fig. 1.2 Chemical structures of first and second generation Grubbs' catalysts.

Replacement of one of the phosphine ligand in Grubbs 1st generation catalyst by *N*-heterocyclic carbenes (NHCs) which were observed as the mimics of phosphine led to Grubbs 2nd generation catalyst (Fig. 1.2).[68] In fact, the reactivity as well as the stability of second-generation Grubbs' catalysts was improved after the involvement of NHC ligands. After that, Grubbs 3rd generation catalyst and Hoveyda catalyst were also synthesized.[69-71] The olefin metathesis reactions proceed in a dissociative fashion according to the mechanism shown in Scheme 1.5.

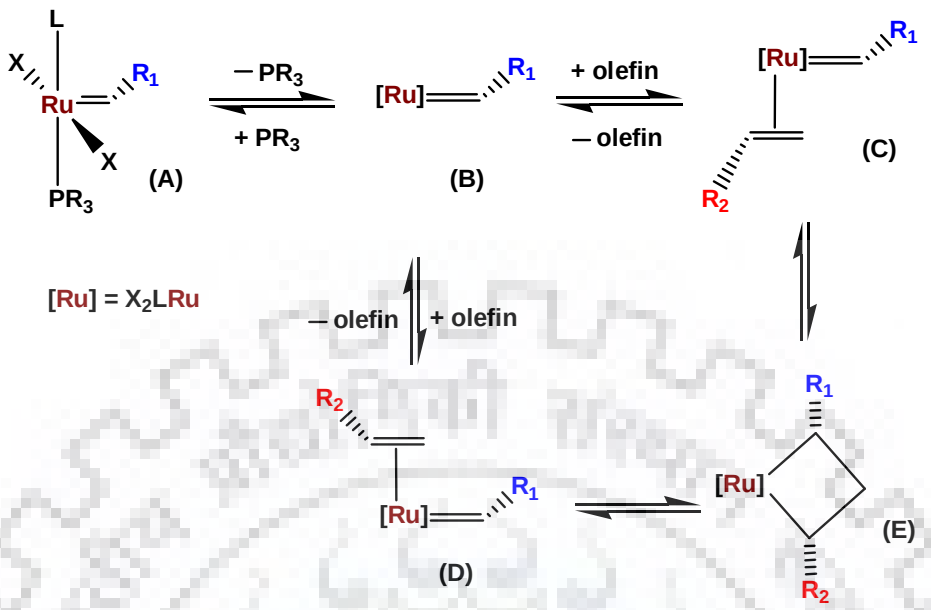

Scheme 1.5 Mechanism of olefin metathesis with Grubbs' catalyst.

1.3.2.2. Hydrogenation and transfer-hydrogenation (TH)

Hydrogenation and transfer hydrogenation (Scheme 1.6) of unsaturated hydrocarbons such as olefins, ketones, and imines to produce alkanes, alcohols and amines respectively are amongst the most important synthetic reactions catalyzed by ruthenium complexes not only from academic point of view but also of industrial importance bacause of operational ease, environment-friendliness and economics [72-74] A hydrogen donor such as molecular hydrogen, alcohol, formic acid is catalytically activated by appropriate transition metal complexes to deliver the two hydrogen atoms to unsaturated bonds to produce the corresponding reduced products. The discovery of RuO_2[75,76] and $RuCl_2\{P(C_6H_5)_3\}_3$[77] as selective hydrogenation catalysts provided an opportunity to the development of ruthenium-based catalysts.

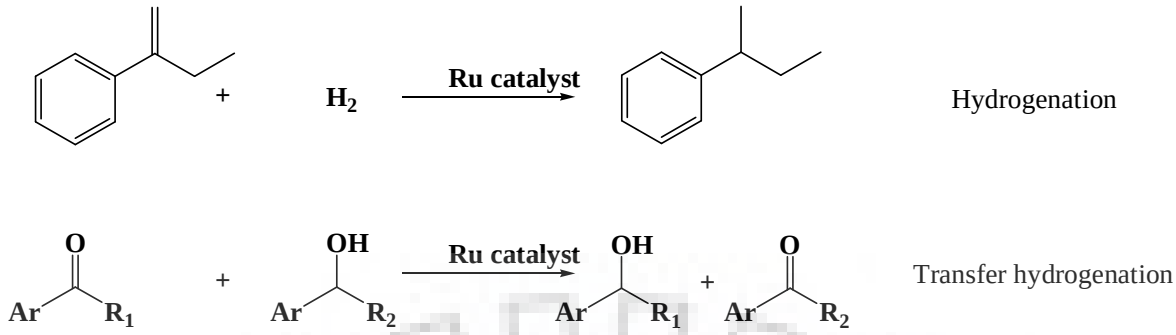

Scheme 1.6 Schematic representation of hydrogenation reactions.

Ruthenium-NHC complexes having a pyridine moiety were well documented as a promising new class of transfer-hydrogenation catalysts.[78,79] Remarkably, a very less catalyst concentration of only 0.1 mol % was found to be adequate for the transfer-hydrogenation of a wide range of ketones and imines.[78] Albrecht and co-workers[80] prepared a family of different donor substituent-functionalized NHCs ruthenium complexes. Among them, the olefin-tethered NHC ruthenium complex was found to be a very efficient and versatile transfer-hydrogenation catalyst for olefins, alkynes, ketones, nitrobenzene, benzonitrile under different conditions.

Singh and co-workers[81] also reported half-sandwich ruthenium(II) complexes as the catalysts bearing tridentate ligands and gave admirable results in the transfer-hydrogenation of ketones. The landmark discovery of the Noyori catalysts in transfer-hydrogenation still inspires the development of new analogues.[82-85]

1.3.3. Ruthenium based complexes in biological system

1.3.3.1. Anti-cancer agents

Cancer, one of the most fatal diseases, embraces a large collection of heinous diseases in the world and causes the death of millions of people every year. It is characterized by the

uncontrolled division of abnormal cells that invade and disrupt tissues. Both, external (e.g., chemicals, radiation, viruses) and internal (e.g., hormones, immune conditions, inherited genes) may be responsible for the initiation and promotion of cancer.[86-89]

Platinum based metallodrugs e.g. cisplatin, carboplatin, oxaliplatin and satraplatin (Fig. 1.3), were widely used as chemotherapeutic agents for cancer treatment. However, tumour resistance and their several side effects like renal toxicity, neurotoxicity, myelosuppression, immunosuppression, severe nausea, vomiting has significantly slowed down the introduction of new platinum-based derivatives into clinical studies. Therefore, the approaches to explore new anticancer drugs based on transition metal complexes with particular attention to ruthenium most likely due to the ability of ruthenium to mimic iron in binding to biomolecules,[89] with similar therapeutic profiles to cisplatin, but without its drawbacks dominate the research in field of cancer.[90,91]

Anti-cancer property of ruthenium(III) complexes was first described by Clarke for Ru(III) ammines; however they were found excessively insoluble to be used in the clinic.[92] Two most promising Ru(III) complexes which have entered clinical trials are trans tetra chlorodimethylsulfoxideimidazoleruthenate(III) (NAMI-A) and trans tetrachlorobis (1H-indazole) ruthenate(III) (KP-1019) (Fig. 1.4).[93] Ruthenium–arene complexes with modified ligands also find their significance as anticancer agent.[94] For example, $[(\eta^6\text{-THA})Ru(en)Cl]^+$ where THA= tetrahydroanthracene and en=ethylenediamine and the ruthenium arene complex $[Ru(arene)Cl_2(PTA)]$, commonly known as RAPTA, (where PTA= 1, 3, 5-triaza-7-phosphaadamantane) (Fig. 1.4) are another examples which have been used as anticancer agents in human cancer cell lines.[95]

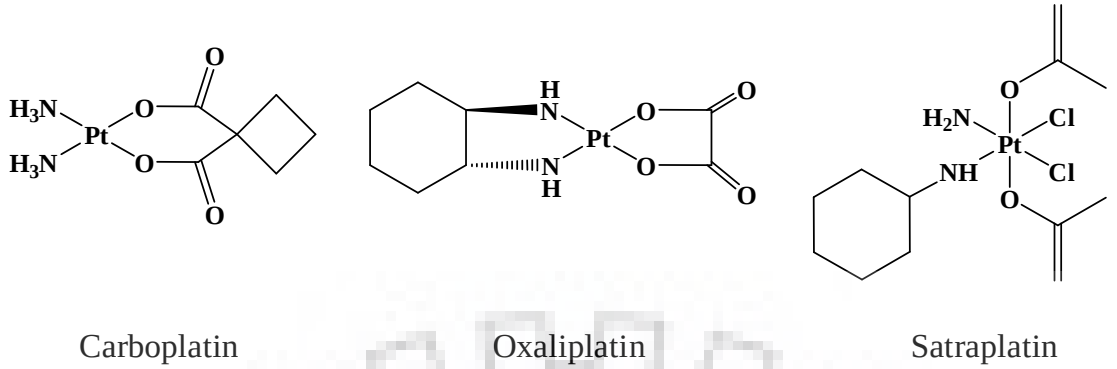

Fig. 1.3 Chemical structures of the carboplatin, oxaliplatin and satraplatin.

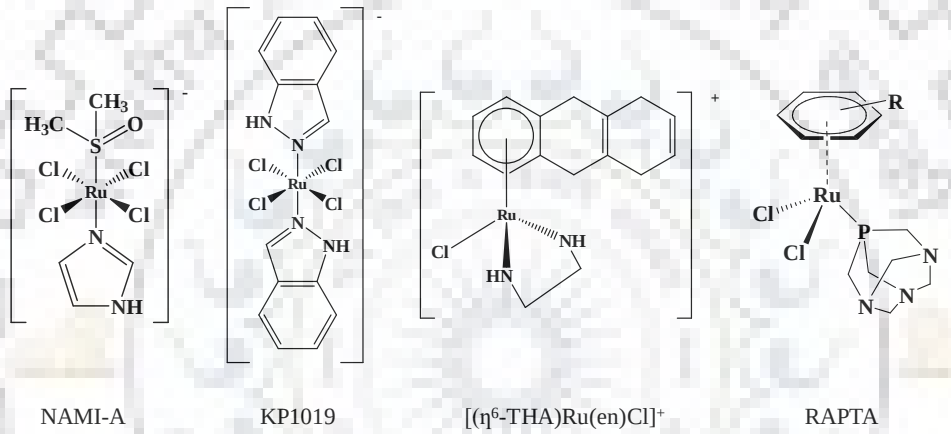

Fig. 1.4 Schematic diagram of ruthenium-based anti-cancer complexes NAMI-A, KP1019, $[(\eta^6\text{-THA})Ru(en)Cl]^+$ and RAPTA.

1.3.3.2. DNA interaction

Transition metal complexes have potential applications in medicinal chemistry and these metal complexes interact with nucleic acids, damage DNA and induce apoptosis in human cells. Ruthenium complexes can also bind with DNA through covalent as well as non-covalent interactions.

Ruthenium complexes $[Ru(phen)_2(dppz)]^{2+}$ and $[Ru(bpy)_2(dppz)]^{2+}$ (Fig. 1.5) containing one intercalating dppz ligand which can readily π-stack into the DNA duplex because of parallel

orientation to the base pairs of the DNA, displayed a significant enhancement in luminescence upon intercalation into duplex DNA.[96,97]

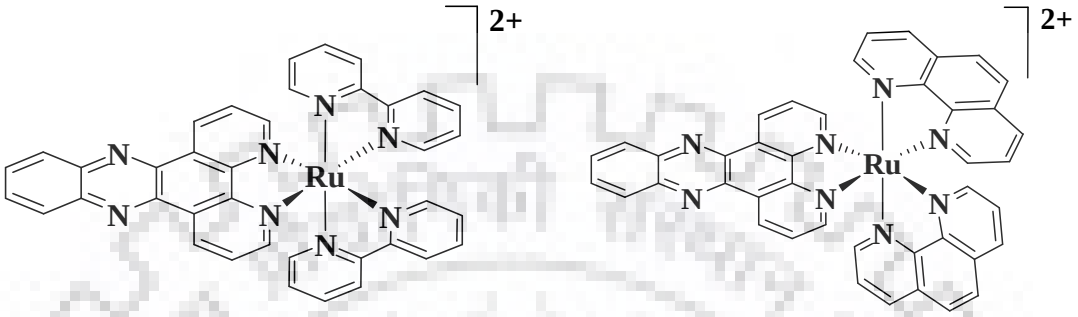

Fig. 1.5 Ruthenium complexes $[Ru(bpy)_2(dppz)]^{2+}$ and $[Ru(phen)_2(dppz)]^{2+}$ utilized for DNA intercalation

Covalent binding of different polypyridyl ruthenium complexes to DNA was demonstrated by Grover and co-workers.[98] Later on, the dinuclear aqua complex $[(bpy)_2Ru(OH_2)]_2O^{4+}$ which was found to bind stereo selectively with CT-DNA and showed more efficient binding over the mononuclear ruthenium complex was reported by the same group.[99] Novakova and co-workers[100] examined polypyridyl ruthenium chloro complexes of chemical formulas [RuCl(bpy)(terpy)]Cl, *cis*-$[Ru(bpy)_2Cl_2]$ and *mer*-$[RuCl_3(terpy)]$ (bpy=2,2'-bipyridyl, terpy=2, 2':6',2''-terpyridine) for DNA binding and among all these complexes *mer*-$[RuCl_3(terpy)]$ complex showed significantly higher DNA interstrand cross-linking as compared to other complexes. The interactions of ruthenium arene complexes such as $[(\eta^6\text{-arene})Ru(en)Cl]^+$ (where arene was biphenyl (BIP), dihydroanthracene (DHA), tetrahydroanthracene (THA), *p*-cymene (CYM) or benzene (BEN) and en was ethylene diamine) to CT-DNA through covalent as well as minor groove binding were investigated by

Sadler and his group.[101,102] In these pseudo-octahedral piano-stool complexes, three coordination sites were occupied by the arene ring and the remaining sites by one halide along with two diamine nitrogens. It was observed that binding of ruthenium (II) arene complexes to DNA was faster as compared to cisplatin. Binuclear ruthenium (II) polypyridyl complex (Fig. 1.6) synthesized by Kumbhar and co-workers[103] was also utilized for the DNA interaction.

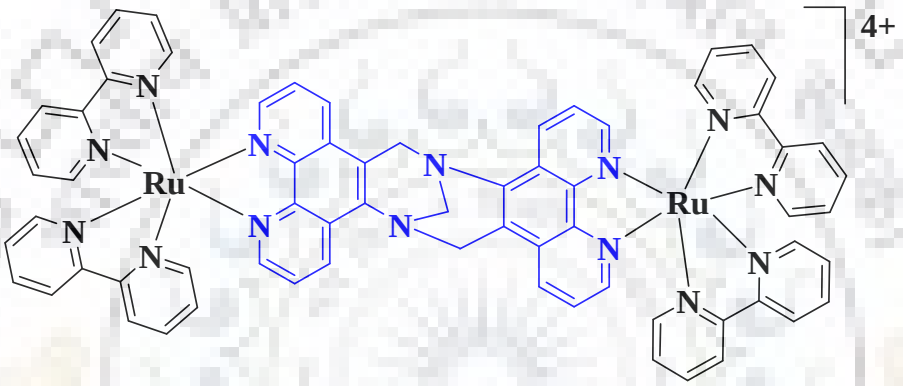

Fig. 1.6 Binuclear ruthenium(II) polypyridyl complex used for DNA interaction.

1.3.3.3. Ruthenium complexes as anti-microbial agents

Because of the capability of ruthenium-based complexes to firmly bind nucleic acids and proteins, the iron mimicking property in binding to biological molecules and ligand exchange kinetics similar to those of their platinum counterparts, these complexes have been largely examined for noteworthy biological activity.[104-108] Moreover, the photophysical properties of many ruthenium(II) complexes make possible flow cytometry and con-focal microscopy studies for cellular accumulation and localization.[105,106] Therapeutic potential of these

complexes as anti-cancer and anti-microbial agents has been demonstrated over the last decade.[109]

Biological activity of polypyridyl metal complexes was initially examined by Dwyer and co-workers.[110] They investigated mononuclear complexes with ligands such as 1,10-phenanthroline, bipyridine and their derivatives coordinated primarily to iron or ruthenium, for the antibacterial activity against Gram-positive, Gram-negative and acid-fast bacteria.[110] $[Ru(phen)_3]^{2+}$ (Fig. 1.7 (a)) was found to be inactive against all the bacterial strains. However, addition of methyl group as substituents on the phenanthroline ligands (Fig. 1.7 (b)), significantly increased the activity against all bacteria indicative of the significance of lipophilicity on the antibacterial action. Mononuclear ruthenium(II) polypyridyl complexes that could bind to DNA through intercalation were examined by Aldrich-Wright and co-workers.[111] These complexes exhibited remarkable bactericidal action against *B. subtilis* and *S. aureus* strains. Moreover, the treatment with the most active compound, $[Ru(2, 9\text{-}Me_2phen)_2(dppz)]^{2+}$ (Fig. 1.7 (c)), increased the survival population of Caenorhabditis elegans that were infected with S. aureus, indicating the relatively less toxicity against eukaryotic systems.[111] Satyanarayana and co-workers also observed that mononuclear ruthenium complexes with derivatives of either dppz or 2-phenyl-imidazo-1,10-phenanthroline ligands had shown moderate activity.[112] In contrast, $[Ru(L)_2bdppz]^{2+}$ {where L= bipyridine or 1, 10-phenanthroline and bdppz=9a,13a-dihydro-4,5,9,14-tetraaza-benzotriphenylene-11-yl)-phenyl-methanone} had shown high anti-microbial activity at 1500 mg ml^{-1} against *S. aureus* and *E. coli*.[113] Although, DNA binding is a considerable factor in terms of anti-microbial activity of the polypyridyl ruthenium(II) complexes, Lam and co-

workers[114] recently explained that a bis(bipyridine)-ruthenium(II) complex having N-phenyl-substituted diazafluorene ligand considerably enhanced the production of reactive oxygen species in MRSA. The authors suggested that high activity observed against MRSA (6.25 mg ml^{-1}) may be due to DNA damage caused by elevation in level of the reactive oxygen species.

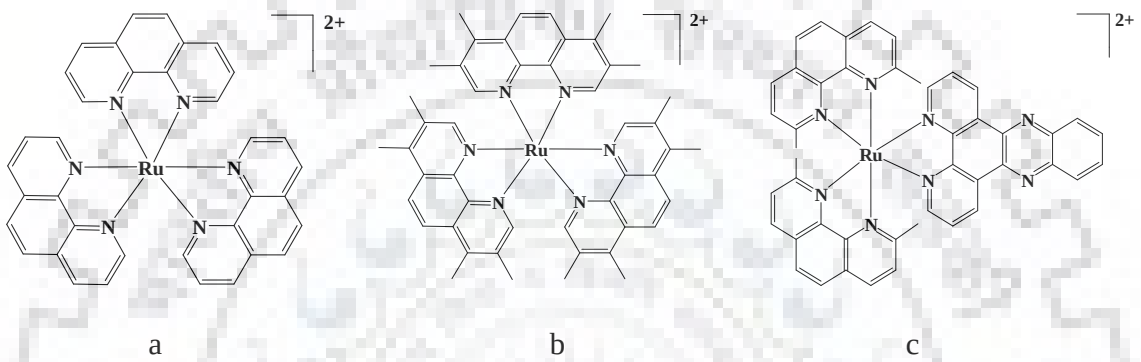

Fig. 1.7 Mononuclear polypyridylruthenium(II) complexes exhibiting antimicrobial activity (a) $[Ru(phen)_3]^{2+}$ (b) $[Ru(Me_4phen)_3]^{2+}$ (c) $[Ru(2, 9\text{-}Me_2phen)_2(dppz)]^{2+}$.

Aldrich-Wright and co-workers studied the intercalative dinuclear complex $[\{Ru(dpq)_2\}_2(m\text{-phen-x-SOS-x-phen})]^{4+}$ (dpq=dipyrido[3,2-d:20 30-f]quinoxaline; SOS=2-mercaptoethyl ether; x=3, 4 or 5) and observed that the complex had a improved DNA binding affinity of 6 $x10^7$ M^{-1}, as compare to the mononuclear analogues $[Ru(dpq)_2(phen)]^{2+}$ ($K=5.4x10^4$ M^{-1}), $[Ru(dpq)_2\text{-(phen-4-SOS)}]^{2+}$ ($K=2.3x10^6$ M^{-1}), or $[Ru(bpy)_2(dpq)]^{2+}$ ($K=5.9 \times 10^4$ M^{-1}).[115,116] Because of having DNA binding capability, Rubbn complexes were highly active against a variety of pathogenic bacteria, particularly Gram positive strains.[117]

1.3.4. Photophysical as well as photochemical properties and applications in DSSC

For many years, there has been a huge current interest to study photophysical properties of ruthenium(II) complexes with polypyridine ligands such as 2, 2'-bipyridine and 1,10-

phenanthroline and their derivatives.[118-120] These complexes have redox optical properties due to the presence of electron accepting polypyridine ligands and an electron-rich metal centre.[121] These particular complexes have applications in different areas including solar energy conversion[122] and molecular electronic devices.[123] Ruthenium polypyridine complexes have ability to absorb a major part of the visible light and the non-radiative decay of metal to ligand charge transfer (MLCT) excited states takes place at room temperature.[121] Decrease in the energy gap between the ground and excited state increases the rate of this decay.[124,125] Hence, absorption bands of low energy gap, make these complexes weak emitters having short-lived excited states. Luminescence properties of the $[Ru(bpy)_3]^{2+}$ and related polypyridine type complexes were illustrated by Crosby and co-workers [126].

Balzani and co-workers[120,121] investigated photochemical and photophysical properties of a series of ruthenium polypyridyl complexes and some of the complexes showed long-lived ligand-centered phosphorescence. They also described the applications of these complexes as luminescent and electroluminescent sensors and solar energy conversion. In 1988, Juris and co-workers[127] reported a series of nine *tris*-heteroleptic ruthenium(II) polypyridyl complexes of the type $[Ru(bpy)(biq)(L)]^{2+}$ (where bpy=2, 2'-bipyridine, biq=2, 2'-biquinoline and L was Me_2-bpy, 1,10-phenanthroline, 3, 3'-biisoquinoline or 2, 2'-bipyrimidine) and the electrochemical behavior as well as luminescence properties were investigated.

Recently, dye sensitized solar cells (DSSCs) have gained considerable attention. Over 20 years ago, Gratzel and co-workers developed the simple method of conversion of solar energy to electricity by dye-sensitized solar cell (DSSC).[128] DSSCs have a wide band-gap semiconductor, generally titanium dioxide (TiO_2) which is covered with a dye to absorb most

of the visible light.[129] Nano-crystalline DSSCs have also gained considerable interest as cost-effective alternatives to present p-n junction photovoltaic devices due to their potential applications and high efficiency.[129,130] Gratzel and O'Regan[131] introduced a dye-sensitized solar cell anchored with the surface of nano-crystalline TiO_2 and an electron is injected from the excited dye to the TiO_2 conduction band upon visible light excitation. Since then, several ruthenium polypyridyl complexes have received great attention in DSSCs as a result of their promising performance as sensitizers.[132,133]

Ruthenium complexes were found to be suitable as sensitizers for DSSC because of their spectral, photophysical and photochemical properties and comparative stability in the oxidized and reduced forms. To absorb in the range of whole visible spectrum, different strategies have been successfully applied in designing ruthenium complexes.[134] To date, several ruthenium(II) polypyridyl complexes particularly [*cis*-(dithiocyanato)Ru-bis(2, 2'-bipyridine-4,4'-dicarboxylate)] complexes commonly known as N3 and N719 dyes (Fig. 1.8) have been used as the most efficient dye sensitizers.[135,136]

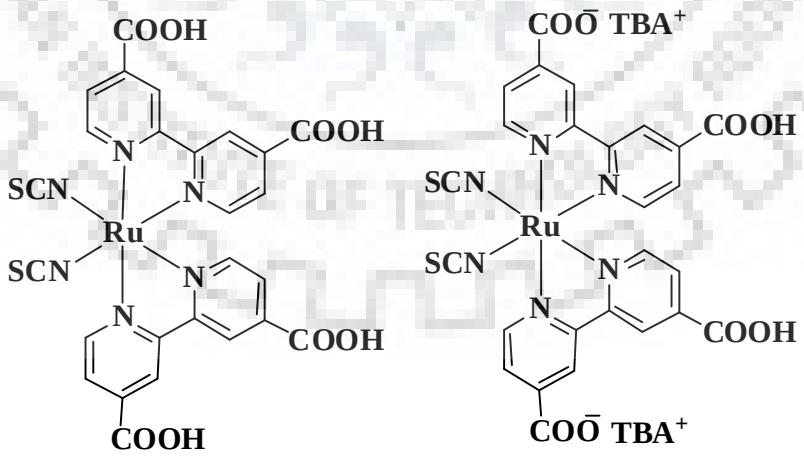

Fig. 1.8 The structures of Gratzel's best DSSC dyes.

1.3.5. NO releasing molecule (NORM)

Nitric oxide, a diatomic gaseous molecule plays very important roles in biological systems.[137] It is one electron paramagnetic strong field ligand. NO was declared as the molecule of the year by *Science* in the year 1992[138] and Nobel Prize for discovery of NO as a signalling molecule was given to three US scientists named as Robert F. Furchgott, Louis J. Ignarro and F. Murad in 1998.

In biosystem, nitric oxide synthase produces NO and various concentration-dependent activities of NO were discovered.[139,140] On the basis of the difference in activities and the Ca^{2+}-dependence, three NOS isoenzymes have been purified and biochemically characterized: neuronal NOS (n-NOS or NOS-1),[141,142] inducible NOS (i-NOS or NOS-2)[143] and endothelial NOS (e-NOS or NOS-3)[144] (Scheme 1.7).

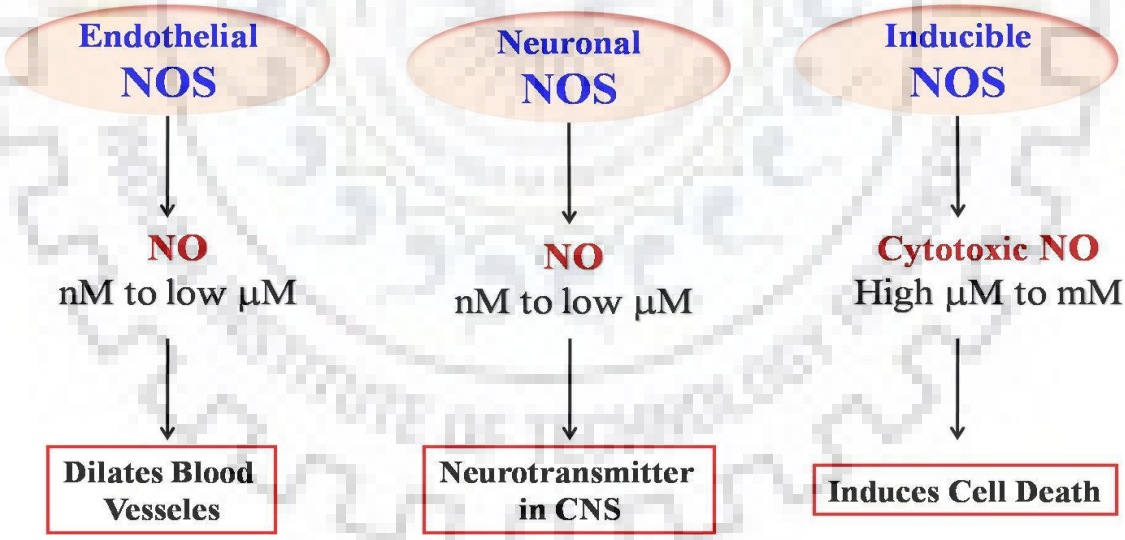

Scheme 1.7 Nitric oxide synthase isoenzymes and their biological functions.

NO is formed as a byproduct during the conversion of semi-essential amino acid L-arginine (L-Arg) into an equal amount of L-citrulline by NOS (Scheme 1.8).[145]

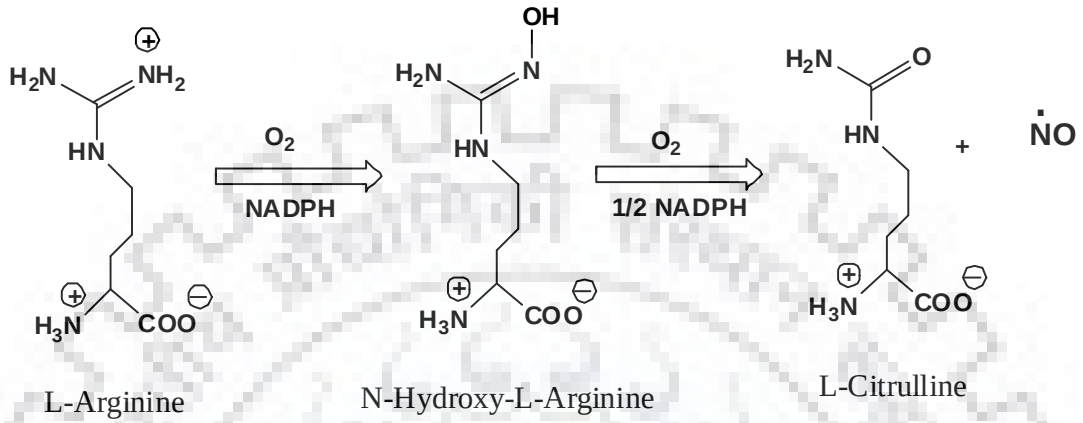

Scheme 1.8 Biosynthesis of nitric oxide (NO) by NOS enzyme.

Oxidation of the substrate carried out by a P450 type heme iron centre requires nicotinamide dinucleotide phosphate (NADPH) and O_2 as co-substrates.[146] Hecker and co-workers[147] explained that L-citrulline can be recycled back to L-arginine to retain the NO production.

1.3.5.1. Organic NO donors

Various organic NO donors have been synthesized and utilized for nitric oxide (NO) donation. Organic nitrites, nitrates and nitrosothiols have been used as potential NO donors.[148] Glyceryl trinitrate (also known as nitroglycerin, GTN) and isosorbide mononitrate (ISMN) have been used as NO donors for the treatment of hypertension and angina pectoris.

Table 1.2 Clinically used NO donor drugs and their applications.[148]

	NO donor drug	Function	Trade name
1.	Glyceryl trinitrate (GTN)	Dilation of blood vessels to treat angina pectoris	Nitroglycerin
2.	Isosorbide mononitrate (ISMN)	Vasodilation	Ismo, Imdur
3.	Isosorbide dinitrate (ISDN)	Vasodilation	Isordil, Sorbitrate, BiDil
4.	Diazeniumdiolates (NONOates)	Treatment of cardiovascular diseases	-
5.	Sodium nitroprusside (SNP)	Lowering of blood pressure	Nitropress
6.	Roussin's black salt	Toxic to melanoma cancer cells	-
7.	Roussin's red salt	Antibacterial	-

Glyceryl trinitrate has three nitrate moieties but it was found that only one molar equivalent of NO is released through enzymatic activation. However, all the molecules are activated by enzymatic pathways and physiological changes.[149,150] However, these NO donors release two molar equivalents of NO at physiological pH and temperature during spontaneous decomposition in solution. Several NONOates have been used to treat cardiovascular diseases but still not used clinically.[151]

1.3.5.2. Metal nitrosyl complexes: Inorganic NO donors

Spontaneous release of nitric oxide from organic NO donors, make them less useful for biological applications. This prompted the scientists to work on metal nitrosyl complexes which could release NO on demand and as an alternative to organic NO donors. From the past few years, the interaction of transition metals with nitric oxide has been received a

significant awareness.[152–157] Therefore various photoactive metal nitrosyls (metal-NO complexes) were synthesized that release NO in the presence of UV as well as visible light of various wavelengths (Scheme 1.9) and are useful in photodynamic therapy(PDT).

Sodium nitroprusside ($Na_2[Fe(NO)(CN)_5]$, SNP) and Roussin's salts (Fig. 1.9) are well known NO donor drugs. However, these inorganic NO donors were found to be non-specific for PDT as these were sensitive to only UV light[158] Additionally, use of the SNP as NO donor was somewhat restricted due to the toxicity of photoproducts. SNP can cause cyanide poisoning and found to be unstable in biological media.

Hence, sensitivity towards visible light was an essential criterion for a metal nitrosyl complex to be useful in photodynamic therapy (PDT) because limit of light penetration in skin is 700-1100 nm (optical window). Several groups produced metal nitrosyl complexes which could donate NO on demand upon light illumination.[158-161]

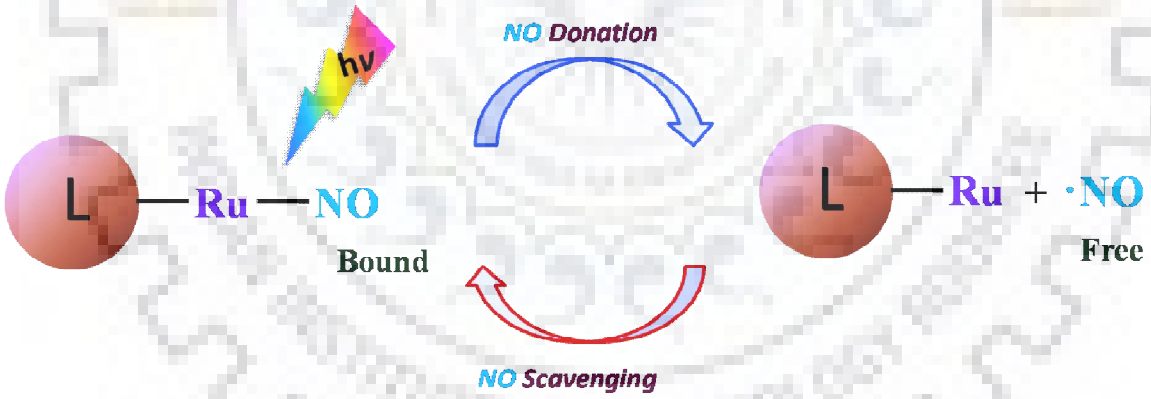

Scheme 1.9 Nitric oxide (NO) donation as well as scavenging in the presence of light.

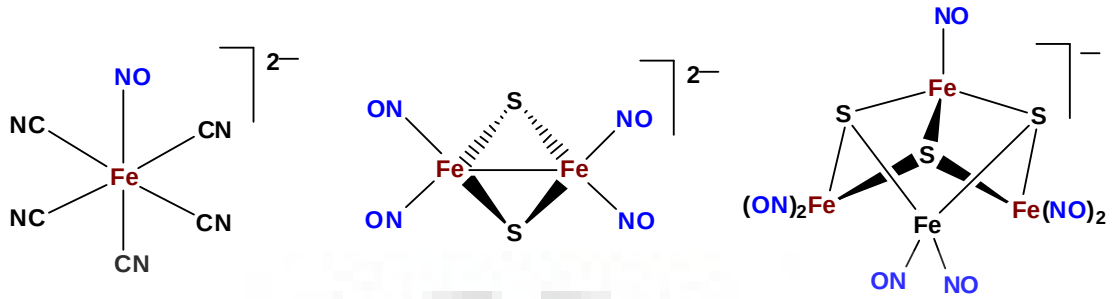

Sodium nitroprusside **Roussin's red salt** **Roussin's black salt**

Fig. 1.9 Clinically used inorganic NO donating drugs: SNP, Roussin's red salt and Roussin's black salt.

Mascharak and co-workers utilized an iron nitrosyl complex namely $[(PaPy_3)Fe(NO)](ClO_4)_2$ (where $PaPy_3$ was *N*,*N'*-bis(2-pyridylmethyl)amine-*N*-ethyl-2-pyridine-2-carboxamide)[160,162] to study the photolability and observed that it was less stable in the aqueous media although photolabile under low-intensity visible light. A number of nitrosyl complexes with other transition metals including manganese,[163–165] chromium[160,166] and molybdenum.[159] were also reported which demand applications in PDT.

1.3.5.3. Photoactive ruthenium nitrosyls

Because of high stability of the ruthenium nitrosyls in aqueous media, these were found to be appropriate for biological activities (under physiological condition, pH ~ 7.0). Ruthenium nitrosyls which can liberate NO under illumination of visible as well as near infrared light are useful for photodynamic therapy (PDT). Generally, one coordinated ligand (L) is replaced by a solvent molecule under illumination of light. Behavior of NO in the presence of light was extensively studied in the different metal nitrosyls by Mascharak and his coworkers.[167–175]

Franco and co-workers[176] have reported some photoactive ruthenium nitrosyls having the ammonia (NH_3) as additional ligands and investigated the dissociation of ammonia (NH_3) as well as photorelease of NO in acidic aqueous solutions upon light illumination.

In the recent years, the heme based nitrosyl complexes containing $\{Fe–NO\}^6$ species has gained a valuable attention. In the biosystem, NO was associated with several processes targeting heme-containing enzymes like guanylate cyclase, myoglobin and cytochrome *c* oxidase.[177–180] Ford and coworkers[181,182] have extensively studied the photochemistry of ruthenium nitrosyls having $\{Ru–NO\}^n$ (n = 6,7) species containing porphyrin ligands. Ruthenium nitrosyls such as [Ru(TPP)(NO)(Cl)] and [Ru(OEP)(NO)(Cl)] released the NO during the photolysis of the Ru–NO bond but these nitrosyls were not used for efficient NO delivery due to the fast rate of NO-recombination.

Several ruthenium nitrosyl complexes with polypyridine ligands were synthesized by Lahiri and coworkers.[183] They have investigated the transformation of nitroso group into the corresponding nitro derivative in the aqueous medium and the rate of conversion was examined spectrophotometrically at various temperatures. At this moment, they did not observed the photochemical behavior of NO. The electrochemistry and photophysical properties of some other ruthenium-terpyridine complexes such as $[Ru^{II}(trpy)(L)(X)](ClO_4)_n]$ [trpy = 2,2′:6′,2″-terpyridine; L = 2,2′-dipyridylamine; and X = Cl^-, n = 1; H_2O, n = 2; NO_2^-, n = 1 ; NO^+, n = 3] (Fig. 1.13) including a 2,2′-dipyridylamine ancillary ligand have been discussed later.[184]

Lahiri and coworkers[185] further synthesized the polypyridyl-based ruthenium nitrosyls $[Ru^{II}(trpy)(L)(NO^+)Cl]BF_4$ and $[Ru^{II}(trpy)(L)(NO^+)](BF_4)_2$, (trpy = 2,2′:6′,2″-terpyridine, L^-

= deprotonated form of unsymmetrical quinaldic acid) (Fig. 1.10). The crystal structures of the both nitrosyls were authenticated by X-ray crystallography.

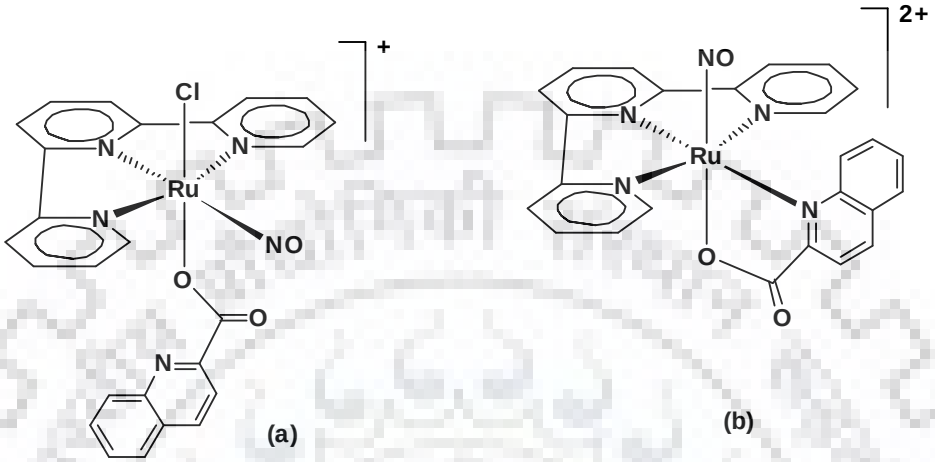

Fig. 1.10 Polypyridyl-based ruthenium nitrosyls: (a) $[Ru^{II}(trpy)(L)(NO^{+})Cl]BF_4$ and (b) $[Ru^{II}(trpy)(L)(NO^{+})](BF_4)_2$ (where L = deprotonated form of unsymmetrical quinaldic acid).

In the complex $[Ru^{II}(trpy)(L)(NO^{+})Cl]BF_4$, the ligand ($L^{-}$) is attached to the ruthenium ion in via carboxylate oxygen ($-COO^{-}$) but in the complex $[Ru^{II}(trpy)(L)(NO^{+})](BF_4)_2$, the ligand ($L^{-}$) is bound through carboxylate oxygen ($-COO^{-}$) as well as N donor atoms. The nitrosyl complexes liberated NO upon illumination of light and formed the solvent bound ruthenium(II)–photopruducts. The photoreleased NO was also trapped by reduced myoglobin (Mb) in the aqueous solution and Mb–NO adduct was characterized by absorption band at λ_{max} = 420 nm. Da Silva and his group[186,187] investigated the sensitivity of pyrazine bridged binuclear ruthenium nitrosyls such as $[Ru(NH_3)_4(L)(pz)Ru(NO)(bpy)_2]^{5+}$ (where L = NH_3 or pyridine, pz = pyrazine and bpy = bipyridine) upon illumination of visible light.

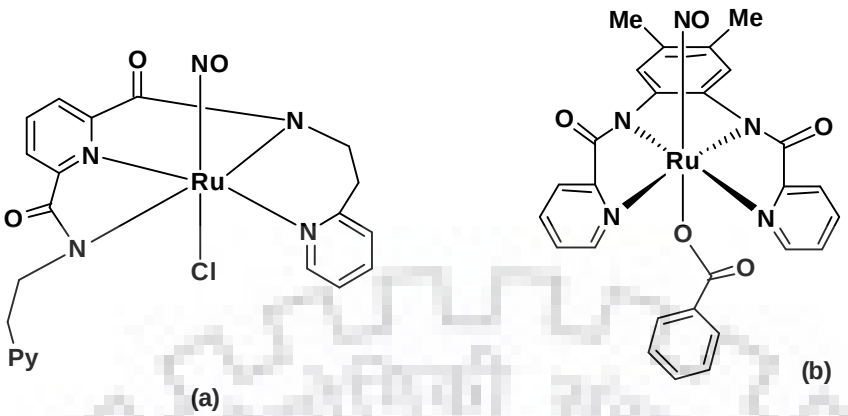

Fig. 1.11 Structures of nitrosyl complexes with carboxamido groups: (a) [(Py_3P)Ru(NO)(Cl)] and (b) [(Me_2bpb)Ru(NO)(OBz)].

Mascharak and co-workers have synthesized carboxamido group based ruthenium nitrosyl complexes[188,189] namely [($PaPy_3$)Ru(NO)]$^{2+}$ and [(Py_3P)Ru(NO)(Cl)] (Fig. 1.11) (where $PaPy_3H$ = *N*,*N*-bis(2-pyridylmethyl)amine-*N*-ethyl-2-pyridine-2-carboxamide and Py_3PH_2 = *N*,*N*-bis(2-(2-pyridyl)ethyl)pyridine-2,6-dicarboxamide, where H = dissociable protons) and examined the photolability of these complexes under UV light.

Ruthenium nitrosyls [(Me_2bpb)Ru(NO)(FlEt)] and [(($OMe)_2$IQ1)Ru(NO)(FlEt)] (where Me_2bpb = 1,2-bis(pyridine-2-carboxamido)5-dimethylbenzene, FlEt = fluorescein ethyl ester and $(OMe)_2$-IQ1 = 1,2-bis(isoquinoline-1-carboxamido)-4,5-dimethoxybenzene) (Fig. 1.12) derived from two new fluorescein-tethered tetradentate ligands with carboxamido-N donors have been synthesized and characterized by Mascharak and his group.[190]

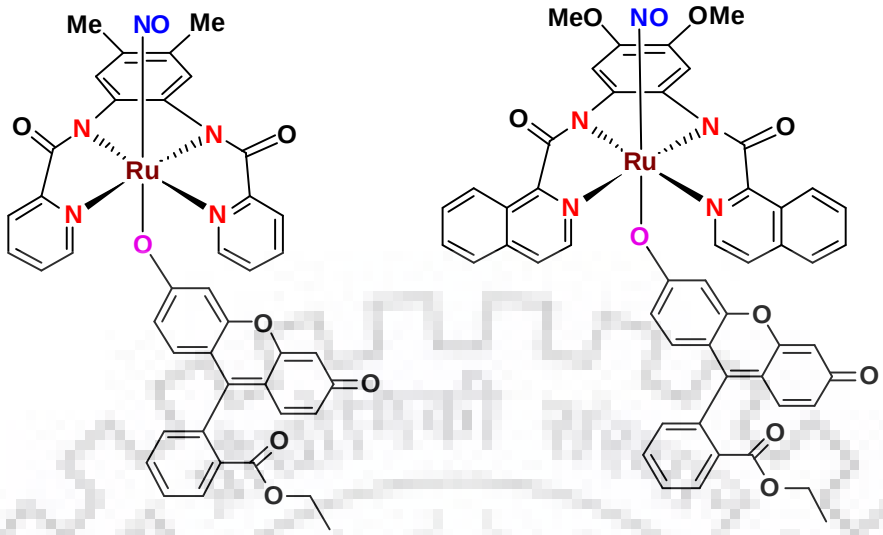

Fig. 1.12 Ruthenium nitrosyls derived from fluorescein-tethered tetradentate ligands.

In very recent years, ruthenium nitrosyls with modified ligand systems were reported by Malfant and her group.[191-194] A novel cyclometalated ruthenium nitrosyl namely [Ru(η^2-phpy)(trpy)(NO)][PF_6]$_2$ (where phpy = 2-phenyl pyridine and trpy = 2,2′:6′,2″-terpyridine) containing {RuNO}^{6} moiety have been synthesized by Crutchley and coworkers.[195] Ghosh et al[196] have been reported a novel cyclometalated nitrosyl complex [Ru(L^{PB1})(PPh_3)$_2$(NO)Cl](ClO_4) (where L^{PB1}H = 5-methyl-7-nitro-2-(4-nitrophenyl)benzoxazole) derived from the nitrosylation of [Ru(L^{SB1})(PPh_3)$_2$Cl] [where $L^{SB1}H_2$ = 4-methyl-2-(4-nitrobenzylideneamino)phenol] and the ring nitration as well as oxidative cyclization, affording benzoxazole derivative formation was observed (scheme 1.10). The molecular structure of the resultant nitrosyl complex was authenticated by X-ray crystallography. The coordinated NO was found to be photolabile under visible light and ensured *via* trapping by reduced myoblobin.

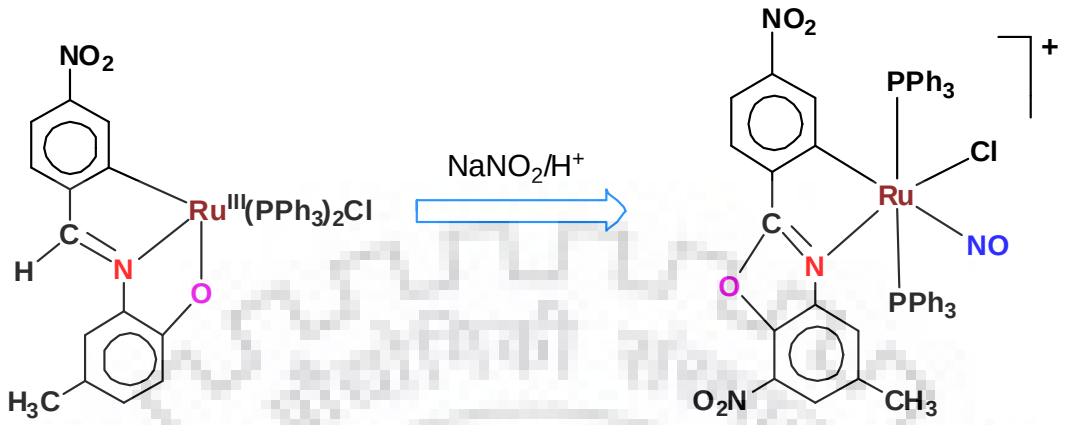

Scheme 1.10 Generation of cyclometalated ruthenium nitrosyl complex.

1.3.6. CO releasing molecule (CORM)

After the discovery of NO as an important signaling molecule in mammals during past few decades, role of carbon monoxide (CO) as signaling molecule also came into picture in past few years and it was found that both CO and NO have similarities in their functions. It is also considered as gasotransmitter such as nitric oxide (NO) and hydrogen sulfide (H_2S) in higher organisms.[197–200] During the catabolism of heme by the enzyme heme oxygenase, CO is produced endogenously and it exerts multiple effects in mammals including anti-inflammatory, anti-apoptotic, anti-proliferative, protection of tissues against hypoxia or ischemia-reperfusion injury and causes vasodilatation. Rational designing of transition metal carbonyls which release CO to a specific site in a controlled manner upon illumination of light has become a fast grown area in the field of research.[201]

In 2002, CO releasing molecule was reported by Motterlini and co-workers.[202] Recently, Mascharak and coworkers reported the mono and dicarbonyl complexes of ruthenium with N, N, S donor tridentate ligand and investigated the photolability of carbonyl complexes

under UV as well as visible light.[203] Schatzschneider and co-workers synthesized Ru(II) polypyridyl carbonyl complexes and examined the CO releasing properties of these photocorms.[204] Kubeil and co-workers synthesized Ru(II) bipyridine carbonyl complexes and the effects of electron withdrawing groups on bipyridine were examined during photorelease of CO.[205]

1.4. Analysis of current work done

In the present report, we have synthesized different ligands having various groups such as diazo (–N=N–), azomethine (–CH=N–) and carboxamide (–CONH–)groups. These ligands were treated with different precursor ruthenium complexes to afford corresponding ruthenium complexes. These ruthenium complexes were characterized by various spectroscopic techniques like IR, UV-Vis spectroscopy, ESI-MS, EPR, ^{1}H as well as ^{31}P NMR spectral studies. Some ruthenium complexes were also treated with *in situ* generated nitric oxide (NO) from acidified sodium nitrite ($NaNO_2$) solution (pH ~ 2-3) to produce ruthenium nitrosyl complexes. Nitrosyl complexes were characterized by IR, UV-Vis spectroscopy, ^{1}H as well as ^{31}P NMR spectral studies. Molecular structures of complexes were authenticated using X-ray crystallography. The redox properties of the ligand as well as metal center in the ruthenium complexes with non innocent ligands were investigated using cyclic voltammetry. Theoretical calculations were also performed on the structure of the complexes to better understand the electronic properties.

Coordinated NO was found to be photolabile under illumination of UV as well as visible light in the nitrosyl complexes and trapping of photoreleased NO was examined by reduced myoglobin (Mb) in the phosphate buffer (pH ~ 6.8) solution using electronic absorption

spectral studies. Anticancer activity studies were investigated using photoreleased nitric oxide from ruthenium nitrosyl complexes upon illumination of visible light. Ruthenium hydrido carbonyl complexes were isolated and utilized further to synthesize cyclometallated ruthenium carbonyl complex which was utilized as a catalyst for transfer hydrogenation of ketones. Photolability of carbonyl complex was also examined under visible light. Half sandwich ruthenium complexes were also utilized for anticancer activity studies.

1.4.1. Ligands and their description

Different types of ligands having azo dyes, schiff bases and carboxamide groups have been utilized which are summarized in Scheme 1.11.

1.4.2. Description of starting material

The ligands described above were reacted with ruthenium(II) precursor complexes which are $[Ru(PPh_3)_3Cl_2]$ and $[(\eta^6\text{-cymene})RuCl_2]_2$. The resultant ruthenium complexes were characterized by IR, NMR, ESI-MS, EPR and UV-visible spectral studies. Molecular structures of complexes were authenticated using X-ray crystallographic study.

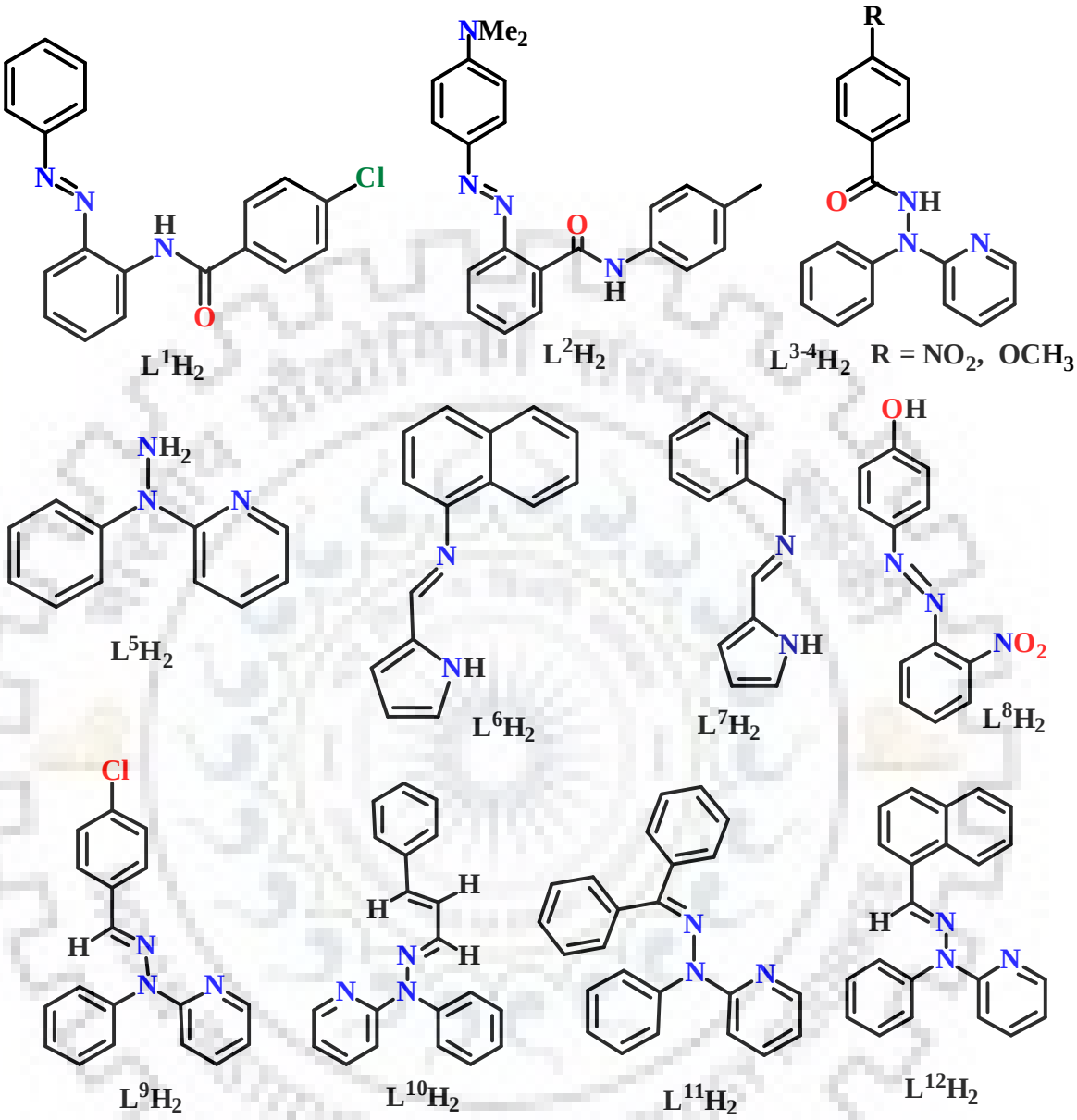

Scheme 1.11 Ligands used in the present thesis.

1.4.3. Description of activity studies

1.4.3.1. Liberation of NO under visible as well as UV light

Photolability of the coordinated NO was examined by exposing dichloromethane solutions of ruthenium nitrosyl complexes upon illumination of visible as well as UV light. In the dark, all the nitrosyl complexes were found to be stable as no changes were observed in electronic absorption spectra. However, NO was released upon illumination of UV as well as visible light. Changes in spectra were observed and the presence of isosbestic points in electronic absorption spectra of nitrosyl complexes after light illumination indicated the formation of new photo products.

1.4.3.2. Transfer of photoreleased NO to myoglobin

In order to confirm the photorelease of NO, trapping experiment of the photoreleased NO by reduced myglobin in the phoshphate buffer (pH = 6.8) was performed. In the electronic absorption spectrum of oxidized myoglobin (Mb), an intense band near 409 nm (an intense Soret band) was observed. After the addition of sodium dithionite to the same cuvette, absorption peak of reduced myoglobin was obtained near 433 nm. When acetonitrile or dimethyl sulfoxide solution of nitrosyl complexes was added to buffer solution of reduced myoglobin, no reaction was observed under dark conditions. But, under the illumination of UV light (λ_{max}= 365 nm) or visible light for a limited time, the absorption spectrum near 420 nm showed the formation of Mb–NO adducts.

Preparation of phosphate buffer solution and myoglobin stock solution: A 50 mM phosphate buffer of pH 6.8 was prepared by adding 0.3283 g of anhydrous Na_2HPO_4 and 0.4192 g of $NaH_2PO_4.2H_2O$ to 50 mL of MilliQ water and making the volume to 100 mL in a

volumetric flask. 5 mg equine skeletal muscle myoglobin (Mb) was dissolved in 5 mL of the above prepared buffer solution.

1.4.3.3. Liberation of CO under visible light

Photolability of the coordinated CO was examined by exposing dichloromethane solution of ruthenium carbonyl complex upon illumination of visible light. In the dark, no changes were observed in electronic absorption spectrum of carbonyl complex and it was found to be stable. However, CO was released upon illumination of visible light and changes in spectra were observed. The presence of isosbestic points in electronic absorption spectrum after light illumination indicated the formation of new photo products.

1.4.3.4. Antiproliferative activity studies using ruthenium nitrosyl complexes

(i) MTT assay

In-order to see the invitro-cytotoxic nature of nitrosyl compounds, the MTT [3-(4,5-dimethylthiazol-2-yl)-2,5-diphenyltetrazolium bromide] colorimetric assay was performed in human cervical cancer cell line (HeLa cells). HeLa cells were grown in 30-50% confluency before treating with the compounds. After mixing the compounds cells were irradiated with visible light to release NO from the compounds. The MTT assay was performed after 24 hours of the treatment.

(ii) Acridine orange and ethidium bromide (AO-EB) staining

Nitric oxide (NO) is a potential inducer of apoptosis. To find out whether treatment with nitrosyl compounds induces cancer cells to enter into apoptotic cycle, the acridine orange and ethidium bromide (AO/EB) dual staining was performed. Acridine orange and ethidium bromide both are fluorescent nucleic acid dye, the former one is permeable to both live and

dead cells whereas the later one (ethidium bromide) enters only into dead cells those lost membrane integrity. The treated cells upon illumination with visible light showed orange yellow fluorescence indicating apoptosis due to release of NO from the nitrosyl compounds.

(iii) Hoechst-Rhodamine staining

Next, to check the nuclear and cytoplasmic integrity, the treated cells were stained with Hoechst 33342 (a fluorescent DNA intercalating dye makes nucleus blue) and Rhodamin B (selectively stained cytoplasm in red). The data showed significant DNA fragmentation as multi-lobed nucleus (red) surrounded by a faint boundary were seen in most of the cells after 6 hours post-treatment with the nitrosyl compounds. After 12 hours post treatment, the DNA fragmentation was more severe; the lobes were separated from each other and mixed with cytoplasmic compartment of the cells.

(iv) DNA fragmentation assay

The DNA fragmentation of cancer cells induced by nitrosyl compounds was also checked by performing agarose gel electrophoresis. The genomic DNA was purified from treated and untreated cells and then resolved in 0.6% agarose gel. Appearance of smear in agarose gel suggested severe degradation of genomic DNA obtained from treated cells, whereas untreated cells showed intact DNA.

(v) Annexin V- Propidium iodide staining

Next, we performed annexin V assay to measure the percentage of cells that belong to late and early apoptosis stages. Hence, binding of annexin V to the cellular surface is an indicative feature for apoptosis. Another dye propidium iodide (membrane impermeable DNA stain) was used in combination of annexin V to discriminate apoptotic versus necrotic

cells (dead cells). Thus, Annexin V negative and PI negative (Annexin V^- and PI $^-$) signal indicates viable, Annexin V positive and PI negative (Annexin V^+ and PI $^-$) indicates early apoptotic and Annexin V positive and PI positive (Annexin V^+ and PI $^+$) indicates late apoptotic cells.

(vi) Gene Expression studies

Apoptosis occur via two pathways intrinsic mitochondrial or extrinsic via death receptor pathway. Both pathways are well regulated by cascades of signalling genes. In our study, we have analysed the change of expression of two apoptotic markers Bcl2 and Bax after treating cells with nitrosyl compound and expression patterns of the above two genes (Bcl2 and Bax) indicated the NO mediated apoptosis probably occurring through mitochondrial pathway.

1.4.3.5. Catalytic transfer hydrogenation

From the literature study, it was found that ruthenium complexes act as catalysts in transfer hydrogenation of carbonyl compunds. Organometallic ruthenium carbonyl complex was utilized in transfer hydrogenation of ketones. In a microwave reaction vial with a closed cap, a mixture containing ketone (1 mmol), the catalyst (known mol percent) and base (known mol percent) in 5 ml of isopropanol was heated on the oil bath with continous stirring at 85°C for suitable period of time as mentioned. After the usual workup (reported in literature), the reaction product dissolved in hexane was analyzed by GC-MS.

1.4.3.6. Anticancer activity studies using half-sandwich ruthenium complexes

As ruthenium–arene complexes with modified ligands find their significance as anticancer agents. We also studied the cytotoxicity of new half sandwich p-cymene Ru(II) complexes containing N^N- chelating imino-pyridyl ligands on MCF-7, MDA-MB-435s and HEK293

cell lines using MTT assay. We further performed the experiments including apoptosis assay, elevation in reactive oxygen species (ROS) level and human serum albumin (HAS) binding. Among all these complexes, one complex was found to be more potent against MCF-7 and MDA-MB-435s cancer cells as compared to rest of three complexes. However, all the complexes exhibited less cytotoxicity or almost inactivity towards HEK293 normal cells.

1.5. Survey of contents in the thesis

In the present thesis, different ruthenium complexes using different ligands have been synthesized and characterized. The resultant ruthenium complexes were utilized for various activities.

In chapter two, organometallic ruthenium(III) complexes $[Ru(L^1)(PPh_3)_2Cl_2]$ (**1**) (where L^1H_2 =(E)-4-chloro-N-(2-(phenyldiazenyl)phenyl)benzamide and H = dissociable proton) and $[Ru(L^2)(PPh_3)_2Cl]$(**2**)(where L^2H_2 = (E)-2-((4-(dimethylamino)phenyl)diazenyl)-N-(p-tolyl)benzamide and H = dissociable protons) were synthesized through C-H bond activation. Complexes **1** and **2** were treated with acidified nitrite solution to afford organometallic ruthenium nitrosyl complexes $[Ru(L^1)(PPh_3)_2(NO)Cl](ClO_4)$(**3**) and $[Ru(L^2_{NO2})(PPh_3)_2(NO)Cl](PF_6)$(**4**). All the complexes were characterized by UV-vis, IR, ESI-MS, NMR spectroscopic studies. Molecular structures of complexes **3** and **4** were authenticated using X-ray crystallographic studies. Coordinated NO in ruthenium nitrosyls **3** and **4** was found to be photolabile under visible light and photo released NO was transferred to reduced myoglobin. Cytotoxic effects of complexes as well as photo-released NO were investigated. Gene expression studies were performed to understand the different stages of apoptotic cell death.

In chapter three, a novel ruthenium(II) coordinated stable aminyl radical complex $[Ru(L^{5\cdot})(PPh_3)_2Cl_2]$ (**5**), was synthesized using ligands L^{3-5}. Cleavage of most stable amide bond and simultaneous production of nitrogen centred radical took place during the reaction course. Complex **5** was characterized by IR, UV-vis and EPR spectroscopic studies. Molecular structure of **5** was authenticated using single crystal X-ray crystallography. Along with spectroscopic characterization, theoretical calculations completely supported the nitrogen centred radical. The interaction of NO with the complex **5** afforded nitrosyl complex $[Ru(L^{5'})(PPh_3)_2(NO)Cl](ClO_4)$ (**6**). Molecular structure of the resultant nitrosyl complex **6** was authenticated by single crystal X–ray diffraction study. The photolability of coordinated NO was examined by using electronic absorption spectral studies under illumination of UV light.

In chapter four, organometallic ruthenium(II) complex $[Ru(L^6C\hat{}N\hat{}N)(PPh_3)_2(CO)]$ (**7**) [where L^6H_2 is (E)-N-((1H-pyrrol-2-yl)methylene)naphthalen-1-amine] [H represents dissociable proton] was synthesized via C-H bond activation using different synthetic strategies. Ruthenium hydrido carbonyl complexes $[Ru(L^6N\hat{}N)(PPh_3)_2(CO)H]$ (**8**) [where L^6H_2 is (E)-N-((1H-pyrrol-2-yl)methylene)naphthalen-1-amine] and $[Ru(L^7N\hat{}N)(PPh_3)_2(CO)H]$ (**9**) [where L^7H_2 is (E)-N-((1H-pyrrol-2-yl)methylene)-1-phenylmethanamine] were isolated. All the complexes were characterized by UV-Vis, IR and NMR spectral studies. Molecular structures of complexes **7**, **8** and **9** were authenticated using X-ray crystallography. Geometry optimization of the complexes **7**–**9** have been performed using Density Functional Theory (DFT) studies. Time-dependent DFT calculations were performed to better understand the electronic properties of complexes **7**–**9**. Complex **7** was utilized as catalyst in transfer hydrogenation of ketones. On the basis of literature study, the

plausible mechanisms were proposed for hydride formation and catalytic transfer hydrogenation. Coordinated CO in organometallic ruthenium carbonyl complex **7** was found to be photolabile upon visible light illumination.

In chapter five, reaction of (E)-4-((2-nitrophenyl)diazenyl)phenol (L^8H, H = dissociable proton) with $Ru(PPh_3)_3Cl_2$ afforded novel organometallic anion radical complex $[Ru(L_A^{8-\cdot})(Cl)(PPh_3)_2]$ (**10**). During the synthesis of complex **10**, nitro group in ligand converted to nitroso group through oxygen atom transfer to labile triphenylphosphine. One electron reduced nitroso group was coordinated to ruthenium in η^1(N) mode. Complex **10** was treated with acidified nitrite to afford nitrosyl complex $[Ru(L_B^{8-\cdot})(PPh_3)_2(NO)](ClO_4)$(**11**) and it is a rare example of an organometallic ruthenium complex having azo anion radical as well as two different noninnocent ligands coordinated to one metal. Both the complexes were characterized by UV-vis, IR, NMR spectroscopic studies. Redox properties of complex **10** were investigated using cyclic voltammetry. Molecular structures of complexes **10** and **11** were authenticated using X-ray crystallographic studies. DFT calculations were performed to better understand the electronic properties of complex **10**.

In chapter six, half sandwich ruthenium complexes $[(p\text{-cym})Ru^{II}(L^{9\text{-}12})Cl]PF_6$(**12-15**) containing N^N chelating schiff base ligand were successfully designed and synthesized. All the synthesized complexes were characterized by UV-vis, IR, ESI-MS, NMR spectroscopic studies. Molecular structures of **12** and **15** were authenticated using X-ray crystallography. Complexes **12-15** were utilized to investigate the anti-cancer activity studies on MCF-7, MDA-MB-435s and HEK-293 cell lines. Among all the complexes, complex **15** was found to be more potent against MCF-7 and MDA-MB-435s cancer cells as compared to complexes

12-14. However, all the complexes exhibited less cytotoxicity or almost inactivity towards HEK-293 normal cells.

1.6. Physical measurements

Synthesized compounds were characterized by various physical methods which were described in the subsequent chapters.

(i) Infrared spectroscopy

IR spectra were obtained as KBr pellets by using 16 scans with the help of Thermo Nicolet Nexus FT-IR spectrometer and reported in cm^{-1}.

(ii) Mass spectrometry

ESI-MS data were recorded in the positive mode using a Bruker MicroTOF–QII mass spectrometer.

(iii) NMR spectroscopy

^{1}H as well as ^{31}P NMR spectra were obtained in the deuterated solvents using Jeol, 400 MHz and Bruker AVANCE, 500 MHz spectrometer.

(iv) UV-Visible spectrophotometer

Electronic absorption spectra were carried out in different organic solvents with an Evolution 600, Thermo Scientific UV-Visible spectrophotometer. A matched pair of quartz cell of path length 1 cm was used.

(v) Cyclic voltammetry

Cyclic voltammetry measurements were carried out using a CH-600C electroanalyzer in different organic solvents at room temperature and solutions were thoroughly degassed with

nitrogen prior to beginning the experiments, and during the measurements nitrogen atmosphere was maintained.

A conventional three-electrode arrangement consisting of platinum wire as auxiliary electrode, glassy carbon as working electrode and Ag(s)/AgCl electrode as reference electrode, was used. These measurements were performed in the presence of 0.1 M tetrabutylammonium perchlorate (TBAP) as the supporting electrolyte, using complexes concentration of 10^{-3} M. $E_{1/2}$ value for ferrocene/ferrocenium couple *vs* Ag/AgCl was found under the same experimental conditions.

(vi) X-ray structure determinations

The X-ray data collection and processing for representative complexes were performed on Bruker Kappa Apex-II CCD diffractometer using graphite monochromated Mo-Kα radiation (λ = 0.71070 Å). Crystal structures were solved by using direct methods. Structure solution, refinement and data output were performed with the help of SHELXTL program. All non-hydrogen atoms were refined anisotropically. Hydrogen atoms were situated in geometrically calculated positions and then refined using a riding model. Images were created by using the DIAMOND program.

R1, *wR2* and goodness-of-fit (GOF) are given by following equations respectively,

$R1 = \Sigma \| F_o | - | F_c \| / \Sigma F_o |$ eq. 1

$wR2 = [\Sigma[w(F_o^2 - F_c^2)^2] / \Sigma[w(F_o^2)^2]]^{1/2}$ eq. 2

$\mathrm{GOF} = [\Sigma[w(F_o^2 - F_c^2)^2] / M - N)]^{1/2}$ eq. 3

Where, M = number of reflections, N = number of parameters refined

Specific details for every compound will be specified in the concerned chapter.

(vii) Chemicals and solvents

All the solvents and chemicals used were of analytical grade and used as obtained. The purification steps where required, were performed by using standard methods and distilled water was used in all the experiments.

Remarkable effect of position of carboxamido nitrogen in bidentate ligands to synthesize organometallic ruthenium(III) complexes via C-H activation: Organometallic ruthenium nitrosyl complexes and anticancer activity studies

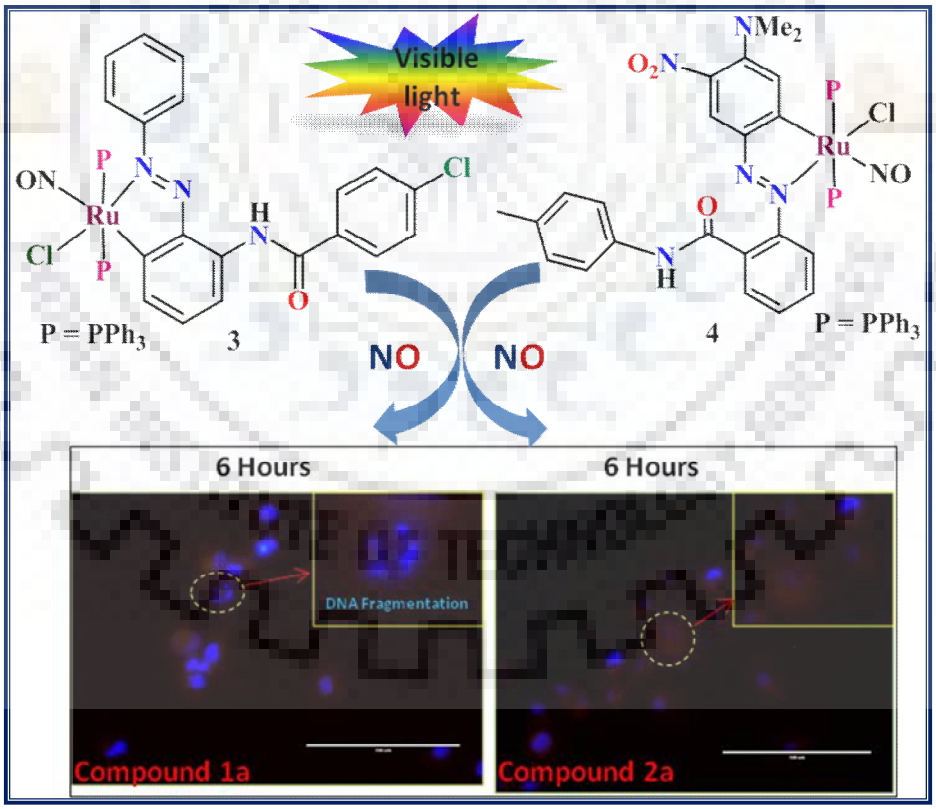

Abstract

Organometallic ruthenium(III) complexes $[Ru(L^1)(PPh_3)_2Cl_2]$ (**1**) (where L^1H_2 =(E)-4-chloro-N-(2-(phenyldiazenyl)phenyl)benzamide and H = dissociable proton) and $[Ru(L^2)(PPh_3)_2Cl]$(**2**)(where L^2H_2 = (E)-2-((4-(dimethylamino)phenyl)diazenyl)-N-(p-tolyl)benzamide and H = dissociable protons) were synthesized through C-H bond activation. Complexes **1** and **2** were treated with acidified nitrite solution to afford organometallic ruthenium nitrosyl complexes $[Ru(L^1)(PPh_3)_2(NO)Cl](ClO_4)$(**3**) and $[Ru(L^2_{NO2})(PPh_3)_2(NO)Cl](PF_6)$(**4**). All the complexes were characterized by UV-vis, IR, ESI-MS, NMR spectroscopic studies. Molecular structures of complexes **3** and **4** were authenticated using X-ray crystallographic studies. Coordinated NO in ruthenium nitrosyls **3** and **4** was found to be photolabile under visible light and photo released NO was transferred to reduced myoglobin. Cytotoxic effects of complexes as well as photo-released NO were investigated. Gene expression studies were performed to understand the different stages of apoptotic cell death.

2.1. Introduction

Nitric oxide (NO) is a diatomic gaseous molecule which is lipophilic and highly diffusible in cellular environment.[206] NO is produced by nitric oxide synthase enzyme (NOS) and this radical molecule could act as a physiological messenger and could regulate vasodilation, immune response, respiration cell migration etc. and hence it exhibits pleotropic biological activity.[207] In the recent years, there has been considerable current interest in the design and synthesis of nitric oxide releasing molecule (NORM).[208-212,167] In this regard those NO-releasing molecules which could deliver NO upon illumination of light could be utilized for site-specific and on demand delivery of nitric oxide. Such molecules which could deliver NO upon illumination of visible and/or infrared lights are of extreme interest in photo dynamic therapy (PDT).[171,213] Hence design and synthesis of NORMs is an important area of chemical research. We have been working with the design and syntheses of organometallic ruthenium nitrosyl (NO complexes having $\{RuNO\}^6$ moiety.[214-217,58,196] As precursor complexes, we always started with Ru(III) organometallic complexes and reacted with acidified nitrite solution to end up with stable diamagnetic organometallic ruthenium nitrosyl complexes. Our recent results for clearly indicated rational design with different combinations of bidentate ligands could give rise to orthometallation via C-H bond activation (shown in Scheme 2.1).

The motivation for the recent study originated from our previous results and we designed ligands (L^1H_2) and (L^2H_2) (shown in Scheme 2.2) to obtain our ruthenium(III) organometallic precursor complexes. The strategic design of such bidentate ligands is important in two ways. First, coordination of amide nitrogen (carboxamido nitrogen) may lead to the activation of C-H bond and second, the presence of azo (-N=N-) group could

provide the photolability of coordinated NO under visible light in the resultant nitrosyl complexes.

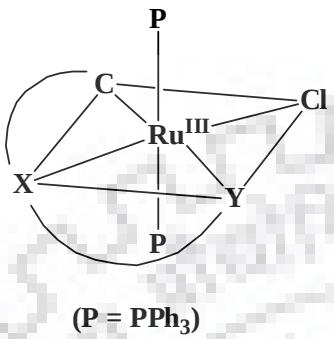

X	Y	Refs.
N_{azo}	O_{phenol}	10(a)
N_{imine}	O_{phenol}	10(b,c,d)
N_{amide}	$N_{pyridine}$	10(e)
N_{azo}	$O_{carboxylato}$	10(f)

Scheme 2.1 Bidentate ligands (X - Y) having different donor atoms (X and Y).

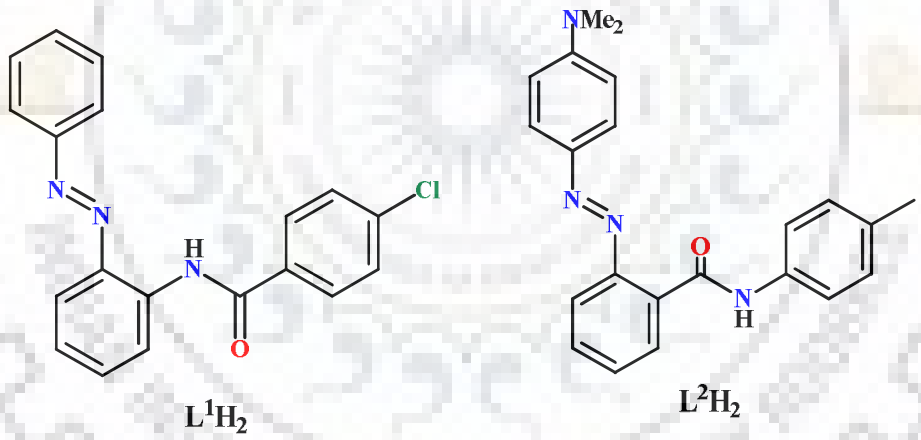

Scheme 2.2 Ligands L^1H_2 and L^2H_2.

In the present study, we describe the design, syntheses and characterization of the novel cyclometalated ruthenium(III) complexes $[Ru(L^1H)(PPh_3)_2Cl_2]$(**1**)(where L^1H_2 =(E)-4-chloro-N-(2-(phenyldiazenyl)phenyl)benzamide and H = dissociable protons) and $[Ru(L^2)(PPh_3)_2Cl]$(**2**)(where L^2H_2 = (E)-2-((4-(dimethylamino)phenyl)diazenyl)-N-(p-

tolyl)benzamide and H = dissociable protons) (shown in Scheme 2.3) and ruthenium nitrosyl complexes $[Ru(L^1H)(PPh_3)_2(NO)Cl](ClO_4)$ (**3**) and $[Ru(L^2_{NO2})(PPh_3)_2(NO)Cl](PF_6)$(**4**) (shown in Scheme 2.3). Molecular structures of **3** and **4** were authenticated using X-ray crystallography. We scrutinized the trans directing effect of carbanion for the coordination and photolability of coordinated NO under visible light.

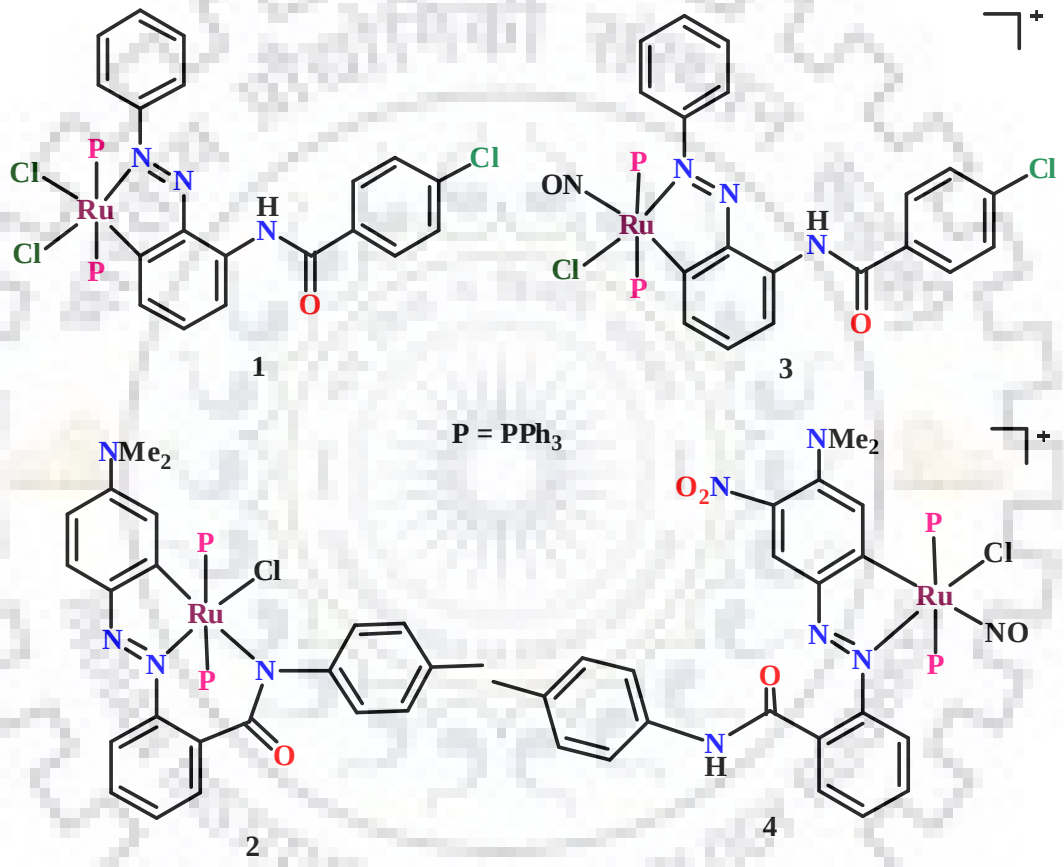

Scheme 2.3 Cyclometalated ruthenium complexes **1**, **2** and nitrosyl complexes **3**, **4**.

According to Ignarro and Buga[218,219] NO was found to have both tumoricidal and tumorigenic effects. Carpenter et al. in recent review[220] mentioned that low and high concentrations of NO may lead to tumor progression and regression respectively. However

we have investigated light induced delivery of NO into HeLa cancer cell-line to study anti-proliferation activity. Cytotoxicity of photo-liberated NO was examined by MTT assay. Further acridine orange and ethidium bromide staining was performed to depict apoptosis in Hela cells. Hoechest as well as rhodamine B staining were employed to investigate the nuclear and cytoplasmic changes upon treatment with photo-released nitric oxide derived from organometallic ruthenium nitrosyls. Anexin V assay was performed to investigate the stages of apoptosis and finally we tried to find out the molecular basis of apoptosis induction by gene expression studies.

2.2. Results and discussion

2.2.1. Syntheses and characterization of ruthenium complexes

Designed ligands L^1H_2 and L^2H_2 were obtained in high yield by condensation reaction of 4-chloro benzoic acid with 2-(phenyldiazenyl)aniline and (2-(N,N-dimethyl-4-aminophenyl) azobenzenecarboxylic acid) (methyl red) with 4-methyl aniline respectively in dimethylformamide in the presence of 1-hydroxybenzotriazole (HOBT) and dicyclohexylcarbodiimide (DCC). $Ru(PPh_3)_3Cl_2$ was added to a hot methanolic solution (20 mL) of the ligands L^1H_2 and L^2H_2 to afford the organometallic ruthenium(III) complexes $[Ru(L^1H)(PPh_3)_2Cl_2]$ (**1**) and $[Ru(L^2)(PPh_3)_2Cl]$ **(2)** respectively (shown in Scheme 2.3). The complexes **1** and **2** were brown and violet in color and highly soluble in dichloromethane, dimethylformamide and dimethylsulphoxide but less soluble in water. The complexes $[Ru(L^1H)(PPh_3)_2(NO)Cl](ClO_4)$(**3**) and $[Ru(L^2{}_{NO2})(PPh_3)_2(NO)Cl](PF_6)$**(4)** were obtained from complexes **1** and **2** respectively (shown in Scheme 2.3). The dichloromethane solutions of complexes **1** and **2** were treated with acidified nitrite ($NaNO_2$) solution with continuous stirring for 2 h and formation of a reddish-orange and reddish violet color, respectively, was

observed. Then, methanolic solutions of $NaClO_4$ and NH_4PF_6 were added to dichloromethane solutions of **3** and **4**, respectively, as the counter anion. Nitrosyl complexes were found to be highly soluble in organic solvents like dichloromethane, dimethylsulphoxide and dimethylformamide.

In the IR spectra of complexes **3** and **4**, the N-O stretching frequency (ν_{NO}) was observed around 1821 cm^{-1} and 1840 cm^{-1}(Table 2.1), which was expected for $\{Ru{-}NO\}^6$ species as reported in literature around 1820-1960 cm^{-1} for $\{Ru{-}NO\}^6$ species.[161,186,221-223] Peaks around 1095 cm^{-1} and 615 cm^{-1} clearly exhibited the presence of perchlorate as counter anion in the complex **3**.[214,58] Peaks around 843 cm^{-1} and 560 cm^{-1} clearly exhibited the presence of hexafluorophosphate as counter anion in the complex **4**.[224] In all the complexes **1-2** and **3-4**, the peaks in the range 747-750 cm^{-1}, 694-695 cm^{-1} and 514-518 cm^{-1} confirmed the presence of axial PPh_3 ligands[214-217,58,196] (Figure 2.1).

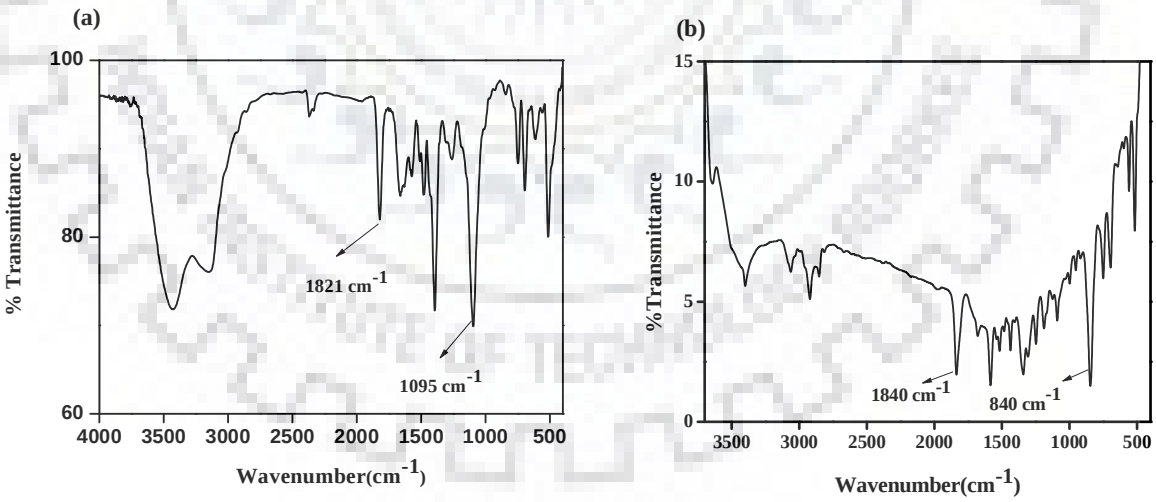

Fig. 2.1 IR spectra of ruthenium nitrosyl complexes (a) **3** and (b) **4**.

Table 2.1 Data for IR spectral studies.

Complex	IR data (cm^{-1}, KBr pellets)				
	ν_{CONH}	$\nu_{N=N}$	ν_{N-O}	ν_{ClO4}	ν_{PPh3}
1	1680	1588	-	-	747, 695, 518
2	1584	1536	-	-	748, 698, 518
3	1666	1576	1821	1095, 623	740, 695, 517
4	1584	1516	1840	-	748, 690, 518

The electronic absorption spectra of complexes **1** and **3** were displayed in Figure 2.2. In complex **1**, we observed charge transfer band with λ_{max} near 480 nm which was probably due to ligand–to–metal charge transfer (LMCT) transition.[51,56,58,225] In complex **3**, bands near 305 nm, 445 nm (Table 2.2) were recognized to be metal to ligand charge transfer (MLCT) transition dπ(Ru)→π*(NO) type and this transition has been responsible for the photolability of the coordinated NO.[161,186,168,188] The electronic absorption spectra of complexes **2** and **4** were displayed in Figure 2.2. In complex **2**, we observed charge transfer bands with λ_{max} near 453nm and 593 nm which were probably due to ligand–to–metal charge transfer (LMCT) transition].[58,51,56,225] In complex **4**, band near 501 nm (Table 2.2) was recognized to be metal to ligand charge transfer (MLCT) transition dπ(Ru)→π*(NO) type.

Table 2.2 Electronic spectral data for complexes **1-4**.

Complex	λ_{max}/nm (ε / $M^{-1}cm^{-1}$)
1	480 (6495), 656 (601)
2	232 (68776), 285 (56415), 453 (18126), 593 (29328)
3	232 (32555), 305 (24888), 441 (4888)
4	231 (99890), 311 (34732), 501 (30399)

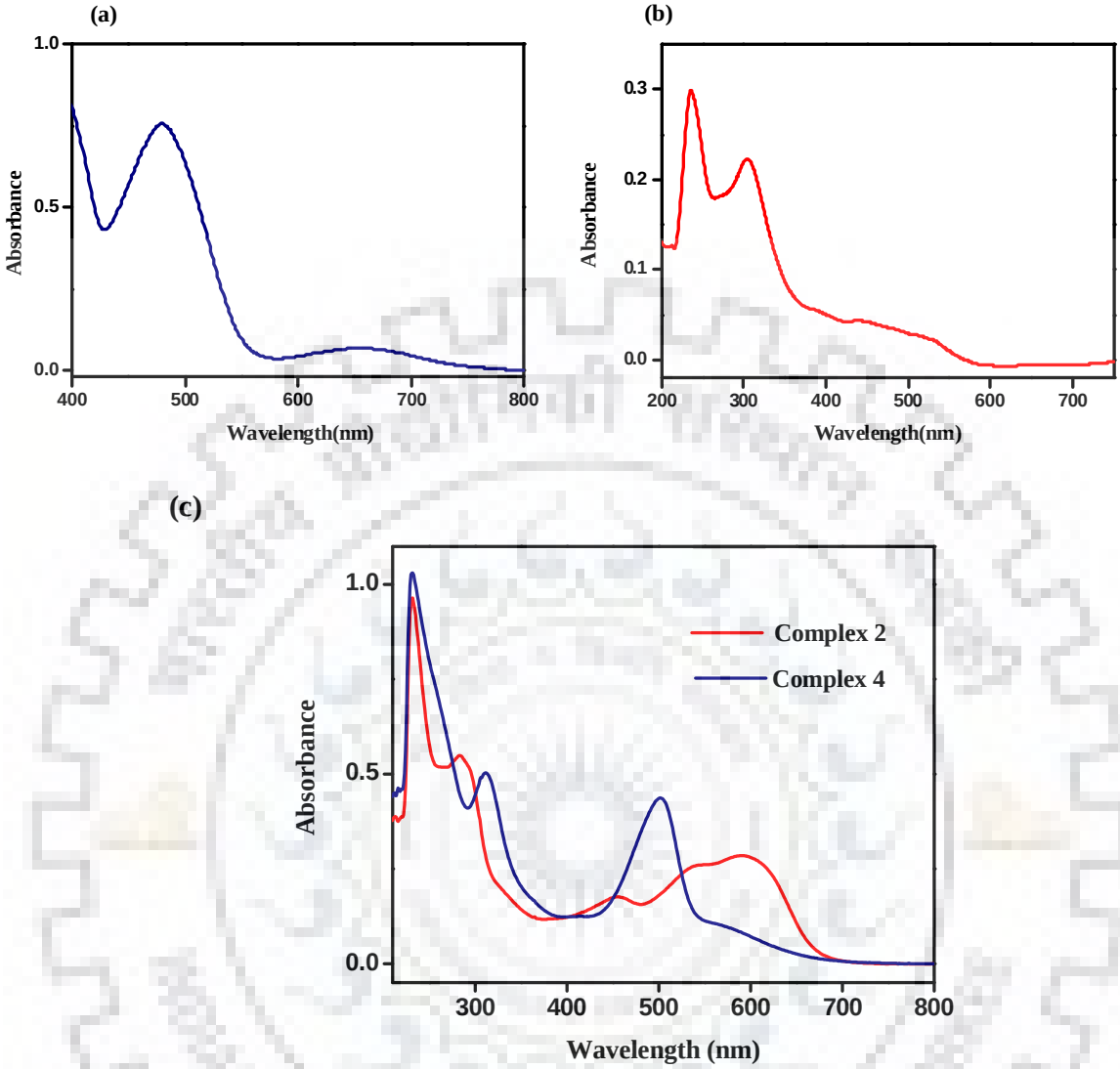

Fig. 2.2 Electronic absorption spectra of complexes (a) **1** (b) **3** and (c) **2**, **4** in dichloromethane solvent.

In ^{1}H NMR spectra for the ligands ($L^{1}H_2$) and ($L^{2}H_2$) (Figure 2.3-2.4), we observed peaks near 11.68 ppm and 11.21 ppm respectively, which were assigned to be carboxamido (–CONH–) proton. The ruthenium nitrosyl complexes **3** and **4** were found to be diamagnetic which was confirmed by ^{1}H and ^{31}P NMR spectral studies (Table 2.3). The ^{1}H and ^{31}P NMR spectra of **3** and **4** were displayed in Figures 2.5-2.6 and 2.7-2.8 respectively. We obtained

single peaks near 20.24 ppm and 22.39 ppm for **3** and **4**, respectively, in ^{31}P NMR spectra corresponding to the presence of trans PPh_3 groups.[214-217,58,196]

Table 2.3 NMR spectral data for ligands and ruthenium complexes **3–4**.

Complex	^{1}H NMR (δ /ppm)	^{31}P NMR (δ /ppm)[a]
$\mathbf{L^1H_2}$	11.68 (s, 1H), 8.84 (d, 1H), 8.39 (d, 2H), 8.13 (d, 2H), 7.99 (d, 1H), 7.84 (d, 2H), 7.56 (m, 4H), 7.29(t, 1H)	-
$\mathbf{L^2H_2}$	11.21 (s, 1H), 8.50-6.87 (d, 10H)(m, 2H), 3.16 (s, 6H), 2.36(s, 3H)	-
3	9.47 (s, 1H), 7.99 (d, 2H), 7.88 (d, 1H), 7.54 (d, 2H), 7.38 (m, 6H), 7.25 (m, 25H), 7.07 (m, 2H), 6.70 (t, 1H), 6.54 (d, 1H), 6.36 (d, 2H)	20.24
4	10.03 (s, 1H), 7.67 (s, 1H), 7.17 (d, 2H), 7.37-7.52 (m, 35H), 6.58 (d, 1H), 5.93 (s, 1H), 2.61 (s, 6H), 2.32 (s, 3H)	22.39

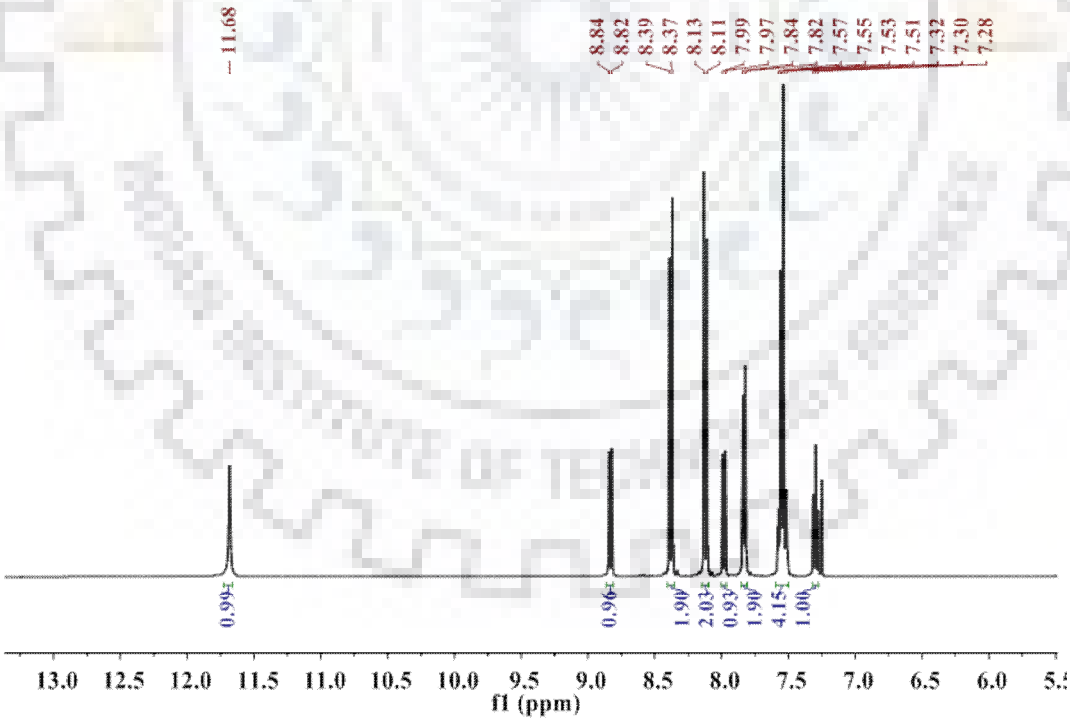

Fig. 2.3 ^{1}H NMR spectrum of $\mathbf{L^1H_2}$ in $CDCl_3$ at room temperature.

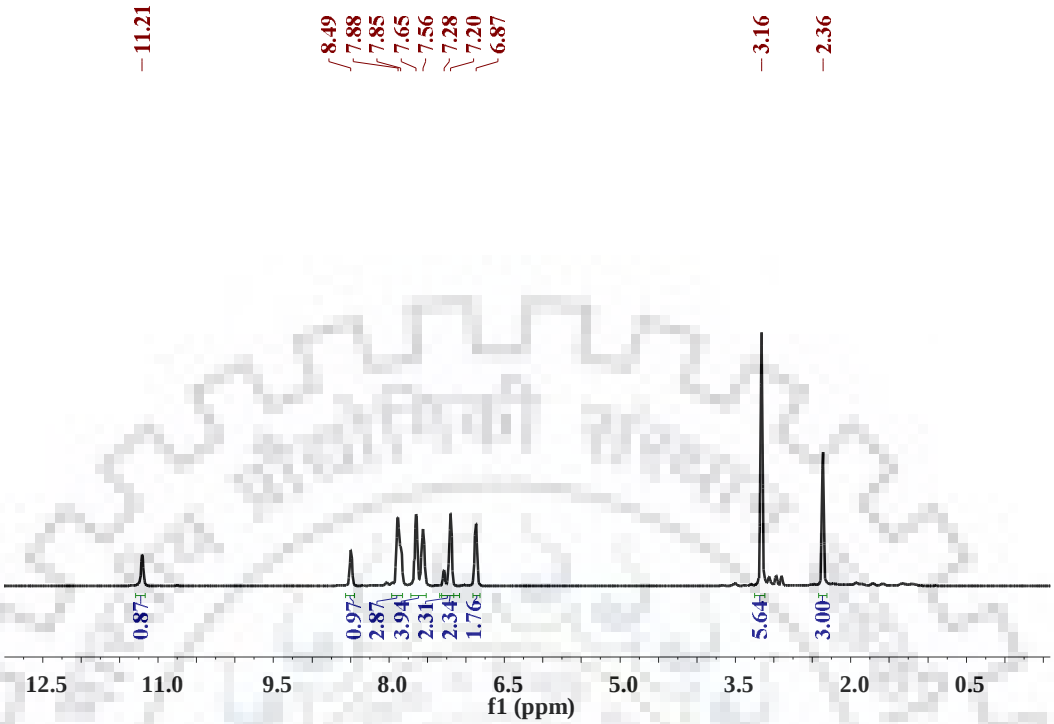

Fig. 2.4 ^{1}H NMR spectrum of $\mathbf{L^2H_2}$ in DMSO-d_6 at room temperature.

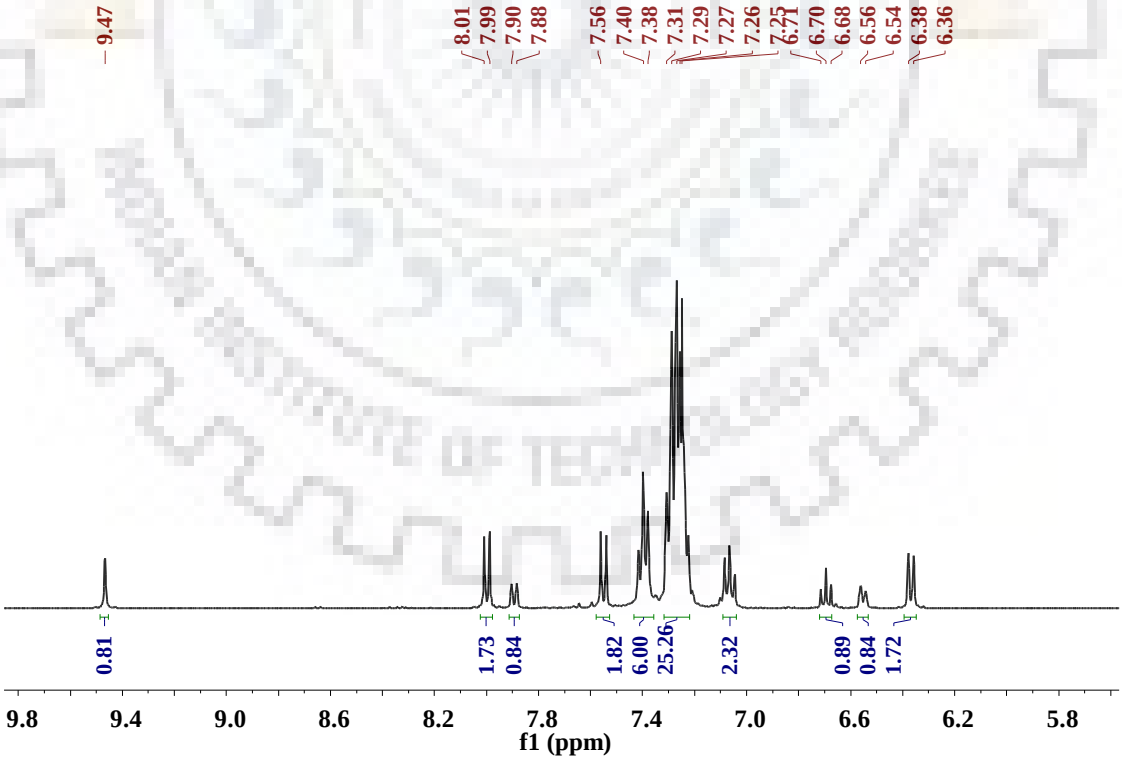

Fig. 2.5 ^{1}H NMR spectrum of complex **3** in $CDCl_3$ at room temperature.

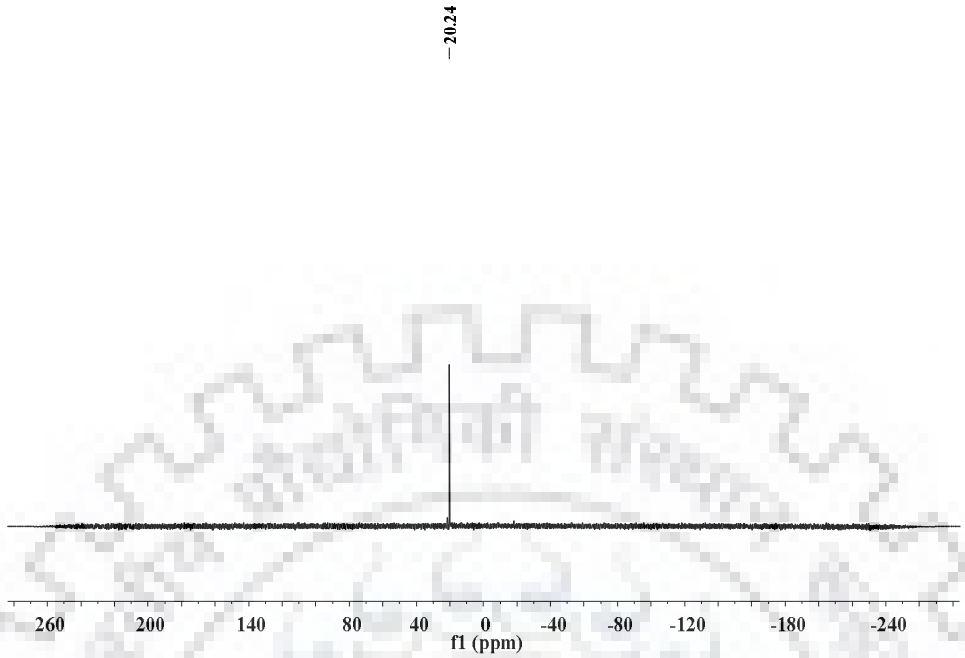

Fig. 2.6 ^{31}P NMR spectrum of complex **3** (δ 20.24 ppm) in $CDCl_3$ at room temperature.

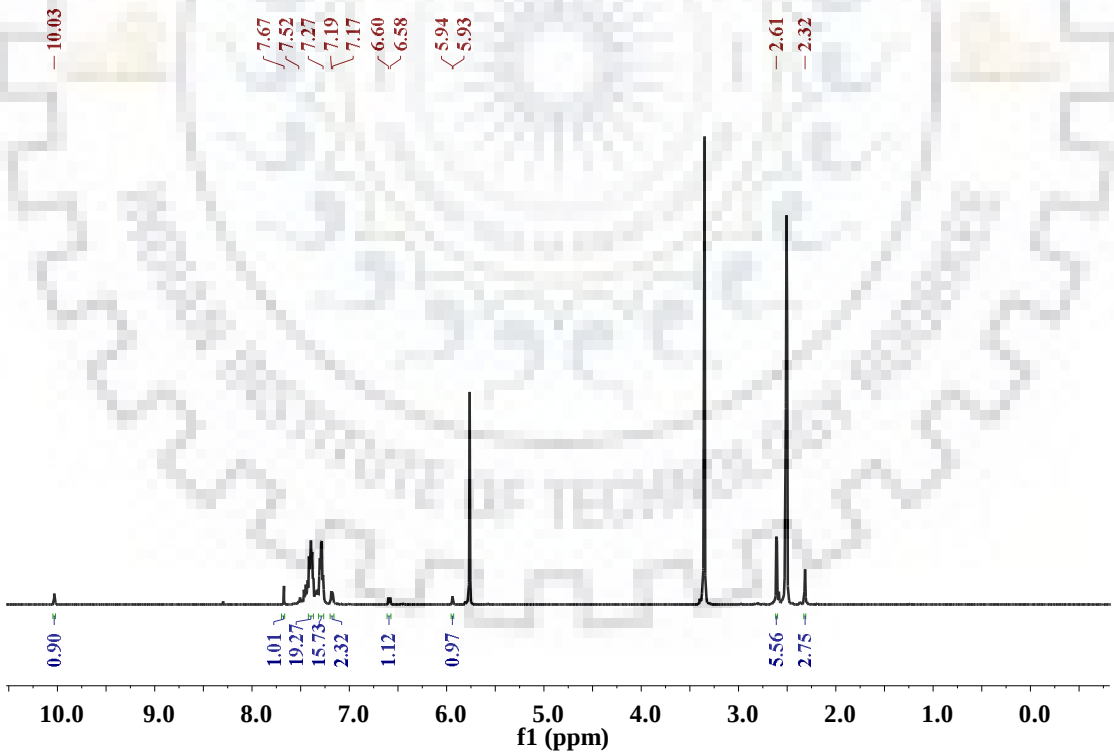

Fig. 2.7 ^{1}H NMR spectrum of complex **4** in DMSO-d_6 at room temperature.

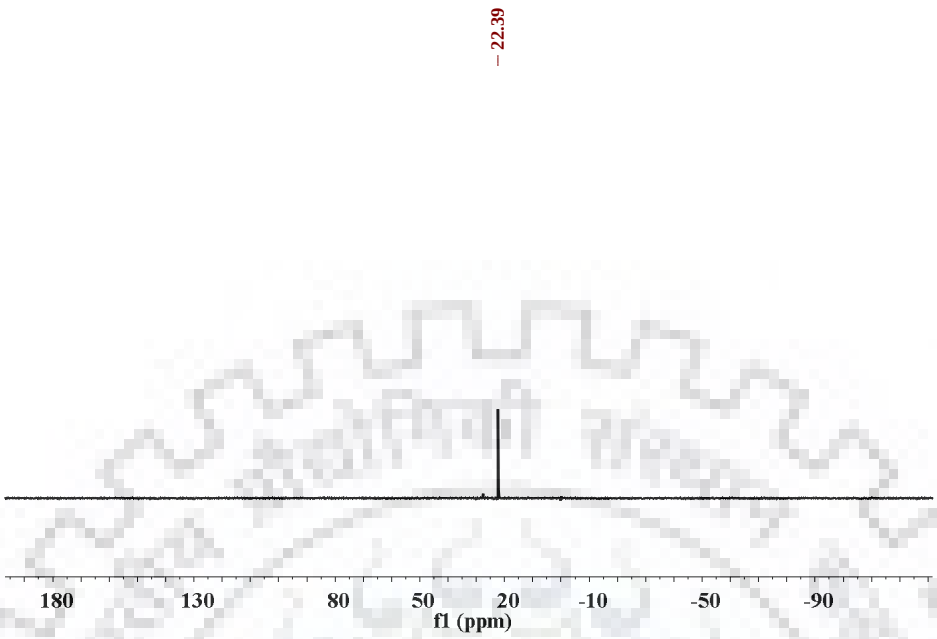

Fig. 2.8 ^{31}P NMR spectrum of complex **4** (δ 22.39 ppm) in DMSO-d_6 at room temperature.

The ESI-MS mass spectra for complexes **1** and **2** (shown in Figures 2.9 and 2.10) in acetonitrile showed peaks at m/z 960.1612[M − 2(Cl)$^-$] and 1018.2278[M+H]$^+$ respectively.

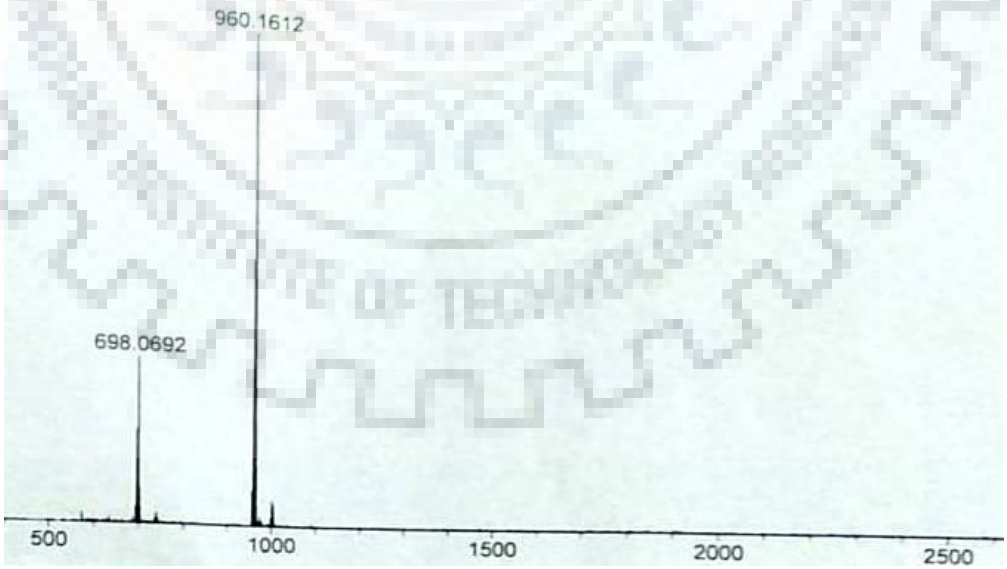

Fig. 2.9 ESI– mass specrtum of complex **1**(in acetonitrile solvent)

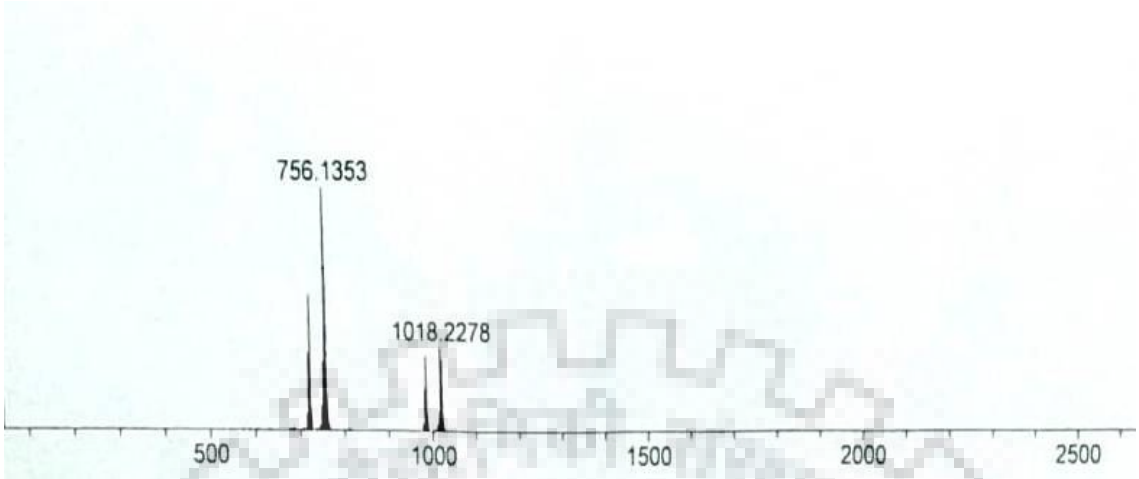

Fig. 2.10 ESI– mass specrtum of complex **2**(in acetonitrile solvent).

2.2.2. Description of molecular structures

The molecular structures of the complexes $[Ru(L^1H)(PPh_3)_2(NO)Cl](ClO_4)$(**3**) and $[Ru(L^2_{NO2})(PPh_3)_2(NO)Cl](PF_6)$**(4)** are depicted in Figure 2.11 and Figure 2.12 respectively.

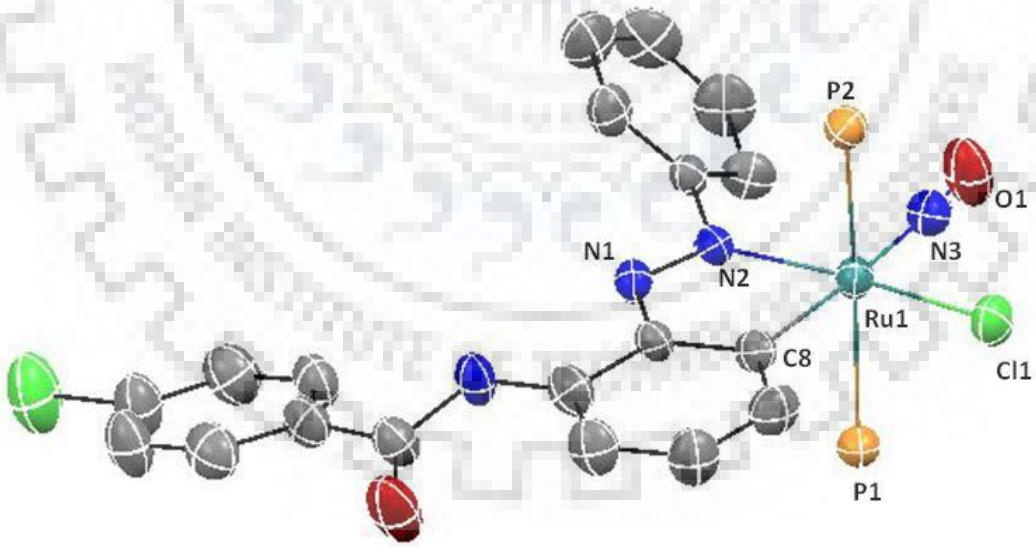

Fig. 2.11 ORTEP diagram (50% probability level) of the $[Ru(L^1H)(PPh_3)_2(NO)Cl](ClO_4)$ (**3**). All hydrogen atoms, counter anion, PPh_3 groups and the crystallized solvent molecules have been omitted for clarity.

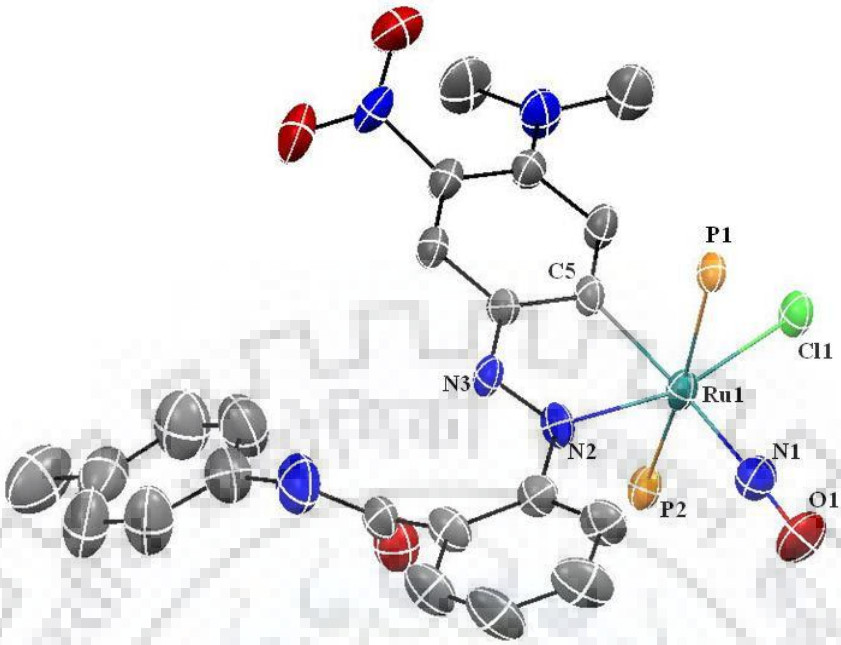

Fig. 2.12 ORTEP diagram (50% probability level) of the $[Ru(L^2_{NO2})(PPh_3)_2(NO)Cl](PF_6)$**(4)**. All hydrogen atoms, counter anion and PPh_3 groups have been omitted for clarity.

The selected bond lengths and bond angles of complexes **3** and **4** are given in Table 2.4.

Crystal data collection and refinement details of the structures of complexes **3** and **4** are summarized in Table 2.5. In the crystal structures of **3** and **4**, the equatorial plane consisted of carbanion, Cl(1), N(azo) and NO. Interestingly in **4**, reversible binding of carboxamido nitrogen was observed during nitrosylation and photorelease of NO. In our previous reports,[214,217] reversible binding of phenolato and carboxylato oxygen was observed in the same manner during the interaction of NO.

We observed that both the phosphine groups were trans to each other at axial positions which was supported by ^{31}P NMR spectral data. The ruthenium centre adopted a distorted-octahedral geometry as reflected in parameters given in Table 2.4.

Table 2.4 Selected bond lengths (Å) and bond angles (˚) for complexes **3** and **4**.

Bond lengths (Å)		Bond angles (°)	
		3·CH_2Cl_2	
Ru(1)−Cl(1)	2.382(3)	N(2)−Ru(1)−Cl(1)	165.9(3)
Ru(1)−C(8)	2.072(13)	N(2)−Ru(1)−N(3)	96.7(5)
Ru(1)−N(2)	2.091(10)	Cl(1)−Ru(1)−N(3)	96.4(4)
N(3)−O(1)	1.125(16)	C(8)−Ru(1)−N(2)	76.7(5)
Ru(1)−P(2)	2.478(3)	Ru(1)−N(3)−O(1)	173.3(12)
Ru(1)−P(1)	2.439(3)	P(1)−Ru(1)− P(2)	170.97(13)
N(1)−N(2)	1.299(14)	C(8)−Ru(1)− N(3)	173.2(6)
Ru(1)−N(3)	1.814(14)	C(8)−Ru(1)−Cl(1)	90.3(4)
		4	
Ru(1)−Cl(1)	2.3666(14)	N(1)−Ru(1)−Cl(1)	95.32(17)
Ru(1)−C(5)	2.079(6)	N(1)−Ru(1)−C(5)	176(2)
Ru(1)−N(1)	1.806(6)	Cl(1)−Ru(1)−N(2)	163.68(15)
Ru(1)−P(1)	2.4689(15)	C(5)−Ru(1)−Cl(1)	87.93(15)
Ru(1)−P(2)	2.4613(15)	N(2)−Ru(1)−N(1)	100.9(2)
Ru(1)−N(2)	2.117(4)	P(1)−Ru(1)−P(2)	171.59(5)
N(1)−O(1)	1.140(7)	C(5)−Ru(1)−N(2)	75.9(2)
N(2)−N(3)	1.275(7)	Ru(1)−N(1)−O(1)	174.3(6)

In the nitrosyl complexes, Ru–$N_{(NO)}$ (~1.80Å),[214,58] NO stretching frequency (ν_{NO}~1820-1840 cm^{-1}) (vide infra) and N–O bond length were consistent with reported values.[58,171] Ru–N and N–O distances in addition to Ru–N–O angle[188] (~174°) revealed the π-acceptor characteristic[51,225] of the coordinated NO^+ in the complex and expressed the $\{Ru^{II}–NO^+\}^6$ description of the $\{RuNO\}^6$ moiety (S = 0 ground state).[214,58,196] Enemark and Feltham suggested a special notation $\{M–NO\}^n$ (where n = total number of electrons present in metal d orbital + NO π* orbital) for all metal nitrosyl complexes to denote a metal–NO bond. For

example, in a ruthenium nitrosyl complex, a $\{Ru–NO\}^6$ unit could show two possible ways to represent a metal–NO bond, namely Ru(III)–$NO^{\bullet}$ and Ru(II)–NO^{+}.

Table 2.5 Summary of crystal data and structural refinement parameters for complexes **3** and **4**.

	3·CH_2Cl_2	**4**
Empirical formula	C_{111} H_{90} C_{l7} N_8 O_8 P_4 Ru_2	C_{58} H_{50} Cl F_6 N_6 O_4 P_3 Ru
Formula weight	2238.08	1238.47
Temperature /K	296(2)	293(2)
Λ (Å) (Mo-Kα)	0.71073	0.71073
Crystal system	Monoclinic	Triclinic
Space group	*P 21*	P-1
a (Å)	10.9304(6)	11.2840(9)
b(Å)	23.1434(11)	13.0023(11)
c (Å)	11.9951(6)	18.8577(15)
α(°)	90.00	93.217(4)
γ (°)	90.00	97.114(4)
β(°)	101.307(3)	96.521(4)
V ($Å^3$)	2975.5(3)	5094(2)
Z	1	2
ρ_{calc} (gcm^{-3})	1.249	1.512
F(000)	1143	1264
Theta range	0.892-27.600	0.896−28.450
Index ranges	$-14<h<13$, $-30<k<29$, $-15<l<15$	$-15<h<15$, $-17<k<17$, $-25<l<25$
Data/restraints/par.	13294/51/667	12651/0/712
GOF[a] on F^2	1.056	0.984
*R*1[b] [$I > 2\sigma(I)$]	0.0907	0.0766
*R*1[all data]	0.1306	0.1341
*wR*2[c] [$I > 2\sigma(I)$]	0.2518	0.2242
*wR*2 [all data]	0.2791	0.2860

[a]$GOF = [\Sigma[w(F_o^2-F_c^2)^2]/M-N]^{1/2}$ (M = number of reflections, N = number of parameters refined). [b] $R1 = \Sigma \| F_o | - | F_c \| / \Sigma | F_o |$. [c] $wR2 = [\Sigma[w(F_o^2-F_c^2)^2]/\Sigma[(F_o^2)^2]]^{1/2}$.

2.2.3. Photolysis experiments

The nitrosyl complexes **3** and **4** were found to be photolabile under visible light. The photolability of coordinated NO was examined by exposing dichloromethane solutions of complexes **3** and **4** under illumination of visible light (Figure 2.13 and 2.14). No change was observed in dark but in the presence of light we observed a change in the spectra of complexes **3** and **4**. On the illumination of light on the solution of complex **3**, the peak intensities decreased near 532 and 305 nm and some new peaks increased near 457 and 270 nm. We observed some isobestic points near 560, 509, 422 and 286 nm (Figure 2.13). On the illumination of light on the solution of complex **4**, peaks near 311, 501 nm disappeared and new peaks near 284, 545 nm appeared. We observed some isobestic points near 272, 302, 339, 462 and 522 nm (Figure 2.14).

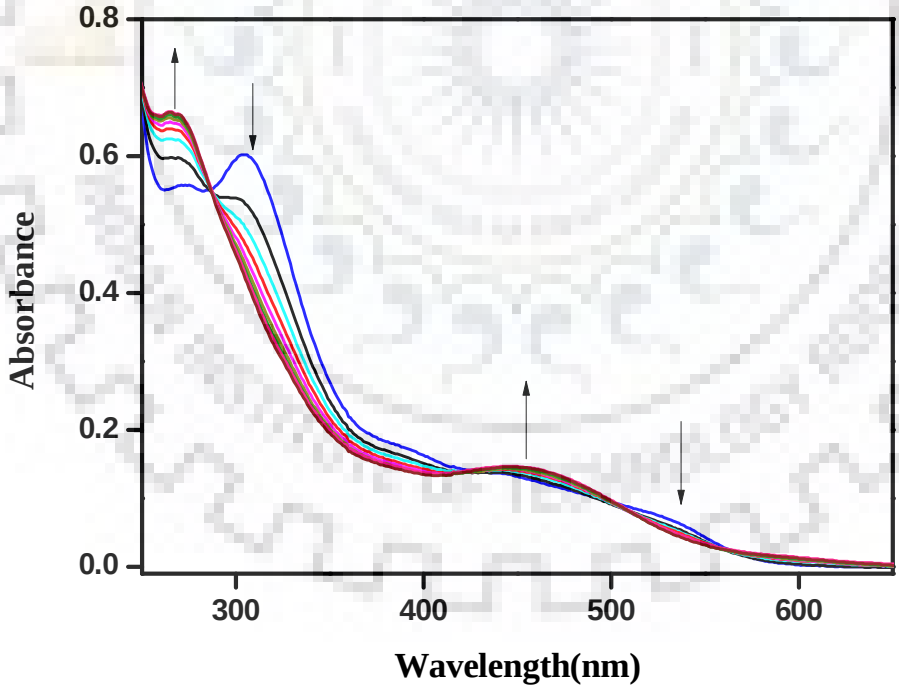

Fig. 2.13 Photocleavage of NO from complex **3** in dichloromethane solution under illumination of visible light (100W). Repetitive scans were taken in 1 min intervals in visible light.

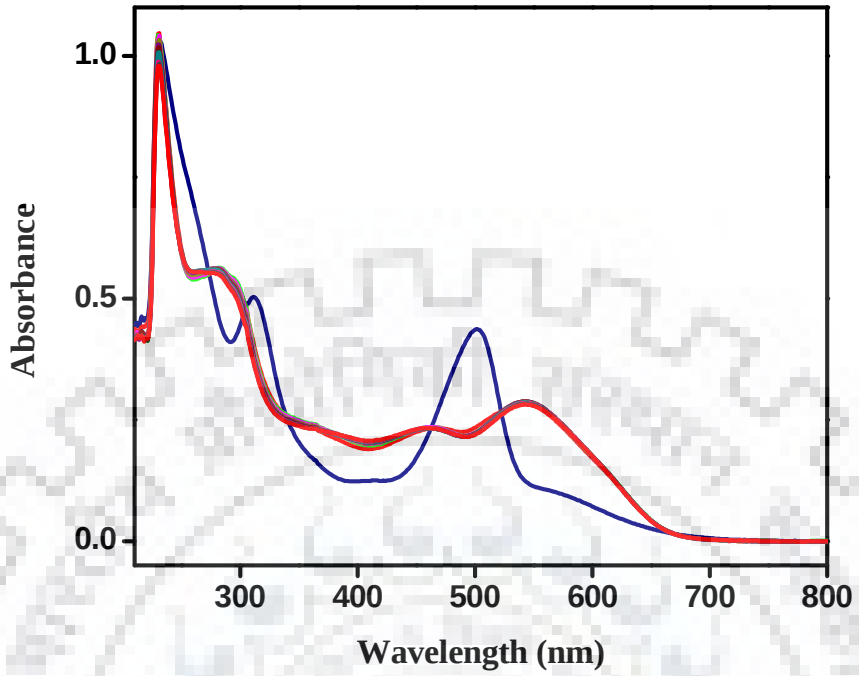

Fig. 2.14 Photocleavage of NO from complex **4** in dichloromethane solution under illumination of visible light (100W). Repetitive scans were taken in 1 min intervals in visible light.

2.2.3.1. Dissociation of NO and retention of amide nitrogen coordination

We have observed the dissociation of ruthenium amide bond (Ru-Ncarboxamido) during NO coordination. This may be due to the formation of {Ru(II)-NO^+}[6] and it is well known in the literature that the carboxamido nitrogen stabilizes higher oxidation state of metal.[216] This prompted us to examine the product after photolytic cleavage of NO. A retention of Ru-Ncarboxamido was observed and complex **4b** was generated. The probable reactions happened are displayed in Scheme 2.4.

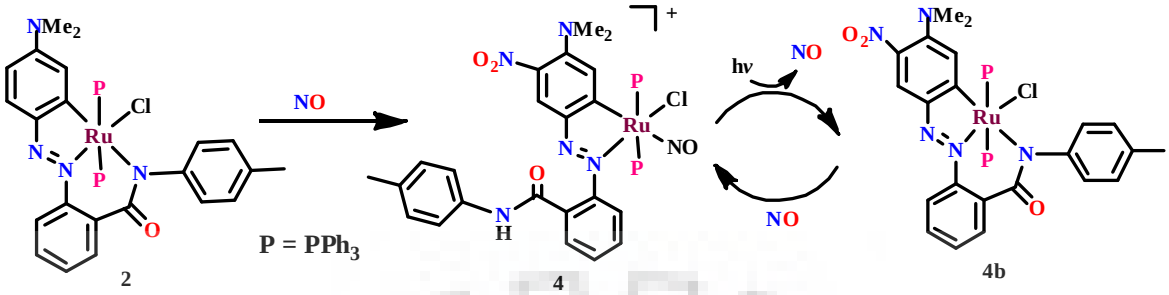

Scheme 2.4 Interconversion of complexes **4** and **4b**.

2.2.4. Trapping of NO by reduced myoglobin

The nitric oxide trapping experiment was carried out using UV–vis spectroscopic technique.[58,196,214] Photoreleased NO from complex **3** was transferred to reduced myoglobin in a phosphate buffer of pH = 6.8. The electronic absorption spectrum of oxidized myoglobin (Mb) showed an intense band near 409 nm (a Soret band). The UV–vis spectrum of reduced myoglobin at 433 nm was obtained by addition of excess sodium dithionite to the same cuvette. Acetonitrile solution of complex **3** was added to the same cuvette but no reaction was observed in dark with the buffer solution of reduced myoglobin. However, when the same mixtures were exposed to the visible light (100 W) for 10 min, absorption band at 422 nm (shown in Figure 2.15) showed the formation of Mb–NO adducts in solution.[58,196,214] The same experiment was performed for complex **4**.

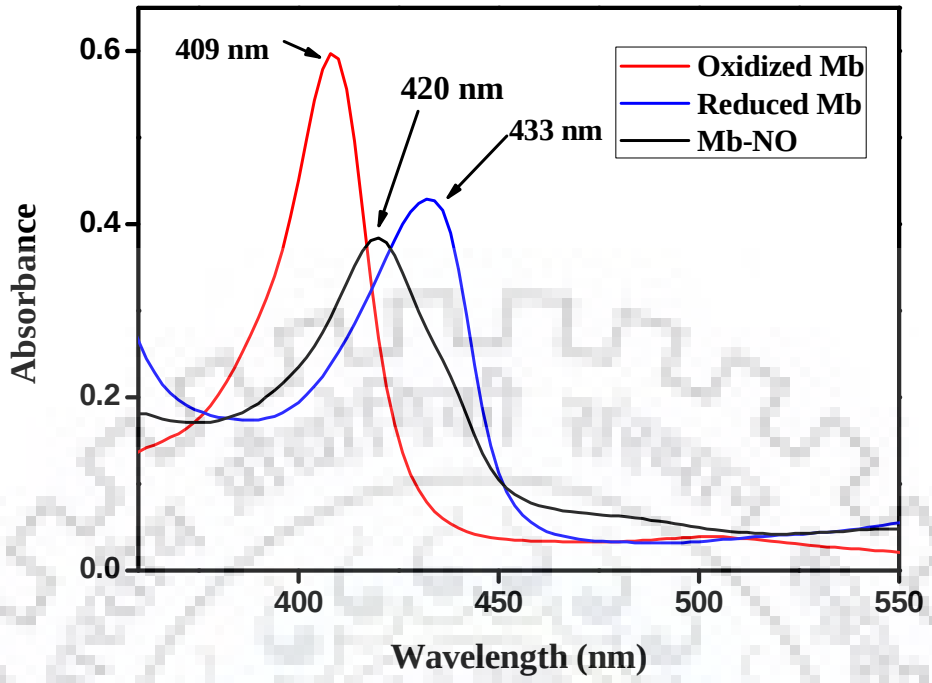

Fig. 2.15 Electronic absorption spectra of conversion of reduced myoglobin to Mb─NO adduct upon reaction with **3** in buffer solution (50 mM phosphate buffer, pH 6.8) under exposure of Visible light(100W) for 10 min.

2.2.5. Concentration dependent cyto-toxicity of compounds 3 and 4

In-order to see the in vitro-cytotoxic nature of both compounds (**3** and **4**), the MTT [3-(4,5-dimethylthiazol-2-yl)-2,5-diphenyltetrazolium bromide] colorimetric assay was performed in human cervical cancer cell line (HeLa cells). HeLa cells were grown in 30-50% confluency before treating with the compounds. After mixing both the compounds cells were irradiated with visible light to release NO from the compounds. The MTT assay was performed after 24 hours of the treatment. The data showed severe concentration (0.2 µM, 0.5 µM, and 0.8 µM up to 2 µM) dependent cytotixicity for both the compounds tested (Figure 2.16). The concentration of 0.8 µM showed almost 50% reduction of live cells; even as low as 0.2 µM concentration for both compounds showed very effective killing of cells within 24 hours (

Figure 2.16) . The solvent DMSO used to dissolve the compounds didn't show any cellular death even after 48 hours. Our group previously described a ruthenium compound which showed severe cytotoxicity at 2 µM concentration, the newly made two compounds showed equivalent cytotoxic effect even at 0.2 µM concentration, suggesting these compounds are 10 times more effective than the previously reported one.[217]

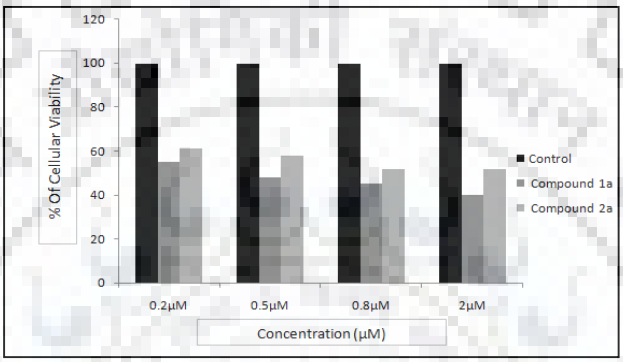

Fig. 2.16 MTT [3-(4,5-dimethylthiazol-2-yl)-2,5diphenyltetrazolium bromide] assay was performed using compound **3** and **4** upon photoactivation. The solvent DMSO was used as control. Four different concentrations (0.2 µM, 0.5µM, 0.8 µM and 2µM) were used to check the cellular toxicity using HeLa cells (human cervical carcinoma cell line). MTT assay showed around 50% cellular viability after treatment with 0.2µM of both the compound. Percentage of cell viability decreases with increase in concentration for both compounds. Control cells (treated with DMSO solvent) didn't show any noticeable reduction of cell numbers.

2.2.6. Photodynamic release of NO from compounds 3 and 4 and its cyto-toxic effect

As both the compounds show anti-cell proliferative activity, next we checked whether the compound itself or the released NO is wrecking the cellular environment, turning to be a potential anti proliferative agent. The HeLa cells were treated with both the compounds (**3** and **4**; concentration 0.2 µM) and irradiated for 10 minutes with visible light. Severe cytotxicity was observed after 6 hours (data not shown) and at 12 hours almost all cells were dead when looked under bright filed microscope (Figure 2.17, Panel 1) . The chloride

derivative of the same compound didn't show any noticeable cyto-toxic effect upon illumination suggesting that the metal ruthenium is not responsible for cellular death. (Figure 2.17, Panel 2) In another control, to show that the compounds itself were not toxic, we illuminated the medium containing compounds for 10 minutes and then transferred the media to 30% confluent HeLa cells. The prior illumination of medium containing compounds will remove NO from the complex and make the compound inactive (residual compound). The data showed the residual compound didn't show any cytotoxic effect suggesting that it is released NO and not the compound responsible for cell death (Figure 2.17, Panel 3). The DMSO solvent added control cells showed 100% viability (Figure 2.17, Panel 4).

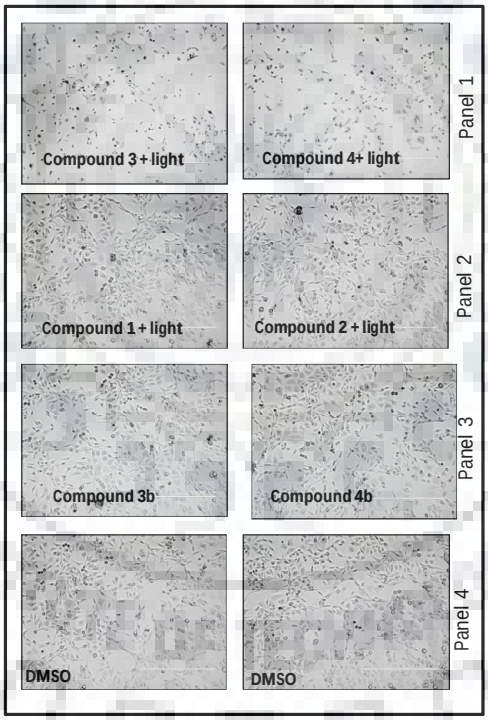

Fig. 2.17 Cell death upon treatment with compound **3** and **4** in Hela cells**. (a)** Panel 1: cells treated with 0.2µM of compound **3** and **4** followed by irradiation with visible light for 10 minutes showed more than 80 % cell death within 24 hours. Panel 2: showed the effects of precursor complexes (ruthenium chloride) (compound **1** and compound **2**) of both the nitrosyl compounds **3** and **4**. Panel 3: showed effects using residual compounds (compound **3b** and compound **4b**) i.e. the effects of compounds after releasing NO. Panel 4: the DMSO control (Healthy cells). Images are taken at 10X magnifications.

2.2.7. Apoptotic induction of cancer cells after treatment with compound 3 and 4

Nitric oxide (NO) is a potential inducer of apoptosis.[226-228] To find out whether treatment with compound **3** and **4** induces cancer cells to enter into apoptotic cycle, the acridine orange and ethidium bromide (AO/EB) dual staining was performed (Figure 2.18). Acridine orange and ethidium bromide both are fluorescent nucleic acid dye, the former one is permeable to both live and dead cells whereas the later one (ethidium bromide) enters only into dead cells those lost membrane integrity.

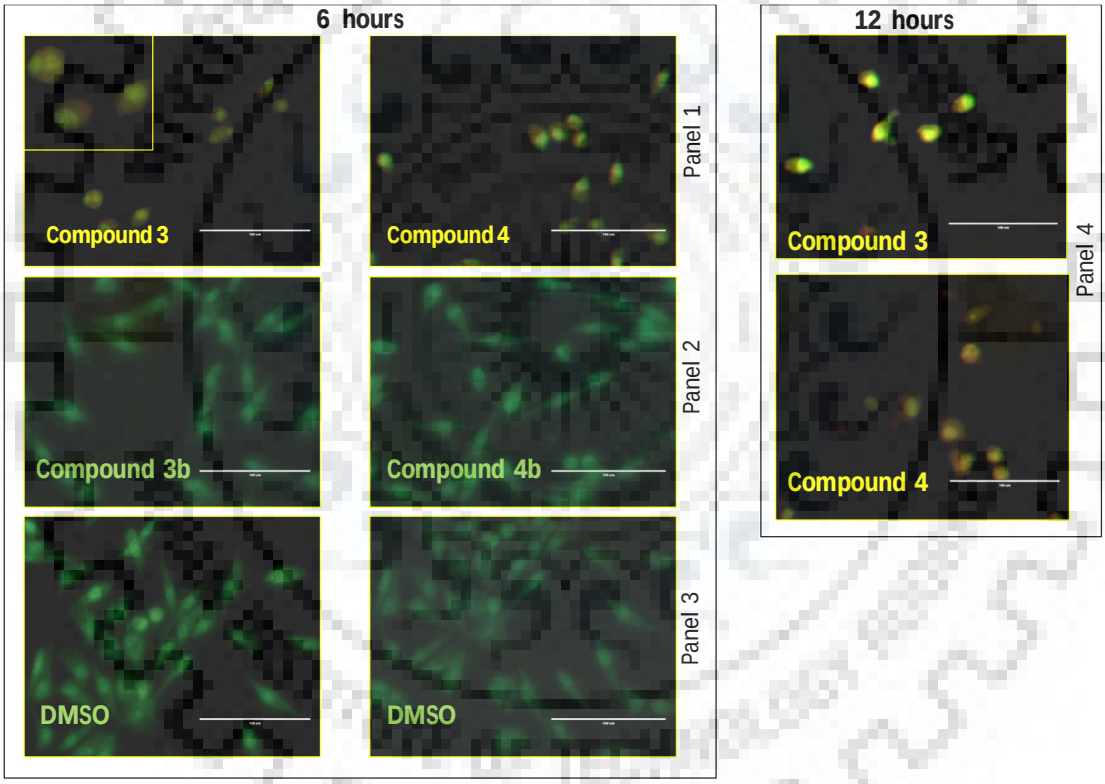

Fig. 2.18 Dual acridine orange and ethidium bromide staining for apoptotic cells. Panel 1. compound **3** and **4** treated cells after 6 hours incubation. Panel 2: compound **3b** and compound **4b** (residual compounds); Panel 3: DMSO control. Panel 4: compound **3** and **4** treated cells after 12 hours incubation.

The treated cells upon illumination with visible light showed orange yellow fluorescence indicating apoptosis due to release of NO from both the compounds (Figure 2.18, Panel 1). Cells treated with compound **3** and **4** without visible light illumination showed uniform green fluorescence suggesting all cells are alive and thus stained with acridine orange only. The same characteristics were observed when cells were treated with residual complexes (compound without NO) and DMSO control (Figure 2.18, Panel 2) and (Figure 2.18, Panel 3), respectively. The intensity of yellow-orange fluorescence increase with longer incubation time (12 hours vs 6 hours) indicating more ethidium bromide staining (Figure 2.18, Panel 4). This also suggests that NO activates signalling pathways which disrupted membrane integrity of the cells allowed ethidium bromide to enter inside cells.

Next, to check the nuclear and cytoplasmic integrity, the treated cells were stained with Hoechst 33342 (a fluorescent DNA intercalating dye makes nucleus blue) and Rhodamin B (selectively stained cytoplasm in red). The data showed significant DNA fragmentation as multi-lobed nucleus (red) surrounded by a faint boundary were seen in most of the cells after 6 hours post-treatment with the compounds **3** and **4** (Figure 2.19, Panel 1). After 12 hours post treatment, the DNA fragmentation was more severe; the lobes were separated from each other and mixed with cytoplasmic compartment of the cells (Figure 2.19, Panel 4). Again residual compound and DMSO control didn't show any DNA fragmentation as evident from intact nucleus and cytoplasm integrity (Figure 2.19, Panel 2 and Panel 3).

2.2.8. DNA fragmentation assay

Total genomic DNA was extracted from HeLa cells with or without treatment with compounds after 6 hours and 12 hours. The isolated DNA was resolved in agarose gel by DNA gel electrophoresis. Equal amount of genomic DNA was loaded in each lane. The DNA

fragmentation of cancer cells induced by both the compounds was also checked by performing agarose gel electrophoresis. The genomic DNA was purified from treated and untreated cells and then resolved in 0.6% agarose gel. Appearance of smear in agarose gel suggested severe degradation of genomic DNA obtained from treated cells, whereas untreated cells showed intact DNA (Figure 2.19, Panel 5).

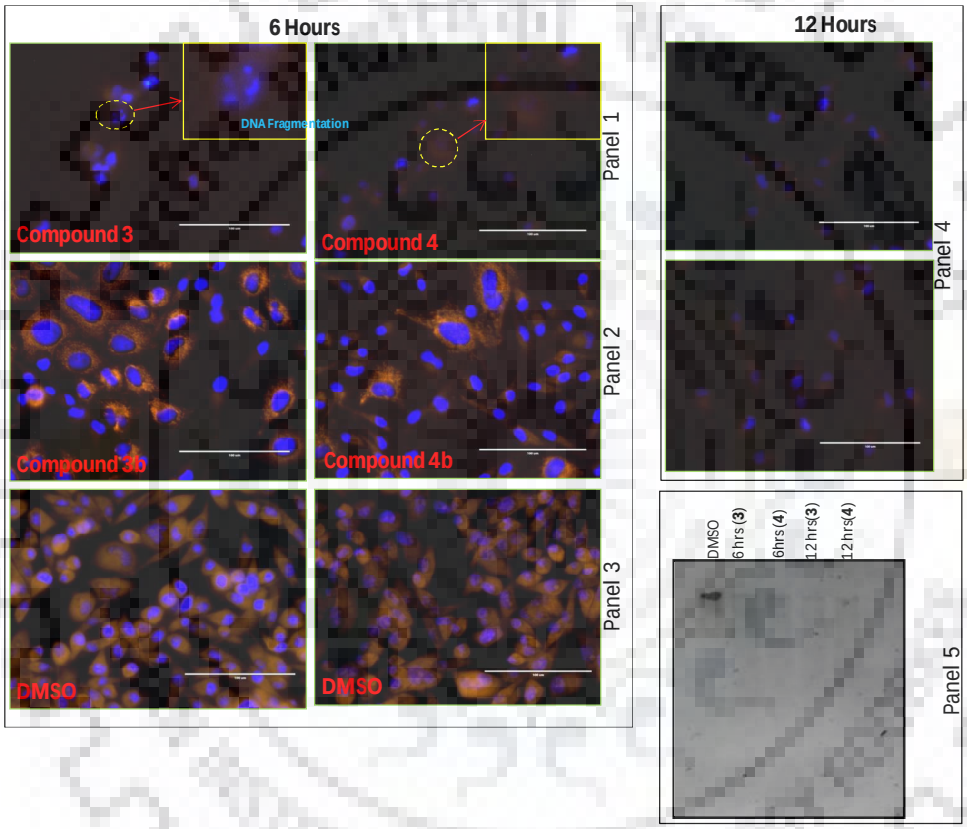

Fig. 2.19 Visualization of altered cytoskeletal and nuclear integrity in treated cells. Cells were stained with Hoechst 3322 (nuclear stain; blue) and Rhodamine B (cytoskeletal stain; red). Panel 1: showed cells after 6 hours post treatment with compound **3** and **4**. Panel 2 showed effect of residual compounds. Panel 3: showed DMSO (solvent) treated cells. Panel 4: showed cells 12 hours post-treatment with compound **3** and **4**. All the images are taken in 40X under proper filter.

2.2.9 Anexin V assay to check stages of apoptosis by fluorescent activated cell sorter

The dual staining (Acridine Orange/Ethidium Bromide and Hoechst 33342/Rhodamine B) and DNA fragmentation assays already confirmed that the released NO from the compounds induces apoptosis in the cancer cells. Next, we performed annexin V assay to measure the percentage of cells that belong to late and early apoptosis stages. Externalization of phosphatidylserine to the outer surface of plasma membrane is a hallmark feature of apoptosis. Hence, binding of annexin V to the cellular surface is an indicative feature for apoptosis. Another dye propidium iodide (membrane impermeable DNA stain) was used in combination of annexin V to discriminate apoptotic versus necrotic cells (dead cells). Thus, Annexin V negative and PI negative (Annexin V^- and PI^-) signal indicates viable, Annexin V positive and PI negative (Annexin V^+ and PI^-) indicates early apoptotic and Annexin V positive and PI positive (Annexin V^+ and PI^+) indicates late apoptotic cells. Treatment of compounds followed by 12 hours incubation showed almost 50% cells are in apoptosis stages (Figure 2.20, Panel 2). Among that 50% apoptotic population, the data showed almost one-third belongs to the early and two-third belong to the late apoptotic stages (Figure 2.20, Panel 2. The DMSO treated cells didn't show any apoptosis induction and sorted as viable cells in the flow sorter (Figure 2.20, Panel 1).

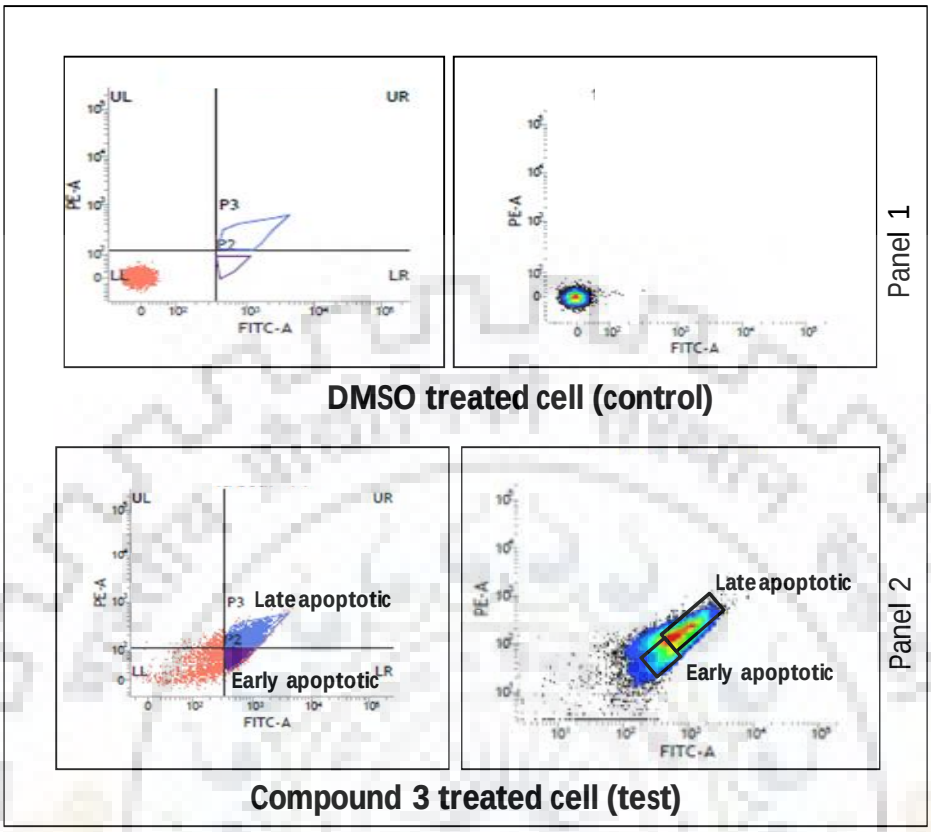

Fig. 2.20 Flow cytometric analysis reveals cells treated with compound **3** after six hours enter early apoptotic phase. Panel 1 showed cells without treatment. Panel 2: showing treated cells with positive staining for both alexa fluore 488 for annexin V and PI (propidium iodide).

2.2.10. Gene Expression studies to check stages of apoptosis

Apoptosis occur via two pathways intrinsic mitochondrial or extrinsic via death receptor pathway. Both pathways are well regulated by cascades of signalling genes. Mitochondrial dysfunction[229] is involved in case of apoptosis as mitochondria release pro-apoptotic factors such as cytochrome C along with other apoptosis inducing factors.[230] The Bcl2 family membranes of proteins[231] play pivotal role to maintain mitochondrial outer membrane integrity. The pro-apoptotic member Bax oligomerizes in the mitochondrial membrane and thus disrupts its integrity whereas pro-survival members (e.g. Bcl2, Bclxl) maintain

mitochondrial membrane.[232] In our study, we have analysed the change of expression of two apoptotic markers Bcl2 and Bax after treating cells with compound **3**. The quality of total RNA isolated from treated cells didn't show any changes when compared with RNA obtained from untreated cells (Figure 2.21, Panel 1). By employing semi quantitative RT-PCR using gene specific primers for Bcl2 and Bax, our data showed the expression of Bax was increased in time-dependent manner; 12 hrs post treatment showed increased expression than 6 hours (Figure 2.21, Panel 2). On contrary, the Bcl2 expression was significantly decreased after 6 hours and no signal was obtained from 12 hours (Figure 2.21, Panel 3). The expression of beta-actin gene was used as control (Figure 2.21, Panel 4). Thus expression patterns of the above two genes (Bcl2 and Bax) indicated the NO mediated apoptosis probably occurring through mitochondrial pathway.

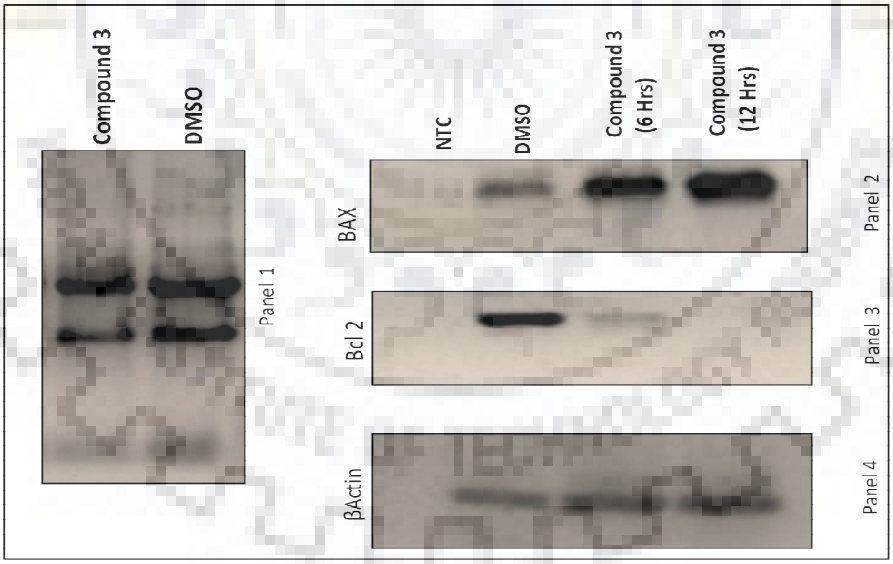

Fig. 2.21 Total cellular RNA isolated from compound **3** and DMSO treated cells. Panel 1: Heat denatured RNA was resolved in neutral 0.8% Agarose gel. Semi quantitative PCR reveals differential expression of Bax and Bcl2 upon apoptosis induction. Panel 2: showing expression of Bax increases after treatment with compound **3** and the increased expression is time dependent. Panel 3: showed decreased time dependent expression of Bcl2. Panel 4: showing expression of beta-actin as control.

2.3. Conclusions

First, ruthenium(III) cyclometallates $[Ru(L^1H)(PPh_3)_2Cl_2]$ (**1**) and $[Ru(L^2)(PPh_3)_2Cl]$(**2**) were synthesized via C-H bond activation and were characterized by different spectroscopic studies. Second, organometallic ruthenium nitrosyl complexes $[Ru(L^1H)(PPh_3)_2(NO)Cl](ClO_4)$ (**3**) and $[Ru(L^2_{NO2})(PPh_3)_2(NO)Cl](PF_6)$(**4**), were synthesized and characterized by different spectroscopic methods. The molecular structures of **3** and **4** were determined by X-ray crystallography. Third, the coordinated NO was found to be photolabile under visible light and we have investigated the liberation of NO via trapping experiment with reduced myoglobin. Presence of azo function in the ligand frame provided NO liberation under visible light. Fourth, photoreleased NO was found to be cytotoxic to HeLa cancer cell-line and utilized to investigate the anti-proliferation activity studies on HeLa cancer cell-line. Fifth, the results of acridine orange and ethidium bromide staining data clearly indicated apoptotic cell death which was consistent with literature. Sixth, cytoplasmic and nuclear changes happened during apoptotic cell death was depicted by Hoechst and Rhodamine B staining. low conc. (0.2)And finally the anexin V assay and the gene expression studies clearly provided the evidences for early stages of apoptotic cell death.

2.4. Experimental section

2.4.1. Reagents and materials

Analytical grade reagents 4-chlorobenzoic acid, 4-methyl aniline, methyl red, ammonium hexafluorophosphate, sodium perchlorate monohydrate, sodium nitrite

(Himedia Laboratories Pvt. Ltd., Mumbai, India) were used as obtained. $RuCl_3.3H_2O$ was purchased from Loba Chemie Pvt. Ltd., Mumbai, India. Triphenylphosphine (SRL, Mumbai, India), disodium hydrogen phosphate anhydrous (RFCL Ltd. New Delhi, India) and sodium dihydrogen phosphate (Chemport India Pvt. Ltd. Mumbai, India) were used as obtained. Double distilled water and distilled solvents were used during the experiments. Equine skeletal muscle myoglobin was obtained from Sigma Aldrich, Steinheim, Germany. The precursor $[Ru(PPh_3)_3Cl_2]$ and 2-(phenyldiazenyl)aniline were prepared by following the procedure reported earlier.[233,234]

2.4.2. Physical measurements

Infrared spectra were obtained as KBr pellets with Thermo Nicolet Nexus FT–IR spectrometer, using 16 scans and were reported in cm^{-1}. Electronic absorption spectra of the complexes were recorded in dichloromethane solvent with an Evolution 600, Thermo Scientific (Shimadzu) UV–vis spectrophotometer. ^1H and ^{31}P NMR spectra were recorded on JEOL, 400 MHz spectrometer in the deuterated solvents. The ESI-mass spectra of the sample (in acetonitrile solvent) were recorded in the positive ion mode using Thermo Finnigan LCQ Deca mass spectrometer.

2.4.3. Syntheses of ligands

2.4.3.1. Synthesis of 4-chloro-N-(2-(phenyldiazenyl)phenyl)benzamide (L^1H_2)

The 4-chloro benzoic acid (5.0 mmol) was taken in 15-20 mL dimethylformamide solution and then cooled on an ice bath. To this solution, 1.48 g (11.0 mmol) of 1-hydroxybenzotriazole (HOBT) as well as 1.13 g (5.5 mmol) of dicyclohexylcarbodiimide (DCC) were added directly and mixture was stirred for half an hour at 0°C. Now a batch of 2-(phenyldiazenyl)aniline(5.0 mmol) was added to the reaction mixture with stirring for next

2 hours on the same ice bath. After, the ice bath was removed and the stirring was continued over night at room temperature. By removing the white precipitate of N,N'-dicyclohexylurea through filtration, the solvent was concentrated to 10 mL. Within 3-4 days, a light orange crystalline solid of ligand L^1H_2 was settled down on the bottom of beaker which was filtered and washed with methanol and diethyl ether. Yield: 58%. Anal. ^{1}H NMR ($CDCl_3$, 400 MHz): δ 11.68 (s, 1H), 8.84 (d, 1H), 8.39 (d, 2H), 8.13 (d, 2H), 7.99 (d, 1H), 7.84 (d, 2H), 7.56 (m, 4H), 7.29(t, 1H) ppm.

2.4.3.2. Synthesis of 2-((4-(dimethylamino)phenyl)diazenyl)-N-(p-tolyl)benzamide (L^2H_2)

Ligand (L^2H_2) was synthesized by reaction of (2-(N,N-dimethyl-4-aminophenyl) azobenzenecarboxylic acid) (methyl red) with 4-methyl aniline following the same procedure as used for ligand L^1H_2. Yield: 55%. Anal. ^{1}H NMR (DMSO-d6, 400 MHz): δ 11.21 (s, 1H), 8.50-6.87 (d, 10H)(m, 2H), 3.16 (s, 6H), 2.36(s, 3H) ppm.

2.4.4. Syntheses of ruthenium complexes

Caution: perchlorate salts of metal complexes with organic ligands are potentially explosive. Only a small amount of material should be prepared and handled with caution.

2.4.4.1. Synthesis of $[Ru(L^1H)(PPh_3)_2(Cl)_2]$ (1)

To a 20 mL methanolic solution of L^1H_2 (0.12 mmol) was added directly ruthenium precursor complex $[Ru(PPh_3)_3Cl_2]$ (0.10 mmol) and mixture was refluxed at 85°C for 1 h on an oil bath to obtain a light brown solid at room temperature and was washed with cold methanol and diethyl ether. Yield: 60%. IR (KBr disk, cm^{-1}): 1588 ($\nu_{N=N}$), 747, 695, 518 (ν_{PPh3}) cm^{-1}. UV-Vis (CH_2Cl_2; λmax, nm (ε, $M^{-1}cm^{-1}$)): 480 (6495), 656(601).

2.4.4.2. Synthesis of $[Ru(L^2)(PPh_3)_2Cl]$ (2)

Complex **2** was synthesized according to procedure followed for the complex **1** by reaction of $[Ru(PPh_3)_3Cl_2]$ with ligand L^2H_2. Yield: 65%. IR (KBr disk, cm^{-1}): 1583 ($\nu_{N=N}$), 748, 698, 518 (ν_{PPh3}) cm^{-1}. UV-Vis (CH_2Cl_2; λmax, nm (ε, $M^{-1}cm^{-1}$)): 231 (99,890), 285(56,415), 453(18,126), 593(29,328).

2.4.4.3. Synthesis of $[Ru(L^1H)(PPh_3)_2(NO)Cl](ClO_4)$ (3)

A batch of (0.1 mmol) of complex **1** was taken in 20mL of dichloromethane to obtain a yellowish red colored solution in round bottom flask of 100 mL. Now 20 mL acidified distilled water was layered over this solution. Sodium nitrite (0.3 g, 4.3 mmol) was added to the bilayer solution and the mixture was stirred at room temperature for 2 hrs to get reddish-orange colored solution of complex **3**. The dichloromethane layer was separated out and $NaClO_4$ (in excess) with 10 mL of methanol was added to this solution. Stirring of this solution was continued for another 2 hour. The solvent mixture was evaporated to get reddish-orange solid. To remove excess of $NaClO_4$, this solid was further dissolved in 10 mL of dichloromethane and was filtered out. Now 10 mL of hexane was added to the filtrate to obtain a reddish-orange precipitate of complex **3**. IR (KBr disk, cm^{-1}): 1821 (ν_{NO}), 1095, 615 (ν_{ClO4}), 750, 694, 514 (ν_{PPh3}) cm^{-1}. UV-vis (CH_2Cl_2; λmax, nm (ε, $M^{-1}cm^{-1}$)): 235 (32555), 305 (24888), 441 (4888). ^1H NMR ($CDCl_3$, 400MHz): δ 9.47 (s, 1H), 7.99 (d, 2H), 7.88 (d, 1H), 7.54 (d, 2H), 7.38 (m, 6H), 7.25 (m, 25H), 7.07 (m, 2H), 6.70 (t, 1H), 6.54 (d, 1H), 6.36 (d, 2H) ppm.^{31}P NMR ($CDCl_3$, 400 MHz): δ 20.24 ppm.

2.4.4.4. Synthesis of $[Ru(L^2_{NO2})(PPh_3)_2(NO)Cl](PF_6)$(4)

Complex **4** was synthesized according to procedure followed for the complex **3** by using complex 2. IR (KBr disk, cm^{-1}): 1840 (ν_{NO}), 843, 560 (ν_{PF6}), 748, 690, 518 (ν_{PPh3}) cm^{-1}. UV-

vis (CH_2Cl_2; λmax, nm (ε, $M^{-1}cm^{-1}$)): 232 (68,776), 311(34,732), 501 (30,399). ^{1}H NMR (DMSO-D6, 400MHz): δ 10.03 (s, 1H), 7.67 (s, 1H), 7.17 (d, 2H), 7.37-7.52 (m, 35H), 6.58 (d, 1H), 5.93 (s, 1H), 2.61 (s, 6H), 2.32 (s, 3H) ppm. ^{31}P NMR (DMSO-D6, 400 MHz): δ 22.39 ppm.

2.4.5. Inter-conversion of complexes [Ru(L^2_{NO2})(PPh_3)$_2$(NO)Cl](PF_6)(4) and [Ru(L^2_{NO2})(PPh_3)$_2$Cl](4b)

(i) Conversion of complex **4** into **4b**. A reddish violet dichloromethane solution of complex 2a was exposed to the light of a tungsten lamp (100W). Within 5 minutes the solution turned from reddish to violet. The solvent was evaporated to obtain a violet colored solid of **4b** and this was washed thoroughly with methanol and diethyl ether. From the electronic absorption spectra of complexes **2** and **4b** (Figure 2.22), it was found that both the spectra are similar and after photorelease of NO from **4**, again, there is binding of carboxamido nitrogen to ruthenium as in complex **2**.

(ii) Conversion of Complex **4b** into **4**. Complex 2b (0.15 mmol) was dissolved in 25 mL of dichloromethane in a 100 mL round-bottom flask to give a violet colored solution. Then 20 mL of acidified distilled water was layered over this solution. Sodium nitrite was added to the bilayer solution, and the mixture was stirred at room temperature for 2 h to give a reddish solution of complex **4**. The dichloromethane layer was separated out, and NH_4PF_6 (in excess) with 5 mL of methanol was added to this solution. Stirring of this solution was continued for another 1 h. The solution mixture was kept in dark for 2-3 days to obtain a crystalline solid of complex **4** then filtered and washed with methanol and diethyl ether.

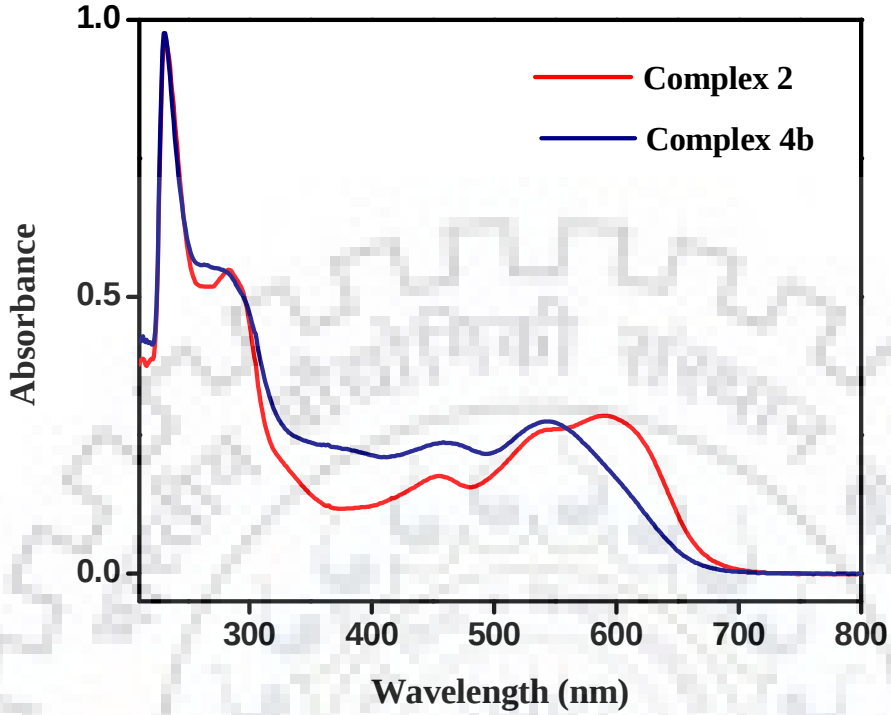

Fig. 2.22 Electronic absorption spectra of **2** and **4b** in dichloromethane solution.

2.4.6. Preparation of myoglobin stock solution

50 mM phosphate buffer solution of 6.8 pH was prepared by adding 0.4192 g of $NaH_2PO_4.2H_2O$ and 0.3283 g of anhydrous Na_2HPO_4 to 50 mL of MilliQ water and making the volume to 100 mL in a volumetric flask. 5 mg equine skeletal muscle myoglobin was dissolved in 5 mL of the above prepared buffer solution.

2.5. X–ray crystallography

Crystals of complex **3** and **4** (reddish) were obtained via layering of hexane over a solution of dichloromethane which were suitable for diffraction study. The X–ray data collection and processing for complexes **3** and **4** were performed with Bruker Kappa Apex–II CCD diffractometer by using graphite monochromated Mo–Kα radiation (λ =

0.71073 Å) at 273K. Crystal structures were solved by direct method. Structure solutions, refinement and data output were carried out with the SHELXTL program.[235,236] All non–hydrogen atoms were refined anisotropically. Hydrogen atoms were placed in geometrically calculated positions and refined using a riding model. Image was created with the DIAMOND program.[237]

2.6. Cell culture

The HeLa cells (human cervical cancer cell line) were maintained in a tissue culture incubator at 5% CO2, 37°C in high glucose Dulbecco's modified Eagle medium (DMEM) supplemented with 10% fetal bovine serum (Gibco, Thermo Fisher Scientific) and 100 U/ml penicillin-streptomycin (Gibco, Thermo Fisher Scientific). For all experiments cell lines were seeded into a 35 mm plate to achieve 30-50% confluency. All cells were routinely checked for mycoplasma contamination.

2.6.1. Cytotoxicity assay

The cyto-toxic effect of compunds was measured by MTT assay well-established cell viability 3-(4,5- dimethylthiazol-2-yl)-2,5-diphenyltetrazolium bromide (MTT) assay. . (SH1/2). To perform the assay, Hela cells were seeded at a density of 10^4 cells per well into 96-well plates in complete culture medium and allowed to grow for 12 hours to achieve 30-50% confluency. Cells were then treated with compounds dissolved in DMSO. In order to release NO from compounds, the media containing compounds and cells was irradiated with visible light for 10 minutes duration. Immediately after light exposure cells were incubated for 24 hours to the cell cuture incubator. After 24 hours of incubation, media was removed and cells were washed for one time with 500 ul sterile 1X PBS (137mM NaCl and 2.7 mM KCl). After that 100 ul solution A [composition of

solution A: 90 µl of fresh incomplete DMEM media and 10 µl of MTT (Sigma-Aldrich, USA) dye (5 mg ml^{-1} stock)] was added to each well and cells were incubated at 37^0C in cell culture incubator for 3-4 hours. The incubation of cells with solution A formed intracellular punctate purple precipitate can be seen under microscope. After incubation the solution A was carefully removed from each well and immediately 100 ul DMSO (Dimethyl sulfoxide) was added to solubilize the formazine crystals. The plate was again incubated for another 30 minutes in dark with gentle swirling after regular interval. The absorbance was measured using multimode reader (Cytation3, Biotek) at 570 nm and background control at 690 nM. All the assays were performed in triplicate. Cell viability was measured according to the absorbance by using the formula; Cell viability = (A570–A690) treated /(A570–A690) control × 100, A570 and A690 are the absorbance values obtained at 570 nm and 690 nm, respectively.

2.6.2. Determination of cell death using bright field microscopy

Around 2×10^5 Hela cells were seeded in 35 mm culture plates and the plates were kept in cell culture incubated for 12 hours to achieve 30-50 % confluency. The compounds dissoved in DMSO were then mixed with cells. To release NO from the compounds, visible light was exposed for 10 minutes to the cell culture plates inside laminar hood. To make residual compound (compound minus NO), the compound containing media (without any cell) was first irradiated with visible light for 10 minutes and then mixed with cells. The residual compound was used to see the effects of ruthenium metal toxicity on human cancer cells. The working concentration used for all the compound was 0.2 µM. After the incubation morphology and cell death was observed under bright field microscope, EVOS cell imaging system (Life Technologies, USA).

2.6.3. Acridine orange/ethidium bromide dual staining

To perform acridine orange and ethidium bromide (AO/EB) dual staining, Hela cells seeded at a concentration of around 2×10^5 in 35 mm culture plates and cells were allowed to grow for another 12 hours to get around 30-50 % confluency. Next cells were treated with compounds and incubated for 6 and 12 hours in cell culture incubator. After incubation, cells were washed with ice cold 1X PBS and stained with AO/EB fluorescent stain solution (working conc. 10 ug/ml) after incubation at 37°C for 10 min. Immediately after the incubation cells were washed two times with 1 X ice cold PBS to remove excess dye. Cells were then fixed using ice chilled 100 % methanol for 10 minutes at room temperature and then washed briefly with 1X PBS. Finally the cells were examined under EVOS cell imaging system (Life Technologies, USA). The above experiment was repeated three times.

2.6.4. Hoechst 33342 and Rhodamine B (Rho B) staining

To stain with Hoechst 33342 and Rhodamine B (Rho B) dyes, cell were grown and treated with the compounds as described previously. Next cells were washed with ice cold 1X PBS and treated with Hoechst 33342 (Life Technologies, USA) and Rhodamine B (Rho B) [2 µl Hoechst dye {stock conc: 10 mg ml−1} and 3 µl Rho B {stock conc: 1 mg ml−1}] for 10 minutes at room temperature. The excess stains was removed by washing with 1XPBS and images were taken using, EVOS cell imaging system (using specific excitation and emission wavelengths, Rho B at an excitation of 540 nm and emission of 625 nm and Hoechst 33342 dye at an excitation of 352 nm and emission of 460 nm). The above experiment was repeated thrice.

2.6.5. DNA fragmentation assay

Cells were grown and treated with the compounds as described in the previous section. After 12 hours incubation, genomic DNA was isolated using DNA easy blood and tissue kit (Qiagen) and subjected to gel electrophoresis in 0.6% agarose gel in 1XTBE buffer (90 mM Tris-borate/2 mM EDTA) at 70 Volts for 45- 60 minutes. Integrity of the isolated genomic DNA was compared with the control and the ethidium bromide stained gel image was captured in Gel documentation systems.

2.6.6. Anexin V assay and flow cytometry

The cells were treated with the compounds as described in previous section. After 6 hrs post treatment, cells were harvested by centrifugation at 2000 X g for 2 minutes at 4^0C. The cell pellet was washed three times with ice cols 1X PBS (2000 X g, 2 minutes s at 4^0C) and re-suspended in 1X annexin binding buffer (Invitrogen) to achieve around 1X 10^6 cells/ml. For each 100 µl of cell suspension 5 µl of Alexa fluor 488 annexin V and 1 µl Propidium Iodide (PI) (working solution conc. 100 µg/ml) was added. Next, cells were incubated at room temperature for 15 minutes and proceeded for flow cytometry (BD-FACS) .

2.6.7. Isolation of total RNA and Quantitative RT PCR

Total RNA was isolated using RNA-Xpress reagent (Himedia) as per protocol from the supplier. Quality and integrity of RNA was measured by gel electrophoresis in 1% agarose in 1X TBE. Isolated RNA was then proceeded for DNase treatment. The RNA volume 5 µl (2 µg/ul) was mixed with 1.5 µl of 10X DNase reaction buffer and lµ of DNase enzyme (invitrogen) in a 15 µl reaction mixture and then incubated at 37^0C for 30 minutes. The reaction was stopped by adding EDTA (final conc. 1mM) and incubating at

65^0C for 5 minutes. The DNA free RNA (0.5 µg) was then subjected for cDNA synthesis by Revert-aid First strand cDNA synthesis kit (Thermo Scientific) following manufacturer's protocol. The synthesized cDNA is used for PCR reaction. The following primers were used for RT-PCR analysis.

β-actin

Forward: 5'-CTGTCTGGCGGC ACCACCAT-3'

Reverse: 5'-GCAACTAAGTCATAGTCCGC -3'

Bax

Forward: 5'-AAGCTGAGCGAGMTCTCAAGC GC-3'

Reverse: 5'-TCCCGCCACAAAGATGGTC ACG-3'

Bc1-2

Forward: 5'-AGATGTCCAGCC AGCTGCACCTGAC-3'

Reverse: 5'-AGATAGGC ACCCAGGGTGATGC AAGCT-3'

Unprecedented cleavage of amide bond and spontaneous generation of stable aminyl radical coordinated to ruthenium: Spectroscopic characterization, X-ray crystal structure and theoretical calculations

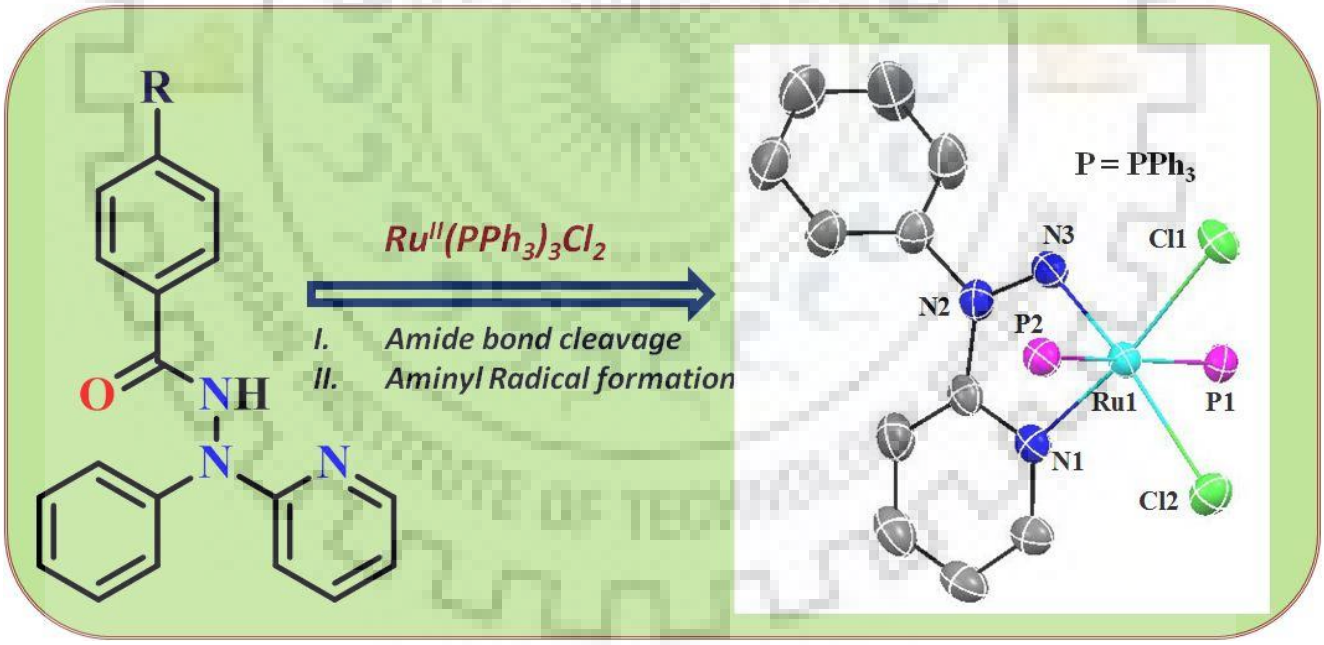

Abstract

Novel ruthenium(II) coordinated stable aminyl radical complex $[Ru(L^{5\cdot})(PPh_3)_2Cl_2]$ (**5**), was synthesized using ligands $L^{3\text{-}5}$. Cleavage of most stable amide bond and simultaneous production of nitrogen centred radical took place during the reaction course. Complex **5** was characterized by IR, UV-vis and EPR spectroscopic studies. Molecular structure of **5** was authenticated using single crystal X-ray crystallography. Along with spectroscopic characterization, theoretical calculations completely supported the nitrogen centred radical. The interaction of NO with the complex **5** afforded nitrosyl complex $[Ru(L^{5'})(PPh_3)_2(NO)Cl](ClO_4)$ (**6**). Molecular structure of the resultant nitrosyl complex **6** was authenticated by single crystal X–ray diffraction study. The photolability of coordinated NO was examined by using electronic absorption spectral studies under illumination of UV light.

3.1. Introduction

Formation of radicals is extremely important in catalytic cycle of several metalloenzymes. For example, generation of phenoxyl radical is crucial in catalytic cycle of galactose oxidase enzyme. This oxygen centred radical is formed in a post translationally modified tyrosine residue. It is well known in literature that carbon centred glycyl radical is important in catalytic cycle of pyruvate formase lyase. In biosystem, sulphur centred thiyl radical is involved in catalytic cycle of ribonucleotide reductases.[238] Among nitrogen centred radicals, aminyl radicals have received considerable current attention because of their similarity with phenoxyl radicals as both are isoelectronic. Aminyl radicals are relatively less stable due to their short life time and it is very difficult to isolate them. These are stabilized by coordination to an electron rich metal centre or an electron donating group is attached with lone pair of electron or extended conjugation. These radicals play an important role in various chemical transformations by abstracting hydrogen from organic substrates.[239,240]

First time, Grutzmacher and coworkers reported rhodium coordinated aminyl radical with the contribution of 57% spin density over the N donor atom.[2] Later on, Grutzmacher and coworkers also reported other aminyl radicals coordinated to rhodium, iridium and cobalt.[241-243] Recently, Thomas and coworkers also reported nickel and cobalt coordinated aminyl radical complexes.[240,244] Peters and coworkers also reported copper coordinated aminyl radical complexes.[245] However, very few reports are available on ruthenium coordinated aminyl radical complexes.[246-248] Herein, we report direct and one-pot synthesis of aminyl radical complex of ruthenium $[Ru(L^{5\cdot})(PPh_3)_2Cl_2]$ (**5**) (Scheme 3.2) in different ways using ligands L^{3-5} (Scheme 3.1). Complex **5** was characterized by various spectroscopic methods like IR, UV-vis and EPR spectral studies . Molecular structure of **5** was

authenticated using X-ray crystallography. Along with spectroscopic characterizations, theoretical calculations were also performed to address the location of electron in radical complex **5**.

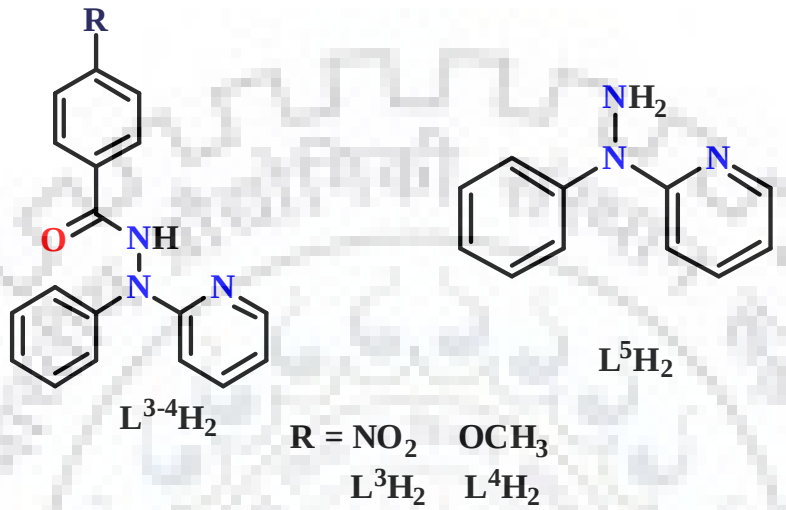

Scheme 3.1 Schematic drawing of ligands L^{3-5}.

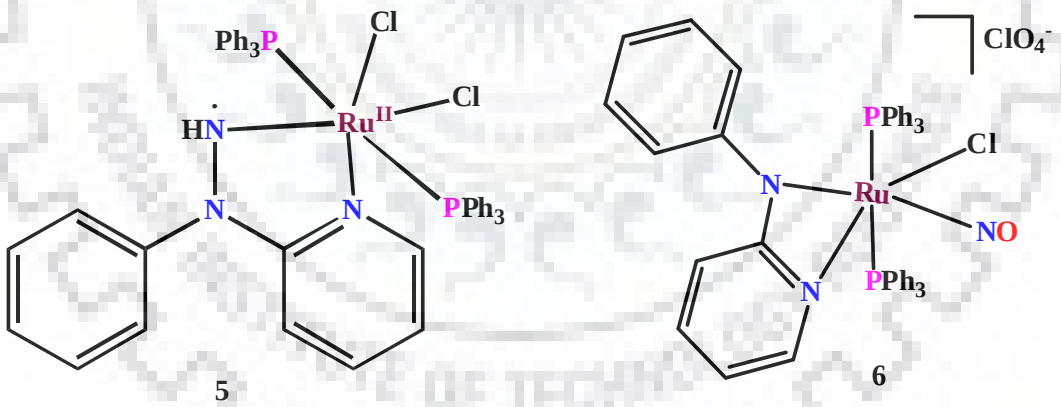

Scheme 3.2 Schematic drawings of ruthenium complexes **5** and **6**.

The interaction of NO with the complex **5** afforded the formation of nitrosyl complex $[Ru(L^{5'})(PPh_3)_2(NO)Cl](ClO_4)$ (**6**) (Scheme 3.2). Molecular structure of the resultant nitrosyl

complex **6** was authenticated by single crystal X–ray diffraction study. The photolability of coordinated NO was examined by using electronic absorption spectral studies under illumination of UV light.

3.2. Results and discussion

3.2.1. Syntheses and characterization of ruthenium complexes

Ligands L^3H_2 and L^4H_2 were obtained in high yield by condensation reaction of 4-nitrobenzoic acid and 4-methoxybenzoic acid with 2-(1-phenylhydrazinyl)pyridine respectively in dimethylformamide in the presence of 1-hydroxybenzotriazole (HOBT) and dicyclohexylcarbodiimide (DCC). $Ru(PPh_3)_3Cl_2$ was added to benzene solution (20 mL) of the ligands $L^{3\text{-}5}H_2$ to afford the complex $[Ru(L^{5\cdot})(PPh_3)_2Cl_2]$(**5**) (shown in Scheme 3.2). Complex **5** was green in color and highly soluble in dichloromethane, but insoluble in water. Dichloromethane solution of complex **5** was treated with acidified nitrite ($NaNO_2$) solution with continuous stirring for 2 h and color of solution turned to a greenish blue. Then, methanolic solution of $NaClO_4$ was added to above solution, as the counter anion. After complete evaporation of solvent, crystalline greenish blue colored nitrosyl complex **6** was obtained and it was found to be highly soluble in dichloromethane, dimethylsulfoxide.

In the IR spectrum of **6**, the N-O stretching frequency (ν_{NO}) was observed around 1821 cm^{-1}, which was expected for $\{Ru{-}NO\}^6$ species as reported in literature around 1820-1960 cm^{-1} for $\{Ru{-}NO\}^6$ species. [161,186,221-223] Peaks around 1091 cm^{-1} and 616 cm^{-1} (Table 3.1) clearly exhibited the presence of perchlorate as counter anion in the complex **6**. [214,58] In both the complexes **5** and **6**, the peaks in the range 743-749 cm^{-1}, 691-693 cm^{-1} and 512-519 cm^{-1} confirmed the presence of axial PPh_3 ligands (shown in Figure 3.1). [214-217,58,196]

Table 3.1 Data for IR spectral studies.

Complex	IR data (cm^{-1}, KBr pellets)		
	ν_{N-O}	ν_{ClO4}	ν_{PPh3}
5	-	-	743, 693, 519
6	1821	1091, 616	749, 691, 512

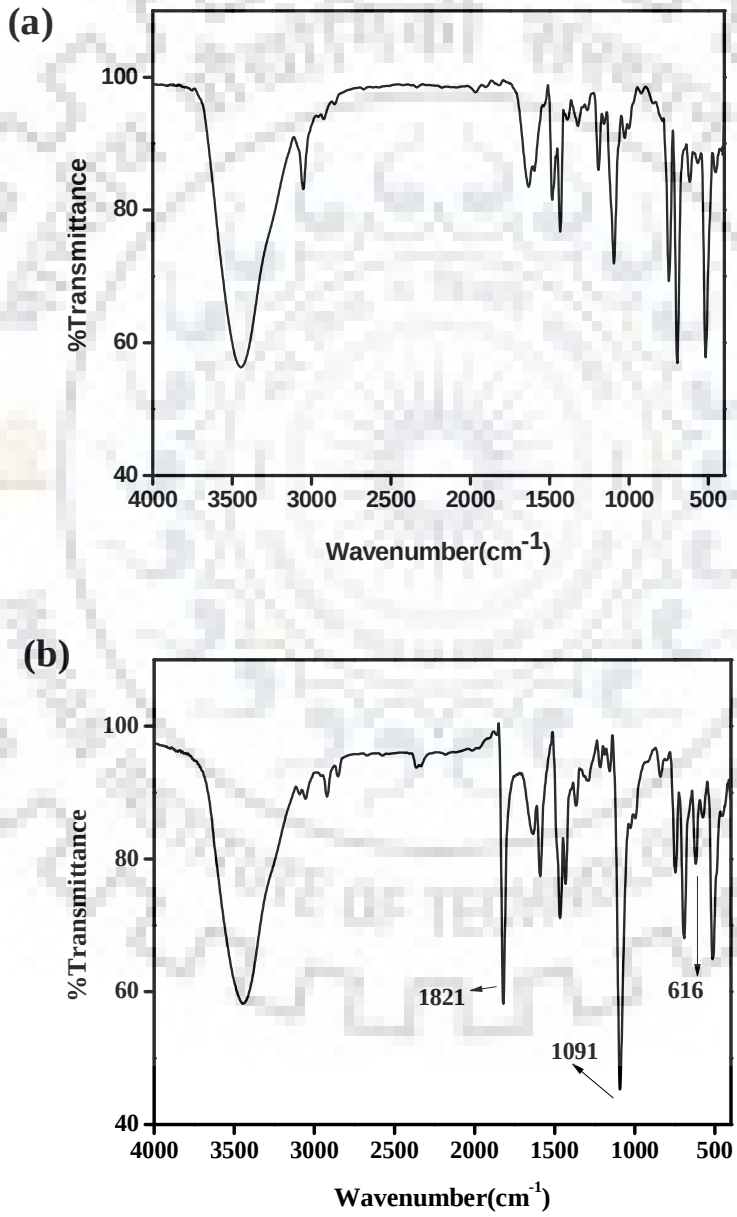

Fig. 3.1 Infrared spectra of complexes (a) **5** and (b) **6**.

The electronic absorption spectra of complexes **5** and **6** were displayed in Figure 3.2. In complex **5**, we observed bands with λ_{max} near 431, 695, 880 nm (Table 3.2) which were probably due to metal to ligand charge transfer transition (MLCT), mixed metal-ligand to ligand charge transfer (MMLLCT) transition and aminyl radical centered transition in NIR region.[248] In complex **6**, bands near 310, 592 nm were recognized to be metal to ligand charge transfer (MLCT) transition dπ(Ru)→π*(NO) type and this transition has been responsible for the photolability of the coordinated NO.[161,186,168,188]

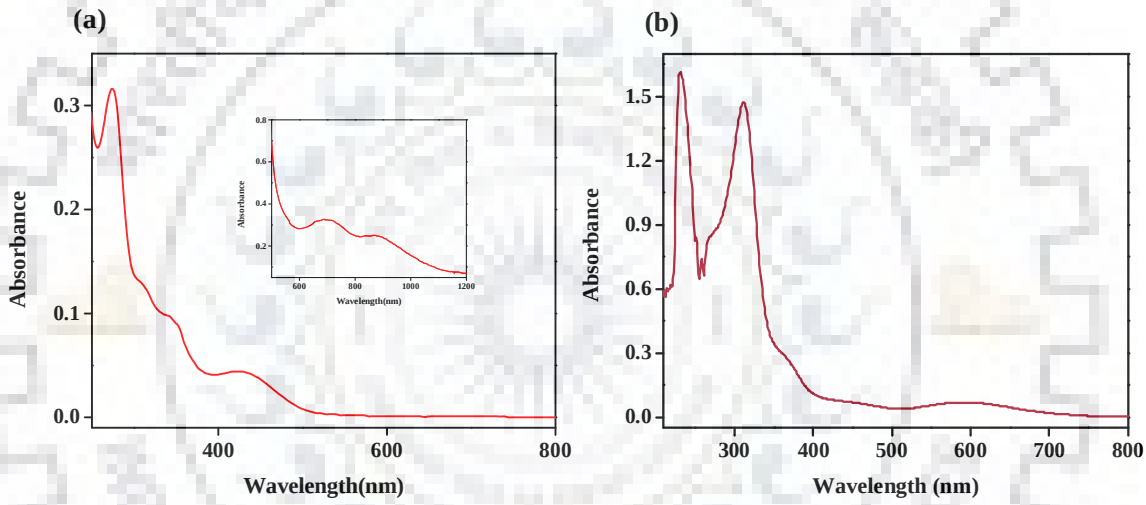

Fig. 3.2 Electronic absorption spectra of complexes (a) **5** and (b) **6** in dichloromethane solutions.

Table 3.2 Electronic spectral data for ruthenium complexes **5** and **6** in dichloromethane solutions.

Complex	λ_{max}/nm (ε / $M^{-1}cm^{-1}$)
5	311 (23529), 345 (17647), 431 (7843), 695 (1200), 880 (500)
6	231 (43223), 310 (39220), 592 (2134)

In the ligands (L^3H_2) and (L^4H_2), we observed peaks near 11.63 ppm and 11.16 ppm (Table 3.3), which were due to the presence of carboxamido (–CONH–) proton displayed in Figures 3.3 and 3.4 respectively. The ruthenium nitrosyl complex **6** was found to be diamagnetic which was confirmed by ^{1}H and ^{31}P NMR spectral studies. The ^{1}H and ^{31}P NMR spectra of **6** were displayed in Figures 3.5 and 3.6 respectively. We obtained single peak near 17.52 ppm for **6** in ^{31}P NMR spectrum corresponding to the presence of trans PPh_3 groups.[214-217,58,196]

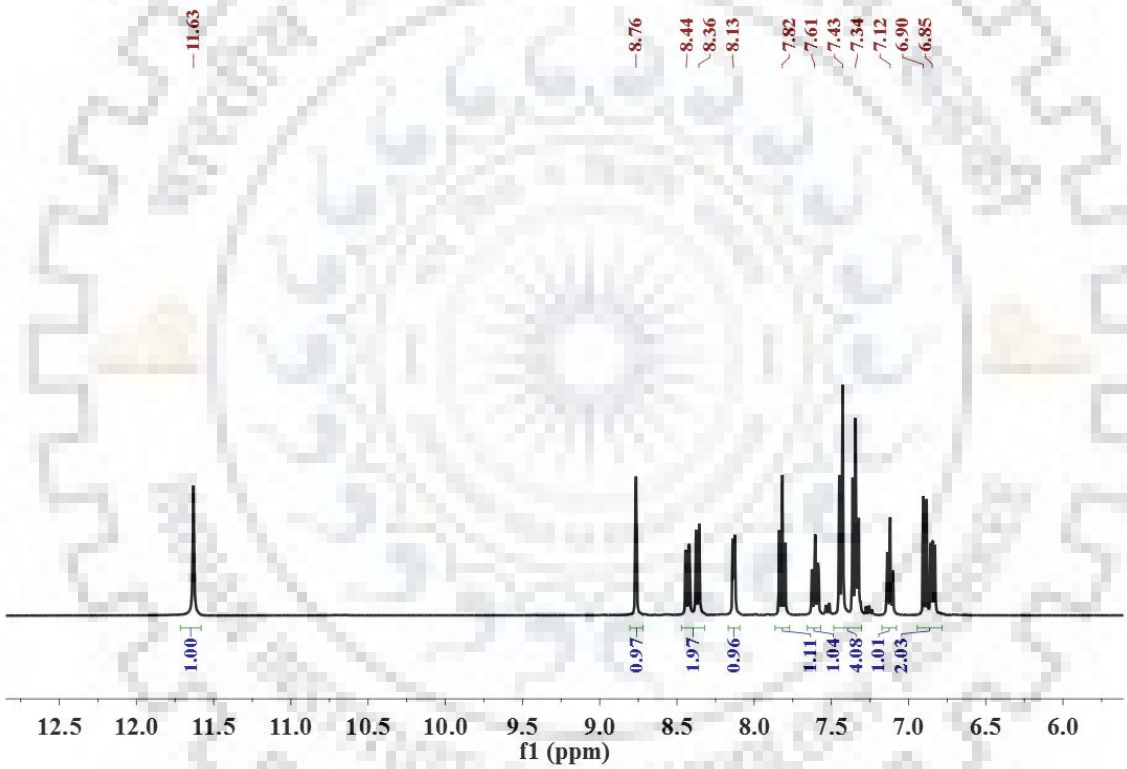

Fig. 3.3 ^{1}H NMR spectrum of ligand $\mathbf{L^3H_2}$ in DMSO-d_6 at room temperature.

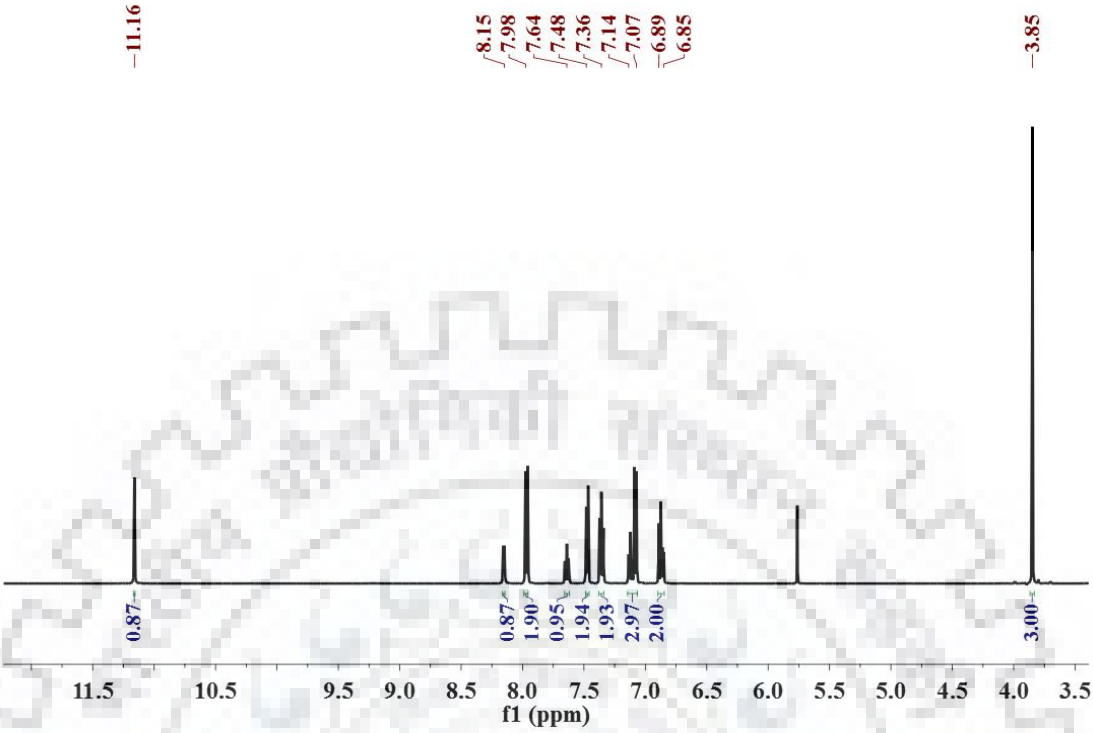

Fig. 3.4 ^{1}H NMR spectrum of ligand **L^{4}H$_2$** in DMSO-d$_6$ at room temperature.

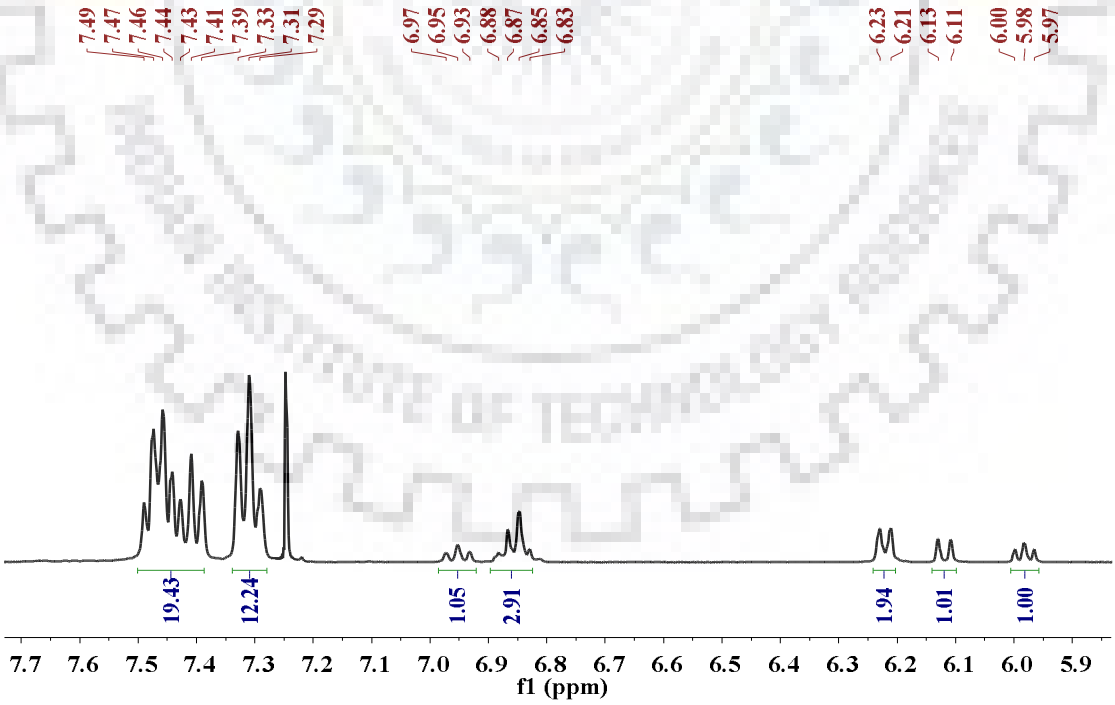

Fig. 3.5 ^{1}H NMR spectrum of complex **6** in CDCl$_3$ at room temperature.

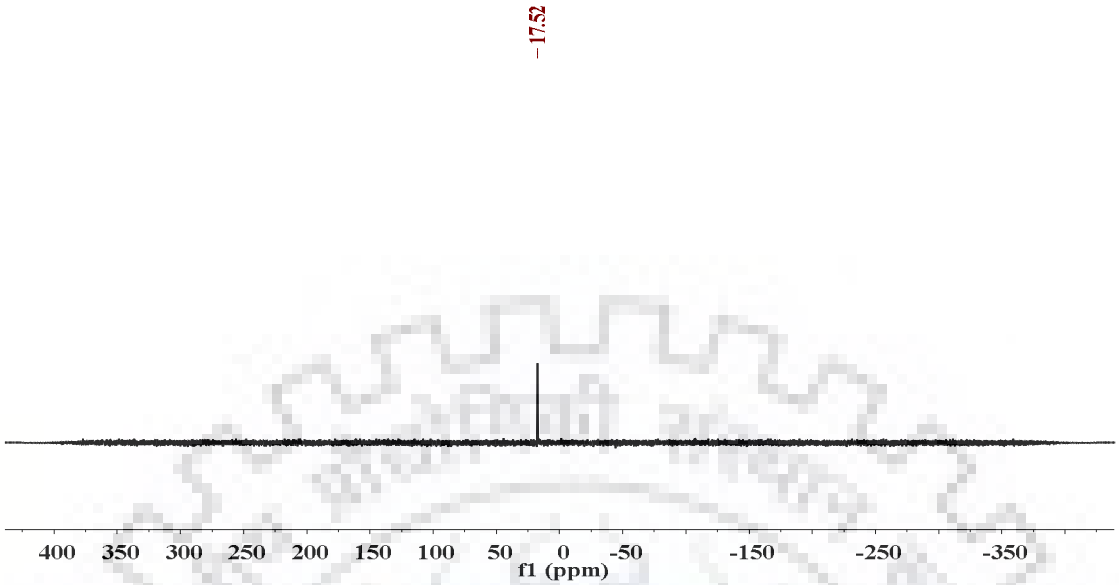

Fig. 3.6 ^{31}P NMR spectrum of complex **6** in $CDCl_3$ at room temperature.

Table 3.3 NMR spectral data for ligands $\mathbf{L^{3\text{-}4}H_2}$ and ruthenium nitrosyl complex **6**.

Complex	^{1}H NMR (δ /ppm)	^{31}P NMR (δ /ppm)
$\mathbf{L^3H_2}$	11.63 (s, 1H), 8.76(s, 1H), 8.36-8.44(m, 2H), 8.13 (d, 1H), 7.82 (t, 1H), 7.61 (t, 1H), 7.34-7.43 (m, 4H), 7.12 (t, 1H), 6.8-6.9 (m, 2H)	-
$\mathbf{L^4H_2}$	11.16 (s, 1H), 8.15(d, 1H), 7.98(d, 2H), 7.64 (t, 1H), 7.48 (d, 2H), 7.36 (t, 2H), 7.14-7.07 (m, 3H), 6.89-6.85 (m, 2H), 3.85 (s, 3H)	-
6	7.49-7.29 (m, 31H), 6.97-6.83 (m, 4H), 6.23 (d, 2H), 6.13 (d, 1H), 6.00 (t, 1H)	17.52

The EPR spectrum of complex **5** in CH_2Cl_2 solvent at room temperature exhibited a sharp signal at g = 2.146 (Figure 3.7). The shifting of g value away from the free radical value is in the support of the small contribution of the metal d orbital to the SOMO of complex **5** and the data was well corroborated with the reported literature.[248]

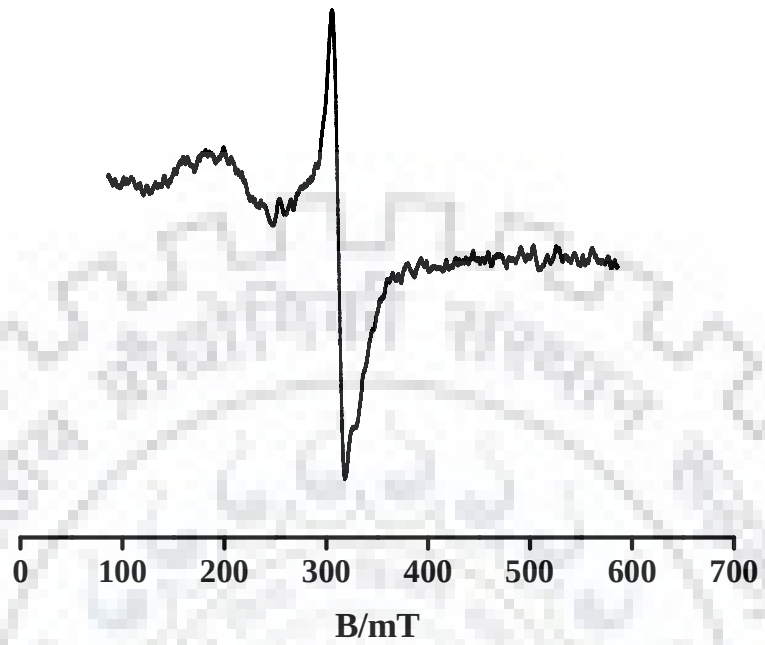

Fig. 3.7 X-Band EPR spectrum of complex $[Ru(L^{5\cdot})(PPh_3)_2Cl_2]$ (**5**) in dichloromethane at room temperature.

3.2.2. Description of molecular structures

The molecular structures of the complexes $[Ru(L^{5\cdot})(PPh_3)_2Cl_2]$(**5**) and $[Ru(L^{5'})(PPh_3)_2(NO)Cl](ClO_4)$(**6**) are depicted in Figure 3.8 and Figure 3.9 respectively.

In the crystal structure of **5**, the equatorial plane consisted of Cl(2), Cl(1), N(py) and N(hydrazyl). In the crystal structure of **6**, the equatorial plane consisted of Cl(1), N(py), $N_{(NO)}$ and N(hydrazyl). We observed that both the phosphine groups were trans to each other at axial positions which was supported by ^{31}P NMR spectral data. The ruthenium centre adopted a distorted-octahedral geometry as reflected in parameters given in Table 3.4. In the nitrosyl complex, $Ru–N_{(NO)}$ (1.741(6) Å), NO stretching frequency (ν_{NO}~1821 cm^{-1}) and N–O bond length were consistent with reported values.[58,171]

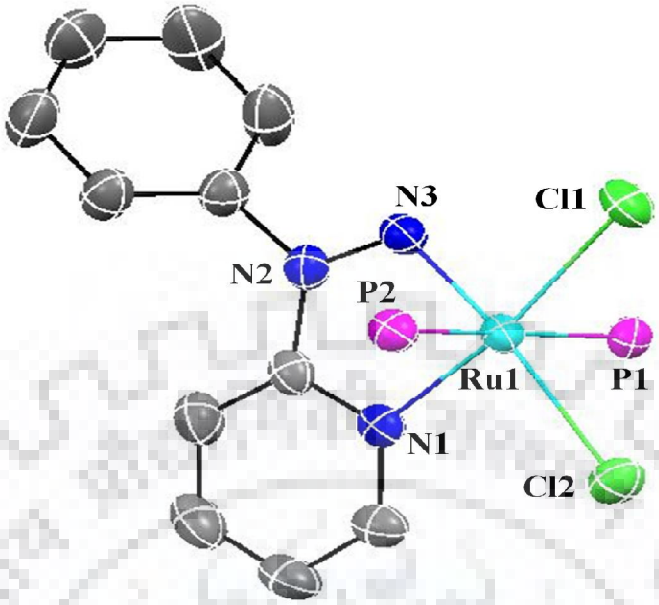

Fig. 3.8 ORTEP diagram (50% probability level) of the $[Ru(L^{5\cdot})(PPh_3)_2Cl_2]$ (**5**). All hydrogen atoms and PPh_3 groups have been omitted for clarity.

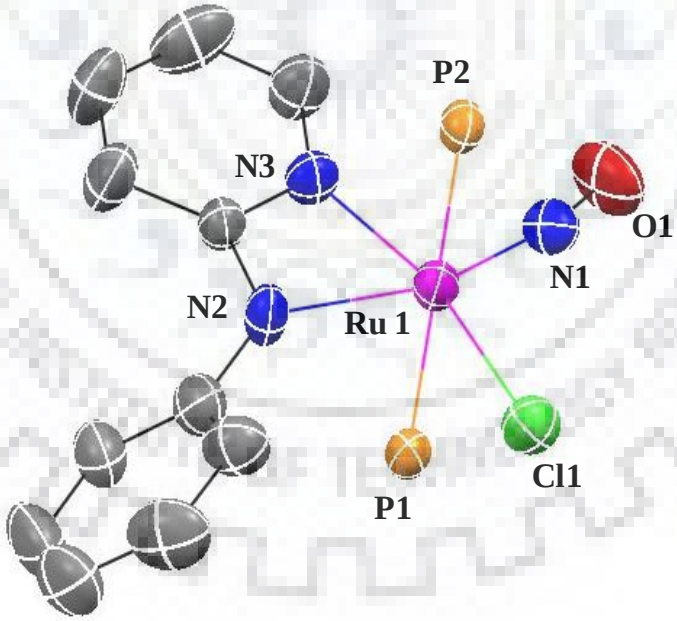

Fig. 3.9 ORTEP diagram (50% probability level) of the $[Ru(L^{5'})(PPh_3)_2(NO)Cl](ClO_4)$ (**6**). All hydrogen atoms, counter anion, PPh_3 groups and the crystallized solvent molecules have been omitted for clarity.

The selected bond lengths and bond angles of complexes **5** and **6** are given in Table 3.4. Crystal data collection and refinement details of the structures of complexes **5** and **6** are summarized in Table 3.5.

Table 3.4 Selected bond lengths (Å) and bond angles (deg.) of complexes **5** and **6**.

Bond lengths (Å)		Bond angles (°)	
		5	
Ru(1)−Cl(1)	2.417(2)	N(1)−Ru(1)−Cl(1)	171.26(5)
Ru(1)−Cl(2)	2.497(1)	N(1)−Ru(1)−N(3)	81.03(7)
Ru(1)−P(1)	2.403(1)	N(1)−Ru(1)−Cl(2)	92.17(5)
Ru(1)−P(2)	2.425(1)	P(1)−Ru(1)− P(2)	173.84(2)
N(2)−N(3)	1.318(3)	Cl(2)−Ru(1)− N(3)	173.10(6)
Ru(1)−N(3)	1.866(2)	Cl(2)−Ru(1)−Cl(1)	96.56(2)
Ru(1)−N(1)	2.050(2)	N(3)−Ru(1)−Cl(1)	90.24(6)
		6	
Ru(1)−Cl(1)	2.3695(19)	N(1)−Ru(1)−Cl(1)	102.1(2)
Ru(1)−N(3)	2.057(6)	N(1)−Ru(1)−N(3)	95.6(3)
Ru(1)−N(1)	1.741(6)	Ru(1)−N(1)−O(1)	166.1(7)
Ru(1)−P(1)	2.4533(19)	N(3)−Ru(1)−Cl(1)	161.98(18)
Ru(1)−P(2)	2.4626(19)	N(2)−Ru(1)−N(1)	158.9(3)
Ru(1)−N(2)	2.087(5)	P(1)−Ru(1)−P(2)	176.47(6)
N(1)−O(1)	1.162(8)	N(3)−Ru(1)−N(2)	63.4(2)

Table 3.5 Summary of crystal data and structural refinement parameters for complexes **5** and **6**.

	5	**6**
Empirical formula	$C_{47}H_{40}Cl_2N_3P_2Ru$	$C_{47}H_{39}Cl_2N_3O_5P_2Ru$
Formula weight	880.73	959.72
Temperature /K	293	296(2)
Λ (Å) (Mo-Kα)	0.71073	0.71073
Crystal system	monoclinic	monoclinic
Space group	P 21/n	P 21/n
a (Å)	13.0906(8)	16.1034(8)
b(Å)	18.1036(10)	15.0569(7)
c (Å)	17.6343(10)	19.8284(10)
α(°)	90	90
γ (°)	90	90
β(°)	102.367(2)	92.695(3)
V (Å^3)	4082.1(4)	4802.4(4)
Z	4	4
ρ_{calc} (gcm^{-3})	1.433	1.327
F(000)	1804	1960
Theta range	0.865−28.290	1.593−28.353
Index ranges	$-17< h< 17$, $-24< k< 24$, $-23< l< 23$	$-21<h< 21$, $-20<k< 18$, $-26<l< 25$
Data/restraints/par.	10142/0.0673/221	12017/0/542
GOF^a on F^2	1.034	1.225
$R1^b$ [$I > 2\sigma(I)$]	0.0673	0.1107
$R1$[all data]	0.0915	0.1825
$wR2^c$ [$I > 2\sigma(I)$]	0.1782	0.3057
$wR2$ [all data]	0.1782	0.3619

3.2.3. Photolysis experiment of nitrosyl complex

The nitrosyl complex **6** was found to be photolabile under UV light. The photolability of coordinated NO was examined by exposing dichloromethane solution of complex **6** under illumination of UV light (Figure 3.10). No change was observed in dark but in the presence of light we observed changes in the electronic absorption spectra of complex **6**. On the illumination of light on the solution of complex **6**, the peak intensities decreased near 595 and 306 nm and some new peaks increased near 420 nm. We also observed some isobestic points near 510 and 375 nm.

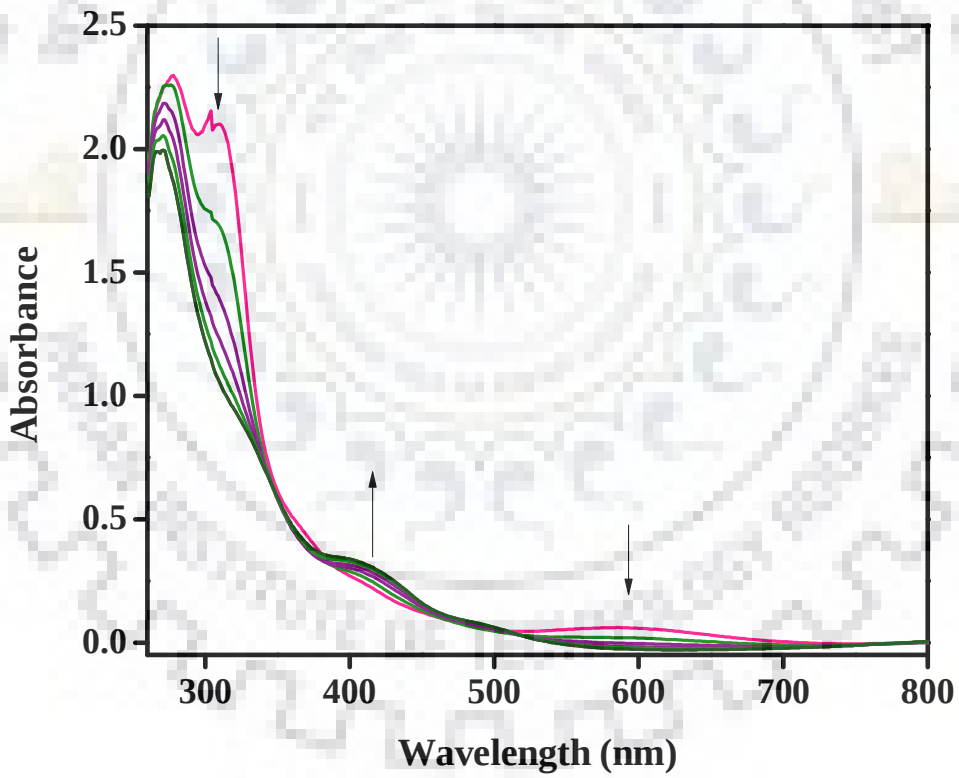

Fig. 3.10 Photocleavage of NO from complex **6** in dichloromethane solution under illumination of low intensity UV lamp (λ_{max}= 365 nm). Repetitive scans were taken in 2 min intervals.

3.2.4. Density functional theory (DFT) calculations

DFT calculation for complex **5** was performed at B3LYP level[249] using LANL2DZ basis set[250] for ruthenium metal and 6-31G(d) basis set for non metal atoms (C, H, N, P and Cl). The singly occupied molecular orbital (SOMO) of complex **5** was found to be located over the ligand (72%) along with minor contribution of metal centre (28%). Frontier molecular orbitals of **5** are shown in Figure 3.11.

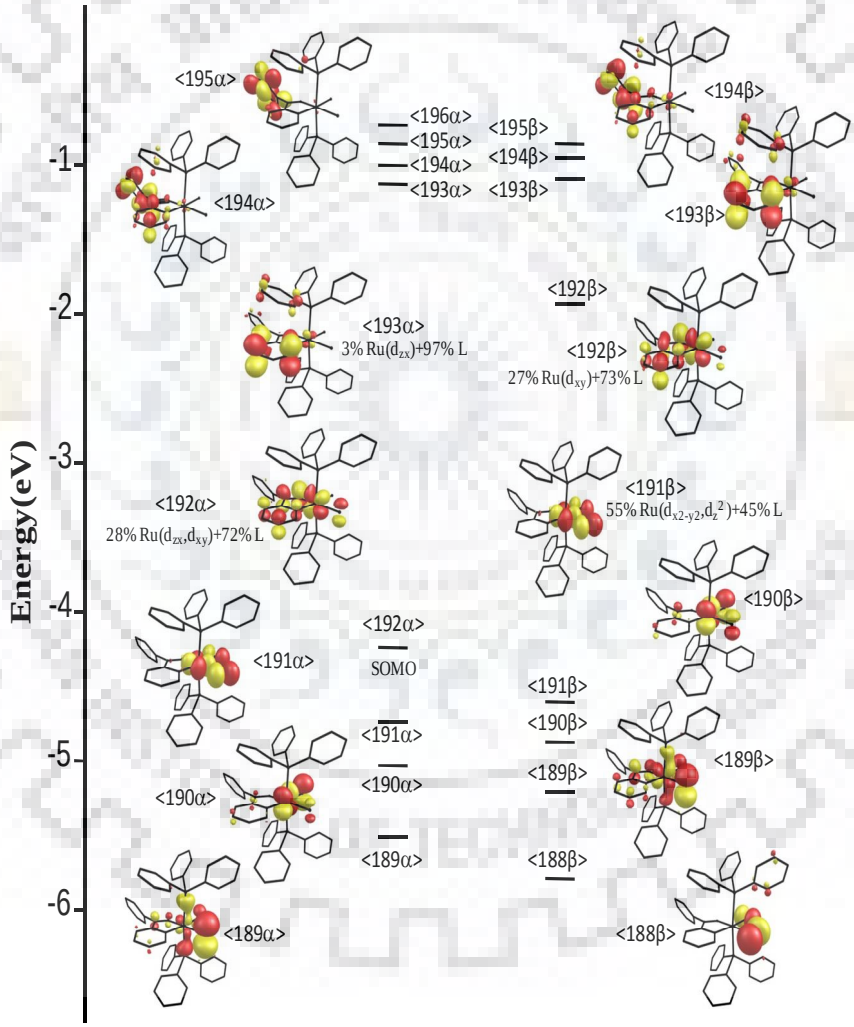

Fig. 3.11 Frontier molecular orbitals of **5**.

The time dependent DFT (TD-DFT) calculation was also carried out to investigate the electronic absorption spectrum of **5**. The bands appeared in the computed spectrum found to be closely related to that of experimental spectrum. The information obtained from the calculated electronic transitions, excitation energies (in eV), and oscillator strengths (*f*) was displayed in Table 3.6. In case of complex **5**, the absorption peaks calculated at 922, 436, 348, 313 and 300 nm were red shifted with respect to the experimental band at 880, 431, 345, 311 and 275 nm, respectively. Absorption peak near 624 nm was blue shifted to the experimental value 695 nm.

The Mulliken spin density plot also confirmed that the 44% spin density is resided over nitrogen and the rest is delocalized over the ligand (shown in Figure 3.12). However, 42% contribution was found from the metal d_{zx} orbital.

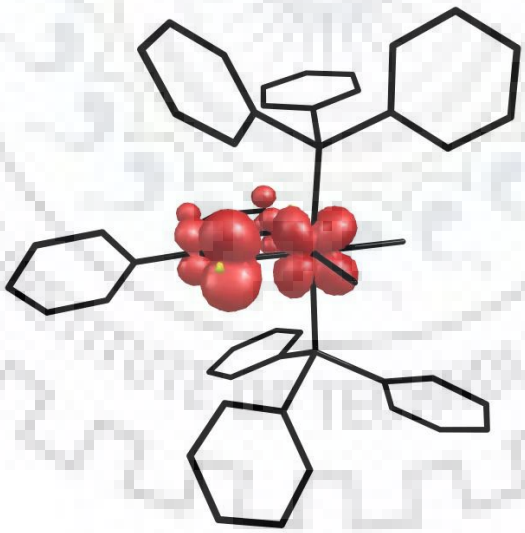

Fig. 3.12 Spin density distribution in complex **5**.

Table 3.6 Calculated TD-DFT excitation energies (in eV), oscillator strengths (*f*), and nature of transitions in the complex **5**.

Transition	λ(nm) Experimental	λ (nm) Theoretical	F (Oscillator strength)	Energy(ev)
HOMO-5(β) – LUMO(β) 11.28% HOMO-3(β) – LUMO(β) 8.22% HOMO-2(β) – LUMO(β) 11.40% HOMO-1(β) – LUMO(β) 69.08%	880	922	0.0012	1.3438
HOMO-1(α) – LUMO+1(α) 7.52% HOMO-1(α) – LUMO+2(α) 19.92% HOMO-1(α) – LUMO+14(α) 5.59% HOMO (β) – LUMO+3(β) 22.23%	695	624	0.0004	1.9871
HOMO-1(α) – LUMO+2(α) 10.95% HOMO (α) – LUMO+1 (α) 9.85% HOMO-3(β) – LUMO(β) 39.71% HOMO (β) – LUMO+3(β) 11.52%	431	436	0.0038	2.8381
HOMO (α) – LUMO+8 (α) 5.75% HOMO-11(β) – LUMO(β) 9.58% HOMO (β) – LUMO+4(β) 6.32%	345	348	0.0052	3.5575
HOMO-2(α) – LUMO+3(α) 10.64% HOMO-2(α) – LUMO+15(α) 6.75% HOMO-1(β) – LUMO+6(β) 8.51% HOMO-1(β) – LUMO+18(β) 7.02%	311	313	0.0094	3.9528
HOMO (α) – LUMO+14 (α) 15.77% HOMO-13(β) – LUMO (β) 13.51% HOMO-14(β) – LUMO (β) 11.35%	275	300	0.0138	4.1204

3.3. Conclusions

Following are the major findings and conclusions of the present study. First, novel ruthenium(II) coordinated stable aminyl radical complex $[Ru(L^{5\cdot})(PPh_3)_2Cl_2]$(**5**), was synthesized and characterized by different spectroscopic studies. Second, nitric oxide reactivity studies afforded ruthenium nitrosyl complex $[Ru(L^{5'})(PPh_3)_2(NO)Cl](ClO_4)$ (**6**) which was characterized by different spectroscopic methods. The molecular structures of **5** and **6** were determined by X-ray crystallography. Third, the coordinated NO was found to be photolabile under UV light. Theoretical calculations were performed using complex **5** to better understand the electronic properties.

3.4. Experimental section

3.4.1. Reagents and materials

Analytical grade reagents 4-nitrobenzoic acid, 4-methoxybenzoic acid, sodium perchlorate monohydrate, sodium nitrite (Himedia Laboratories Pvt. Ltd., Mumbai, India) were used as obtained. $RuCl_3.3H_2O$ was purchased from Loba Chemie Pvt. Ltd., Mumbai, India. Triphenylphosphine (SRL,Mumbai, India). The precursor $[Ru(PPh_3)_3Cl_2]$ and 2-(1-phenylhydrazinyl)pyridine were prepared by following the procedure reported earlier.[233,251] Infrared spectra were obtained as KBr pellets with Thermo Nicolet Nexus FT–IR spectrometer, using 16 scans and were reported in cm^{-1}. Electronic absorption spectra of the complexes were recorded in dichloromethane solvent with an Evolution 600, Thermo Scientific (Shimadzu) UV–vis spectrophotometer. ^1H and ^{31}P NMR spectra were recorded on JEOL, 400 MHz spectrometer in the deuterated solvents.

3.4.2. Preparation of ruthenium complexes

Caution: Perchlorate salts of metal complexes with organic ligands are potentially

explosive. Only a small amount of material should be prepared and handled carefully.

3.4.2.1. Synthesis of 4-nitro-N'-phenyl-N'-(pyridine-2-yl)benzohydrazide (L^3H_2)

The 4-nitrobenzoic acid (5.0 mmol) was taken in 15-20 mL dimethylformaide solution and then cooled on an ice bath. To this solution, 1.48 g (11.0 mmol) of 1-hydroxybenzotriazole (HOBT) as well as 1.13 g (5.5 mmol) of dicyclohexylcarbodiimide (DCC) were added directly and mixture was stirred for half an hour at 0°C. Now a batch of 2-(1-phenylhydrazinyl)pyridine(5.0 mmol) was added to the reaction mixture with stirring for next 2 hours on the same ice bath. After, the ice bath was removed and the stirring was continued overnight at room temperature. By removing the white precipitate of N,N′-dicyclohexylurea through filtration, the solvent was concentrated to 10 mL. Within 3-4 days, a light yellowish crystalline solid of ligand L^3H_2 was settled down on the bottom of beaker which was filtered and washed with methanol and diethyl ether. ^{1}H NMR (DMSO-d_6, 400 MHz): δ 11.63 (s, 1H), 8.76(s, 1H), 8.36-8.44(m, 2H), 8.13 (d, 1H), 7.82 (t, 1H), 7.61 (t, 1H), 7.34-7.43 (m, 4H), 7.12 (t, 1H), 6.8-6.9 (m, 2H) ppm.

3.4.2.2. Synthesis of 4-methoxy-N'-phenyl-N'-(pyridin-2-yl)benzohydrazide (L^4H_2)

Ligand (L^4H_2) was synthesized by reaction of 4-methoxybenzoic acid with 2-(1-phenylhydrazinyl)pyridine following the same procedure as used for ligand L^3H_2. ^{1}H NMR (DMSO-d_6, 400 MHz): δ 11.16 (s, 1H), 8.15(d, 1H), 7.98(d, 2H), 7.64 (t, 1H), 7.48 (d, 2H), 7.36 (t, 2H), 7.14-7.07 (m, 3H), 6.89-6.85 (m, 2H), 3.85 (s, 3H) ppm.

3.4.2.3. Synthesis of $[Ru(L^{5\cdot})(PPh_3)_2Cl_2]$ (5)

A batch of $Ru(PPh_3)_3Cl_2$ (0.1 mmol) was added to a benzene solution (20 mL) of $L^{3\text{-}5}H_2$ (0.15 mmol) and the mixture was refluxed for 4 h at 85 °C with continuous stirring. It was then cooled to room temperature. The green solid was filtered out and washed thoroughly

with methanol and diethyl ether and then dried. UV–vis (CH_2Cl_2; λ_{max}/nm (ε,$M^{-1}cm^{-1}$)): 311 (23529), 345 (17647), 431 (7843), 695 (1200), 880 (500).

3.4.2.4. Synthesis of $[Ru(L^{5'})(PPh_3)_2(NO)Cl](ClO_4)$ (6)

A batch of (0.1 mmol) of complex **5** was taken in 20mL of dichloromethane to obtain a greenish colored solution in round bottom flask of 100 mL. Now 20 mL acidified distilled water was layered over this solution. Sodium nitrite (0.3 g, 4.3 mmol) was added to the bilayer solution and the mixture was stirred at room temperature for 2 hrs to get greenish-blue colored solution of complex **6**. The dichloromethane layer was separated out and $NaClO_4$ (in excess) with 10 mL of methanol was added to this solution. Stirring of this solution was continued for another 2 hrs. The solvent mixture was evaporated and crystalline greenish-blue complex **6** was isolated. IR (KBr disk, cm^{-1}): 1821 (ν_{NO}), 1091, 616 (ν_{ClO4}). UV-vis (CH_2Cl_2; λmax, nm (ε, $M^{-1}cm^{-1}$)): 231 (43223), 310 (39220), 592 (2134). ^1H NMR ($CDCl_3$, 400MHz): δ 7.49-7.29 (m, 31H), 6.97-6.83 (m, 4H), 6.23 (d, 2H), 6.13 (d, 1H), 6.00 (t, 1H) ppm.^{31}P NMR (chloroform-d, 400 MHz): δ 17.52 ppm.

3.4.3. X–ray crystallography

Crystals of complexes **5** and **6** were obtained via layering of hexane over a solution of dichloromethane which was suitable for diffraction study. The X–ray data collection and processing for complexes **5** and **6** were performed with Bruker Kappa Apex–II CCD diffractometer by using graphite monochromated Mo–Kα radiation (λ = 0.71073 Å) at 273K. Crystal structures were solved by direct method. Structure solutions, refinement and data output were carried out with the SHELXTL program.[235,236] All non–hydrogen atoms were refined anisotropically. Hydrogen atoms were placed in geometrically calculated positions and refined using a riding model. Image was created with the DIAMOND program.[237]

Naphthyl C8-H hydrogen activation and synthesis of organometallic ruthenium complex: Crystal structure of hydride intermediates and catalytic transfer hydrogenation

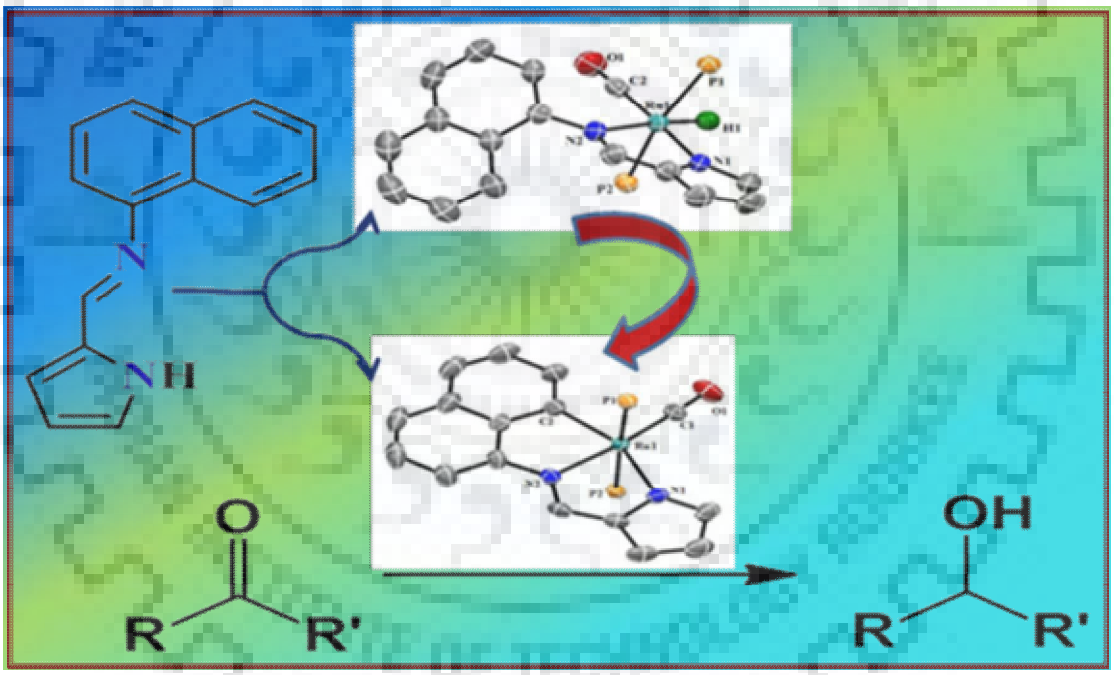

Abstract

Organometallic ruthenium(II) complex [Ru(L^6C^N^N)(PPh_3)$_2$(CO)] (**7**) [where L^6H_2 is (E)-N-((1H-pyrrol-2-yl)methylene)naphthalen-1-amine] [H represents dissociable proton] was synthesized via C-H bond activation using different synthetic strategies. Ruthenium hydrido carbonyl complexes [Ru(L^6N^N)(PPh_3)$_2$(CO)H] (**8**) [where L^6H_2 is (E)-N-((1H-pyrrol-2-yl)methylene)naphthalen-1-amine] and [Ru(L^7N^N)(PPh_3)$_2$(CO)H] (**9**) [where L^7H_2 is (E)-N-((1H-pyrrol-2-yl)methylene)-1-phenylmethanamine] were isolated. All the complexes were characterized by UV-Vis, IR and NMR spectral studies. Molecular structures of complexes **7**, **8** and **9** were authenticated using X-ray crystallography. Geometry optimization of the complexes **7–9** have been performed using Density Functional Theory (DFT) studies. Time-dependent DFT calculations were performed to better understand the electronic properties of complexes **7–9**. Complex **7** was utilized as catalyst in transfer hydrogenation of ketones. On the basis of literature study, the plausible mechanisms were proposed for hydride formation and catalytic transfer hydrogenation. Coordinated CO in organometallic ruthenium carbonyl complex **7** was found to be photolabile upon visible light illumination.

4.1. Introduction

Cyclometalation, one of the most convenient methods for synthesis of organometallic entities, has gained significant current interest probably because of mildest route followed for activation of strong C-H bonds.[34] The chemistry of organometallic compounds has become fast grown area in the field of chemical research because of vast applications of these complexes in catalysis, organic transformation , bioorganometallic chemistry, photophysical devices etc.[34] Our recent reports[58,196,214,216,217] on ruthenium organometallics clearly indicated the necessity of at least one hard donor present in the bidentate ligand frame to synthesize cyclometalated ruthenium complexes, but none of the report describes the naphthyl C8-H bond activation. However, only few reports are available in literature on naphthyl C-H activation using ruthenium complexes[252-259] and it still remains the challenging area of chemical research.

It is well known that hydrides are reactive intermediates or catalysts in various chemical reactions.[260] Both, the laboratory and industrial applications of transition metal hydrides including hydrogenation, catalytic and stoichiometric transformations, olefin isomerization and hydroformylation reactions, electrochemical H_2 evolution, reduction of CO_2 to carbon-based fuels, have made their chemistry an important area of research.[261] These prompted us to investigate the chemistry of ruthenium hydride complexes.

From literature study, it was found that deprotonated pyrrole nitrogen is a hard donor and stabilizes metal in higher oxidation state.[262,263] This encouraged us to synthesize ligands L^6H_2 and L^7H_2 (shown in Scheme 4.1).

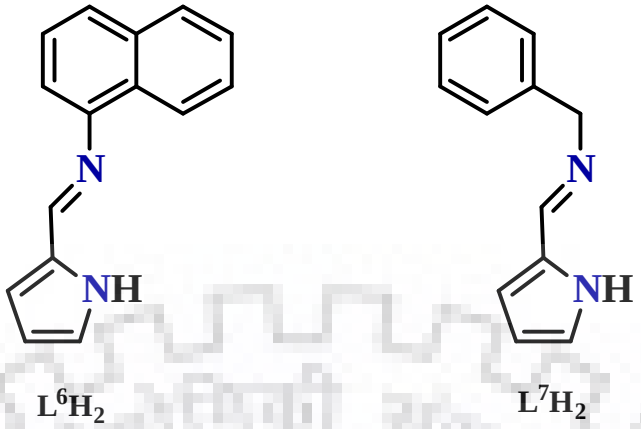

Scheme 4.1 Ligands $\mathbf{L^6H_2}$ and $\mathbf{L^7H_2}$.

In the present report, we describe the syntheses and spectral characterization of organometallic ruthenium(II) complex $[Ru(L^6C^\wedge N^\wedge N)(PPh_3)_2(CO)]$ (**7**) (shown in Scheme 4.2) and ruthenium hydrido carbonyl complexes $[Ru(L^6N^\wedge N)(PPh_3)_2(CO)H]$ (**8**) [where L^6H_2 is (E)-N-((1H-pyrrol-2-yl)methylene)naphthalen-1-amine] and $[Ru(L^7N^\wedge N)(PPh_3)_2(CO)H]$ (**9**) [where L^7H_2 is (E)-N-((1H-pyrrol-2-yl)methylene)-1-phenylmethanamine] [H represents dissociable proton] (shown in Scheme 4.2). Complex **7** was utilized for transfer hydrogenation of ketones. Geometries of **7**, **8** and **9** were authenticated using X-ray crystallography.

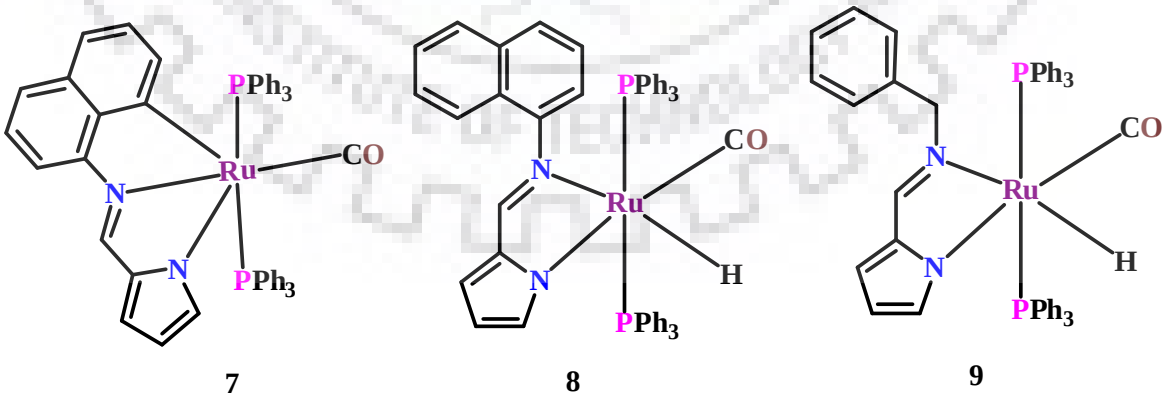

Scheme 4.2 Complexes **7**, **8** and **9**.

4.2. Results and discussion

4.2.1. Syntheses and characterization of ruthenium complexes

Ligands L^6H_2 and L^7H_2 were obtained by condensation reaction of pyrrole-2-carbaldehyde with naphthalene-1-amine and phenylmethanamine, respectively, in 20 mL methanol with continuous stirring. Complex $[Ru(L^6C^\wedge N^\wedge N)(PPh_3)_2(CO)]$ (**7**) was synthesized in two different ways (shown in Scheme 4.3). The complexes $[Ru(L^6N^\wedge N)(PPh_3)_2(CO)H]$ (**8**) and $[Ru(L^7N^\wedge N)(PPh_3)_2(CO)H]$ (**9**) were synthesized (shown in Scheme 4.3) by the reaction of $Ru(PPh_3)_3Cl_2$ in methanol and triethylamine with the Schiff base ligands L^6H_2 and L^7H_2 (shown in Scheme 4.1), respectively. Plausible mechanism for the syntheses of complexes **7** and **8** (shown in Scheme 4.4) is in accordance with reported literature.[254-257,52] Complex **9** was formed in a similar way as for complex **8**. All the complexes were soluble in dichloromethane and dimethylsulfoxide.

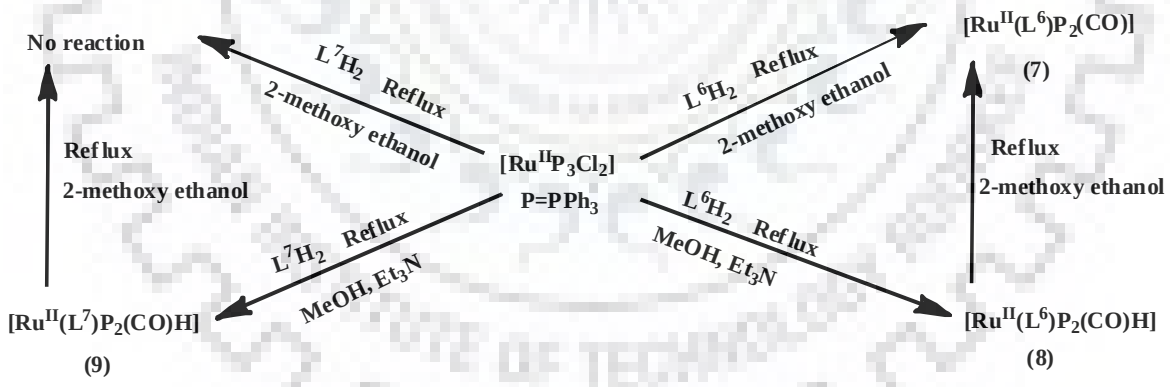

Scheme 4.3 Synthetic routes of complexes **7**, **8**, and **9**.

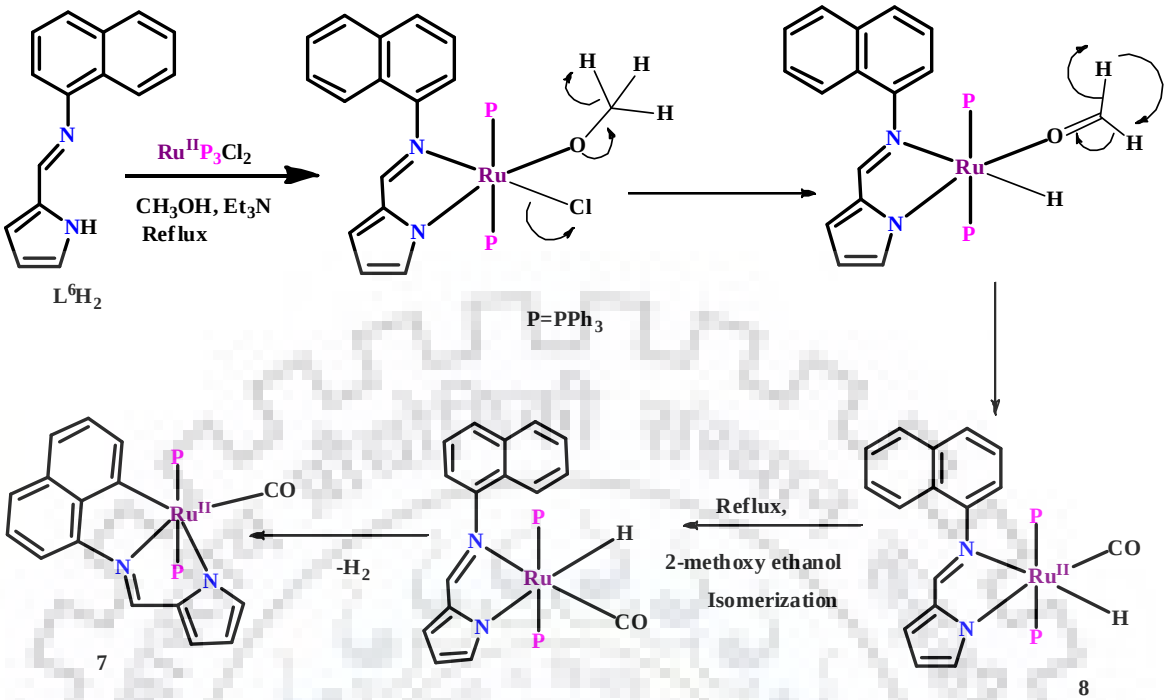

Scheme 4.4. Plausible mechanism for the syntheses of complexes **7** and **8**.

In the IR spectra of complexes **7-9**, the C-O stretching frequency (ν_{CO}) was observed around 1910-1920 cm^{-1}.[254-257,52] In all the complexes **7-9**, the peaks in the range 745-750 cm^{-1}, 690-695 cm^{-1} and 514-520 cm^{-1} confirmed the presence of axial PPh_3 ligands (Table 4.1).[254-257,52] The infrared spectra of complexes **7**, **8** and **9** are shown in Fig. 4.1.

Table 4.1 Data for IR spectral studies.

Complex	IR data (cm^{-1}, KBr pellets)		
	$\nu_{C=N}$	ν_{CO}	ν_{PPh3}
7	1588	1913	753, 692, 520
8	1555	1924	744, 695, 517
9	1586	1910	743, 693, 519

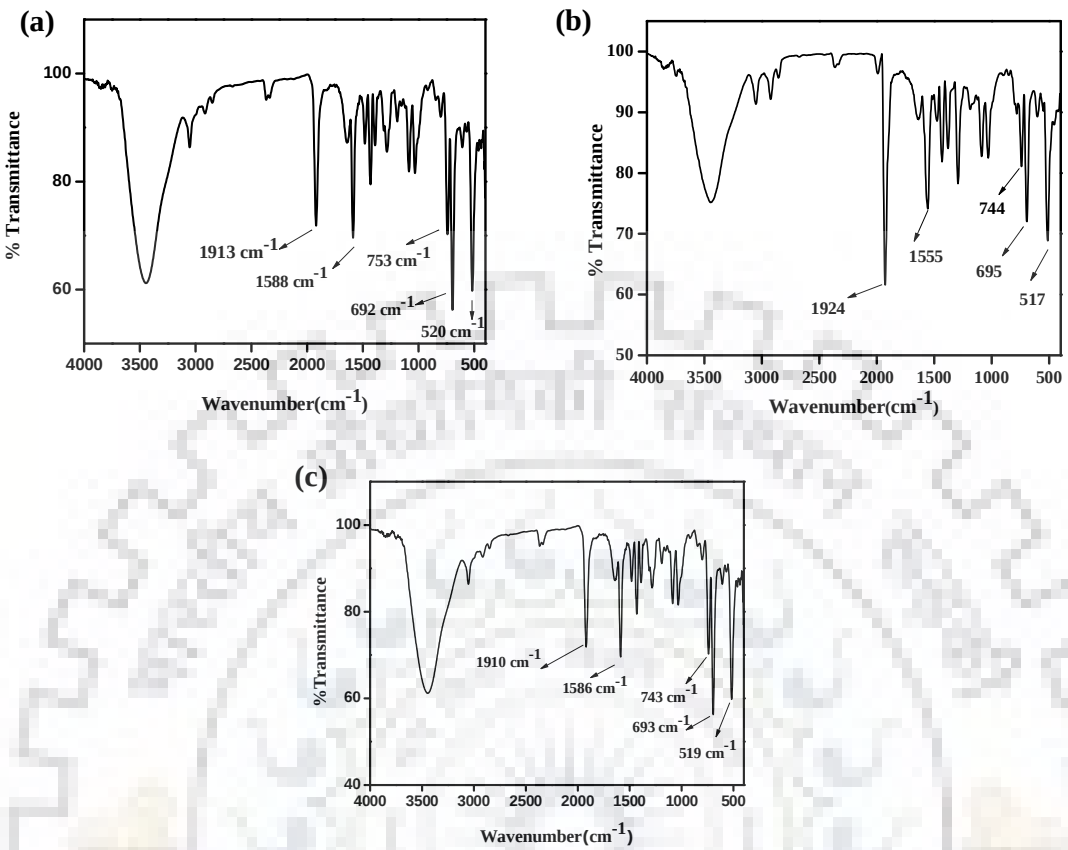

Fig. 4.1 Infrared spectra of ruthenium(II) carbonyl complexes (a) **7**, (b) **8** and (c) **9**.

The electronic absorption spectra of complexes **7-9** were displayed in Fig. 4.2 and Fig. 4.3 respectively. In complex **7**, band near 275 nm probably due to ligand centred charge transfer transition was observed and bands at 405 nm, 485nm, 517nm were recognized to be metal to ligand charge transfer (MLCT) transition. In complex **8**, we observed a band with λ_{max} near 239 nm probably due to ligand centred charge transfer transition and a band with λ_{max} near 397nm which was probably due to metal to ligand charge transfer (MLCT) transition. In complex **9**, a band with λ_{max} near 338 nm was recognized to be metal to ligand charge transfer (MLCT) transition. Electronic absorption spectral data of ligands and all the complexes were shown in (Table 4.2).

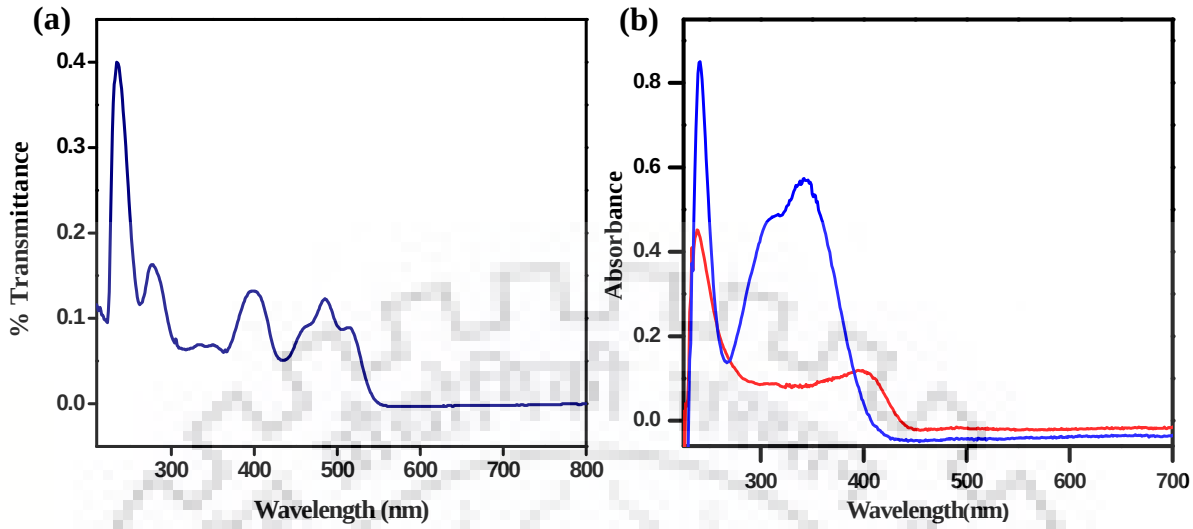

Fig. 4.2 Electronic absorption spectra of (a) complex **7** and (b) $\mathbf{L^6H_2}$ (—) and **8** (—) in dichloromethane solutions.

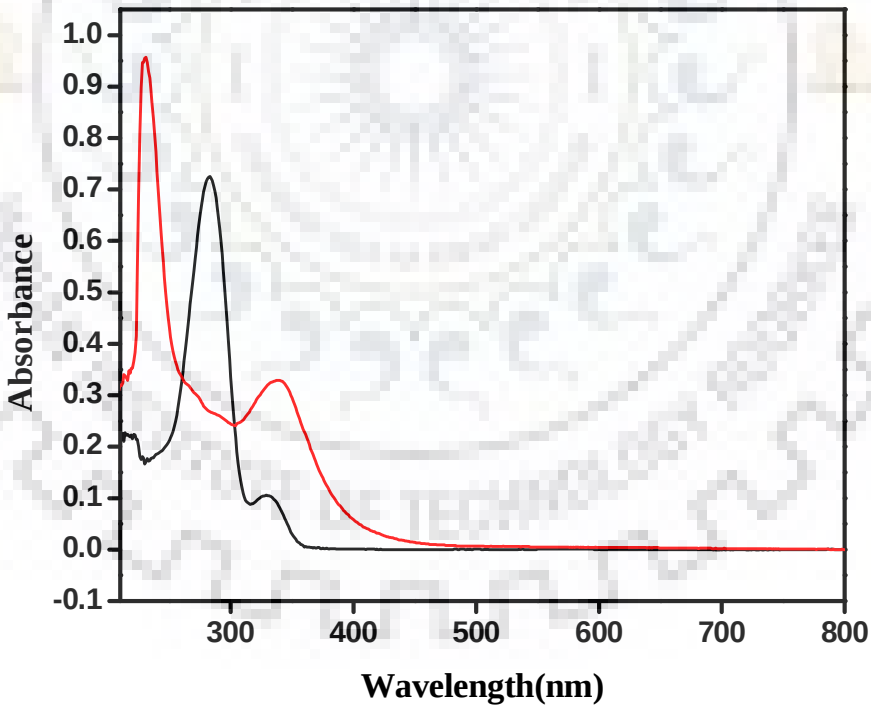

Fig. 4.3 The electronic absorption spectra of $\mathbf{L^7H_2}$ (—) and **9** (—) in dichloromethane solutions.

Table 4.2 Data for electronic absorption spectral studies.

Complex	λ_{max}/nm (ε / $M^{-1}cm^{-1}$)
L^6H_2	241 (69,900), 341 (47,600)
L^7H_2	282 (1,47000), 330 (22494)
7	275 (40,000), 405 (23,330), 485 (20,000), 517 (16,660)
8	239 (13812), 397 (3500)
9	230 (100,000), 338 (34,659)

In the ligands (L^6H_2) and (L^7H_2), we observed peaks near 10.11 ppm and 11.41 ppm respectively, which were due to the presence of pyrole (–NH–) proton (Fig. 4.4 and Fig. 4.5). All the complexes were confirmed to be diamagnetic by ^{1}H NMR spectral studies (Table 4.3). The ^{1}H NMR spectra of **7** and **8** were displayed in Fig. 4.6 and Fig. 4.7 respectively.

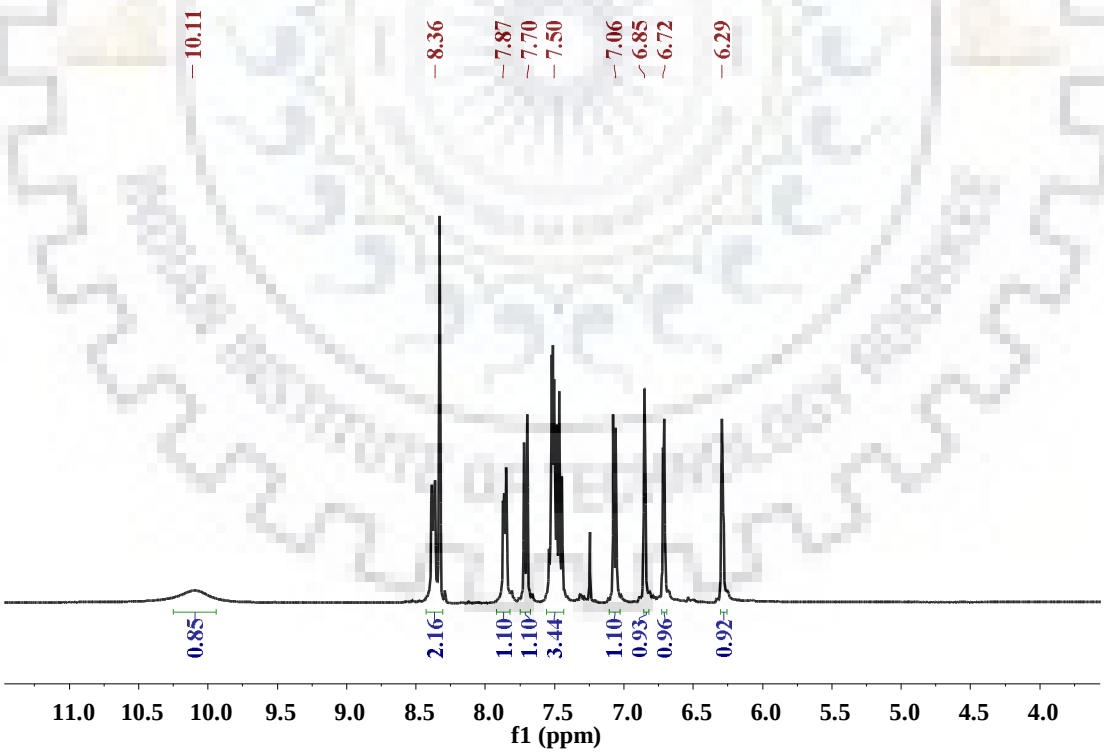

Fig. 4.4 ^{1}H NMR spectrum of ligand $\mathbf{L^6H_2}$ in $CDCl_3$ at room temperature.

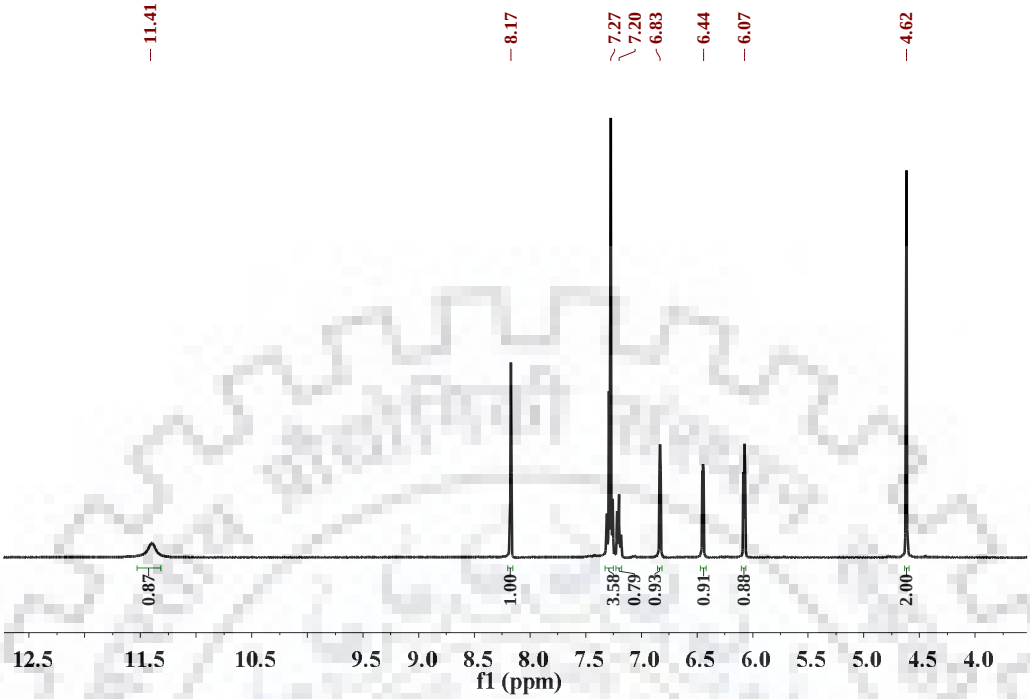

Fig. 4.5 ^{1}H NMR spectrum of ligand $\mathbf{L^7H_2}$ in DMSO-d_6 at room temperature.

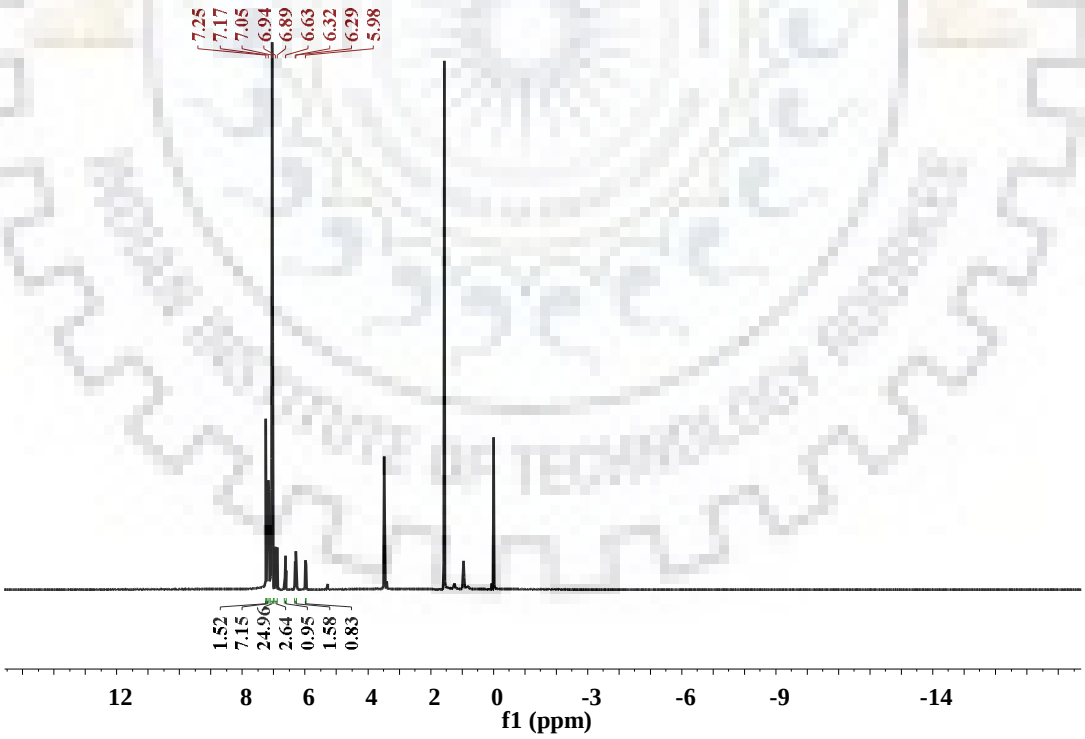

Fig. 4.6 ^{1}H NMR spectrum of complex **7** in $CDCl_3$ at room temperature.

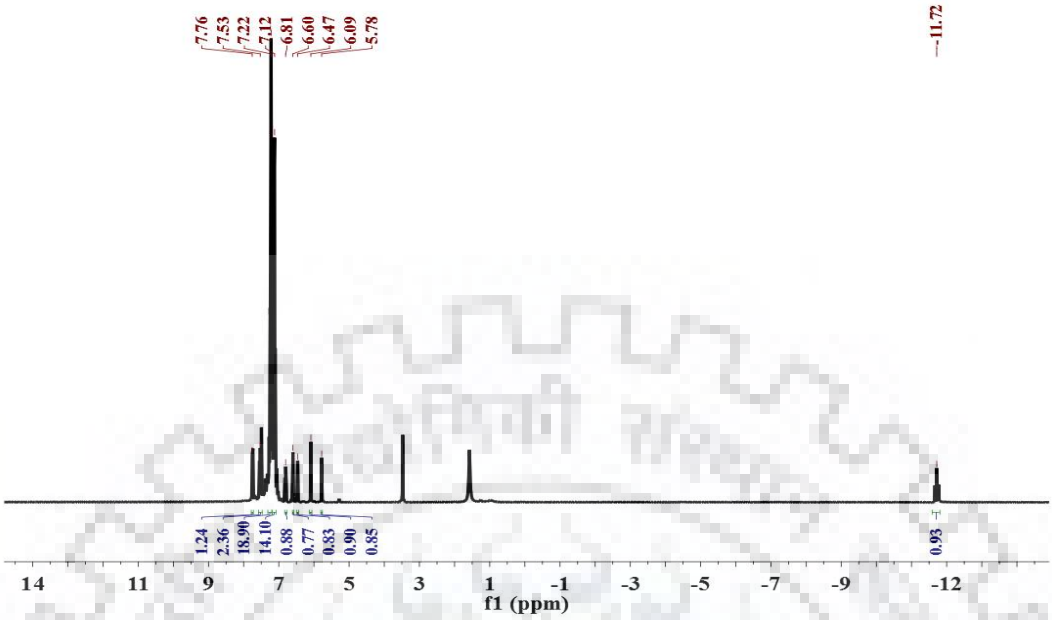

Fig. 4.7 ^{1}H NMR spectrum of complex **8** in $CDCl_3$ at room temperature.

Table 4.3 NMR spectral data for ligands and ruthenium complexes **7–8**.

Complex	^{1}H NMR (δ /ppm)
L^6H_2	10.11 (s, 1H), 8.36-6.28 (11H)
L^7H_2	11.41 (s, 1H), 8.17 (s, 1H), 7.27-6.07 (8H), 4.62 (s, 2H)
7	7.601–7.347 (m, 8H), 7.215–7.081 (m, 27H), 6.804 (t, 1H), 6.735 (d, 1H), 6.541 (d, 1H), 6.441 (d, 1H), 6.081 (m, 2H)
8	-11.72 (t, 1H), 7.601–7.347 (m, 8H), 7.215–7.081 (m, 27H), 6.804 (t, 1H), 6.735 (d, 1H), 6.541 (d, 1H), 6.441 (d, 1H), 6.081 (m, 2H)

4.2.2. Description of molecular structures

The crystal structures of the complexes [Ru(L^6C^N^N)(PPh_3)$_2$(CO)] **(7)**, [Ru(L^6N^N)(PPh_3)$_2$(CO)H] (**8**) and [Ru(L^7N^N)(PPh_3)$_2$(CO)H] **(9)** and are depicted in Fig. 4.8, Fig. 4.9 and Fig. 4.10 respectively.

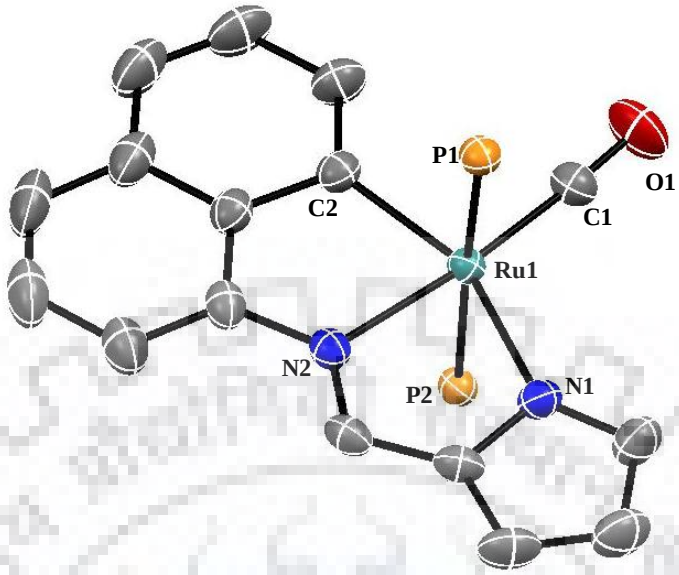

Fig. 4.8 ORTEP diagram (50% probability level) of the [Ru(L^6C^N^N)(PPh_3)$_2$(CO)] **(7)**. All hydrogen atoms and phenyl rings of PPh_3 groups have been omitted for clarity.

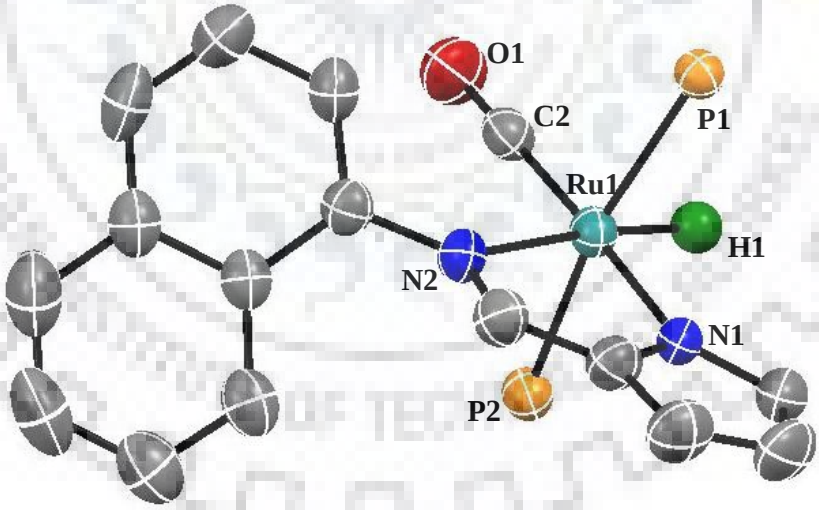

Fig. 4.9 ORTEP diagram (50% probability level) of the [Ru(L^6N^N)(PPh_3)$_2$(CO)H] (**8**). All hydrogen atoms and phenyl rings of PPh_3 groups have been omitted for clarity.

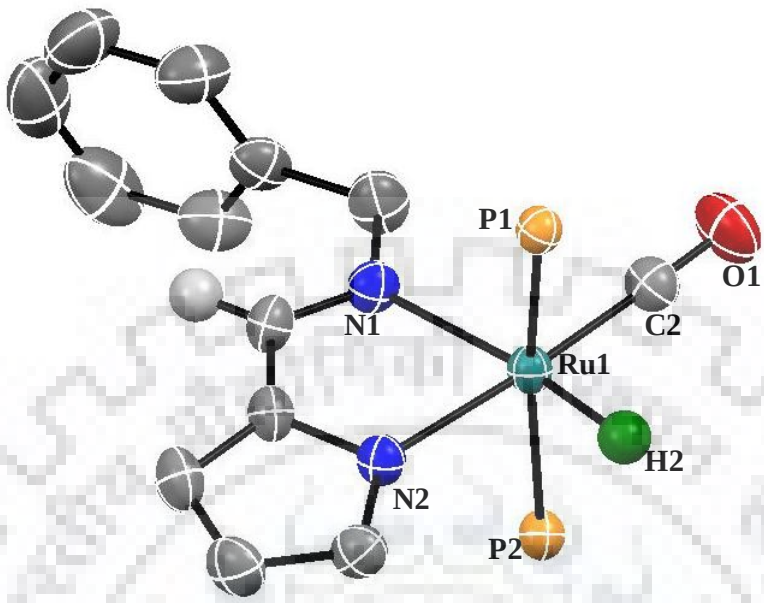

Fig. 4.10 ORTEP diagram (50% probability level) of the [Ru(L^7N^N)(PPh_3)$_2$(CO)H] **(9)**. All hydrogen atoms and phenyl rings of PPh_3 groups have been omitted for clarity.

The selected bond lengths and bond angles of complexes **7-9** along with theoretical values are given in Table 4.4. Crystal data collection and refinement detail of the structures of complexes **7-9** are summarized in Table 4.5. In the crystal structure of **7**, the equatorial plane consisted of N(imine), N(pyrrole), C(carbanion) and CO. In the crystal structures of **8** and **9**, the equatorial plane consisted of N(imine), N(pyrrole), H(hydride) and CO. The ruthenium centre adopted a distorted-octahedral geometry as reflected in parameters given in Table 4.4. In the complexes **7**, **8** and **9**, Ru–H bond length (~ 1.54 Å), CO stretching frequency (ν_{CO}~1920 cm^{-1}) and C–O bond length (~ 1.15 Å) in addition to Ru–C–O angle (~177°) were consistent with reported values.[254-257,52]

Table 4.4 Selected bond lengths (Å) and bond angles (deg.) of complexes **7**, **8** and **9**.

Bond lengths (Å) Experimental [Theoretical]		Bond angles (°) Experimental [Theoretical]	
		7	
Ru(1)−C(2)	2.070(3) [2.090]	C(1)−Ru(1)−N(1)	110.73(11) [108.91]
Ru(1)−C(1)	1.838(3) [1.856]	N(2)−Ru(1)−N(1)	75.76(9) [76.60]
Ru(1)−N(1)	2.193(2) [2.226]	C(1)−Ru(1)−N(2)	173.44(11) [174.47]
C(1)−O(1)	1.160(4) [1.19]	C(2)−Ru(1)−N(1)	155.28(11) [156.13]
Ru(1)−P(1)	2.387(7) [2.504]	Ru(1)−C(1)−O(1)	176.3(3) [176.27]
Ru(1)−P(2)	2.380(7) [2.505]	P(1)−Ru(1)− P(2)	175.77(2) [176]
Ru(1)−N2)	2.100(2) [2.122]	C(2)−Ru(1)−N(2)	79.53(10) [79.53]
		C(2)−Ru(1)−C(1)	93.98(12) [94.94]
		8	
Ru(1)−H(1)	1.54(2) [1.60]	N(1)−Ru(1)−H(1)	95.5(9) [93.34]
Ru(1)−C(2)	1.839(4) [1.863]	N(2)−Ru(1)−N(1)	75.93(11) [76.49]
Ru(1)−N(1)	2.129(3) [2.134]	H(1)−Ru(1)−N(2)	171.5(9) [169.49]
C(2)−O(1)	1.156(4) [1.193]	C(2)−Ru(1)−N(1)	173.93(13) [174.68]
Ru(1)−P(1)	2.333(10) [2.482]	Ru(1)−C(2)−O(1)	178.5(3) [177.02]
Ru(1)−P(2)	2.373(10) [2.496]	P(1)−Ru(1)− P(2)	164.78(3) [160]
Ru(1)−N2)	2.225(3) [2.311]	C(2)−Ru(1)−N(2)	98.28(13) [98.20]
		C(2)−Ru(1)−H(1)	90.2(9) [91.94]
		9	
Ru(1)−H(2)	1.545 [1.623]	N(1)−Ru(1)−H(2)	93.88 [93.34]
Ru(1)−C(2)	1.843(2) [1.861]	N(2)−Ru(1)−N(1)	76.40(6) [76.45]
Ru(1)−N(1)	2.185(17) [2.227]	H(2)−Ru(1)−N(2)	170.09 [169.78]
C(2)−O(1)	1.149(2) [1.195]	C(2)−Ru(1)−N(1)	100.20(8) [99.43]
Ru(1)−P(1)	2.349(5) [2.476]	Ru(1)−C(2)−O(1)	177.80(19) [177.46]
Ru(1)−P(2)	2.365(5) [2.477]	P(1)−Ru(1)− P(2)	169.02(19) [168.80]
Ru(1)−N2)	2.122(16) [2.133]	C(2)−Ru(1)−N(2)	176.44(8) [175.84]
		C(2)−Ru(1)−H(2)	89.47 [90.77]

Table 4.5 Summary of crystal data and structural refinement parameters for complexes **7**, **8** and **9**.

	7	**8**	**9**
Empirical formula	$C_{52}H_{40}N_2OP_2Ru$	$C_{52}H_{42}N_2OP_2Ru$	$C_{49}H_{42}N_2OP_2Ru$
Formula weight	871.87	873.89	837.86
Temperature /K	296(2)	293(2)	293(2)
Λ (Å) (Mo-Kα)	0.71073	0.71073	0.71073
Crystal system	triclinic	triclinic	triclinic
Space group	P –1	P –1	P –1
a (Å)	9.3156(6)	9.5709(8)	10.6182(7)
b(Å)	12.7447(8)	12.9221(11)	12.6532(8)
c (Å)	19.3338(12)	18.2006(15)	17.0944(11)
α(˚)	103.616(3)	81.560(4)	106.237(3)
γ (˚)	109.517(2)	79.282(4)	109.064(3)
β(˚)	95.394(3)	80.456(4)	97.359(3)
V (Å^3)	2065.0(2)	2165.4(3)	2022.3(2)
Z	2	2	2
ρ_{calc} (gcm^{-3})	1.402	1.340	1.376
F(000)	896	900	864
Theta range	1.10-28.30	2.188-25.499	1.279-28.398
Index ranges	$-12<h<12$, $-17<k<17$, $-25<l<25$	$-11<h<11$, $-15<k<15$, $-21<l<22$	$-12<h<14$, $-16<k<16$, $-22<l<22$
Data/restraints/par.	10145/0/523	8062/0/527	9948/0/504
GOF^a on F^2	0.722	1.002	1.071
$R1^b$ [$I > 2\sigma(I)$]	0.0352	0.0464	0.0312
$R1$[all data]	0.0546	0.0897	0.0431
$wR2^c$ [$I > 2\sigma(I)$]	0.0987	0. 0796	0.0692
$wR2$ [all data]	0.1406	0.0945	0.0809

4.3. Catalytic transfer hydrogenation

Role of ruthenium complexes as catalyst in transfer hydrogenation of carbonyl compounds, has gained considerable current attention, most likely due to the relatively mild route of reaction and benign nature of reagents used.[254-257,264] We began our study to utilize complex **7** as a catalyst in transfer hydrogenation of ketones and reaction conditions were optimized using acetophenone as a substrate by varying base (like NaOH, KOH and KO^tBu), solvent, time and amount of catalyst used. However, yield was poor in case of KO^tBu. After careful optimization, we concluded that 0.3 mol% catalyst, 2-propanol as a solvent and 0.3 mmol KOH, provided admirable yield at 85 °C reaction temperature and 6 hrs of reaction time. Table 4.6 provides data of various substrates used for transfer hydrogenation. From entries 5 and 6 in Table 4.6, it is clear that catalyst is completely inactive for substrates 2-pyridyl acetone and 2-amino benzophenone respectively, probably due to the chelate formation of these substrates after coordination to metal centre.[254] Plausible mechanism for the catalytic transfer hydrogenation of carbonyl compounds using complex **7** is given in Scheme 4.5.[254,255,257] In the first step, deprotonated isopropanol is coordinated to ruthenium in catalyst **A** through oxygen atom as isopropoxide and there is simultaneous breaking of Ru-C bond followed by protonolysis of naphthyl ring to generate the intermediate **B**. In the second step, coordinated isopropoxide ligand undergoes β-hydride elimination to generate the Ru-H species in the intermediate **C** which is considered to be catalytically active species during the transfer hydrogenation.[254,255,257] In the third step, there is insertion of carbonyl substrate into Ru-H bond to generate the intermediate **C**. In the last step, there is elimination of hydrogenated product alcohol with simultaneous regeneration of catalyst.

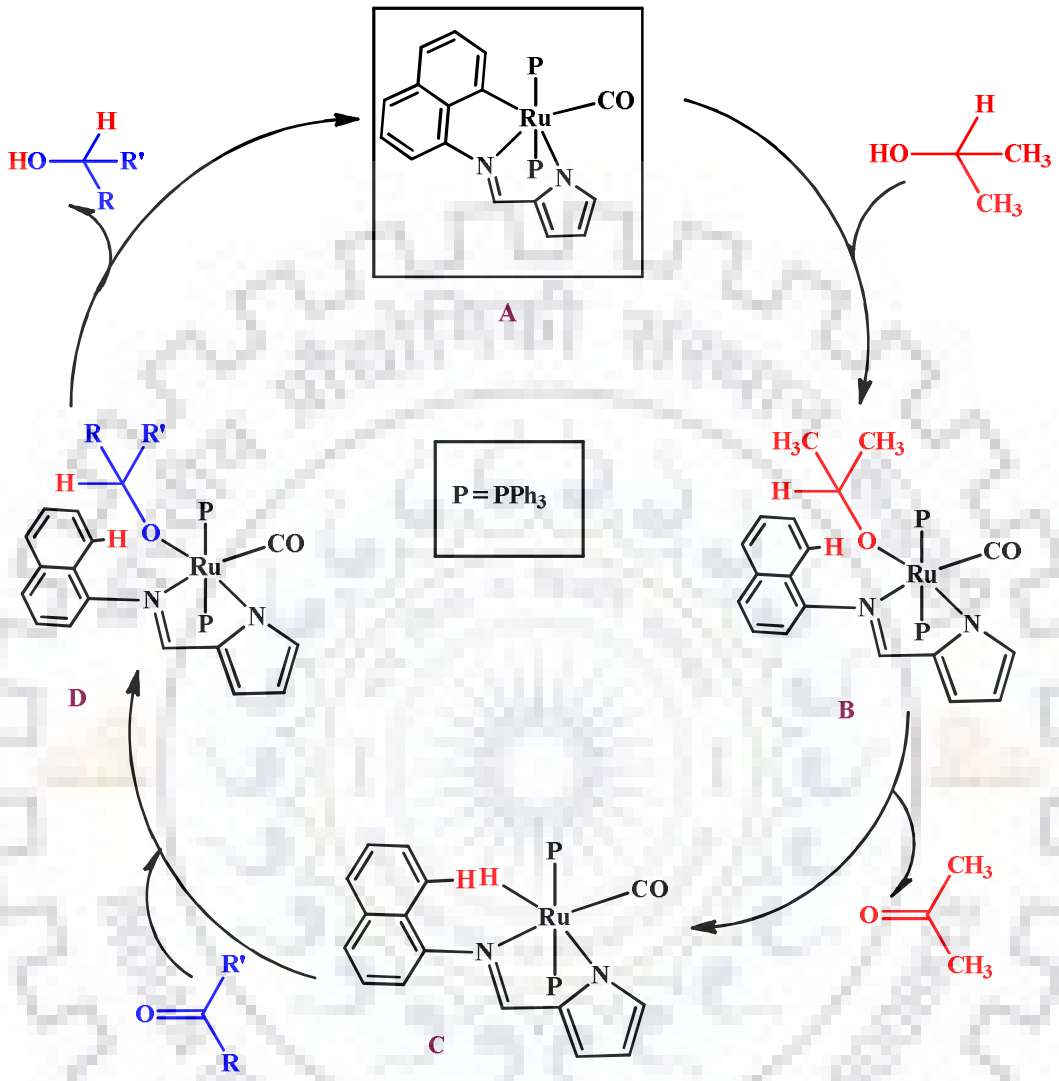

Scheme 4.5 Plausible mechanism for the catalytic transfer hydrogenation of carbonyl compounds using complex **7**.

Table 4.6 Catalytic transfer hydrogenation of ketones.[a]

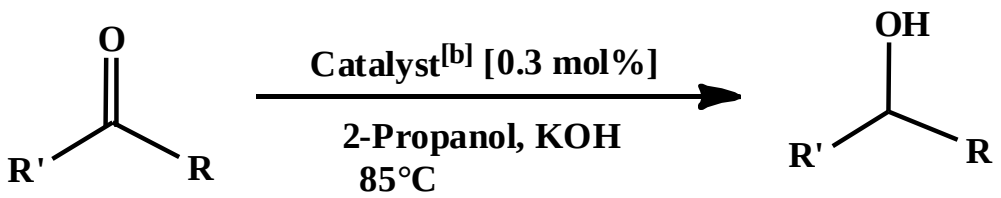

Entry	Substrate	Yield[c] (%)	TON[d]
1	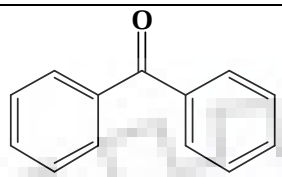	100	333
2	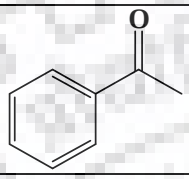	87	290
3	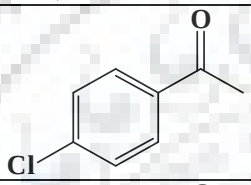	80	266
4	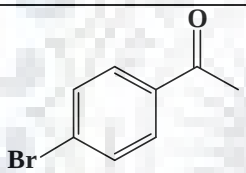	85	283
5	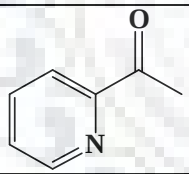	0	0
6	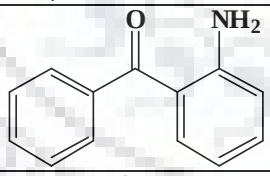	0	0
7		97	323
8	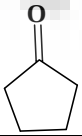	100	333

[a]Reaction conditions: ketone (1.0 mmol), KOH (0.3 mmol), 2-propanol (5 mL), 85 °C. [b] Catalyst: [Ru(L^6C^N^N)(PPh_3)$_2$(CO)](**7**). [c] Determined by GC–MS. [d] TON = turnover number

4.4. DFT studies

The optimisation of geometries for complexes **7-9** were performed at the B3LYP level of DFT using LANL2DZ basis set for ruthenium metal. Contour plots of HOMO and LUMO for the all complex **7-9** are shown in Figure 4.11. Compositions of selected frontier molecular orbitals (HOMO and LUMO) of complexes **7-9** are given in Table 4.7. Moreover, the bond length and bond angle parameters of the optimised structures were compared with data obtained from X-ray calculation in order to validate the experimental data with theoretical (Table 4.4). The experimental bond length and bond angle values are consistent with theoretical values.

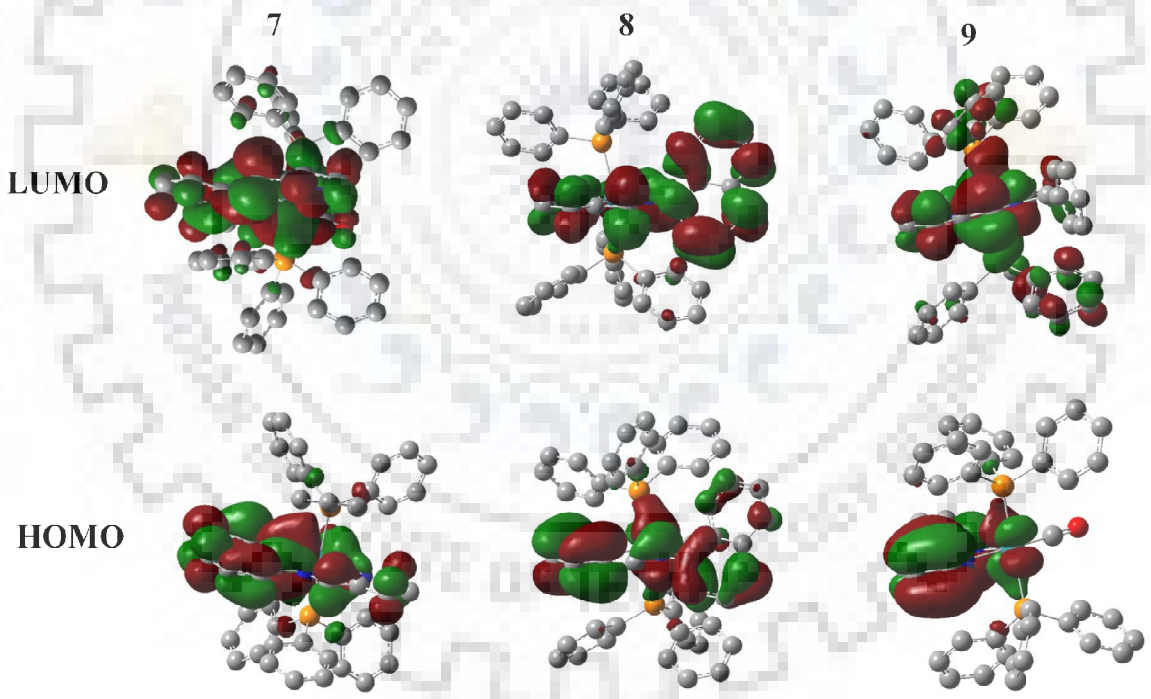

Fig. 4.11 Contour plots of HOMO and LUMO of complex **7**, **8** and **9**.

Table 4.7 Compositions of HOMO and LUMO of complexes **7**, **8**, **9**.

Complex	Fragments	Contribution [%] of fragments to	
		HOMO	LUMO
(7)	Ru	16	2
	CO	0	2
	PPh_3	5	7
	L^1	79	89
(8)	Ru	16	4
	H	0	0
	CO	0	1
	PPh_3	10	10
	L^1H	74	85
(9)	Ru	16	17
	H	0	0
	CO	0	3
	PPh_3	12	4
	L^2H	72	76

4.4.1. TDDFT and excited state analysis

To provide insight into the nature of the experimentally derived electronic absorptions, TDDFT calculations were performed on all complexes **7-9**. The results of the TDDFT calculations are summarized in Tables 4.8. The bands appearing in the computed absorption spectra were found to be closely related to those of experimental spectra. The TD-DFT spectrum of complex **7** showed transitions at 385 and 477 nm with oscillator strengths (*f*) of 0.0038 and 0.0949 respectively, which were mainly assigned to H → L+3 and H → L transitions respectively. The TD-DFT spectrum of complex **8** showed a transition at 393 nm with oscillator strength (*f*) of 0.0588 which was mainly assigned to H → L+1 transition.

Similarly, the TD-DFT spectrum of complex **9** showed a transition at 344 nm, with oscillator strength (*f*) of 0.0168 which was mainly assigned to H → L+1 transition.

Table 4.8 Main calculated transitions for complexes **7**, **8**, **9** with composition in terms of molecular orbital contribution of the transition, excitation energies, and oscillator strength.

Complex	Excited state	Composition	λ(nm) Experimental	λ (nm) Theoretical	F (Oscillator strength)	Energy(ev)
7	i	HOMO → LUMO+3 (76%) HOMO → LUMO+1 (14%)	405	385	0.0038	3.2197
	ii	HOMO → LUMO (90%) HOMO-1→ LUMO (7%)	485	477	0.0949	2.5977
8	i	HOMO-1→ LUMO+1 (16%) HOMO → LUMO+1 (50%) HOMO → LUMO (7%) HOMO-2 → LUMO+1 (3%)	397	393	0.0588	3.1519
9	i	HOMO-1→ LUMO (28%) HOMO → LUMO+1 (60%)	338	344	0.0168	3.6003

4.5. Photolysis experiment of coordinated CO

Coordinated CO in carbonyl complex **7** was found to be photolabile under visible light. The photolability of coordinated CO was examined by exposing dichloromethane solution of complex **7** under illumination of visible light (Figure 4.12). No change was observed in dark but in the presence of light we observed a change in the electronic absorption spectra of complex **7**. Upon the illumination of light on the solution of complex **7**, the peak intensities

decreased near 485, 400 and 275 nm and some isobestic points near 376 and 296 nm (Figure 4.12) were observed.

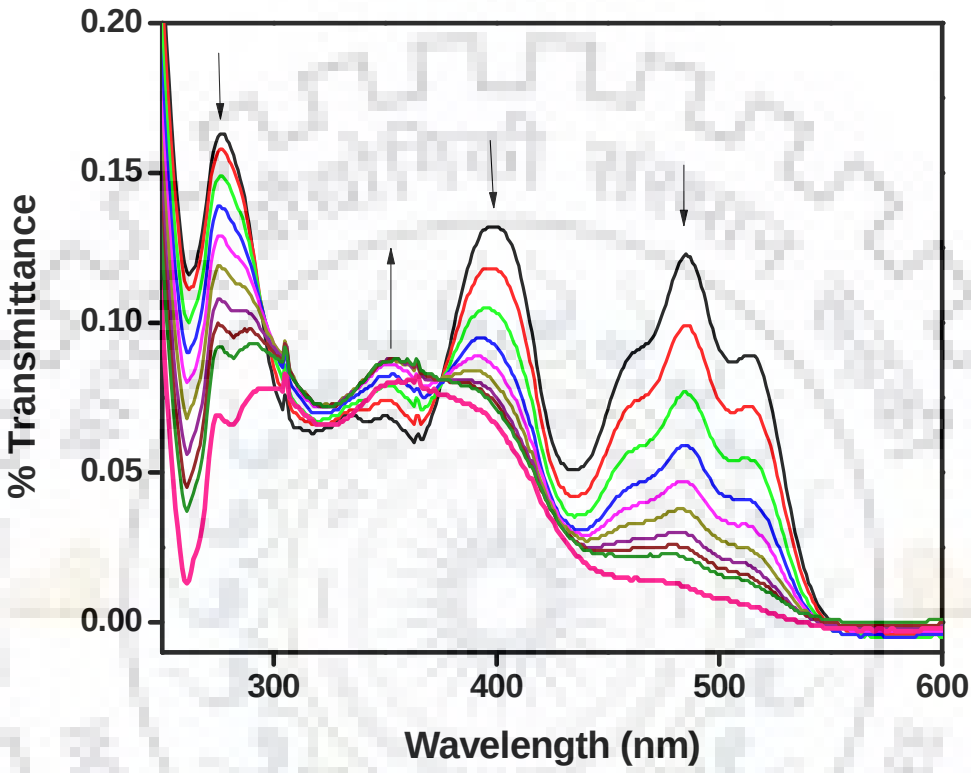

Fig. 4.12 Photocleavage of CO from complex **7** in dichloromethane solution under illumination of visible light (100W). Repetitive scans were taken in 1 min intervals in visible light.

4.6. Conclusions

The major findings and conclusions of the present study are following: (**a**) Organometallic ruthenium(II) complex [Ru(L^6C^N^N)$(PPh_3)_2$(CO)] (**7**) was synthesized by reaction of [Ru$(PPh_3)_3Cl_2$] with ligand L^6H_2 directly and from complex **8** (intermediate) via C-H bond activation and was characterized by different spectroscopic studies. (**b**) Ruthenium hydrido

carbonyl complexes [Ru(L^6N^N)(PPh_3)$_2$(CO)H] (**8**) and [Ru(L^7N^N)(PPh_3)$_2$(CO)H] (**9**) were synthesized by reaction of [Ru(PPh_3)$_3$$Cl_2$] with ligands L^6H_2 and L^7H2, respectively, and characterized by various spectroscopic studies. (**c**) The molecular structures of **7-9** were authenticated by X-ray crystallography. (**d**) Complex **7** was found to be an effective catalyst in transfer hydrogenation reactions of ketones. (**e**) A theoretical study on the structures of the complexes **7**–**9** have been investigated and time-dependent DFT methods were used to aid in the assignment of the intense UV-vis absorption bands found for complexes. (**f**) The plausible mechanisms for formation of complexes **7**, **8** and catalytic transfer hydrogenation using complex **7** were proposed on the basis of literature. (**g**) Coordinated CO in complex **7** was found to be photolabile upon illumination of visible light.

4.7. Experimental section

4.7.1. Reagents and materials

All the reagents naphthalene-1-amine, phenylmethanamine, pyrrole-2-carbaldehyde, (Himedia Laboratories Pvt. Ltd., Mumbai, India) were of analytical grade. $RuCl_3.3H_2O$ was purchased from Loba Chemie Pvt. Ltd., Mumbai, India. Triphenylphosphine (SRL, Mumbai, India) was used as obtained. The precursor [Ru(PPh_3)$_3$$Cl_2$] was synthesized using the procedure reported earlier.[233] Infrared spectra were recorded with Thermo Nicolet Nexus FT–IR spectrometer, as KBr pellets using 16 scans and were reported in cm^{-1}. ^{1}H NMR spectra of all complexes in the deuterated solvents were recorded on JEOL, 400 MHz spectrometer. Electronic absorption spectra of all complexes in dichloromethane solvent were recorded with an Evolution 600, Thermo Scientific (Shimadzu) UV–vis spectrophotometer.

4.7.2. Syntheses of ligands

4.7.2.1. N-((1H-pyrrol-2-yl)methylene)naphthalen-1-amine (L^6H_2)

A solution of pyrrole-2-carbaldehyde (3 mmol) in 5 mL methanol was added dropwise to solution of naphthalene-1-amine (3 mmol) in 10 mL methanol with stirring. After 1 day of continous sstirring the brown colored precipitate was filtered and washed with small amount of methanol. Yield: (70 %). UV–vis (CH_2Cl_2; λ_{max}, nm (ε, M^{-1} cm^{-1})): 241 (69,900), 341 (47,600). ^{1}H NMR ($CDCl_3$, 400MHz): δ 10.11 (s, 1H), 8.36-6.28 (11H).

4.7.2.2. N-((1H-pyrrol-2-yl)methylene)-1-phenylmethanamine (L^7H_2)

Ligand L^7H_2 was synthesized from the reaction of pyrrole-2-carbaldehyde with phenylmethanamine in the same way as for ligand L^6H_2. Yield: (75 %). UV–vis (CH_2Cl_2; λ_{max}, nm (ε, M^{-1} cm^{-1})): 282 (1,47000), 330 (22494). ^{1}H NMR (DMSO-d_6, 400MHz): δ 11.41 (s, 1H), 8.17 (s, 1H), 7.27-6.07 (8H), 4.62 (s, 2H).

4.7.3. Syntheses of ruthenium complexes

4.7.3.1. Synthesis of [Ru(L^6C^N^N)(PPh_3)$_2$(CO)] (7)

Complex **7** was synthesized in two ways: (i) A batch of $Ru(PPh_3)_3Cl_2$ (0.1 mmol) was added directly to a solution of ligand L^6H_2 (0.15 mmol) in 2-methoxy ethanol and colour of solution was transformed to reddish after 10 min. This reddish solution was refluxed for 1 h and orange coloured solid was precipitated out, which was filtered and washed with small amount of methanol. Yield: 60% (ii) Complex [Ru(L^6C^N^N)(PPh_3)$_2$(CO)] (**7**) was also synthesized from the complex **8** by refluxing in 2-methoxy ethanol for 10 min. IR (KBr disk, in cm^{-1}): 1913(ν_{CO}), 1588 ($\nu_{C=N}$), 753, 692, 520 (ν_{PPh3}) cm^{-1}. UV–vis (CH_2Cl_2; λ_{max}, nm (ε, M^{-1} cm^{-1})): 275 (40,000), 405 (23,330), 485 (20,000), 517 (16,660). ^{1}H NMR ($CDCl_3$, 400MHz): δ 7.601–7.347 (m, 8H), 7.215–7.081 (m, 27H), 6.804 (t, 1H), 6.735 (d, 1H), 6.541 (d, 1H), 6.441 (d, 1H), 6.081 (m, 2H).

4.7.3.2. Synthesis of [Ru(L^6N^N)(PPh_3)$_2$(CO)H] (8)

To a solution of ligand L^6H_2 (0.15 mmol) and triethylamine in methanol, a batch of $Ru(PPh_3)_3Cl_2$ (0.1 mmol) was added and colour of solution was changed to light reddish brown. This reddish brown solution was refluxed for 4 h and yellowish brown coloured solid was precipitated out, filtered and washed with small amount of methanol. Yield: (65 %). IR (KBr disk, in cm^{-1}): 1924(ν_{CO}), 1555 ($\nu_{C=N}$), 744, 691, 516 (ν_{PPh3}) cm^{-1}. UV–vis (CH_2Cl_2; λ_{max}, nm (ε, M^{-1} cm^{-1})): 239 (13812), 397 (3500). ^{1}H NMR ($CDCl_3$, 400MHz): δ -11.72 (t, 1H), 7.601–7.347 (m, 8H), 7.215–7.081 (m, 27H), 6.804 (t, 1H), 6.735 (d, 1H), 6.541 (d, 1H), 6.441 (d, 1H), 6.081 (m, 2H).

4.7.3.3. Synthesis of [Ru(L^7N^N)(PPh_3)$_2$(CO)H] (9)

Complex [Ru(L^7N^N)(PPh_3)$_2$(CO)H] (**9**) was synthesized by following the same procedure as for **8** from the reaction of $Ru(PPh_3)_3Cl_2$ with ligand L^7H_2. Yield: 70% . IR (KBr disk, in cm^{-1}): 1910(ν_{CO}), 1587 ($\nu_{C=N}$), 745, 695, 520(ν_{PPh3}) cm^{-1}. UV–vis (CH_2Cl_2; λ_{max}, nm (ε, M^{-1} cm^{-1})): 230 (100,000), 338 (34,659).

4.7.4. X–ray crystallography

Single crystal of complexes **7**, **8** and **9** were obtained via layering of hexane over a solution of dichloromethane which were suitable for diffraction study. The X–ray data collection and processing of complexes **7**, **8** and **9** were carried out using Bruker Kappa Apex–II CCD diffractometer and graphite monochromated Mo–Kα radiation (λ = 0.71073 Å) at 273K. Structure solutions, refinement and data output were carried out with the SHELXTL program.[235,236] All non–hydrogen atoms were refined anisotropically and hydrogen atoms were placed in geometrically calculated positions and refined using a riding model. Images were produced with the DIAMOND program.[237]

4.7.5. DFT study and computational details

The DFT calculations for complexes **7**, **8** and **9** were carried out using Gaussian 09 program package.[249,250] The Becke's three parameters hybrid exchange functional with the Lee–Yang–Parr (LYP) nonlocal correlation functional was used throughout the computational study.[249,250] A LANL2DZ basis set for ruthenium metal was used in the calculation. Coordinates from single crystal X-ray structures of all the complexes were used as input data for the optimisation of geometries. Pictorial representations of frontier molecular orbitals were created using the Gauss View-5 program. To evaluate the electronic transitions, time dependent density functional theory (TD-DFT) calculations were also performed on the optimised geometries.

4.7.6. Synthetic procedure for catalytic transfer hydrogenation

In a microwave reaction vial with a closed cap, a mixture containing ketone (1 mmol), the catalyst (known mol percent) and base (known mol percent) in 5 ml of isopropanol was heated on the oil bath with continous stirring at 85°C for suitable period of time as mentioned. After the usual workup (reported in literature), the reaction product dissolved in hexane was analyzed by GC-MS.

In-situ ligand modification to generate anion radical in organometallic ruthenium complex: A rare example of isolation of organometallic azo anion radical during nitric oxide reactivity

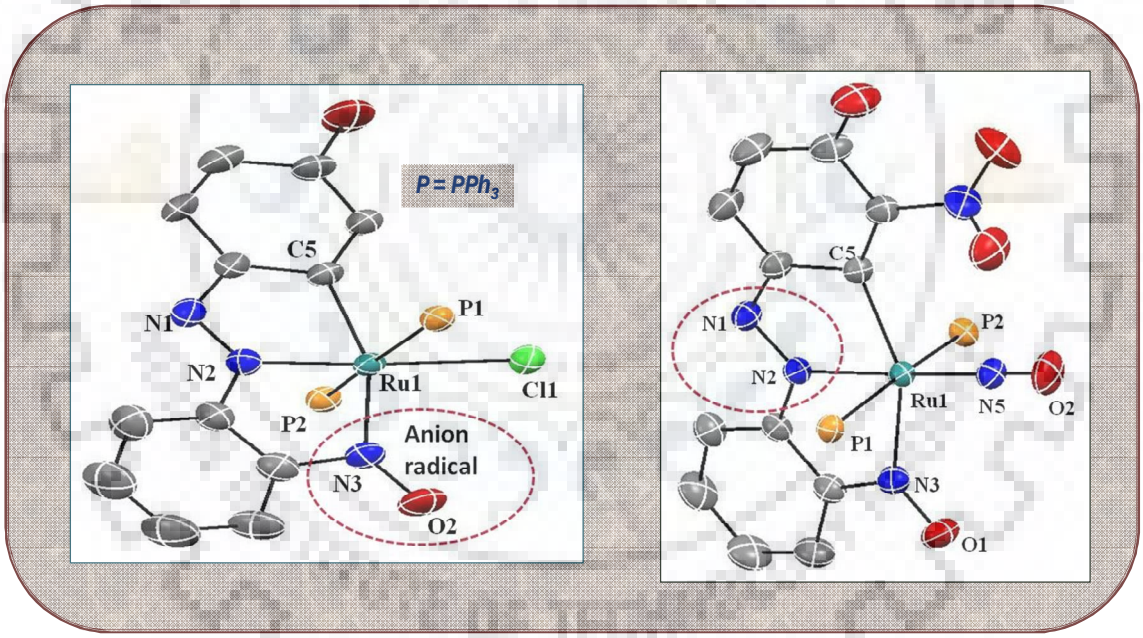

Abstract

The reaction of (E)-4-((2-nitrophenyl)diazenyl)phenol (L^8H, H = dissociable proton) with $Ru(PPh_3)_3Cl_2$ afforded novel organometallic anion radical complex $[Ru(L_A^{8-\cdot})(Cl)(PPh_3)_2]$ (**10**). During the synthesis of complex **10**, nitro group in ligand converted to nitroso group through oxygen atom transfer to labile triphenylphosphine. One electron reduced nitroso group was coordinated to ruthenium in η^1(N) mode. Complex **10** was treated with acidified nitrite to afford nitrosyl complex $[Ru(L_B^{8-\cdot})(PPh_3)_2(NO)](ClO_4)$(**11**) and it is a rare example of an organometallic ruthenium complex having azo anion radical as well as two different noninnocent ligands coordinated to one metal. Both the complexes were characterized by UV-vis, IR, NMR spectroscopic studies. Redox properties of complex **10** were investigated using cyclic voltammetry. Molecular structures of complexes **10** and **11** were authenticated using X-ray crystallographic studies. DFT calculations were performed to better understand the electronic properties of complex **10**.

5.1. Introduction

Coordination chemistry of transition metal complexes with redox noninnocent ligands have gained considerable interest during past few years inspired by the fact that both ligand as well as metal-centered redox events are invloved in biological processes, organic transformations etc.[265,266] Organic radicals are highly reactive and their isolation in the crystalline state has become a challenging area of chemical research. In this regard, syntheses of coordination complexes of transition metal ions with possibilities of multiple oxidation states as a carrier of redox noninnocent ligands have been successfully used as an alternative.[267]

Among all the redox active ligands, nitrogen centered redox-active noninnocent ligands have been well-known.[268] Azo aromatic ligands, one of the nitrogen centered redox active ligands have been utilized significantly for the syntheses of coordination complexes with transition metals during past few years[269-271] however, isolation of the first two azo-anion-radical stabilized by ruthenium and copper was carried out simultaneously in the pure crystalline state in 1998.[272,273]

From investigation of literature, it was found that organic nitro compounds are used as oxidants in various organic transformations and conversion of nitro group to nitroso group is mediated by transition metals by oxygen atom transfer from nitro group in M-NO_2 or organic nitro compounds to CO, alkenes, phosphines to get corresponding oxidized product CO_2, epoxides, phosphine oxides respectively (shown in Scheme 5.1). The nitroso ligand can coordinate to metal through η^1-N, η^1-O, and η^2-(N, O) binding modes. Based on the previous reports, mechanism of the O-transfer from nitro groups may involve either the nucleophilic

attack of the nitro oxygen on the oxidizable group L or outer and inner sphere electron transfer pathway.[274-278]

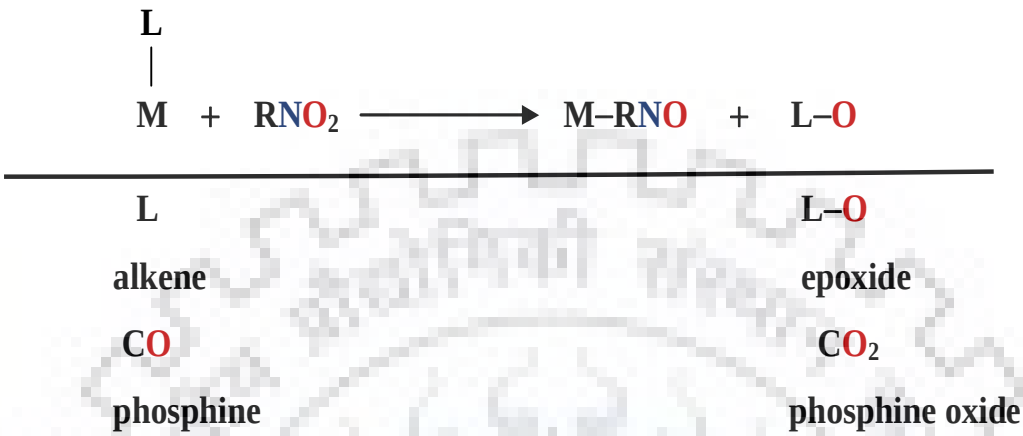

Scheme 5.1 O-atom transfer from nitro group to oxidizable groups L

Inspired by these valuable findings, in the present report, we designed and synthesized the ligand L^8H systematically (shown in Scheme 5.2).

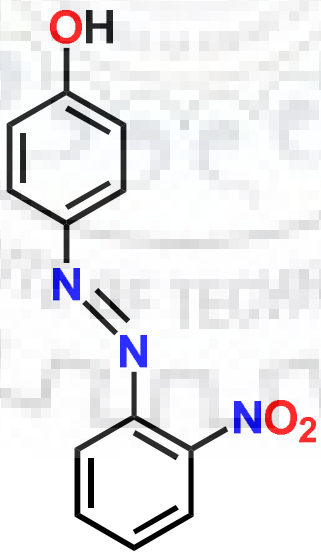

Scheme 5.2 Ligand **L^8H**

Organometallic ruthenium complex $[Ru(L_A^{8-\cdot})(Cl)(PPh_3)_2]$ (**10**) (shown in Scheme 5.3) having one electron reduced nitroso group coordinated to ruthenium as η^1-N was isolated during reduction of nitro group in ligand L^8H with simultaneous formation of triphenylphosphine oxide. To, the best of our knowledge, this is the first example of coordination of nitro aryl group to ruthenium in $\eta^1(N_{nitroso})$ mode during oxygen atom transfer. Complex **10** is rare example of having unpaired electron on both ligand (nitroso group) as well as metal center and both are not coupled to each other. In most of the cases, the unpaired electron of the coordinated ligand gets coupled with unpaired electrons on another radical ligand or on the metal. Consequently, transition metal complexes with stable, uncoupled radicals are rare in the literature.[279] Complex **10** was reacted with acidified sodium nitrite solution to get organometallic ruthenium nitrosyl complex $[Ru(L_B^{8-\cdot})(NO)(PPh_3)_2](ClO_4)$(**11**) (shown in Scheme 5.3)

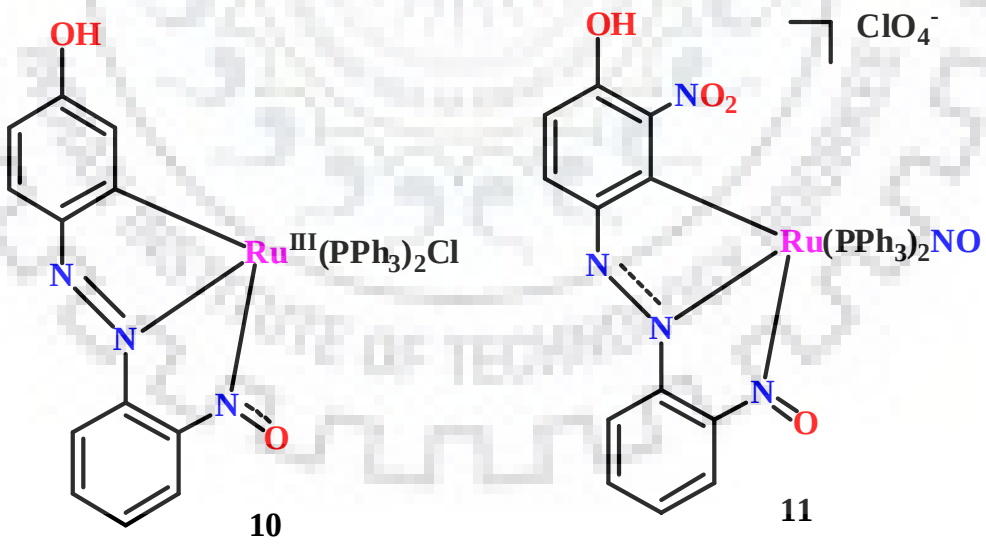

Scheme 5.3 Schematic drawings of complexes **10** and **11**.

Interestingly, during the synthesis of ruthenium nitrosyl **11**, unpaired electron from coordinated nitroso in **10** was shifted to azo group considered as sink of electron and formation of azo anion radical takes place.

Apart from coordination complexes of M-L type in which only one redox active noninnocent ligand is present, complexes of L^1-M-L^2 type with two different noninnocent ligands coordinated to one redox active transition metal are rare in literature.[280]

To, the best of our knowledge, complex **11** is first example of organometallic ruthenium complex having azo anion radical and it is a rare example of a molecule having two different noninnocent ligands coordinated to one metal.

5.2. Results and discussion

5.2.1. Syntheses and characterization of ligand and ruthenium complexes

Ligand L^8H was obtained in high yield by coupling reaction of diazotized 2-nitro aniline with phenol. $Ru(PPh_3)_3Cl_2$ was added directly to a hot methanolic solution (20 mL) of the ligand L^8H to afford the organometallic ruthenium(III) complex $[Ru(L_A^{8-\cdot})(Cl)(PPh_3)_2]$(**10**). $[Ru(L_B^{8-\cdot})(NO)(PPh_3)_2](ClO_4)$(**11**) was obtained from the complex **10** during nitric oxide reactivity. The complexes **10** and **11** were green and greenish blue in color and highly soluble in dimethylformamide, dichloromethane and dimethylsulphoxide but insoluble in water.

In the IR spectrum of complex 1**1,** the N-O stretching frequency (ν_{NO}) around 1874 cm^{-1} was expected for $\{Ru{-}NO\}^6$ species as reported in literature around 1820-1960 cm^{-1} for $\{Ru{-}NO\}^6$ species.[161,186,221-223] Characteristic peaks of perchlorate as counter anion in the complex **11** were observed around 1093 cm^{-1} and 622 cm^{-1}.[214,58] In both the complexes **10** and **11**, the peaks in the range 747-750 cm^{-1}, 694-695 cm^{-1} and 514-518 cm^{-1} (Table 5.1) confirmed the presence of axial PPh_3 ligands.[214-217,58,196] (shown in Figure 5.1).

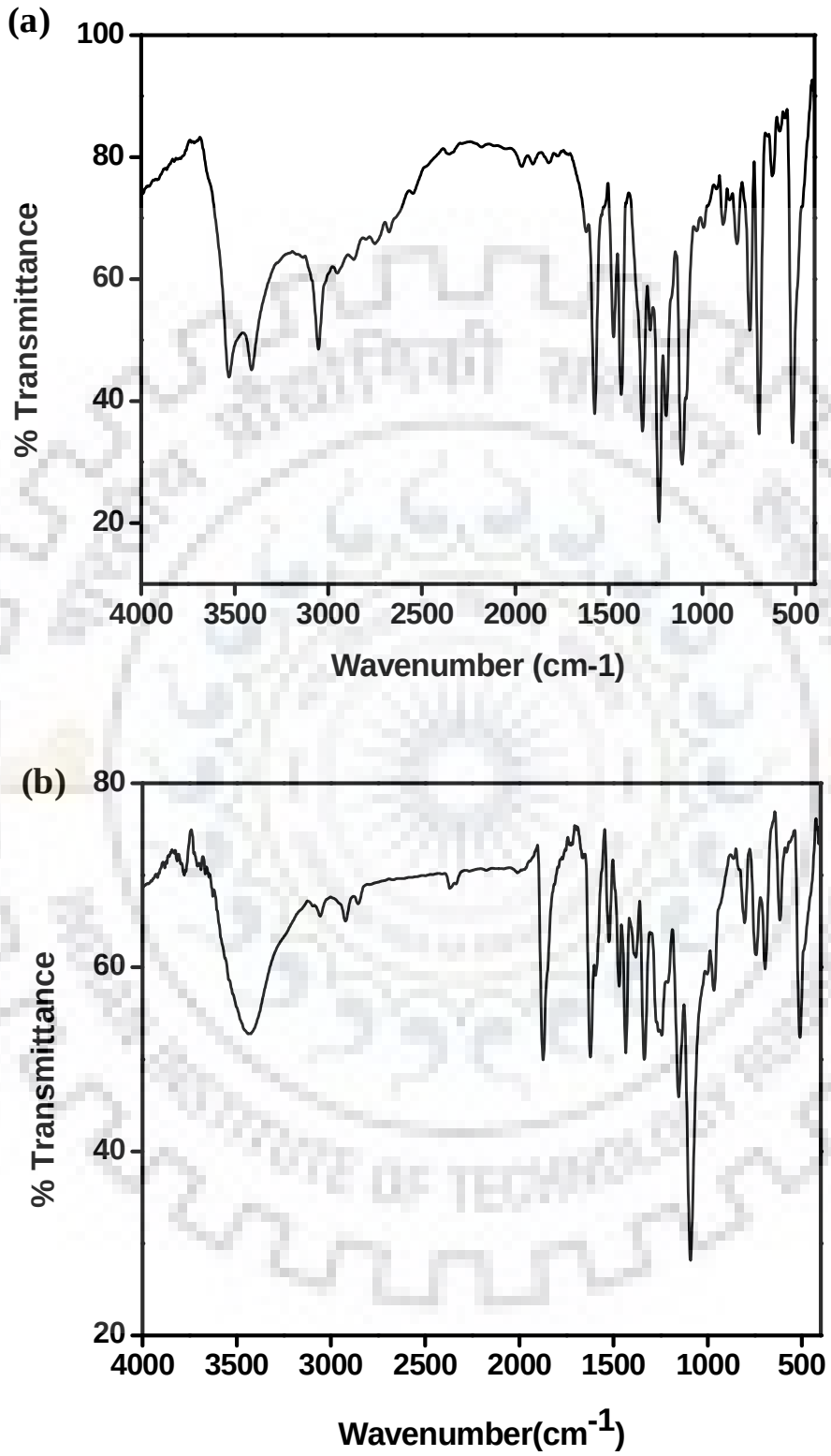

Fig. 5.1 Infrared spectra of complexes (a) **10** and (b) **11**.

Table 5.1 Data for IR spectral studies.

Complex	IR data (cm^{-1}, KBr pellets)			
	$\nu_{N=N}$	ν_{N-O}	ν_{ClO4}	ν_{PPh3}
10	1574	-	-	743, 692, 513
11	-	1874	1093, 622	745, 695, 520

The electronic absorption spectra of complexes **10** and **11** were displayed in Figure 5.2. In complex **10**, we observed charge transfer band with λ_{max} near 497 nm which was probably due to ligand–to–metal charge transfer (LMCT) transition.[51,56,58,225] In complex **11**, bands near 583 nm, 743 nm (Table 5.2) were recognized to be metal to ligand charge transfer (MLCT) transition $d\pi(Ru)\rightarrow\pi^*(NO)$ type and this transition has been responsible for the photolability of the coordinated NO.[161,186,168,188]

Table 5.2 Electronic absorption spectral data for ruthenium complexes **10** and **11** in dichloromethane solutions.

Complex	λ_{max}/nm (ε / $M^{-1}cm^{-1}$)
10	366(13068), 423(7500), 497(4909), 646(3181)
11	369(26205), 583(14256), 743(1969).

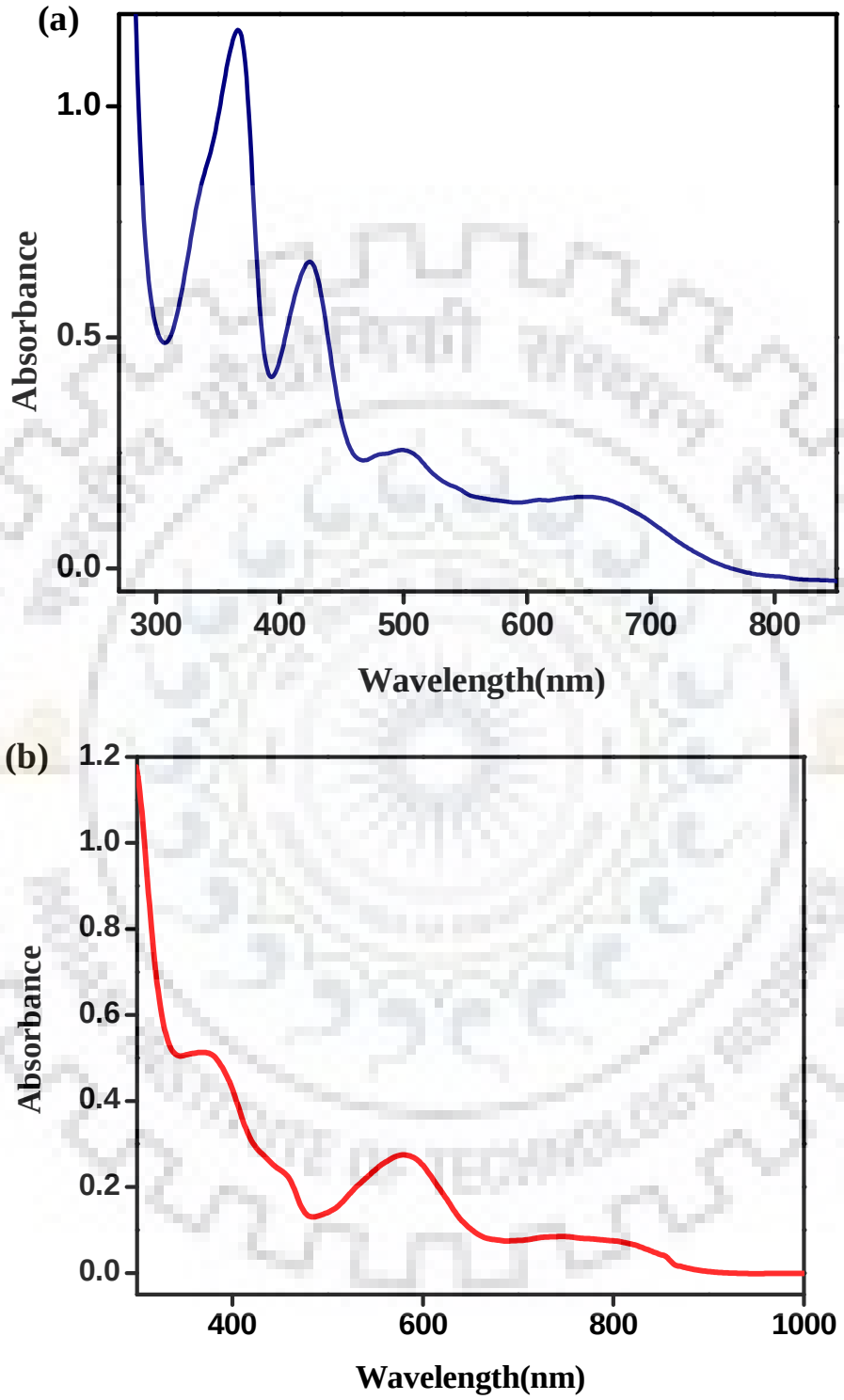

Fig. 5.2 Electronic absorption spectra of complexes (a) **10** and (b) **11** in dichloromethane solutions.

In the ligand (L^8H), we observed peak near 10.56 ppm, which was due to the presence of phenol (–OH) proton (Figure 5.3). Although complex **11** is one electron paramagnetic, but it provided NMR spectra and the ^1H and ^{31}P NMR spectra of **11** were displayed in Figure 5.4 and Figure 5.5 respectively. Single peak around 20.18 ppm (Table 5.3) was obtained for **11** in ^{31}P NMR spectrum corresponding to the presence of trans PPh_3 groups.[214-217,58,196]

Table 5.3 NMR spectral data for ligand **L^8H** and ruthenium nitrosyl complex **11**.

Complex	^1H NMR (δ /ppm)	^{31}P NMR (δ /ppm)
L^8H	10.56 (s, 1H), 8.02 (d, 1H), 7.72 (m, 5H), 6.93 (d, 2H)	-
11	7.59 (s, 1H), 7.50-7.14 (m, 32H), 6.59 (s, 1H), 6.34(d, 1H), 6.25(d, 1H)	20.18

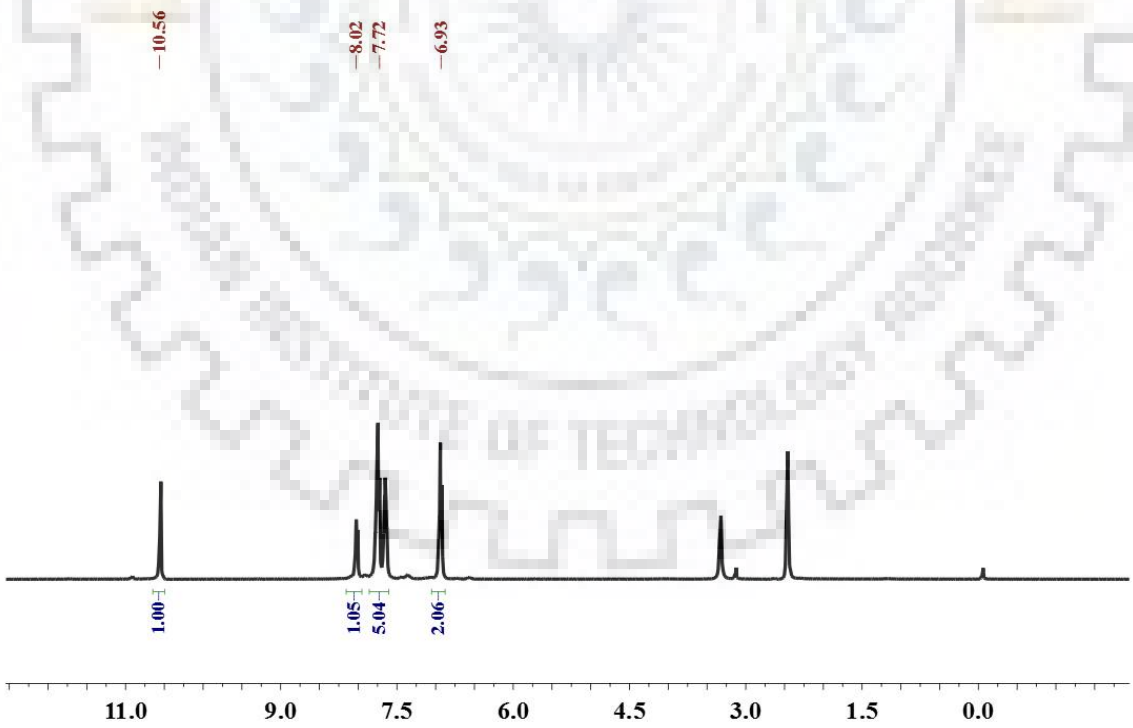

Fig. 5.3 ^1H NMR spectrum of **L^8H** in DMSO-d_6 at room temperature.

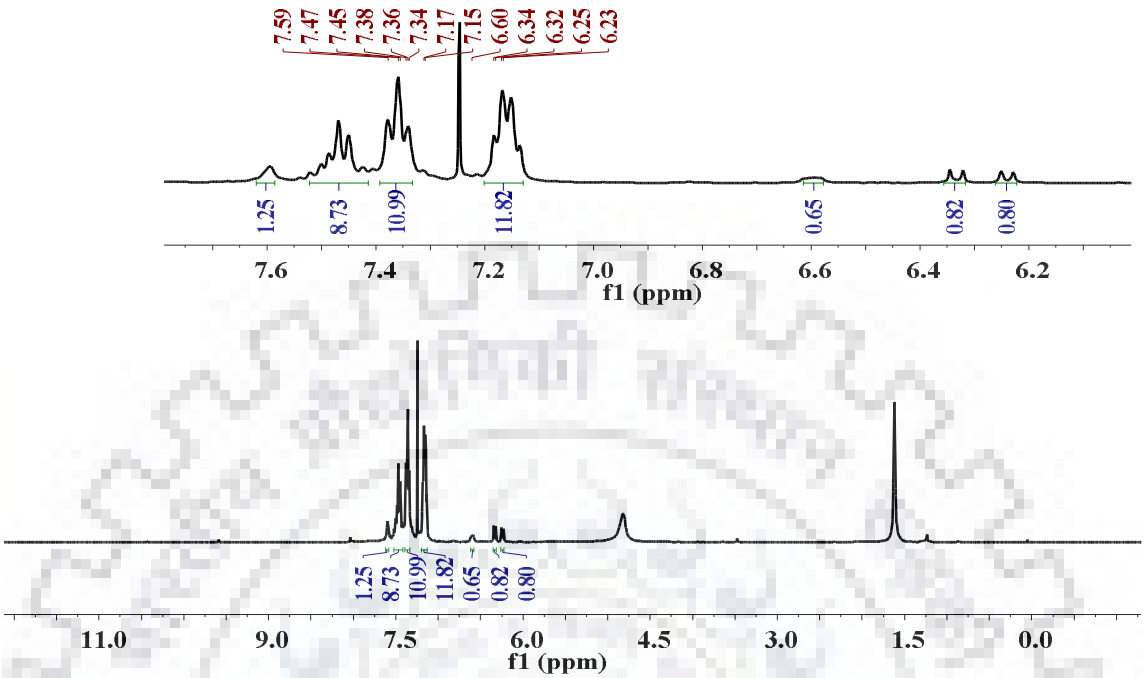

Fig. 5.4 ^{1}H NMR spectrum of complex **11** in $CDCl_3$ at room temperature.

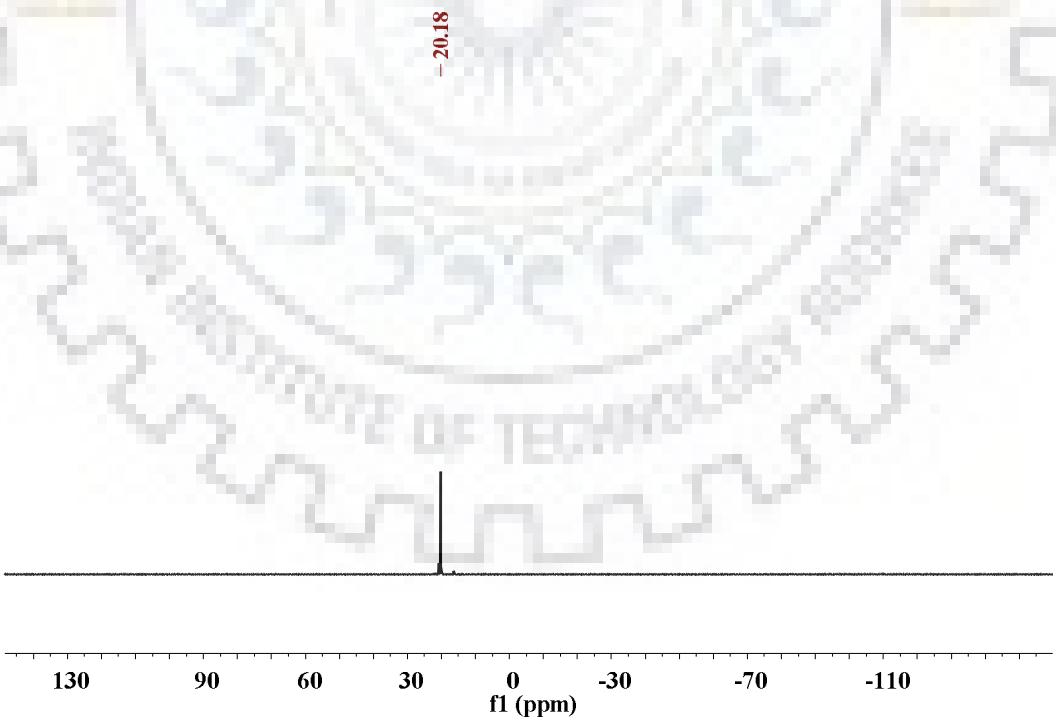

Fig. 5.5 ^{31}P NMR spectrum of complex **11** in $CDCl_3$ at room temperature.

5.2.2. Description of molecular structures

The molecular structures of the complexes $[Ru(L_A^{8-\cdot})(Cl)(PPh_3)_2]$ **(10)** and $[Ru(L_B^{8-\cdot})(NO)(PPh_3)_2](ClO_4)$(**11**) are shown in Figure 5.6 and Figure 5.7 respectively.

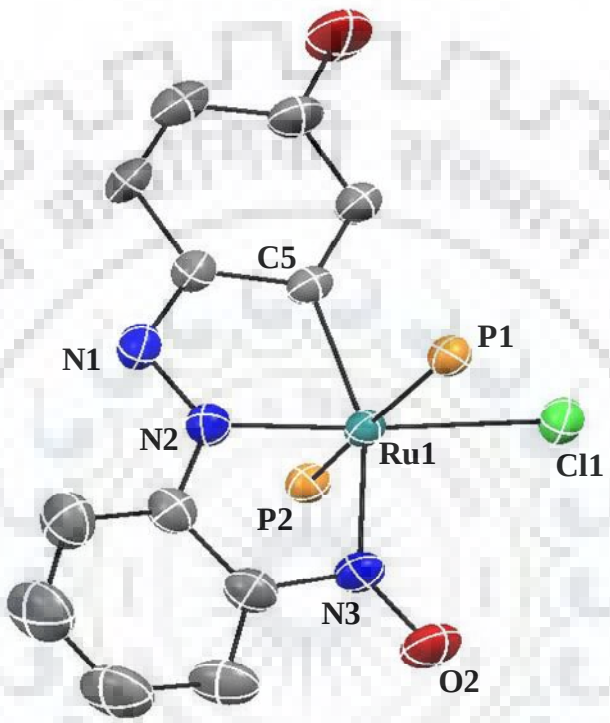

Fig. 5.6 ORTEP diagram (50% probability level) of the $[Ru(L_A^{8-\cdot})(Cl)(PPh_3)_2]$ (**10**). All hydrogen atoms, crystallized solvent molecules and the PPh_3 groups have been omitted for clarity.

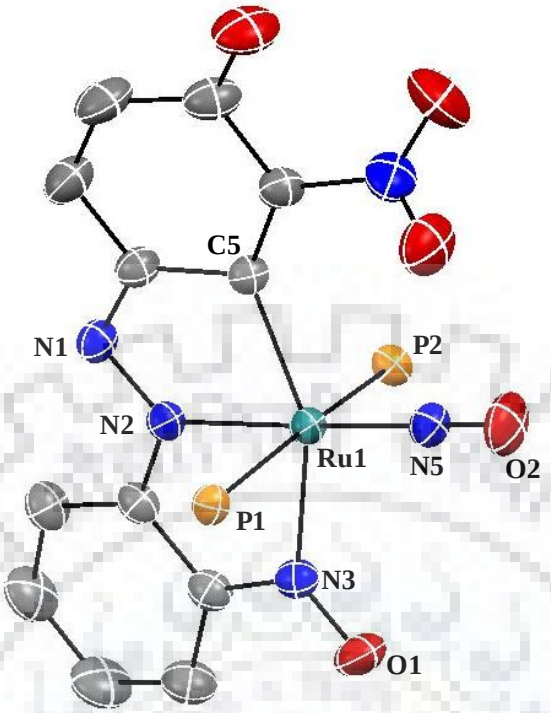

Fig. 5.7 ORTEP diagram (50% probability level) of the $[Ru(L_B^{8-})(NO)(PPh_3)_2](ClO_4)$(**11**). All hydrogen atoms, counter anion, crystallized solvent molecules and the PPh_3 groups have been omitted for clarity.

The selected bond lengths and bond angles of complexes **10** and **11** are given in Table 5.4 and Table 5.5 respectively. Crystal data collection and refinement details of the structures of complexes **10** and **11** are summarized in Table 5.6. In the molecular structure of **10**, carbanion (C5), Cl(1), azo nitrogen (N2) and the nitroso nitrogen N(3) constituted the equatorial plane while both the PPh_3 groups were at axial position. Hence, the geometry around Ru(III) centre was considered to be distorted octahedral as reflected in metric parameters. In the crystal structure of **11**.CH_2Cl_2, the equatorial plane was comprised of carbanion (C5), azo nitrogen (N2), nitroso nitrogen N(3) and N(5) of NO. However, after nitrosylation, the phosphine groups were intact at axial positions. In addition, ligand nitration was observed in the phenyl ring containing the –OH group, at ortho position to

the –OH group and carbanion (C5) function. All the bond distance and bond angle values were consistent with the values reported in the literature.[58,171,188,272,281]

Table 5.4 Selected bond lengths (Å) and bond angles (deg.) of complex **10**.

Bond lengths(A°)		Bond angles(°)	
Ru(1)–N(2)	1.955(13)	N(2)−Ru(1)−N(3)	80.64(19)
Ru(1)–N(3)	2.059(8)	N(2)−Ru(1)−Cl(1)	176.16(14)
N(1)–N(2)	1.301(7)	N(2)−Ru(1)−C(5)	78.02(20)
Ru(1)–Cl(1)	2.450(15)	P(1)−Ru(1)−P(2)	168.71(5)
Ru(1)–P(1)	2.388(5)	Cl(1)−Ru(1)−N(3)	102.76(14)
Ru(1)–P(2)	2.407(3)	C(5)−Ru(1)−N(3)	158.66(21)
Ru(1)–C(5)	2.056(7)	C(12)−N(3)−O(2)	114.18(47)
N(3)–O(2)	1.266(7)		

Table 5.5 Selected bond lengths (Å) and bond angles (deg.) of complex **11**.

Bond lengths(A°)		Bond angles(°)	
Ru(1)–N(2)	2.005(3)	N(2)−Ru(1)−N(5)	176.65(9)
Ru(1)–N(3)	2.126(7)	N(3)−Ru(1)−N(5)	106.12(9)
N(1)–N(2)	1.339(5)	N(2)−Ru(1)−C(5)	76.96(8)
Ru(1)–N(5)	1.767(3)	P(1)−Ru(1)−P(2)	172.28(2)
Ru(1)–P(1)	2.464(3)	C(5)−Ru(1)−N(3)	153.61(8)
Ru(1)–P(2)	2.474(3)	C(5)−Ru(1)−N(5)	100.12(9)
Ru(1)–C(5)	2.102(9)	Ru(1)−N(3)−O(1)	126.86(16)
N(5)–O(2)	1.140(4)	Ru(1)−N(5)−O(2)	177.7(2)
N(3)–O(1)	1.246(5)	N(2)−Ru(1)−N(3)	76.72(8)

Table 5.6 Summary of crystal data and structural refinement parameters for complexes **10** and **11**.

	10	**11**
Empirical formula	$C_{48}H_{38}ClN_3O_2P_2Ru$	$C_{49}H_{38}Cl_3N_5O_9P_2Ru$
Formula weight	887.27	1110.20
Temperature /K	293	293
Λ (Å) (Mo-Kα)	0.71073	0.71073
Crystal system	Triclinic	Triclinic
Space group	P –1	P–1
a (Å)	11.1635(16)	11.9194(12)
b(Å)	11.8631(18)	12.5733(13)
c (Å)	17.078(2)	17.6570(17)
α (˚)	101.425(6)	98.422(5)
γ (˚)	103.173(6)	110.836(4)
β (˚)	105.491(7)	100.834(5)
V (Å^3)	2039.8(5)	2362.6(4)
Z	2	2
ρ_{calc} (gcm^{-3})	1.445	1.561
F(000)	908.0	1128.0
Theta range	1.29-28.640	1.21−28.340
Index ranges	$-14< h< 14$, $-15< k< 15$, $-23< l< 23$	$-15< h< 15$, $-16< k< 16$, $-23< l< 23$
Data/restraints/par.	10195/0/514	11632/0/622
GOF^a on F^2	1.191	1.045
$R1^b$ [$I > 2\sigma(I)$]	0.0659	0.0345
$R1$[all data]	0.0881	0.0447
$wR2^c$ [$I > 2\sigma(I)$]	0.2040	0.0858
$wR2$ [all data]	0.2315	0.0948

5.2.3. Electrochemistry

The redox property of the complex **10** was measured by cyclic voltammetry in a dichloromethane solution by using 0.1 M TBAP as the supporting electrolyte. Complex **10** exhibited three voltammetric response, one reversible oxidation couple with $E_{1/2}$ value near +0.60 V probably due to the oxidation of nitroso group in the ligand frame, one irreversible reduction with $E_{1/2}$ value –0.83V and one quasi-reversible reduction couple

with $E_{1/2}$ value –1.36 V *vs*. Ag/AgCl (Figure 5.8). Two cathodic peaks were observed probably due to reduction of azo group and nitroso group in ligand frame.[281]

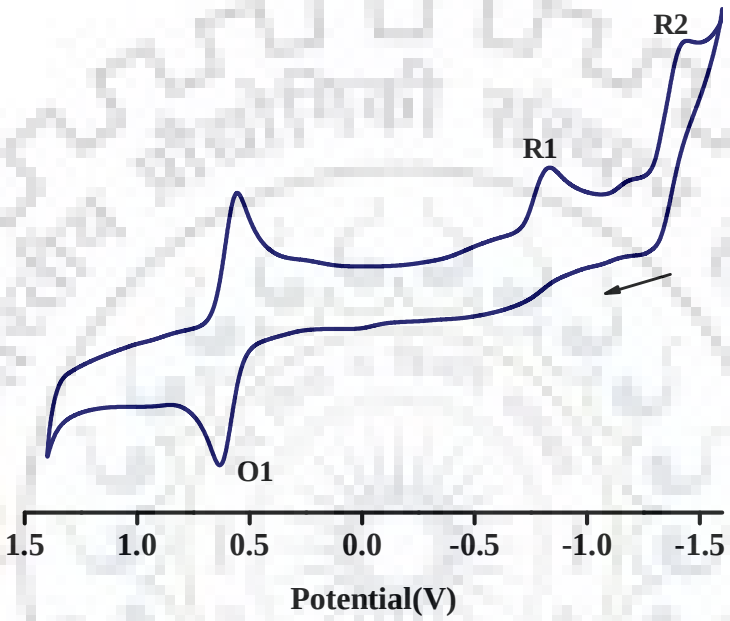

Fig. 5.8 Cyclic voltammogram of 10^{-3} M solution of complex **10** in the presence of 0.1 M tetrabutylammonium perchlorate (TBAP), using a working electrode (glassy-carbon), reference electrode (Ag/AgCl) and auxiliary electrode (platinum wire), scan rate = 0.1 Vs^{-1}.

5.2.4. GC-MS spectrum of triphenylphosphine oxide(TPPO)

During the synthesis of complex **10**, oxygen atom transfer took place from nitro group of ligand L^8H to one of labile triphenylphosphine of $Ru(PPh_3)_3Cl_2$ and triphenylphosphine oxide was extracted from the filtrate. It was characterized using GC-MS chromatography and GC-MS spectrum of TPPO is given in Figure 5.9.

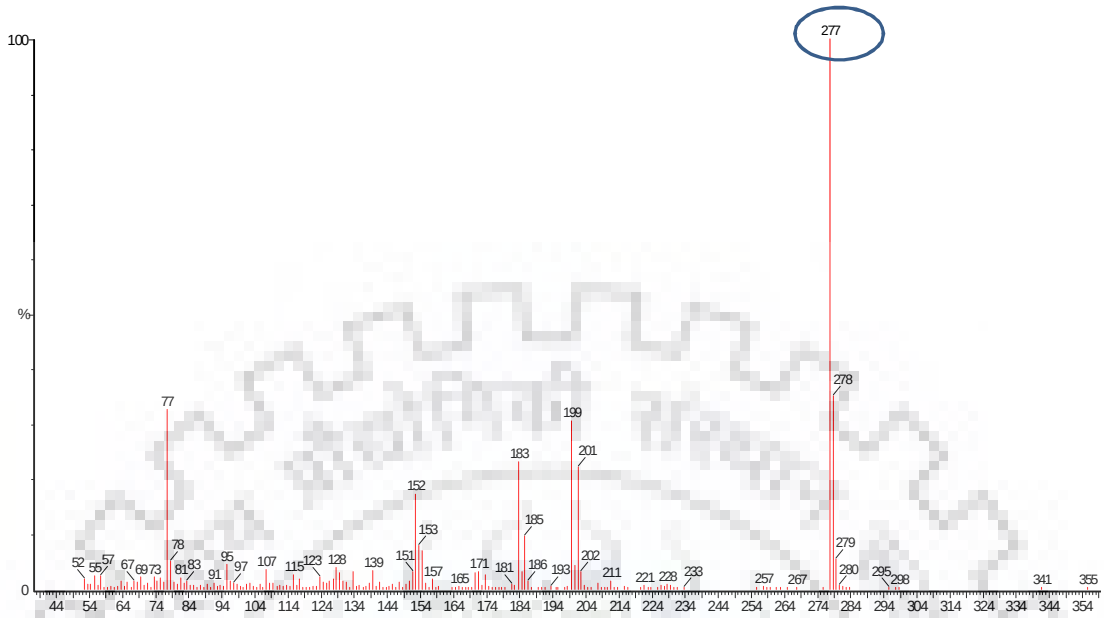

Fig. 5.9 GC-MS spectrum of triphenylphosphine oxide.

5.2.5. Density functional theory (DFT) calculations

All DFT optimizations have been carried out by employing a B3LYP hybrid functional using the Gaussian 09, revision B.01, package software package.[282] The method used was Becke's three parameter hybrid exchange functional, the nonlocal correlation provided by the Lee, Yang, and Parr expression, and Vosko, Wilk, and Nuair 1980 correlation functional (III) for local correction.[283-285] The basis set was LANL2DZ for ruthenium atom and 6-31g+(d,p) for carbon, nitrogen, oxygen, chlorine, phosphorous and hydrogen atoms. The coordinates are taken directly from the single crystal X-ray data and subsequently unconstrained geometry optimization of the molecules are done keeping the spin-state (low-spin) constant both for ruthenium with the complex having overall charge 0 and spin multiplicity of 3 for ferromagnetic interactions. The symmetry-broken,[286] singlet-diradical wave function of the complex was subsequently optimized. Frequency calculations were also executed on all optimized structures to ensure that there are zero or very few imaginary frequencies.

The Mulliken spin density plot of complex **10** showed that the total 92% spin density is distributed over the coordinated nitroso group (44% spin density is distributed over nitrogen and 48% spin density is distributed over oxygen of nitroso group) which confirmed the presence of one unpaired electron over the ligand and 72% spin density is located over metal center corresponding to one unpaired electron (shown in Figure 5.10). From spin density distribution, it was confirmed that there are two unpaired electrons in complex **10**.

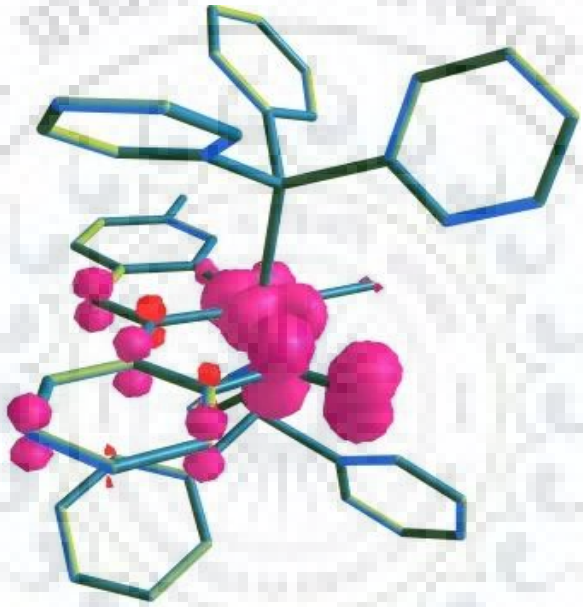

Fig. 5.10 Spin density plot of complex **10**.

The singly occupied molecular orbital (SOMO) of complex **10** (shown in Figure 5.11) was found to be located over the ligand (84%) along with minor contribution of metal centre (13%).

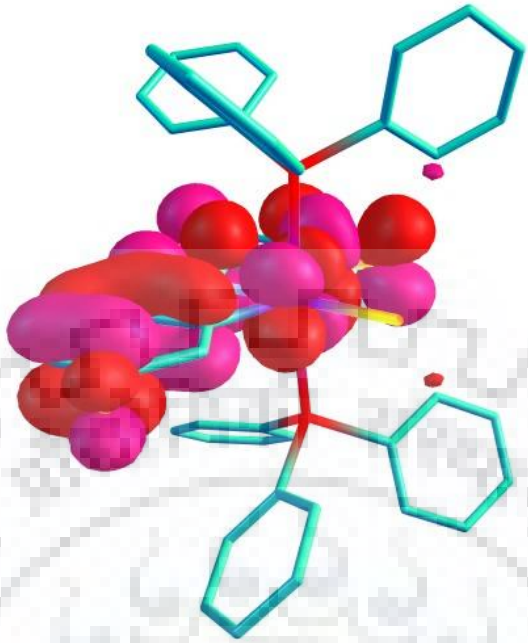

Fig. 5.11 SOMO of complex **10**.

5.3. Conclusions

Following are the major findings and conclusions of the present study (**a**) Non innocent ligand L^8H was systematically designed and synthesized (**b**) Reduction of nitro group to nitroso and oxygen atom transfer to triphenylphosphine was extremely important during synthesis of organometallic ruthenium complex **10**. (**c**) A rare example of generation of anion radical on nitroso group in **10** during the reduction of nitro group and C-H bond activation. (**d**) A rare example of generation of organometallic azo anion radical in **11** during the nitrosylation of complex **10**. (**e**) Both the complexes were characterized using IR, UV-vis, NMR spectroscopy (**f**) Molecular structures of both the complexes were authenticated using X-ray crystallography (**g**) Redox properties of complex **10** were investigated using cyclic voltammetry. (**h**) DFT calculations were performed to better understand the electronic properties of complex **10**.

5.4. Experimental section

5.4.1. Reagents and materials

All the reagents used were of analytical grade. 2-nitroaniline, phenol, sodium perchlorate monohydrate, sodium nitrite (Himedia Laboratories Pvt. Ltd., Mumbai, India) were used as obtained. $RuCl_3.3H_2O$ was purchased from Loba Chemie Pvt. Ltd., Mumbai, India. Triphenylphosphine (SRL,Mumbai, India) were used as obtained. Distilled solvents were used during the experiments. The precursor $[Ru(PPh_3)_3Cl_2]$ was prepared by following the procedure reported earlier.[233]

Infrared spectra were obtained as KBr pellets with Thermo Nicolet Nexus FT–IR spectrometer, using 16 scans and were reported in cm^{-1}. ^1H and ^{31}P NMR spectra were recorded on JEOL, 400 MHz spectrometer in the deuterated solvents. Electronic absorption spectra of the complexes were recorded in dichloromethane solvent with an Evolution 600, Thermo Scientific (Shimadzu) UV–vis spectrophotometer.

5.4.2. Synthesis of ligand and ruthenium complexes

5.4.2.1. Synthesis of (E)-4-((2-nitrophenyl)diazenyl)phenol(L^8H))

Ligand L^8H was synthesized by coupling reaction of diazotized 2-nitro aniline with phenol. ^1H NMR (DMSO-d_6, 400 MHz): δ 10.56 (s, 1H), 8.02 (d, 1H), 7.72 (m, 5H), 6.93 (d, 2H) ppm.

5.4.2.2. Synthesis of $[Ru(L_A^{8-\cdot})(Cl)(PPh_3)_2]$ (10)

A batch of $Ru(PPh_3)_3Cl_2$ (0.1 mmol) was added to a methanol solution (35 mL) of L^8H (0.15 mmol) and the mixture was refluxed for 4 h at 85 °C with continuous stirring. It was then cooled to room temperature. The dark green solid was filtered out and washed thoroughly with methanol and diethyl ether and then dried. Yield: (61%). IR (KBr disk, in cm–1): 1574

(νN=N), 743, 692, 513 (νPPh3). UV–vis (CH_2Cl_2; λmax, nm (ε, $M^{-1}cm^{-1}$)): 366(13068), 423(7500), 497(4909), 646(3181).

5.4.2.3. Synthesis of $[Ru(L_B^{8-\cdot})(NO)(PPh_3)_2](ClO_4)$ (11)

A batch of (0.090 g, 0.1 mmol) of complex **10** was taken in 30 mL of dichloromethane to obtain a green colored solution in round bottom flask of 100 mL. Now 20 mL acidified distilled water (p^H ~2.5) was added to this solution. Sodium nitrite (0.4 g) was added to the above solution and stirred at room temperature for 2.5 hours to get dark greenish blue colored solution. Sodium perchlorate dissolved in 10 mL of methanol was added to the dichloromethane layer which was separated out. And above solution was further stirred for 1 hour. The solvent mixture was evaporated to get dark greenish blue solid of complex **11**. To remove excess of sodium perchlorate, solid was further dissolved in dichloromethane and filtered out. Yield: 58 %. IR (KBr disk, cm^{-1}): 1874 (ν_{NO}), 745, 695, 520 (ν_{PPh3}), 1093, 622 (ν_{ClO4}), cm^{-1}. UV-Vis (CH_2Cl_2; λ_{max}/nm (ε, $M^{-1}cm^{-1}$)): 369(26205), 583(14256), 743(1969). ^1H NMR ($CDCl_3$, 400MHz): δ 7.59 (s, 1H), 7.50-7.14 (m, 32H), 6.59 (s, 1H), 6.34(d, 1H), 6.25(d, 1H) ppm. ^{31}P NMR ($CDCl_3$, 400 MHz): δ 20.24 ppm.

5.5. X–ray crystallography

Crystals of complexes **10** and **11** were obtained via layering of hexane over a solution of dichloromethane which were suitable for diffraction study. The X–ray data collection and processing for complexes **10** and **11** were performed with Bruker Kappa Apex–II CCD diffractometer using graphite monochromated Mo–Kα radiation (λ = 0.71073 Å) at 273K. Crystal structures were solved by direct method. Structure solutions, refinement and data output were carried out by the SHELXTL program.[235,236] All non–hydrogen atoms were

refined anisotropically and hydrogen atoms were placed in geometrically calculated positions and refined using a riding model. Image was created using DIAMOND program.[237]

Anticancer Properties of Half-Sandwich Ruthenium(II) Schiff Base Complexes

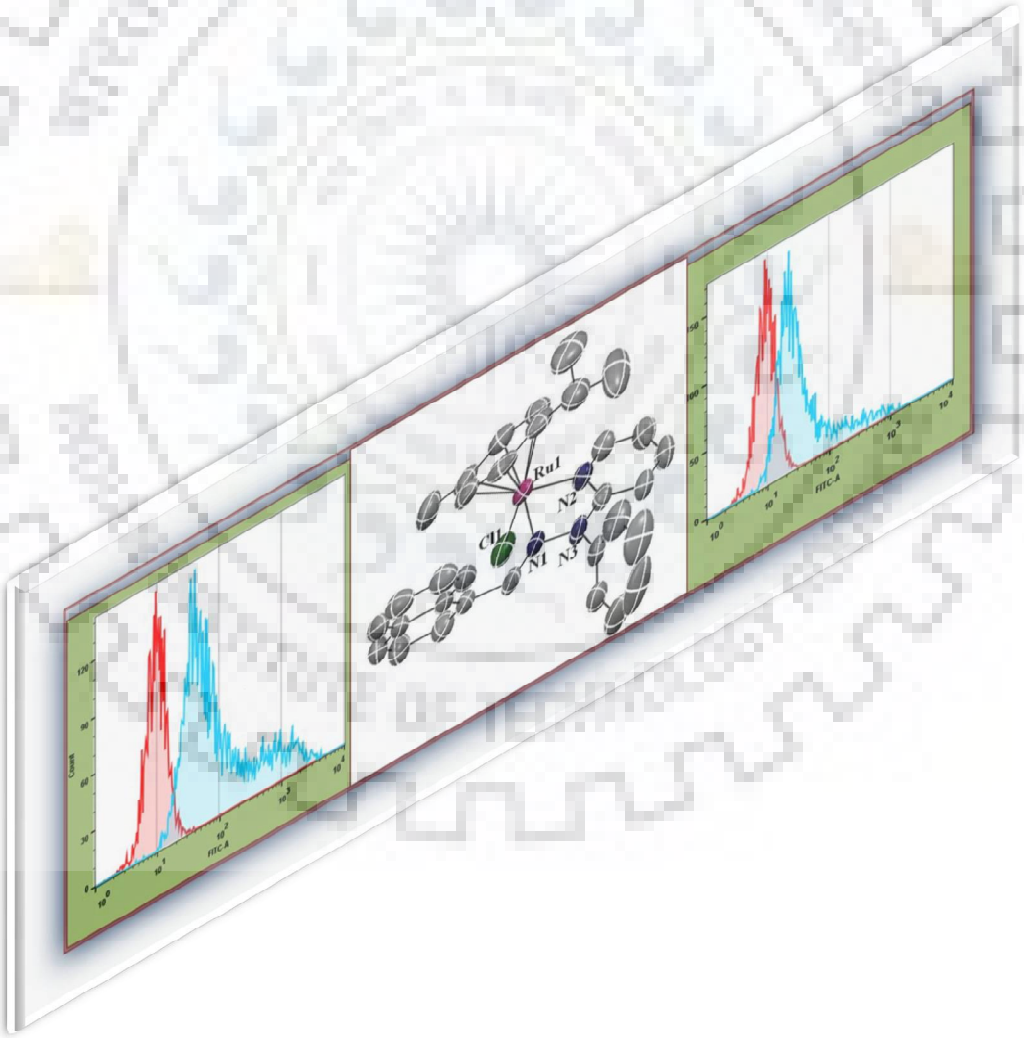

Chapter 6

Abstract

Half sandwich ruthenium complexes [(p-cym)$Ru^{II}(L^{9-12})Cl]PF_6$(**12-15**) containing N^N chelating schiff base ligand were successfully designed and synthesized. All the synthesized complexes were characterized by UV-vis, IR, ESI-MS, NMR spectroscopic studies. Molecular structures of **12** and **15** were authenticated using X-ray crystallography. Complexes **12-15** were utilized to investigate the anti-cancer activity studies on MCF-7, MDA-MB-435s and HEK-293 cell lines. Among all the complexes, complex **15** was found to be more potent against MCF-7 and MDA-MB-435s cancer cells as compared to complexes **12-14**. However, all the complexes exhibited less cytotoxicity or almost inactivity towards HEK-293 normal cells.

6.1. Introduction

Cancer, one of the most fatal diseases, embraces a large group of dreadful diseases in the world and causes the death of millions of people every year. It is characterized by the division of abnormal cells in an uncontrolled manner that disrupt tissues. Factors responsible for cancer may be either external such as chemicals, radiation, viruses or internal such as hormones, immune conditions, inherited genes.[86-89]

Platinum based metallodrugs e.g. cisplatin, carboplatin and oxaliplatin are broadly used for cancer treatment as chemotherapeutic agents. However, tumour resistance and their several side effects like immunosuppression, renal toxicity, myelosuppression, neurotoxicity, severe nausea, vomiting has significantly slowed down the introduction of new platinum-based derivatives into clinical studies. Therefore, the approaches to explore alternative anticancer drugs derived from transition metal complexes with similar therapeutic profiles to cisplatin, but without its drawbacks dominate the research in field of cancer.[90,91]

A large number of metal complexes with aromatic N, P, O, S donor ligands with particular attention to ruthenium most likely due to the iron mimicking ability of ruthenium in binding to biomolecules,[89] have been used as promising anticancer agents.[224,287-290] Even though, a wide range of ruthenium complexes have been reported, ruthenium–arene complexes with modified ligands find their significance as anticancer agents.[88,89,291-298]

The N^N-chelating ligands which coordinate to a wide range of metals in coordination chemistry, have found vast applications in medicinal chemistry.[288] Inspired by these valuable findings, herein we designed and synthesized a series of new half sandwich p-cymene Ru(II) complexes $[(p\text{-cym})Ru^{II}(L^{9\text{-}12})Cl]PF_6$(**12-15**) containing N^N- chelating imino-pyridyl ligands (Scheme 6.1). We also studied the cytotoxicity of all the complexes **12-15** on MCF-7,

MDA-MB-435s and HEK293 cell lines using MTT assay. We further performed the experiments including apoptosis assay, elevation in reactive oxygen species (ROS) level and human serum albumin (HAS) binding. Among all these complexes, complex **15** was found to be more potent against MCF-7 and MDA-MB-435s cancer cells as compared to complexes **12-14**. However, all the complexes exhibited less cytotoxicity or almost inactivity towards HEK293 normal cells.

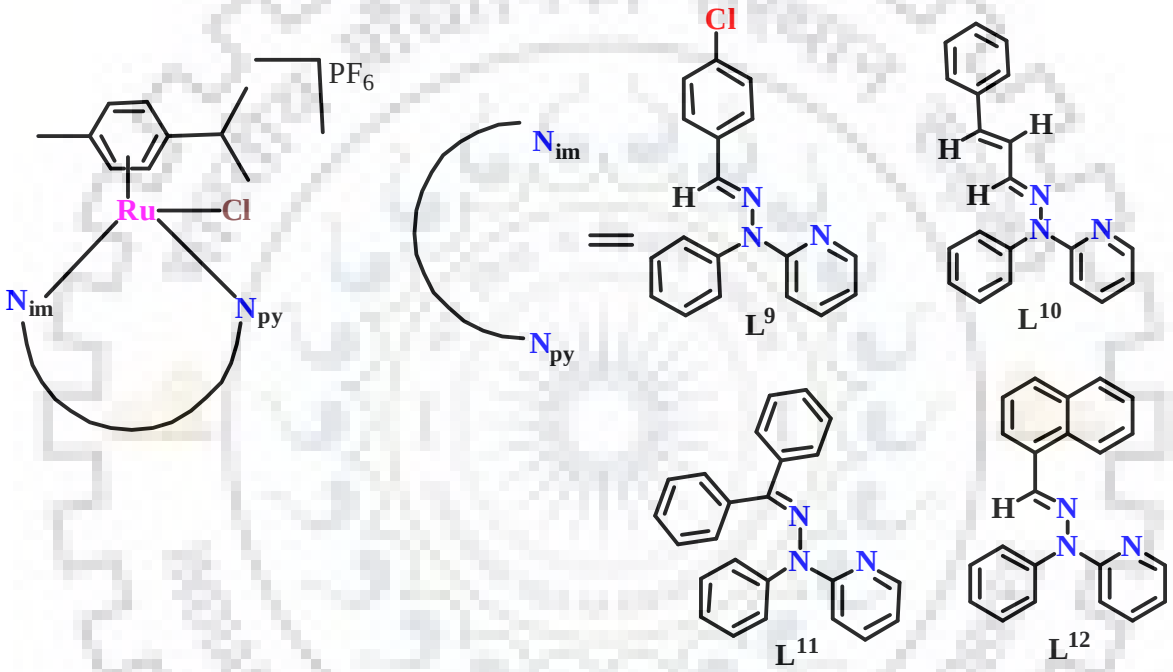

Scheme 6.1 Complexes **12-15** with ligands **L**$^{9-12}$

6.2. Results and discussion

6.2.1. Syntheses and characterization of ligands and ruthenium complexes

Ligands L^{9-12} were obtained in high yield by condensation reaction of 2-(1-phenylhydrazinyl)pyridine with p-chloro benzaldehyde, cinnamaldehyde, benzophenone, naphthaldehyde respectively in methanol. $[(\eta^6\text{-cymene})RuCl_2]_2$ was added to methanolic

solution (20 mL) of the ligands L^{9-12} to afford the ruthenium(II) complexes [(η^6-cymene)$Ru^{II}(L^{9-12})Cl]PF_6$ (**12-15**) respectively. The complexes **12, 13, 15** were yellow and complex **14** was orange in color. All the complexes were highly soluble in dichloromethane, dimethylformamide and dimethylsulphoxide but less soluble in water.

In the IR spectra of complexes **12-15** (Figure 6.1), peaks around 840 cm^{-1} and 560 cm^{-1} confirmed the presence of hexafluoro phosphate as counter anion (Table 6.1).[224]

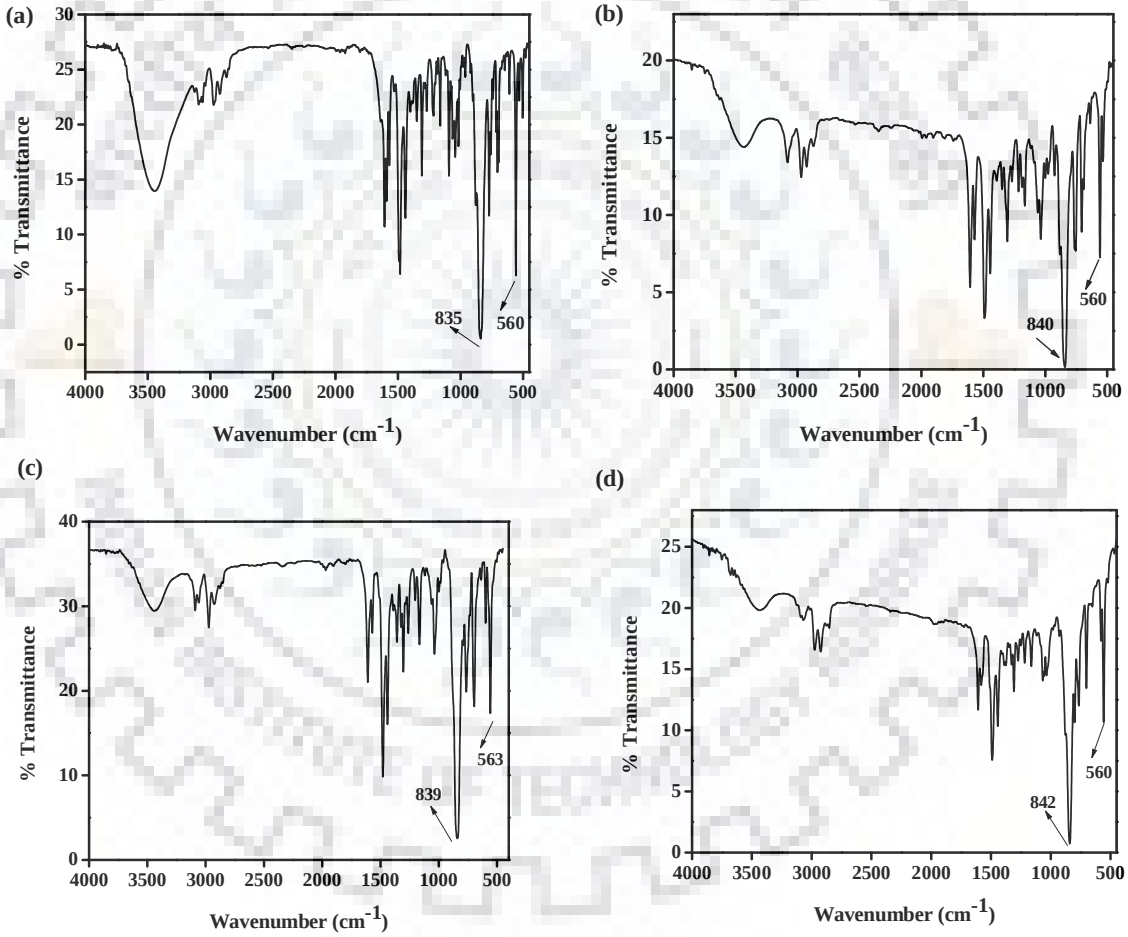

Fig. 6.1 Infrared spectra of ruthenium complexes (a) **12** (b) **13** (c) **14** and (d) **15**.

Table 6.1 Data for IR spectral studies.

Complex	IR data (cm^{-1}, KBr pellets)	
	$\nu_{C=N}$	ν_{PF6}
12	1613	835, 560
13	1605	840, 560
14	1617	839, 563
15	1611	842, 560

The electronic absorption spectra of complexes **12-15** were displayed in Figure 6.2. In all the complexes **12-15**, charge transfer band with λ_{max} above 300 nm (Table 6.2) observed which was probably due to metal to ligand charge transfer (MLCT) transition.

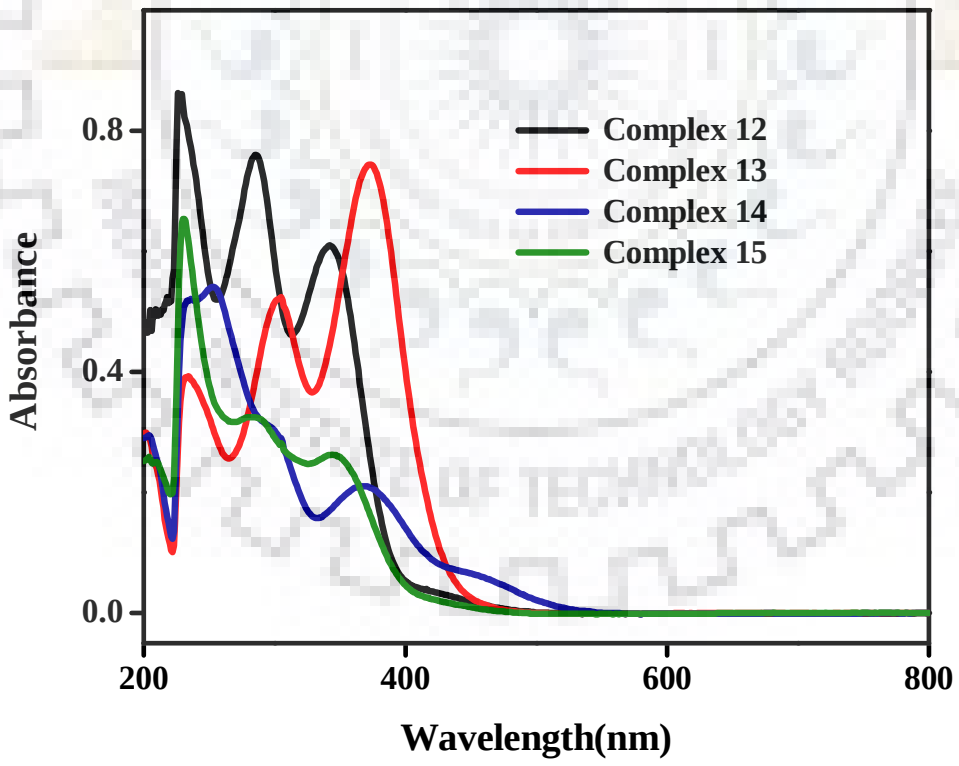

Fig. 6.2 Electronic absorption spectra of **12-15** in dichloromethane solutions.

Table 6.2 Electronic absorption spectral data for ruthenium complexes **12-15**.

Complex	λ_{max}/nm (ε / $M^{-1}cm^{-1}$)
12	226 (10963), 284(9686), 340(7764)
13	233 (18073), 303(24082), 370(34403)
14	253(16355), 367(6476), 450(2169)
15	230 (24962), 285(12310), 345(10075)

The ^{1}H NMR spectra of the ligands (L^{9-12}) were displayed in Figures 6.3-6.6, respectively. All the complexes were found to be diamagnetic which was confirmed by ^{1}H NMR spectral studies (Table 6.3). The ^{1}H NMR spectra of complexes **12-15** were displayed in Figures 6.7-6.10, respectively.

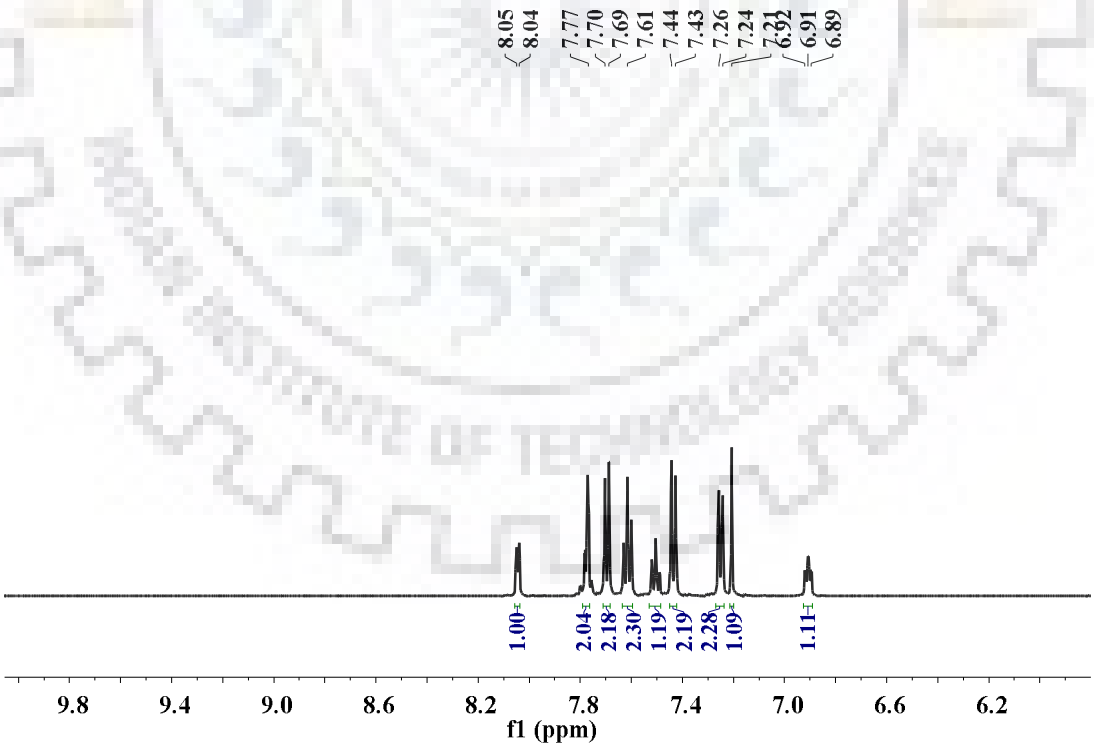

Fig. 6.3 ^{1}H NMR spectrum of ligand $\mathbf{L^9}$ in DMSO-d_6 at room temperature.

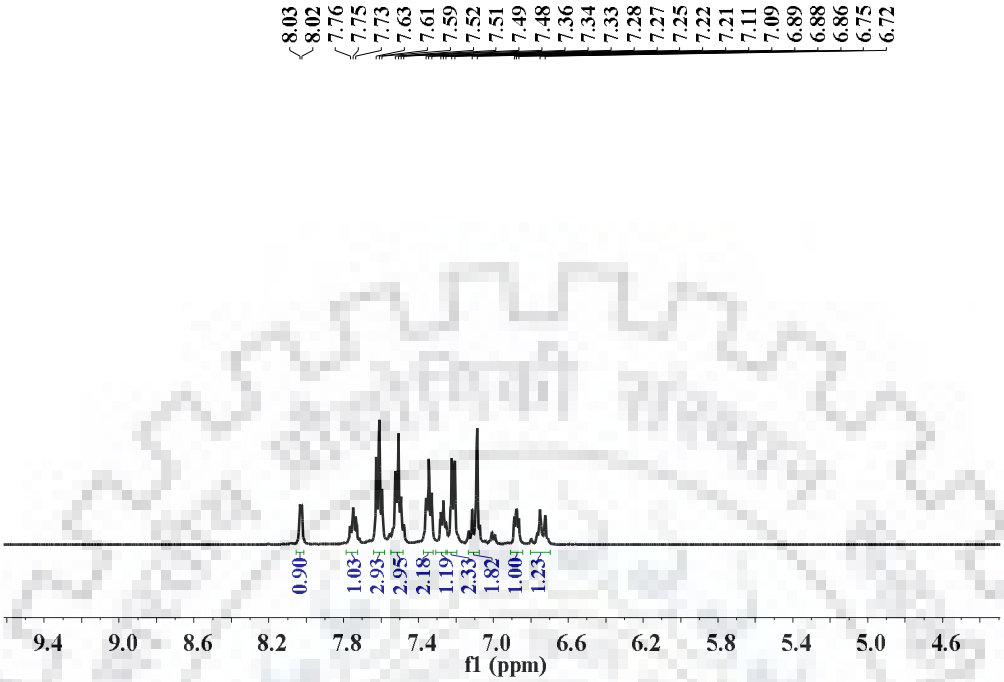

Fig. 6.4 ^{1}H NMR spectrum of ligand **L**^{10} in DMSO- d_6 at room temperature.

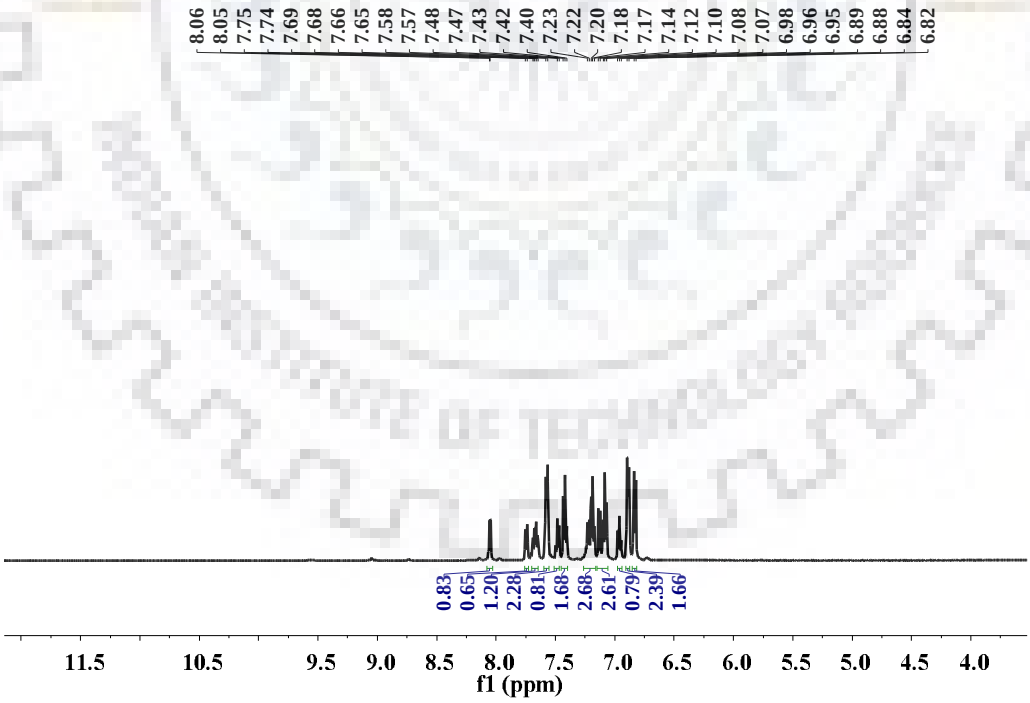

Fig. 6.5 ^{1}H NMR spectrum of ligand **L**^{11} in DMSO- d_6 at room temperature.

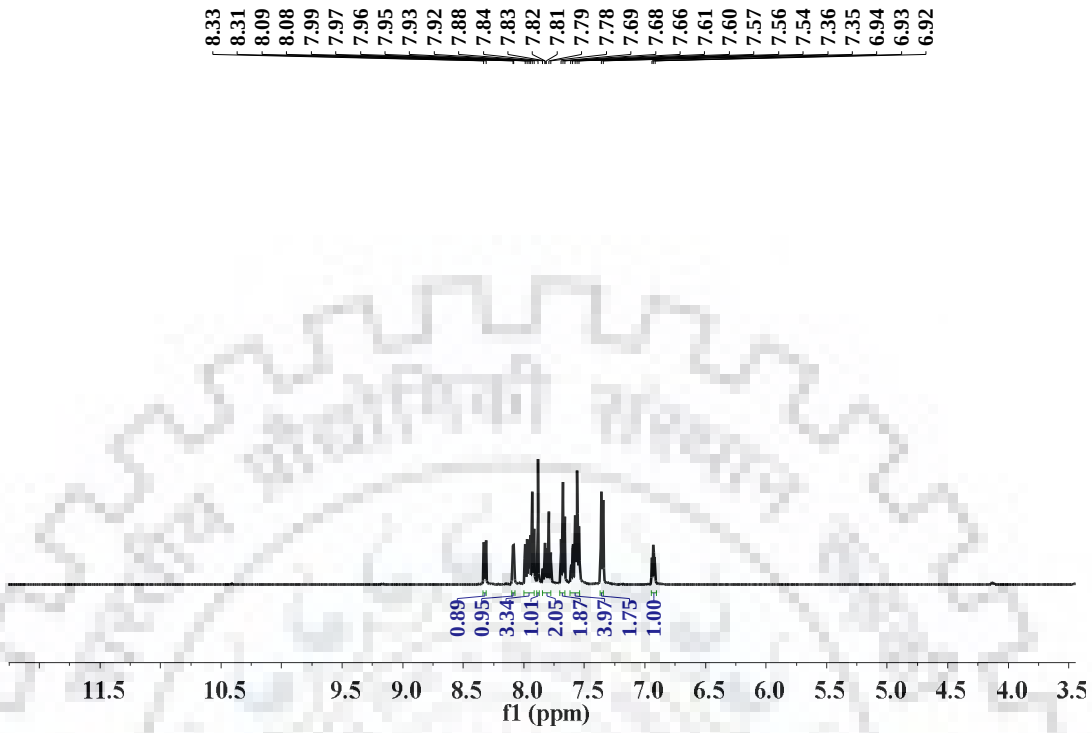

Fig. 6.6 ^{1}H NMR spectrum of ligand **L**^{12} in DMSO- d_6 at room temperature.

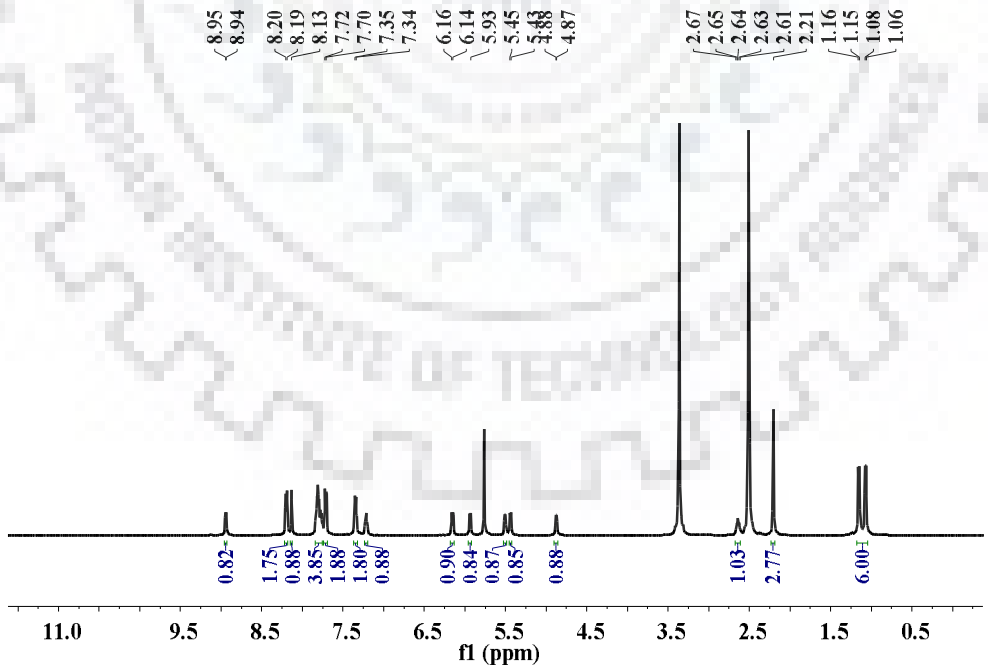

Fig. 6.7 ^{1}H NMR spectrum of complex **12** in DMSO- d_6 at room temperature.

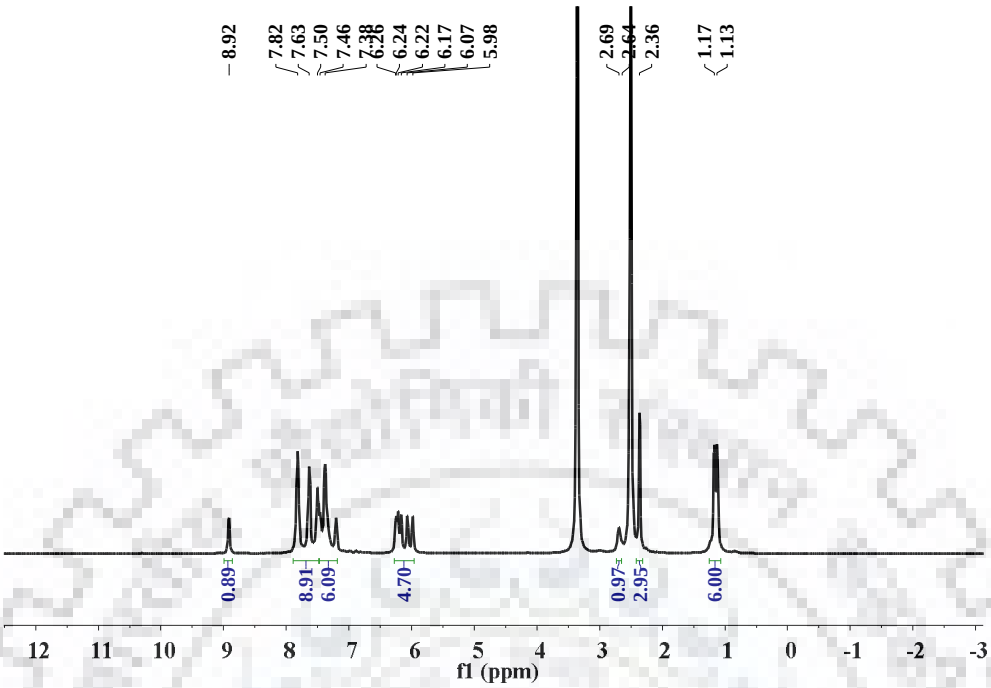

Fig. 6.8 ^{1}H NMR spectrum of complex **13** in DMSO- d_6 at room temperature.

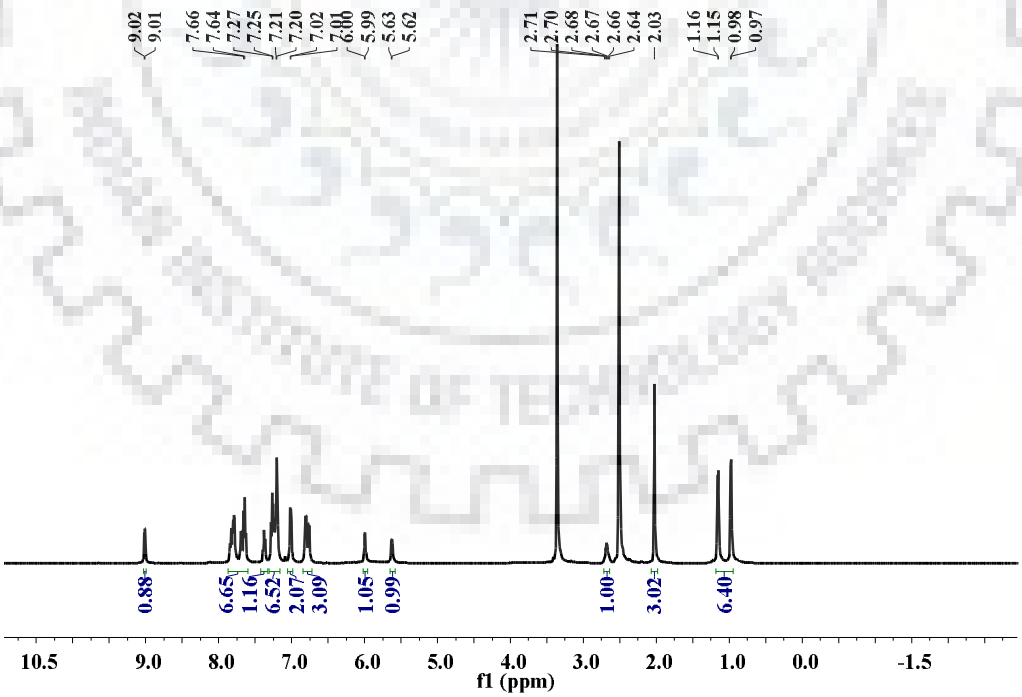

Fig. 6.9 ^{1}H NMR spectrum of complex **14** in DMSO- d_6 at room temperature.

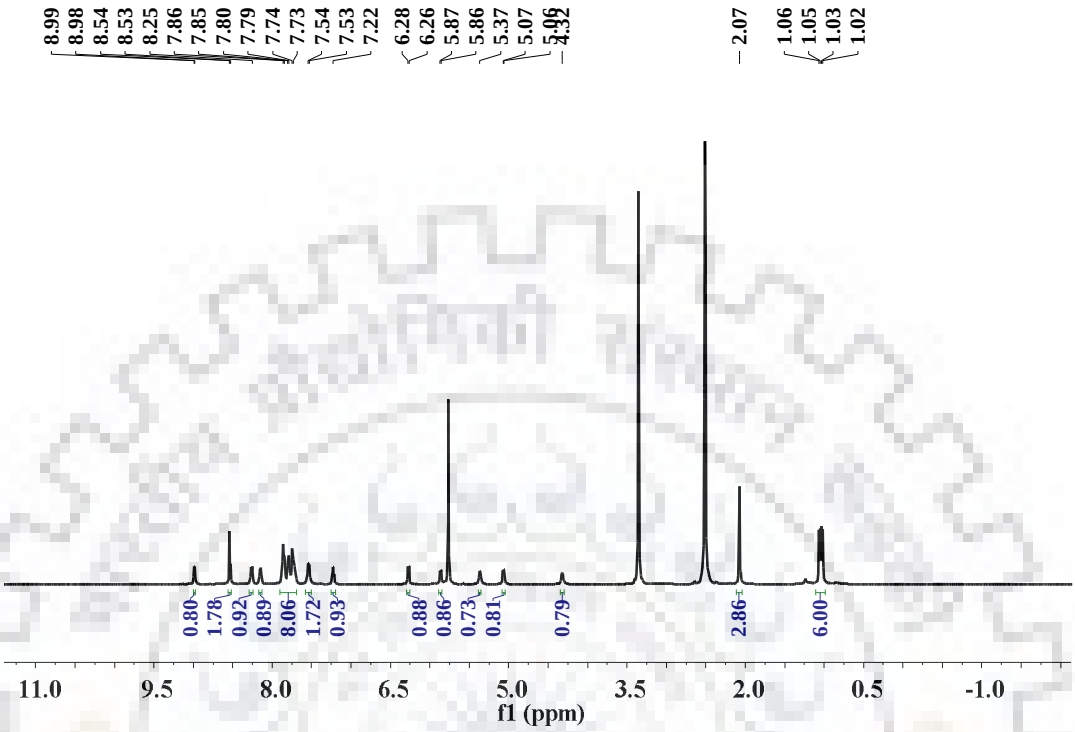

Fig. 6.10 ^{1}H NMR spectrum of complex **15** in DMSO- d_6 at room temperature.

The ESI-MS spectra for complexes **13** and **14** in acetonitrile showed mass peak at m/z 570.1246$[M - PF_6]^+$ and 620.1401$[M - PF_6]^+$ respectively shown in Figure 6.11-6.12.

Table 6.3 NMR spectral data for ligands $\mathbf{L^{9-12}}$ and ruthenium complexes **12-15**.

Complex	^{1}H NMR (δ /ppm)
$\mathbf{L^9}$	8.05-8.04 (d, 1H), 7.80-7.76 (m, 2H), 7.70-7.69 (d, 2H), 7.63-7.60 (t, 2H), 7.52-7.49 (t, 1H), 7.44-7.43 (d, 2H), 7.26-7.24 (d, 2H), 7.21 (s, 1H), 6.92-6.89 (t, 1H)
$\mathbf{L^{10}}$	8.03-8.02 (d, 1H), 7.76-7.73 (t, 1H), 7.63-7.59 (t, 3H), 7.52-7.48 (m, 3H), 7.36-7.33 (t, 2H), 7.28-7.25 (t, 1H), 7.22-7.21 (d, 2H), 7.11-7.09 (d, 2H), 6.89-6.86 (t, 1H), 6.75-6.72 (d, 1H)
$\mathbf{L^{11}}$	8.06-8.05 (d, 1H), 7.75-7.74 (d, 1H), 7.69-7.65 (m, 1H), 7.58-7.57 (d, 2H), 7.48-7.47 (d, 1H), 7.43-7.40 (t, 2H), 7.23-7.17 (m, 3H), 7.14-7.07 (m, 3H), 6.98-6.95 (t, 1H), 6.89-6.88 (d, 2H), 6.84-6.82 (d, 2H)
$\mathbf{L^{12}}$	8.33-8.31 (d, 1H), 8.09-8.08 (d, 1H), 7.99-7.92 (m, 3H), 7.88 (s, 1H), 7.84-7.78 (m, 2H), 7.69-7.66 (t, 2H), 7.61-7.54 (m, 4H), 7.36-7.35 (d, 2H), 6.94-6.92 (t, 1H)
12	8.95-8.94 (d, 1H), 8.20-8.19 (d, 2H), 8.13 (s, 1H), 7.83-7.76 (m, 4H), 7.72-7.70 (d, 2H), 7.35-7.34 (d, 2H), 7.23-7.20 (t, 1H), 6.16-6.14 (d, 1H), 5.94-5.93 (d, 1H), 5.57-5.50 (d, 1H), 5.45-5.43 (d, 1H), 4.88-4.87 (d, 1H), 2.67-2.61 (m, 1H), 2.21 (s, 3H), 1.16-1.15, 1.08-1.06 (d, 3H, d, 3H)
13	8.92 (d, 1H), 8.20-8.19 (d, 2H), 8.13 (s, 1H), 7.83-7.76 (m, 4H), 7.72-7.70 (d, 2H), 7.35-7.34 (d, 2H), 7.23-7.20 (t, 1H), 6.16-6.14 (d, 1H), 5.94-5.93 (d, 1H), 5.57-5.50 (d, 1H), 5.45-5.43 (d, 1H), 4.88-4.87 (d, 1H), 2.67-2.61 (m, 1H), 2.21 (s, 3H), 1.16-1.15, 1.08-1.06 (d, 3H, d, 3H)
14	9.02-9.01 (d, 1H), 7.84-7.63(m, 7H), 7.39-7.36 (t, 1H), 7.28-7.20(m, 7H), 7.02-7.01 (d, 2H), 6.81-6.75(m, 3H), 6.00-5.99 (d, 1H), 5.63-5.62 (d, 1H), 2.71-2.64 (m, 1H), 2.03 (s, 3H), 1.16-1.15, 0.98-0.97 (d, 3H, d, 3H)
15	8.99-8.98 (d, 1H), 8.54-8.53 (m, 2H), 8.27-8.25 (d, 1H), 8.16-8.14 (d, 1H), 7.86-7.73 (m, 8H), 7.54-7.53 (d, 2H), 7.24-7.21 (t, 1H), 6.28-6.26 (d, 1H), 5.87-5.86 (d, 1H), 5.37-5.36 (d, 1H), 5.07-5.06 (d, 1H), 4.32 (s, 1H), 2.07 (s, 3H), 1.06-1.02 (m, 6H)

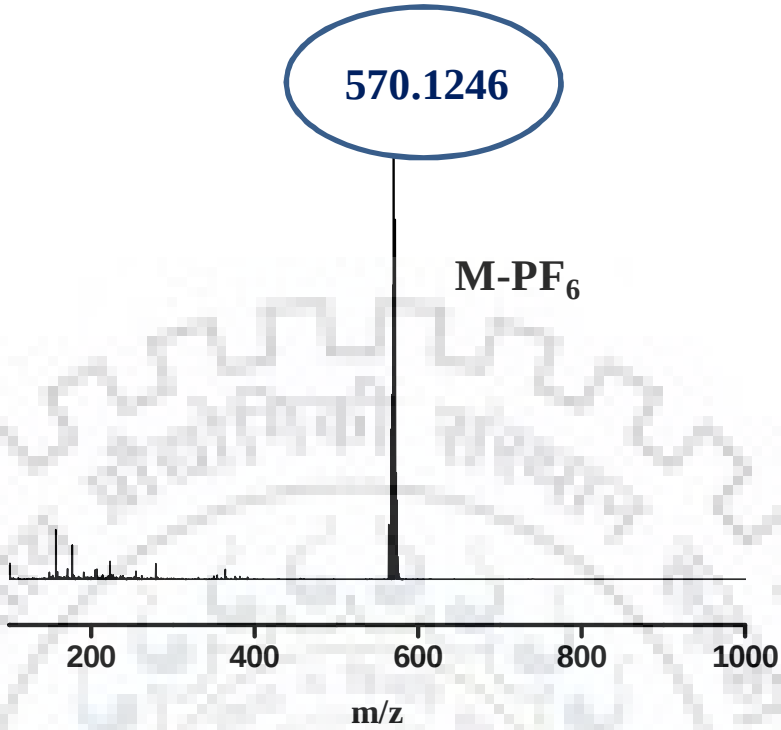

Fig. 6.11 ESI–MS positive ion specrtum of complex **13** (acetonitrile solvent was used). Units *m*/*z* in Da.

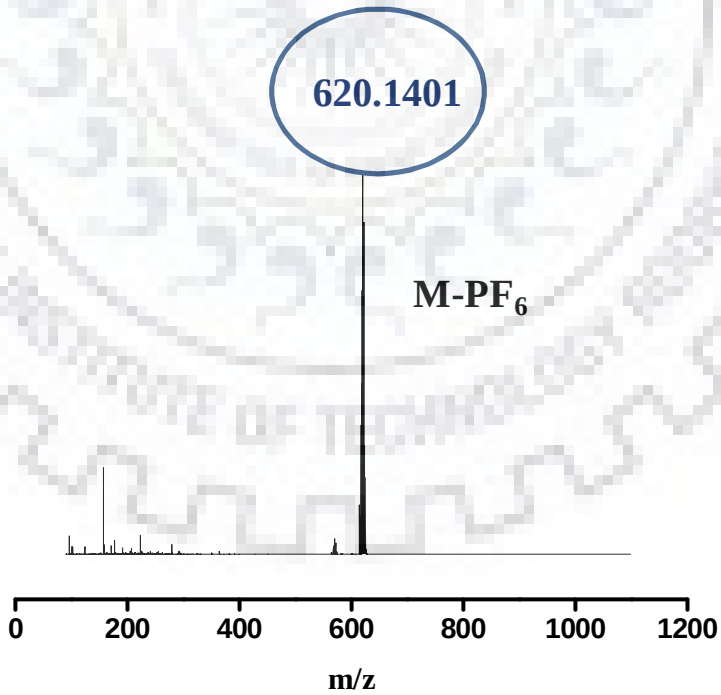

Fig. 6.12 ESI–MS positive ion specrtum of complex **14** (acetonitrile solvent was used). Units *m*/*z* in Da.

6.2.2. Description of molecular structures

The molecular structures of the complexes [(η^6-cymene)$Ru^{II}(L^9)$Cl]PF_6 (**12**) and [(η^6-cymene)$Ru^{II}(L^{12})$Cl]PF_6 (**15**) are depicted in Fig. 6.13 and Fig. 6.14 respectively.

The selected bond lengths and bond angles of complexes **12** and **15** are given in Table 6.4. Crystal data collection and refinement details of the structures of complexes **12** and **15** are summarized in Table 6.5. In the crystal structures of **12** and **15**, the ruthenium centre adopted a distorted-octahedral geometry as reflected in parameters given in Table 6.4. In all the complexes, PF_6 stretching frequency (ν_{PF6}~840cm^{-1}) was consistent with reported values.[224]

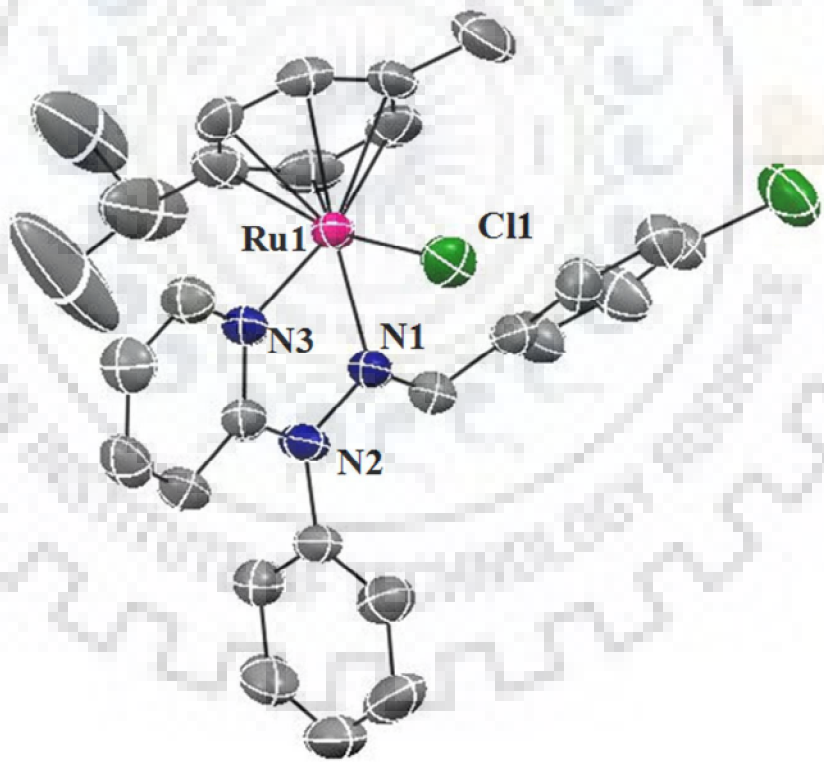

Fig. 6.13 ORTEP diagram (50% probability level) of the [(η^6-cymene)$Ru^{II}(L^9)$Cl]PF_6 (**12**). All hydrogen atoms, counter anion have been omitted for clarity.

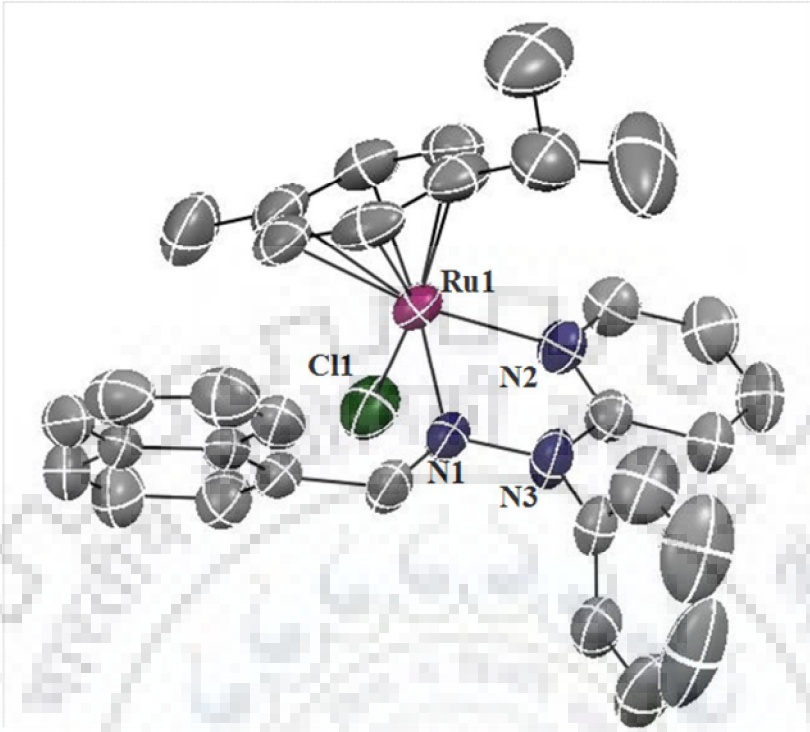

Fig. 6.14 ORTEP diagram (50% probability level) of the $[(\eta^6\text{-cymene})Ru^{II}(L^{12})Cl]PF_6$ (**15**). All hydrogen atoms, counter anion have been omitted for clarity.

Table 6.4 Selected bond lengths (Å) and bond angles (deg.) of complexes **12** and **15**.

Bond lengths (Å)		Bond angles (°)	
		12	
Ru(1)−Cl(1)	2.387(9)	N(1)−Ru(1)−Cl(1)	88.13(7)
Ru(1)−N(3)	2.064(3)	N(1)−Ru(1)−N(3)	76.96(10)
Ru(1)−N(1)	2.116(2)	Cl(1)−Ru(1)−N(3)	84.43(8)
		15	
Ru(1)−Cl(1)	2.386(10)	N(1)−Ru(1)−Cl(1)	90.68(9)
Ru(1)−N(2)	2.068(3)	N(1)−Ru(1)−N(2)	76.49(11)
Ru(1)−N(1)	2.120(3)	Cl(1)−Ru(1)−N(2)	82.68(9)

Table 6.5 Summary of crystal data and structural refinement parameters for complexes **12** and **15**.

	12	**15**
Empirical formula	C_{28} H_{28} Cl_2 N_3 Ru, F_6 P	C_{32} H_{31} Cl N_3 Ru, F_6 P
Formula weight	723.47	739.09
Temperature /K	296(2)	293(2)
Λ (Å) (Mo-Kα)	0.71073	0.71073
Crystal system	Monoclinic	Monoclinic
Space group	P 21/c	P 21/c
a (Å)	14.9108(6)	12.769(2)
b(Å)	10.0858(4)	14.750(3)
c (Å)	20.2271(7)	17.519(3)
α(°)	90.00	90.00
γ (°)	90.00	90.00
β(°)	97.559(2)	104.902(7)
V (Å^3)	3015.5(2)	3188.7(10)
Z	4	4
ρ_{calc} (gcm^{-3})	1.594	1.540
F(000)	1456.0	1496.0
Theta range	0.850-28.300	0.871−28.300
Index ranges	$-19<h<19$, $-23<k<23$, $-26<l<26$	$-17<h<17$, $-19<k<19$, $-23<l<23$
Data/restraints/par.	7431/0/373	7877/0/401
GOF^a on F^2	1.039	1.152
$R1^b$ [$I > 2\sigma(I)$]	0.0424	0.0521
$R1$[all data]	0.0563	0.0775
$wR2^c$ [$I > 2\sigma(I)$]	0.1070	0.1396
$wR2$ [all data]	0.1183	0.1736

6.2.3. Cell proliferation assay

Initially, the all synthesized complexes **12-15** were evaluated for their anti-proliferative properties on MCF-7, MDA-MB-435s and HEK293 cell lines by MTT assay. Each complex was screened in the concentration range of 0-250 µM, and treatments were given for 24 and 48 h. The cell viability results had shown that in the studied concentration range the complex **15** inhibit the proliferation of both the cancerous cell lines significantly, whereas complexes **12-14** inhibit the growth at very high concentration range (shown in the Figure 6.15). These results suggested that the complex **15** is more potential molecule than complexes **12**, **13** and **14**.

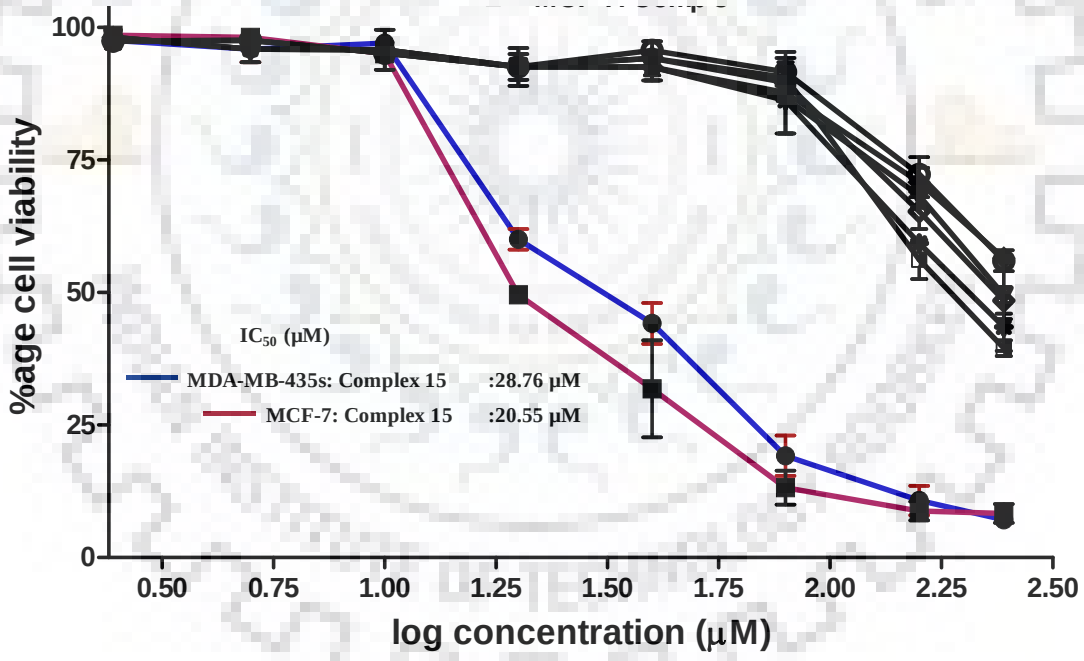

Fig. 6.15 Cell proliferation studies of selected cancer cells with complexes **12-15**. Outcome from the viability studies of MCF-7 and MDA-MB-435s cells in presence of increasing concentrations of each complex, treatment was given for 48 h. Cell viabilities were presented as the percentage of the number of viable cells to that of the control. Each data point shown is the mean ± SD from n=3. (For anticancer activities paclitaxel has been taken as positive control).

It was interesting that in the studied concentration range all of the synthesized complexes don't show any cytotoxicity towards HEK-293 cell lines (normal cells) (shown in the Figure 6.16). The IC_{50} values for the complex **15** have been shown in the inset of Figure 6.15. For complex **15**, the IC_{50} values were found to be 28.76 ± 0.82 μM for MDA-MB-435s cells and 20.55 ± 0.24 μM for MCF-7 cells. Further, the cytotoxicity of complex **15** at its respective IC_{50} value was also studied on HEK293 cells, it was observed that more than 85% of embryonic kidney cells are viable even after 72 h of treatment. These cell viability results clearly indicated that though all the synthesized complexes (**12-15**) are non-toxic to normal cells and, but complex **15** is more potent towards studied cancerous cells. Thus, complex **15** was taken for further cell based studies such as apoptosis and reactive oxygen species (ROS) production.

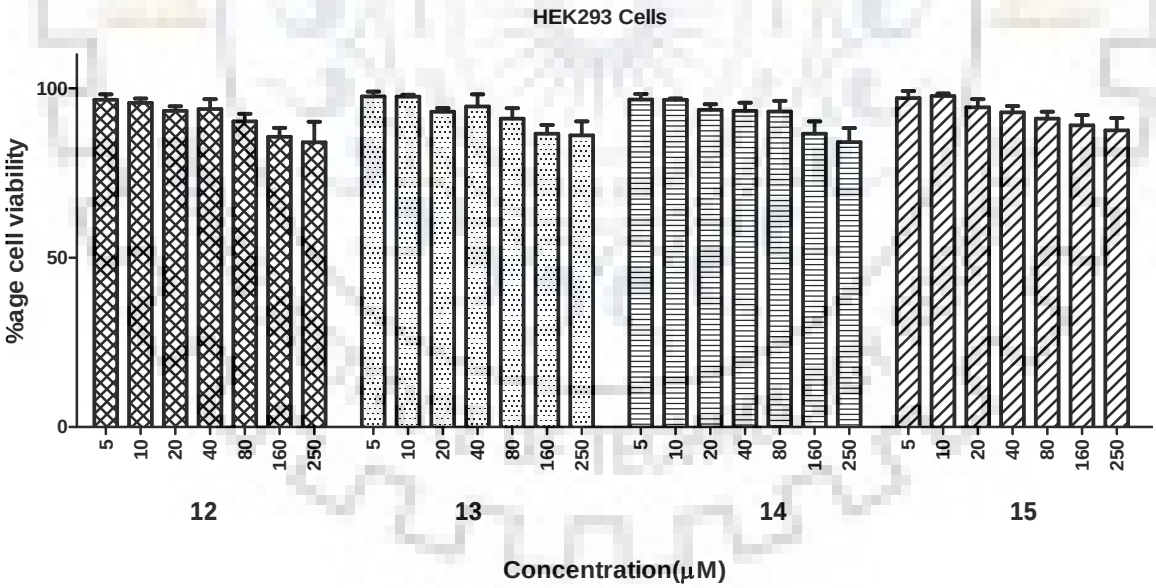

Fig. 6.16 Outcome from the cell viability studies of HEK293 cells in presence of increasing concentrations of complexes **12-15**, treatment was given for 48 h. Cell viabilities were presented as the percentage of the number of viable cells to that of the control.

6.2.4. Apoptosis assay

Evasion of apoptosis is a striking hallmark of all the cancerous cells, though it is an indispensable process abnormal cell growth, in case of cancerous cells impaired signaling helps them to overcome it.[299] Thus, it was of interest to see whether the decrease in cell viability in studied cancerous cells (MCF-7 and MDA-MB-435s) after the treatment of complex **15** is apoptosis mediated or not. The cells (MCF-7 and MDA-MB-435s) were starved in reduced serum medium and treated with IC_{50} dose of complex **15** for 24 h and subsequently annexin-V staining was used to evaluate the apoptotic potential of complex **15**. The annexin-V stained cells were analyzed by flow cytometry and it was found that the treatment of complex **15** considerably induces the apoptosis in both the cancerous cells (shown in Figure 6.17).

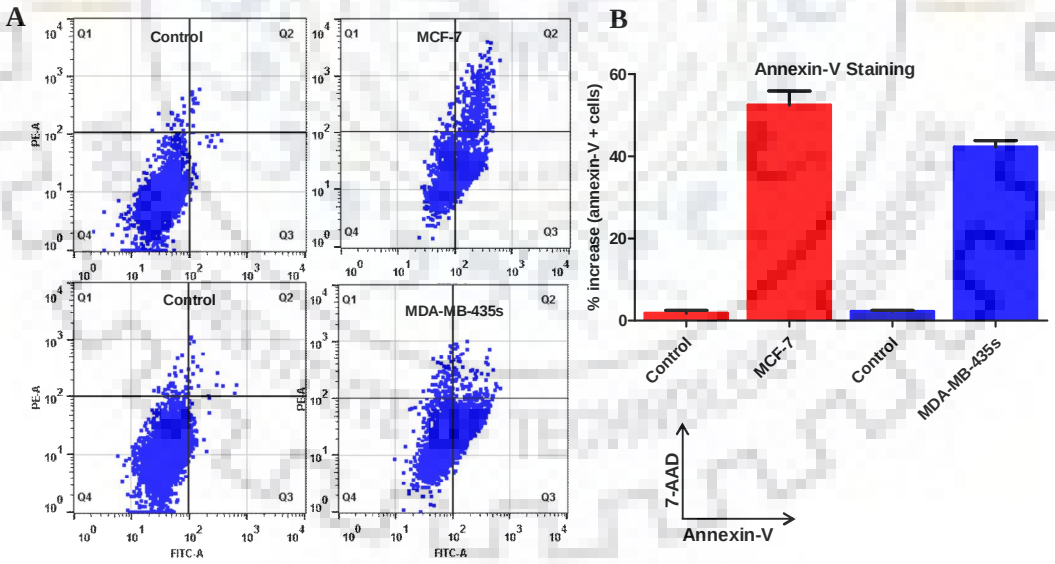

Fig. 6.17 MCF-7 and MDA-MB-435s cells were treated with IC_{50} concentrations of complex **15** for 24 h and apoptosis induction was studied using Annexin V-PI apoptosis kit **(A)** Histogram showing the distribution of anti-FITC-Annexin-V stained cells after the treatment of complex **15**. **(B)** Bar graphs represent the percentage of MCF-7 and MDA-MB-435s cells undergoing apoptosis for duplicate measurements ± SD.

Analysis of results suggested that treatment cells with IC_{50} dose of complex **15** induces apoptosis in 55.87 %, of MCF-7 cells and 40.71 %, of MDA-MB-435s cells as compared to the control cells (shown in Figure 6.17). Thus, the results of apoptosis studies suggested that the death of studied cancerous cells after the treatment of complex **15** is apoptosis mediated. These results are also in accordance of previously published results that treatment of cancerous cells with transition metal based drugs or Ru-based complexes causes cell death via apoptosis induction.[295,300]

6.2.5. ROS estimation

The mitochondrial metabolism is the main source of ROS which has the capacity to induce cell apoptosis.[301] Thus on the basis of apoptosis results, it was of significant importance to study the production of ROS after the treatment of cells with complex **15**. Both the cells were treated with IC_{50} dose of complex **15** for 5-6 h and the levels of ROS were measured with the help of flow cytometry by using 2-Dichlorofluorescein diacetate (DCFDA) staining. Results of ROS measurements clearly suggested that the treatment of cells with complex **15** increases the production of ROS (Figure 6.18). The treatment of cells with complex **15** shifts the position of respective histogram towards right (higher value), which indicates higher level of ROS. This increase in the level of ROS after the treatment of cells with complex **15** might be also be contributed to the cell death. These results were found to be consistent with the earlier studies that the increased levels of ROS after the treatment of some anticancer drugs/metal based drugs can activate a sequence of pro-apoptotic pathways, which eventually leads to malfunctioning at cellular level and leads to apoptosis.[295,301,302] All of these results suggested that the complex **15** inhibits the growth of cancerous cells and demonstrate great

potential of it for promising anticancer lead molecule.

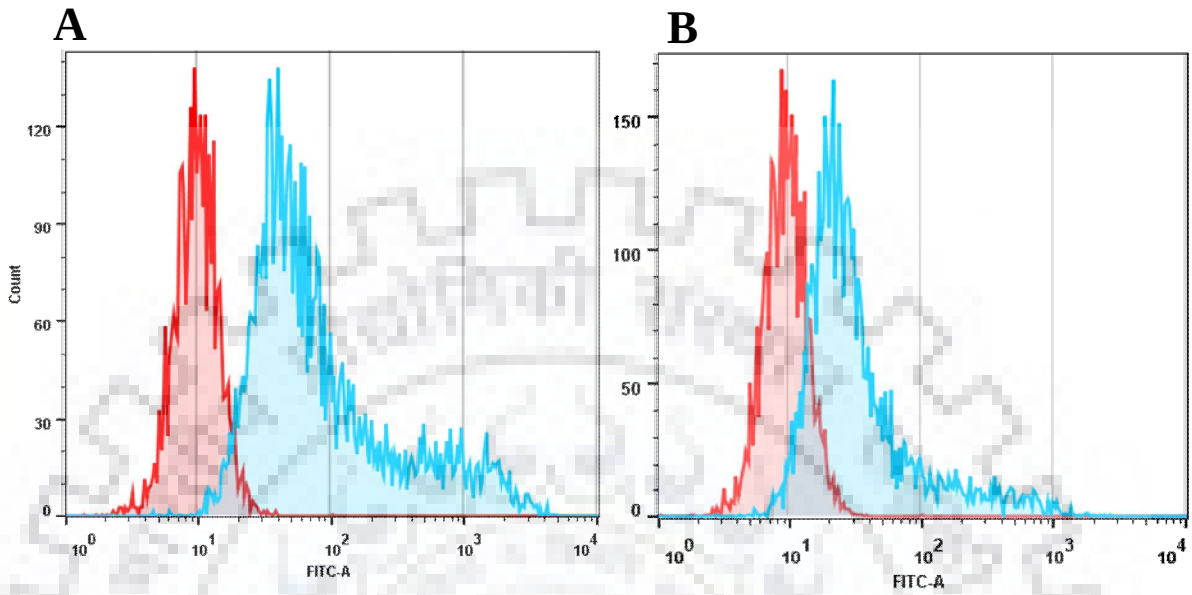

Fig. 6.18 (A) Histogram showing the level of ROS in untreated (red colour) and treated MCF-7 (cyan colour) cells. **(B)** Histogram showing the level of ROS in untreated (red colour) and treated MDA-MB-435s (cyan colour) cells. Cells were treated with IC_{50} dose of complex **15** for 5-6 h and processed for ROS measurements using DCFDA staining by FACS. Shifting of histogram towards right shows higher levels of ROS.

6.2.6. HSA Binding

Due to the abundance of serum albumin in blood stream and its importance in drug delivery system, we analyzed the binding of complex **15** with HSA with the help of fluorescence emission measurements. HSA sample was excited at 280 nm and emission spectra were recorded in the range of 300-400 nm with the increasing concentrations of complex **15** (0-100 μM). The significant decrease in fluorescence intensity while increasing the concentration of complex **15** is fitted in the modified Stern-Volmer equation and the binding

constant (K_a) and number of binding site per protein molecule (*n)* were estimated (shown in Figure 6.19). With the successive addition of complex **15** in HSA a progressive decrease in the fluorescence emission has been observed (shown in Figure 6.19). These results suggested that complex **15** interacted with HSA. The value of binding constant was 2.08×10^4 M^{-1}. The value of binding constant suggested that the complex **15** possesses medium binding affinity for HSA.

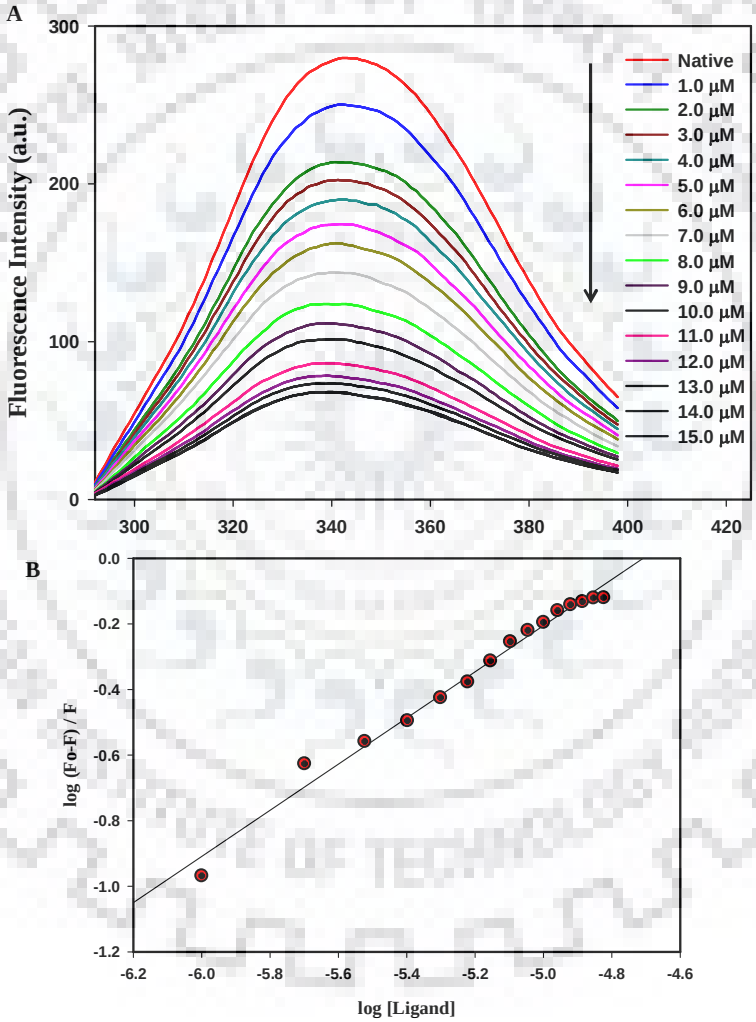

Fig. 6.19 (A) Fluorescence emission spectra of HSA with the increasing concentration of complex **15** (see inset for concentrations)**,** excitation wavelength was fixed at 280nm and emission was recorded in 300-400 nm **(B)** Modified Stern-Volmer plot showing quenching of HSA fluorescence with increasing concentration of complex **15**, this plot was used to calculate binding affinity (K_a) and number of binding sites (*n*).

6.3. Conclusions

Following are the major findings and conclusions of the present study. First, half sandwich ruthenium complexes [(p-cym)$Ru^{II}(L^{9-12})Cl]PF_6$ (**12-15**) were synthesized and characterized by IR, UV-VIS, ESI-MS, NMR spectroscopic studies. Second, the molecular structures of **12** and **15** were determined by X-ray crystallography. Third, all the complexes were utilized to investigate the anti-proliferation activity studies on MCF-7, MDA-MB-435s and HEK293 cell lines. Fourth, apoptosis assay, elevation in ROS level and HSA binding studies were examined. Fifth, among all the complexes, complex **15** was found to be more potent against MCF-7 and MDA-MB-435s cancer cells as compared to complexes **12-14**. However, all the complexes exhibited less cytotoxicity or almost inactivity towards HEK-293 normal cells.

6.4. Experimental section

6.4.1. Reagents and materials

Analytical grade reagents 4-chlorobenzaldehyde, cinnamaldehyde, benzophenone, naphthaldehyde, ammonium hexafluorophosphate were used as obtained. $RuCl_3.3H_2O$ was purchased from Loba Chemie Pvt. Ltd., Mumbai (India). Triphenylphosphine (SRL, Mumbai, India) was used as obtained. The precursor $[(\eta^6\text{-cymene})RuCl_2]_2$ and 2-(1-phenylhydrazinyl)pyridine were prepared by following the procedure reported earlier.[251,303]

6.4.2. Physical measurements

Infrared spectra were recorded with Thermo Nicolet Nexus FT–IR spectrometer, as KBr pellets using 16 scans and were reported in cm^{-1}. ^1H NMR spectra of all complexes in the deuterated solvents were recorded on Bruker, 500 MHz spectrometer. Electronic absorption spectra of all complexes in dichloromethane solvent were recorded with an Evolution 600, Thermo Scientific (Shimadzu) UV–vis spectrophotometer. The ESI-mass spectra of the

complexes **2** and **3** (in acetonitrile solvent) were recorded with Thermo Finnigan LCQ Deca mass spectrometer in the positive ion mode

6.4.3. Syntheses of Ligands

6.4.3.1. Synthesis of 2-(2-(4-chlorobenzylidene)-1-phenylhydrazinyl)pyridine (L^9)

A solution of p-chloro benzaldehyde (3 mmol) in methanol (10 ml) was added dropwise to a solution of 2-(1-phenylhydrazinyl)pyridine (3 mmol) in methanol (10 ml) with stirring. After 3 h of continous stirring, the pinkish white colored precipitate was filtered and washed thoroughly with small amount of methanol. Yield: 72%. Anal.^{1}H NMR (DMSO-d_6, 500 MHz): δ 8.05-8.04 (d, 1H), 7.80-7.76 (m, 2H), 7.70-7.69 (d, 2H), 7.63-7.60 (t, 2H), 7.52-7.49 (t, 1H), 7.44-7.43 (d, 2H), 7.26-7.24 (d, 2H), 7.21 (s, 1H), 6.92-6.89 (t, 1H) ppm.

6.4.3.2. Synthesis of 2-((E)-1-phenyl-2-((E)-3-phenylallylidene)hydrazinyl)pyridine (L^{10})

Ligand (L^{10}) was synthesized from reaction of cinnamaldehyde with 2-(1-phenylhydrazinyl)pyridine in the same way as for ligand L^9. Yield: 70%. Anal.^{1}H NMR (DMSO- d_6, 500 MHz): δ 8.03-8.02 (d, 1H), 7.76-7.73 (t, 1H), 7.63-7.59 (t, 3H), 7.52-7.48 (m, 3H), 7.36-7.33 (t, 2H), 7.28-7.25 (t, 1H), 7.22-7.21 (d, 2H), 7.11-7.09 (d, 2H), 6.89-6.86 (t, 1H), 6.75-6.72 (d, 1H) ppm.

6.4.3.3. Synthesis of 2-(2-(diphenylmethylene)-1-phenylhydrazinyl)pyridine (L^{11})

Ligand (L^{11}) was synthesized from reaction of benzophenone with 2-(1-phenylhydrazinyl)pyridine in the same way as for ligand L^9. Yield: 65%. Anal.^{1}H NMR (DMSO- d_6, 500 MHz): δ 8.06-8.05 (d, 1H), 7.75-7.74 (d, 1H), 7.69-7.65 (m, 1H), 7.58-7.57 (d, 2H), 7.48-7.47 (d, 1H), 7.43-7.40 (t, 2H), 7.23-7.17 (m, 3H), 7.14-7.07 (m, 3H), 6.98-6.95 (t, 1H), 6.89-6.88 (d, 2H), 6.84-6.82 (d, 2H) ppm.

6.4.3.4. Synthesis of 2-(2-(naphthalen-1-ylmethylene)-1-phenylhydrazinyl)pyridine (L^{12})

Ligand (L^{12}) was synthesized from reaction of naphthaldehyde with 2-(1-phenylhydrazinyl)pyridine in the same way as for ligand L^9. Yield: 68%. Anal.^{1}H NMR (DMSO- d_6, 500 MHz): δ 8.33-8.31 (d, 1H), 8.09-8.08 (d, 1H), 7.99-7.92 (m, 3H), 7.88 (s, 1H), 7.84-7.78 (m, 2H), 7.69-7.66 (t, 2H), 7.61-7.54 (m, 4H), 7.36-7.35 (d, 2H), 6.94-6.92 (t, 1H) ppm.

6.4.4. Syntheses of ruthenium complexes

6.4.4.1. Synthesis of [(η^6-cymene)Ru^{II}(L^9)Cl]PF_6 (12)

To a 20 mL methanolic solution of L^9 (0.2 mmol), a batch of ruthenium precursor complex [(η^6-cymene)$RuCl_2$]$_2$ (0.1mmol) was added directly and mixture was stirred at room temperature for 1h, after that NH_4PF_6 (0.25 mmol) was added to above solution and stirring was continued further for 1h. The yellow colored precipitate separated out and was filtered with filter paper, washed with methanol and diethyl ether and dried under vacuum. Yield: 68%. IR (KBr disk, cm^{-1}): 835, 560 (ν_{PF6}) cm^{-1}. UV-Vis (CH_2Cl_2; λmax, nm (ε, $M^{-1}cm^{-1}$)): 226 (10963), 284(9686), 340(7764). ^{1}H NMR (DMSO- d_6, 500 MHz): δ 8.95-8.94 (d, 1H), 8.20-8.19 (d, 2H), 8.13 (s, 1H), 7.83-7.76 (m, 4H), 7.72-7.70 (d, 2H), 7.35-7.34 (d, 2H), 7.23-7.20 (t, 1H), 6.16-6.14 (d, 1H), 5.94-5.93 (d, 1H), 5.57-5.50 (d, 1H), 5.45-5.43 (d, 1H), 4.88-4.87 (d, 1H), 2.67-2.61 (m, 1H), 2.21 (s, 3H), 1.16-1.15, 1.08-1.06 (d, 3H, d, 3H) ppm.

6.4.4.2. Synthesis of [(η^6-cymene)Ru^{II}(L^{10})Cl]PF_6 (13)

Complex **13** was synthesized according to procedure followed for the complex **12** by reaction of [(η^6-cymene)$RuCl_2$]$_2$ with ligand L^{10}. Yield: 62%. IR (KBr disk, cm^{-1}): 840, 560 (ν_{PF6}) cm^{-1}. UV-Vis (CH_2Cl_2; λmax, nm (ε, $M^{-1}cm^{-1}$)): 233 (18073), 303(24082), 370(34403). ^{1}H

NMR (DMSO- d_6, 500 MHz): δ 8.92 (d, 1H), 8.20-8.19 (d, 2H), 8.13 (s, 1H), 7.83-7.76 (m, 4H), 7.72-7.70 (d, 2H), 7.35-7.34 (d, 2H), 7.23-7.20 (t, 1H), 6.16-6.14 (d, 1H), 5.94-5.93 (d, 1H), 5.57-5.50 (d, 1H), 5.45-5.43 (d, 1H), 4.88-4.87 (d, 1H), 2.67-2.61 (m, 1H), 2.21 (s, 3H), 1.16-1.15, 1.08-1.06 (d, 3H, d, 3H) ppm.

6.4.4.3. Synthesis of [(η^6-cymene)Ru^{II}(L^{11})Cl]PF_6 (14)

Complex **14** was synthesized according to procedure followed for the complex **12** by reaction of [(η^6-cymene)$RuCl_2$]$_2$ with ligand L^{11}. Yield: 58%. IR (KBr disk, cm^{-1}): 839, 563 (ν_{PF6}) cm^{-1}. UV-Vis (CH_2Cl_2; λmax, nm (ε, $M^{-1}cm^{-1}$)): 253(16355), 367(6476), 450(2169) . ^1H NMR (DMSO- d_6, 500 MHz): δ 9.02-9.01 (d, 1H), 7.84-7.63(m, 7H), 7.39-7.36 (t, 1H), 7.28-7.20(m, 7H), 7.02-7.01 (d, 2H), 6.81-6.75(m, 3H), 6.00-5.99 (d, 1H), 5.63-5.62 (d, 1H), 2.71-2.64 (m, 1H), 2.03 (s, 3H), 1.16-1.15, 0.98-0.97 (d, 3H, d, 3H) ppm.

6.4.4.4. Synthesis of [(η^6-cymene)Ru^{II}(L^{12})Cl]PF_6 (15)

Complex **15** was synthesized according to procedure followed for the complex **12** by reaction of [(η^6-cymene)$RuCl_2$]$_2$ with ligand L^{12}. Yield: 64%. IR (KBr disk, cm^{-1}): 842, 560 (ν_{PF6}) cm^{-1}. UV-Vis (CH_2Cl_2; λmax, nm (ε, $M^{-1}cm^{-1}$)): 230 (24962), 285(12310), 345(10075). ^1H NMR (DMSO- d_6, 500 MHz): δ 8.99-8.98 (d, 1H), 8.54-8.53 (m, 2H), 8.27-8.25 (d, 1H), 8.16-8.14 (d, 1H), 7.86-7.73 (m, 8H), 7.54-7.53 (d, 2H), 7.24-7.21 (t, 1H), 6.28-6.26 (d, 1H), 5.87-5.86 (d, 1H), 5.37-5.36 (d, 1H), 5.07-5.06 (d, 1H), 4.32 (s, 1H), 2.07 (s, 3H), 1.06-1.02 (m, 6H) ppm.

6.4.5. X–ray crystallography

Crystals of complex **12** and **15** (yellowish) suitable for diffraction study were obtained via layering of hexane over a solution of dichloromethane. The X–ray data collection and processing for complexes **12** and **15** were performed using graphite monochromated Mo–Kα

radiation (λ = 0.71073 Å) with Bruker Kappa Apex–II CCD diffractometer at 273K. Direct method was used to solve the crystal structures. Structure solutions, refinement and data output were carried out using SHELXTL program.[235,236] All non–hydrogen atoms were refined anisotropically, hydrogen atoms were placed in geometrically calculated positions and refined using a riding model. Images were formed using DIAMOND program.[237]

6.4.6. Cell culture

HEK-293, MDA-MB-435s and MCF-7 cell lines were grown and maintained in a DMEM supplemented with 10% heat-inactivated fetal bovine serum (Gibco) and 1% penicillin, streptomycin solution (Gibco), in a 5% CO_2 humidified incubator at 37°C. For MTT assay the cells were seeded in triplicate in 96-well plate containing a cell count of approximately 9000-10000 cells/well and incubated for 24 h in a CO_2 incubator. The cells were then incubated with increasing concentrations of test compounds (5–250μM) in a final volume of 200 μL for 48 h at 37 °C in a CO_2 incubator. The mixture of culture medium and compounds were removed after 48 h of incubation at 37 °C and cells were washed twice with phosphate buffer saline (pH 7.4) solution. After that, freshly prepared 20 μL MTT at a concentration of 5 mg/mL in PBS and 100 μL of DMEM were added in each well and the plates were incubated for 4-5 h at 37°C in the CO_2 incubator. DMSO (150 μL per well) was added to solubilize the formazan crystals, the metabolized MTT product, and were allowed a short incubation of 10 min at room temperature. The absorbance was recorded at 570 nm on the multiplate ELISA reader (Bio-Rad, USA). Percent viability was taken as the relative absorbance of treated vs. untreated control cells and plotted as a function of concentration of compounds.[304,305]

6.4.7. Cell apoptosis assay

To study the apoptotic potential of synthesized half sandwich ruthenium(II) complexes, Annexin-V staining was used as described previously.[304,305] Briefly, the cells were dosed with IC_{50} concentration of complex **15** for 24 h at 37ºC. The control cells were treated with media only. After 24 h treatment, nearly 2.0-2.5 x10^6 cells were trypsinized and collected by centrifuging the cell suspension at 1800 rpm for 4 min. Collected cells were washed two times with 5 ml of PBS. Finally, cells were stained with FITC labeled Annexin-V antibodies using FITC-Annexin-V kit according to the manufacturer's guidelines (BD-Biosciences, USA). Approximately, 10,000 events were analyzed for each sample through flow cytometry on BD LSR II Flow Cytometry Analyzer and FlowJo software.

6.4.8. Fluorescence measurements

Binding affinity of complex **15** with HSA was measured by observing the fluorescence intensity change of emission spectrum of HSA by following our previously published protocol.[302] Each titration of protein was performed in triplicates and the average was taken for analysis. A significant decreased in fluorescence intensity of protein with increase in the concentration of complex **15** were used as the criteria for deducing the binding constant (K_a) as well as number of binding sites (n) present on the protein molecule using the modified Stern-Volmer equation[306]:

$$\log (F_o\text{-}F)/F = \log K_a + n\log[L] \qquad (1)$$

where, F_o = Fluorescence intensity of native protein, F = Fluorescence intensity of protein in the presence of ligand, K_a = Binding constant, n = number of binding sites, L = concentration

of ligand. The values for binding constant (K_a) and number of binding sites (*n*) were derived from the intercept and slope, respectively.

6.4.9. Reactive oxygen species measurement

To analyze the reactive oxygen species (ROS) level inside the cell DCFDA staining was used as described earlier.[302,307] Briefly, the selected cells (70-80% confluent) were incubated with IC_{50} dose of complex **15** and positive control H_2O_2, respectively in a 24-well culture plates. After 5-6 h incubation of cells with complex **15**, cells were gently washed with 500µl of pre-warmed (at 37°C) Krebs Ringer buffer (20 mM HEPES, 2 mM $MgSO_4$, 10 mM dextrose, 127 mM NaCl, 1 mM $CaCl_2$ and 5.5 mM KCl), subsequently 10 µM DCFDA (Invitrogen Grand Island, NY) has been added to each well and incubated further for 30 min in dark at 37°C in a humidified CO_2 incubator. After 30 min incubation, the cells were collected by trypsinization and ROS levels were measured through flow cytometry on BD LSR II Flow Cytometry Analyzer and samples were analysed by FlowJo.

Summary & Conclusions

In the present study, new complexes of ruthenium (II) and ruthenium (III) were synthesized and characterized by IR, UV-Vis, NMR and EPR spectral studies. Molecular structures of representative complexes were authenticated by X- ray crystallography. In few cases, redox properties of the metal complexes were also investigated and theoretical calculations were performed to better understand the experimental results.

In the present report, we have synthesized ruthenium organometallics *via* C-H activation. Aminyl radical coordinated ruthenium complex was also isolated. Oxygen atom transfer and formation of anion radical on coordinated nitroso group was also observed. Organometallic azo anion radical in ruthenium nitrosyl was also characterized. Ruthenium nitrosyls were also synthesized and photolytic dissociation of NO was examined by performing UV-Visible spectral studies. Photoreleased NO was transferred to reduced myoglobin. Ruthenium hydride complexes were isolated. Organometallic ruthenium (II) carbonyl complex was also synthesized and utilized for catalytic transfer hydrogenation. Coordinated CO was found to be photolabile under visible light. Photoreleased NO under visible light was utilized for anticancer activity studies. Half-sandwich ruthenium complexes were also synthesized and utilized for anticancer activity studies.

The work of the present thesis provided several interesting results and avenues and we got ideas for several experiments. Detailed investigations regarding few complexes are under progress. The results obtained from this thesis prompted us to explore further the interesting chemistry of ruthenium.

References

1. Cotton, F. A.; Wilkinson, G.; Murillo, C. A.; Bochmann, M. "Advanced inorganic chemistry" 6th ed.; Wiley, New York, **1999**.
2. Bertini, I.; Gray, H. B.; Lippard, S. J.; Valentine, J. S. "Bioinorganic chemistry" South Asian ed.; University Science Books, **1998**.
3. Frausto da Silva, J. J. R.; Williams, R. J. P. "The biological chemistry of the elements: The inorganic chemistry of life" 2nd ed.; Oxford University Press, New York, **2001**.
4. Patra, A. K.; Olmstead, M. M.; Mascharak, P. K. "Spontaneous reduction of a low-spin Fe(III) complex of a neutral pentadentate N_5 Schiff base ligand to the corresponding Fe(II) species in acetonitrile" *Inorg. Chem.* **2002**, *41*, 5403.
5. Kundu, T.; Sarkar, B.; Mondal, T. K.; Mobin, S. M.; Urbanos, F. A.; Fiedler, J.; Jemenez-Aparicio, R.; Kaim, W.; Lahiri, G. K. "Redox-rich spin-spin-coupled semiquinoneruthenium dimers with intense near-IR absorption" *Inorg. Chem.* **2011**, *50*, 4753.
6. Das, A.; Scherer, T. M.; Chowdhury, A. D.; Mobin, S. M.; Kaim, W.; Lahiri, G. K. "Asymmetrical diruthenium complex bridged by a redox-active ligand" *Inorg. Chem.* **2012**, *51*, 1675.
7. Das, A.; Scherer, T. M.; Mobin, S. M.; Kaim, W.; Lahiri, G. K. "9-oxidophenalenone: A noninnocent β-diketonate ligand?" *Inorg. Chem.* **2012**, *51*, 4390.
8. Jain, P. U.; Munshi, P.; Walawalkar, M. G.; Rath, S. P.; Rajak, K. K.; Lahiri, G. K. "Ruthenium dithiophosphates: Synthesis, X-ray crystal structure, spectroscopic and electrochemical properties" *Polyhedron* **2000**, *19*, 801.
9. Juris, A.; Balzani, V. "Ru(II) polypyridine complexes: Photophysics, photochemistry, electrochemistry and chemiluminescence" *Coord. Chem. Rev.* **1988**, *84*, 85.

10. Sauvage, J.-P.; Collin, J.-P.; Chambron, J.-C.; Guillerez, S.; Coudret, C.; Balzani, V.; Barigelletti, F.; Cola, L. D.; Flamigni, L. "Ruthenium(II) and osmium(II) bis(terpyridine) complexes in covalently-linked multicomponent systems: Synthesis, electrochemical behavior, absorption spectra, photochemical and photophysical properties" *Chem. Rev*. **1994**, *94*, 993.
11. Endicott, J. F.; Schlegel, H. B.; Uddin, Md. J.; Seniveratne, D. S. "MLCT excited states and charge delocalization in some ruthenium ammine-polypyridyl complexes" *Coord. Chem. Rev*. **2002**, *229*, 95.
12. Shan, B.-Z.; Zhao, Q.; Goswami, N.; Eichhorn, D. M.; Rillema, D. P. "Structure, NMR and other physical and photophysical properties of ruthenium(II) complexes containing the 3,3'-dicarboxyl-2,2'-bipyridine ligand" *Coord. Chem. Rev*. **2001**, *211*, 117.
13. Barnard, C. F. J.; Bennett, S. C. "Oxidation states of ruthenium and osmium" *Platin. Met. Rev*. **2004**, *48*, 157.
14. Greenwood, N. N.; Earnshaw, A. "Chemistry of the elements" 2nd ed.; Butterworth-Heinemann, Oxford, UK, **1997**.
15. Tommos, C.; Babcock, G. T. "Oxygen production in nature: A light-driven metalloradical enzyme process" *Acc. Chem. Res.* **1998**, *31*, 18.
16. Ruttinger, W.; Dismukes, G. C. "Synthetic water-oxidation catalysts for artificial photosynthetic water oxidation" *Chem. Rev*. **1997**, *97*, 1.
17. Chen, Z.; Meyer, T. J. "Copper(II) catalysis of water oxidation" *Angew. Chem. Int. Ed*. **2013**, *52*, 700.

18. Xie, Y.; Shaffer, D. W.; Andralojc, A. L.; Szalda, D. J.; Concepcion, J. J. "Water Oxidation by Ruthenium Complexes Incorporating Multifunctional Bipyridyl Diphosphonate Ligands" *Angew. Chem. Int. Ed*. **2016**, *55*, 8067.

19. Gersten, S. W.; Samuels, G. J.; Meyer, T. J. "Catalytic oxidation of water by an oxo-bridged ruthenium dimer" *J. Am. Chem. Soc*. **1982**, *104*, 4029.

20. Liu, F.; Concepcion, J. J.; Jurss, J. W.; Cardolaccia, T.; Templeton, J. L.; Meyer, T. J. "Mechanisms of water oxidation from the blue dimer to photosystem II" *Inorg. Chem.* **2008**, *47*, 1727.

21. Chronister, C. W.; Binstead, R. A.; Ni, J.; Meyer, T. J. "Mechanism of water oxidation catalyzed by the μ-oxo dimer $[(bpy)_2(OH_2)Ru^{III}ORu^{III}(OH_2)(bpy)_2]^{4+}$ " *Inorg. Chem.* **1997**, *36*, 3814.

22. Sens, C.; Romero, I.; Rodriguez, M.; Llobet, A.; Parella, T.; Benet-Buchholz, J. "A new Ru complex capable of catalytically oxidizing water to molecular dioxygen" *J. Am. Chem. Sec*. **2004**, *126*, 7798.

23. Romero, I.; Rodriguez, M.; Sens, C.; Mola, J.; Kollipara, M. R.; Francas, L.; Mas-Marza, E.; Escriche, L.; Llobet, A. "Ru complexes that can catalytically oxidize water to molecular dioxygen" *Inorg. Chem*. **2008**, *47*, 1824.

24. Romain, S.; Bozoglian, F.; Sala, X.; Llobet, A. "Oxygen-oxygen bond formation by the Ru-Hbpp water oxidation catalyst occurs solely via an intramolecular reaction pathway" *J. Am. Chem. Soc*. **2009**, *131*, 2768.

25. Hurst, J. K.; Cape, J. L.; Clark, A. E.; Das, S.; Qin, C. "Mechanisms of water oxidation catalyzed by ruthenium diimine complexes" *Inorg. Chem*. **2008**, *47*, 1753.

26. Hurst, J. K. "Water oxidation catalyzed by dimeric μ-oxo bridged ruthenium diimine complexes" *Coord. Chem. Rev*. **2005**, *249*, 313.

27. Stull, J. A.; Britt, R. D.; McHale, J. L.; Knorr, F. J.; Lymar, S. V.; Hurst, J. K. "Anomalous reactivity of ceric nitrate in ruthenium "blue dime"-catalyzed water oxidation" *J. Am. Chem. Soc*. **2012**, *134*, 19973.

28. Deng, Z.; Tseng, H.-W.; Zong, R.; Wang, D.; Thummel, R. "Preparation and study of a family of dinuclear Ru(II) complexes that catalyze the decomposition of water" *Inorg. Chem*. **2008**, *47*, 1835.

29. Zhang, G.; Zong, R.; Tseng, H.-W.; Thummel, R. "Ru(II) complexes of tetradentate ligands related to 2,9-di(pyrid-2′-yl)-1,10-phenanthroline" *Inorg. Chem*. **2008**, *47*, 990.

30. Tseng, H.-W.; Zong, R.; Muckerman, J. T.; Thummel, R. "Mononuclear ruthenium(II) complexes that catalyze water oxidation" *Inorg. Chem.* **2008**, *47*, 11763.

31. Concepcion, J. J.; Jurss, J. W.; Templeton, J. L.; Meyer, T. J. "One site is enough. Catalytic water oxidation by $[Ru(tpy)(bpm)(OH_2)]^{2+}$ and $[Ru(tpy)(bpz)(OH_2)]^{2+}$ " *J. Am. Chem. Soc*. **2008**, *130*, 16462.

32. Duan, L.; Fischer, A.; Xu, Y.; Sun, L. "Isolated seven-coordinate Ru(IV) dimer complex with $[HOHOH]^-$ bridging ligand as an intermediate for catalytic water oxidation" *J. Am. Chem. Soc*. **2009**, *131*, 10397.

33. Matheu, R.; Ertem, M. Z.; Buchholz, J. B.; Coronado, E.; Batista, V. S.; Sala, X.; Llobet, A. "Intramolecular Proton Transfer Boosts Water Oxidation Catalyzed by a Ru Complex" *J. Am. Chem. Soc*. **2015**, *137*, 10786.

34. Albrecht, M. "Cyclometalation Using d-Block Transition Metals: Fundamental Aspects and Recent Trends" *Chem. Rev.* **2010**, *110*, 576.

35. Murahashi, S.-I.; Takaya, H.; Naota, T. "Ruthenium catalysis in organic synthesis" *Pure Appl. Chem.* **2002**, *74*, 19.

36. Naota, T.; Takaya, H.; Murahashi, S.-I. "Ruthenium-catalyzed reactions for organic synthesis" *Chem. Rev.* **1998**, *98*, 2599 and references therein.

37. Shahane, S.; Fischmeister, C.; Bruneau, C. "Acceptorless ruthenium catalyzed dehydrogenation of alcohols to ketones and esters" *Catal. Sci. Technol.* **2012**, *2*, 1425.

38. Kakiuchi, F.; Murai, S. "Catalytic C–H/olefin coupling" *Acc. Chem. Res.* **2002**, *35*, 826.

39. Chatani, N.; Asaumi, T.; Yorimitsu, S.; Ikeda, T.; Kakiuchi, F.; Murai, S. "$Ru_3(CO)_{12}$-catalyzed coupling reaction of sp^3 C–H bonds adjacent to a nitrogen atom in alkylamines with alkenes" *J. Am. Chem. Soc* **2001**, *123*, 10935.

40. Chatani, N.; Yorimitsu, S.; Asaumi, T.; Kakiuchi, F.; Murai, S. "$Ru_3(CO)_{12}$-catalyzed C–H/CO/olefin coupling of *N*-Pyridylindolines. Direct carbonylation at a C–H Bond δ to the pyridine nitrogen" *J. Org. Chem.* **2002**, *67*, 7557.

41. Chatani, N.; Kamitani, A.; Murai, S. "Ruthenium-catalyzed reaction of α,β-unsaturated imines with carbon monoxide and alkenes leading to β,γ-unsaturated γ-butyrolactams: Involvement of direct carbonylation at olefinic C–H bonds as a key step" *J. Org. Chem.* **2002**, *67*, 7014.

42. Asaumi, T.; Chatani, N.; Matsuo, T.; Kakiuchi, F.; Murai, S. "Ruthenium-catalyzed C–H/CO/olefin coupling reaction of *N*-arylpyrazoles. Extraordinary reactivity of *N*-arylpyrazoles toward carbonylation at C–H bonds" *J. Org. Chem.* **2003**, *68*, 7538.

43. Kakiuchi, F.; Kochi, T.; Mizushima, E.; Murai, S. "Room-temperature regioselective C–H/olefin coupling of aromatic ketones using an activated ruthenium catalyst with a

carbonyl ligand and structural elucidation of key intermediates" *J. Am. Chem. Sec*. **2010**, *132*, 17741.

44. Aihara, Y.; Chatani, N. "Ruthenium-catalyzed direct arylation of C–H bonds in aromatic amides containing a bidentate directing group: Significant electronic effects on arylation" *Chem. Sci*. **2013**, *4*, 664.
45. Arockiam, P. B.; Bruneau, C.; Dixneuf, P. H. "Ruthenium(II)-catalyzed C–H bond activation and functionalization" *Chem. Rev*. **2012**, *112*, 5879.
46. Singh, K. S.; Dixneuf, P. H. "Ruthenium(II)-catalyzed alkenylation of ferrocenyl ketones *via* C–H bond activation" *Organometallics* **2012**, *31*, 7320.
47. Li, B.; Devaraj, K.; Darcel, C.; Dixneuf, P. H. "Ruthenium(II) catalysed synthesis of unsaturated oxazolines *via* arene C–H bond alkenylation" *Green Chem*. **2012**, *14*, 2706.
48. Li, B.; Darcel, C.; Dixneuf, P. H. "Ruthenium(II)-catalysed functionalisation of C–H bonds via a six-membered cyclometallate: Monoarylation of aryl 2-pyridyl ketones" *ChemCatChem* **2014**, *6*, 127.
49. Ghosh, K.; Chattopadhyay, S.; Pattanayak, S.; Chakravorty, A. "Alkyne insertion into the Ru–C bond of a four-membered metallacycle. Insertion rate and reaction pathway" *Organometallics* **2001**, *20*, 1419.
50. Ghosh, K.; Pattanayak, S.; Chakravorty, A. "Metallacycle expansion by alkyne insertion. Chemistry of a new family of ruthenium organometallics" *Organometallics* **1998**, *17*, 1956.
51. Kannan, S.; Ramesh, R.; Liu, Y. "Ruthenium(III) mediated C–H activation of azonaphthol: Synthesis, structural characterization and transfer hydrogenation of ketones" *J. Organomet. Chem.* **2007**, *692*, 3380.

52. Gupta, P.; Dutta, S.; Basuli, F.; Peng, S.-M.; Lee, G.-H.; Bhattacharya, S. "Ruthenium mediated C-H activation of 2-(arylazo)phenols: Characterization of an intermediate and the final organoruthenium complex" *Inorg. Chem.* **2006**, *45*, 460.

53. Nag, S.; Gupta, P.; Butcher, R. J.; Bhattacharya, S. "Unprecedented migration of a methyl group in 2-(2',6'-dimethylphenylazo)-4-methylphenol mediated by ruthenium" *Inorg. Chem.* **2004**, *43*, 4814.

54. Halder, S.; Acharyya, R.; Peng, S.-M.; Lee, G.-H.; Drew, M. G. B.; Bhattacharya, S. "Synthesis, structure, and electrochemical properties of a family of 2-(arylazo)phenolate complexes of ruthenium with unusual C-C coupling and N=N cleavage" *Inorg. Chem.* **2006**, *45*, 9654.

55. Lahiri, G. K.; Bhattacharya, S.; Mukherjee, M.; Mukherjee, A. K.; Chakravorty, A. "Directed metal oxidation levels in azo-ruthenium cyclometalates. Synthesis and structure of a trivalent" *Inorg. Chem.* **1987**, *26*, 3359.

56. Ghosh, P.; Pramanik, A.; Bag, N.; Lahiri, G. K.; Chakravorty, A. "Paramagnetic organometallics formed by *o*-metallation of phenolic Schiff bases by ruthenium(III)" *J. Organomet. Chem.* **1993**, *454*, 237.

57. Djukic, J.-P.; Sortais, J.-B.; Barloy, L.; Pfeffer, M. "Cycloruthenated compounds – synthesis and applications" *Eur. J. Inorg. Chem.* **2009**, 817.

58. Ghosh, K.; Kumar, S.; Kumar, R.; Singh, U. P. "Ruthenium(III) cyclometalates obtained by site-specific orthometallation and their reactivity with nitric oxide: Photoinduced release and estimation of NO liberated from the ruthenium nitrosyl complexes" *Eur. J. Inorg. Chem.* **2012**, 929.

59. Ammar, H. B.; Le Nôtre, J.; Salem, M.; Kaddachi, M. T.; Dixneuf, P. H. "Synthesis of bis-oxazoline-ruthenium(II)-arene complexes. Combined catalytic isomerisation and claisen rearrangement of bis-allyl ether" *J. Organomet. Chem.* **2002**, *662*, 63.

60. Cariou, R.; Fischmeister, C.; Toupet, L.; Dixneuf, P. H. "A bidentate NHC–alkenyl ruthenium(II) complex via vinyl C–H bond activation" *Organometallics* **2006**, *25*, 2126.

61. Li, B.; Roisnel, T.; Darcel, C.; Dixneuf, P. H. "Cyclometallation of arylimines and nitrogen-containing heterocycles *via* room-temperature C–H bond activation with arene ruthenium(II) acetate complexes" *Dalton Trans*. **2012**, *41*, 10934.

62. Nguyen, S. T.; Grubbs, R. H.; Ziller, J. W. "Syntheses and activities of new single-component, ruthenium-based olefin metathesis catalysts" *J. Am. Chem. Soc*. **1993**, *115*, 9858.

63. Trnka, T. M.; Grubbs, R. H. "The development of L_2X_2Ru=CHR olefin metathesis catalysts: An organometallic success story" *Acc. Chem. Res.* **2001**, *34*, 18.

64. Nguyen, S. T.; Johnson, L. K.; Grubbs, R. H.; Ziller, J. W. "Ring-opening metathesis polymerization (ROMP) of norbornene by a group VIII carbene complex in protic media" *J. Am. Chem. Soc*. **1992**, *114*, 3975.

65. Huang, J.; Schanz, H.-J.; Stevens, E. D.; Nolan, S. P. "Influence of sterically demanding carbene ligation on catalytic behaviour and thermal stability of ruthenium olefin metathesis catalysts" *Organometallics* **1999**, *18*, 5375.

66. Vougioukalakis, G. C.; Grubbs, R. H. "Ruthenium-based heterocyclic carbene-coordinated olefin metathesis catalysts" *Chem. Rev*. **2010**, *110*, 1746.

67. Schwab, P.; France, M. B.; Ziller, J. W.; Grubbs, R. H. 1995. "A series of well-defined metathesis catalysts-synthesis of $[RuCl_2(=CHR')(PR_3)_2]$ and its reactions" *Angew. Chem. Int. Ed.* **1995**, *34*, 2039.

68. Scholl, M.; Ding, S.; Lee, C. W.; Grubbs, R. H. "A series of well-defined metathesis catalysts-synthesis of $[RuCl_2(=CHR')(PR_3)_2]$ and its reactions" *Org. Lett.* **1999**, *1*, 953.

69. Sanford, M. S.; Love, J. A.; Grubbs, R. H. "A versatile precursor for the synthesis of new ruthenium olefin metathesis catalysts" *Organometallics* **2001**, *25*, 5314.

70. Harrity, J. P. A.; La, D. S.; Cefalo, D. R.; Visser, M. S.; Hoveyda, A. H. "Chromenes through metal-catalyzed reactions of styrenyl ethers. Mechanism and utility in synthesis" *J. Am. Chem. Soc*. **1998**, *120*, 2343.

71. Garber, S. B.; Kingsbury, J. S.; Gray, B. L.; Hoveyda, A. H.; April, R. V. "Chromenes through metal-catalyzed reactions of styrenyl ethers. Mechanism and utility in synthesis" *J. Am. Chem. Soc*. **2000**, *122*, 8168.

72. Siegel, S. "Comprehensive Organic Synthesis" (Eds: B. M. Trost, I. Fleming), Pergamon Press, Oxford, **1991**, *8*, Chap. 3.1.

73. Takaya, H.; Noyori, R. "Comprehensive Organic Synthesis" (Eds: B. M. Trost, I. Fleming), Pergamon Press, Oxford, **1991**, *8*, Chap. 3.2.

74. Hudlicky, M. "Reductions in Organic Chemistry" 2nd Ed., American Chemical Society, Washington, DC, 1996, Chapter 13.

75. Behr, L. C.; Kirby, J. E.; MacDonald, R. N.; Todd, C. W. "Synthesis of Alicyclic Diamines" *J. Am. Chem. Soc*. **1946**, *68*, 1296.

76. Barkdoll, A. E.; England, D. C.; Gray, H. W.; Kirk, Jr., W.; Whitman, G. M. "Alicyclic Diamines. Preparation of Bis-(4-aminocyclohexyl)-methane" *J. Am. Chem. Soc.* **1953**, *75*, 1156.

77. Evans, D.; Osborn, J. A.; Jardine, F. H.; Wilkinson, G. "Homogeneous hydrogenation and hydroformylation using ruthenium complexes" *Nature* **1965**, *208*, 1203.

78. Fernández, F. E.; Puerta, M. C.; Valerga, P. "Half-sandwich ruthenium(II) picolyl-NHC complexes: synthesis, characterization and catalytic activity in transfer hydrogenation reactions" *Organometallics* **2011**, *30*, 5793.

79. Fernández, F. E.; Puerta, M. C.; Valerga, P. "Ruthenium(II) picolyl-NHC complexes: synthesis, characterization and catalytic activity in amine N-alkylation and transfer hydrogenation reactions" *Organometallics* **2012**, *31*, 6868.

80. Horn, S.; Albrecht, M. "Transfer hydrogenation of unfunctionalized alkenes using N-heterocyclic carbene ruthenium catalyst precursors" *Chem. Commun.* **2011**, *47*, 8802.

81. Prakash, O.; Sharma, K. N.; Joshi, H.; Gupta, P. L.; Singh, A. K. "Half sandwich complexes of chalcogenated pyridine based Bi-(N, S/ Se) and terdentate (N, S/Se, N) ligands with (η^6-Benzene)-ruthenium (II): synthesis, structure and catalysis of transfer hydrogenation of ketones and oxidation of alcohols" *Dalton Trans.* **2013**, *42*, 8736.

82. Václavík, J.; Kuzma, M.; Prech, J.; Kacer, P. "Asymmetric transfer hydrogenation of imines and ketones using chiral $Ru^{II}Cl(\eta^6$-*p*-cymene)[(S,S)-N-TsDPEN] as a catalyst: A computational study" *Organometallics* **2011**, *30*, 4822.

83. Zhang, B.; Wang, H.; Lin, G. Q.; Xu, M. H. "Ruthenium(II)-catalyzed asymmetric transfer hydrogenation using unsymmetrical vicinal diamine-based ligands: dramatic substituent effect on catalyst efficiency" *Eur. J. Org. Chem.* **2011**, 4205.

84. Soni, R.; Cheung, F. K.; Clarkson, G. C.; Martins, J. E. D.; Graham, M. A.; Wills, M. "The importance of the N-H bond in Ru/TsDPEN complexes for asymmetric transfer hydrogenation of ketones and imines" *Org. Biomol. Chem.* **2011**, *9*, 3290.

85. Dayan, S.; Kalaycioglu, N. O.; Daran, J. C.; Labande, A.; Poli, R. "Synthesis and characterization of half-sandwich ruthenium complexes containing aromatic sulfonamides bearing pyridinyl rings: catalysts for transfer hydrogenation of acetophenone derivatives" *Eur. J. Inorg. Chem.* **2013**, 3224.

86. Alonso, M. M.; Busto, N.; Jalon, F. A.; Manzano, B. R.; Leal, J. M.; Rodríguez, A. M.; García, B.; Espino, G. "Derivation of Structure–Activity Relationships from the Anticancer Properties of Ruthenium(II) Arene Complexes with 2-Aryldiazole Ligands" *Inorg. Chem.*, **2014**, *53*, 11274.

87. Gupta, R. K.; Sharma, G.; Pandey, R.; Kumar, A.; Koch, B.; Li, P. Z.; Xu, Q.; Pandey, D. S. "DNA/Protein Binding, Molecular Docking, and in Vitro Anticancer Activity of Some Thioether-Dipyrrinato Complexes" *Inorg. Chem.*, **2013**, *52*, 13984.

88. Xu, Z.; Kong, D.; He, X.; Guo, L.; Ge, X.; Liu, X.; Zhang, H.; Li, J.; Yang, Y.; Liu, Z. "Mitochondria-targeted half-sandwich ruthenium^{II} diimine complexes: anticancer and antimetastasis via ROS-mediated signalling" *Inorg. Chem. Front.*, **2018**, *5*, 2100.

89. Caruso, F.; Rossi, M.; Benson, A.; Opazo, C.; Freedman, D.; Monti, E.; Gariboldi, M. B.; Shaulky, J.; Marchetti, F.; Pettinari, R.; Pettinari, C. "Ruthenium–Arene Complexes of Curcumin: X-Ray and Density Functional Theory Structure, Synthesis, and Spectroscopic Characterization, in Vitro Antitumor Activity, and DNA Docking Studies of (p-Cymene)Ru(curcuminato)chloro" *J. Med. Chem.*, **2012**, *55*, 1072.

90. Bergamo, A.; Dyson, P. J.; Sava, G. "The mechanism of tumour cell death by metal-based anticancer drugs is not only a matter of DNA interactions" *Coord. Chem. Rev.* **2018**, *360*, 17.

91. Gupta, R. K.; Kumar, A.; Paitandi, R. P.; Singh, R. S.; Mukhopadhyay, S.; Verma, S. P.; Das, P.; Pandey, D. S. "Heteroleptic arene Ru(II) dipyrrinato complexes: DNA, protein binding and anti-cancer activity against the ACHN cancer cell line" *Dalton Trans.*, **2016**, *45*, 7163.

92. Ronconi, L.; Sadler, P. J. "Using coordination chemistry to design new medicines" *Coord. Chem. Rev.* **2007**, *251*, 1633.

93. Dyson, P. J.; Sava, G. "Metal-based anti-tumour drugs in the post genomic era" *Dalton Trans.*, **2006**, 1929.

94. Habtemariam, A.; Melchart, M.; Fernandez, R.; Parsons, S.; Oswald, I. D. H.; Parkin, A.; Fabbiani, F. P. A.; Davidson, J. E.; Dawson, A.; Aird, R. E.; Jodrell, D. I.; Sadler, P. J. "Structure-activity relationships for cytotoxic ruthenium(II) arene complexes containing N,N-, N,O-, and O,O-chelating ligands" *J. Med. Chem.* **2006**, *49*, 6858.

95. Aird, R. E.; Cummings, J.; Ritchie, A. A.; Muir, M.; Morris, R. E.; Chen, H.; Sadler, P. J. "*In vitro* and *in vivo* activity and cross resistance profiles of novel ruthenium(II) organometallic arene complexes in human ovarian cancer" *Br. J. Cancer* **2002**, *86*, 1652.

96. Friedman, A. E.; Chambron, J. C.; Sauvage, J. P.; Turro N. J.; Barton, J. K. "A molecular light switch for DNA: $Ru(bpy)_2(dppz)^{2+}$" *J. Am. Chem. Soc.* **1990**, *112*, 4960.

97. Jenkins, Y.; Friedman, A. E.; Turro N. J.; Barton, J. K. "Characterization of dipyridophenazine complexes of ruthenium(II): The light switch effect as a function of nucleic acid sequence and conformation" *Biochemistry* **1992**, *31*, 10809.

98. Grover, N.; Gupta, Thorp, H. H. "Stereoselective covalent binding of aquaruthenium(II) complexes of DNA" *J. Am. Chem. Soc.* **1992**, *114*, 3390.

99. Grover, N.; Welch, T. W.; Fairley, T. A.; Cory, M.; Thorp, H. H. "Covalent binding of aquaruthenium complexes to DNA" *Inorg. Chem.* **1994**, *33*, 3544.

100. Novakova, O.; Kasparkova, J.; Vrana,O.; Van Vliet, P. M.; Reedijk, J.; Brabec, V. "Correlation between cytotoxicity and DNA binding of polypyridyl ruthenium complexes" *Biochemistry* **1995**, *34*, 12369.

101. Novakova, O.; Chen, H.; Vrana, O.; Rodger, A.; Sadler, P. J.; Brabec, V. "DNA interactions of monofunctional organometallic ruthenium(II) antitumor complexes in cell-free media" *Biochemistry* **2003**, *42*, 11544.

102. Bugarcic, T.; Habtemariam, A.; Deeth, R. J.; Fabbiani, F. P. A.; Parsons, S.; Sadler, P. J. "Ruthenium(II) arene anticancer complexes with redox-active diamine ligands" *Inorg. Chem.* **2009**, *48*, 9444.

103. Ezadyar, S. A.; Kumbhar, A. S.; Kumbhar, A. A.; Khan, A. "Binuclear ruthenium(II) polypyridyl complexes: DNA cleavage and mitochondria mediated apoptosis induction" *Polyhedron* **2012**, *36*, 45.

104. Metcalfe, C.; Thomas, J. A. "Kinetically inert transition metal complexes that reversibly bind to DNA" *Chem. Soc. Rev.* **2003**, *32*, 215.

105. Keene, F. R.; Smith J. A.; Collins, J. G. "Metal complexes as structure-selective binding agents for nucleic acids" *Coord. Chem. Rev.* **2009**, *253*, 2021.

106. M. R. Gill and J. A. Thomas, "Ruthenium(II) polypyridyl complexes and DNA-from structural probes to cellular imaging and therapeutic" *Chem. Soc. Rev.* **2012**, *41*, 3179.

107. Gill, M. R.; Garcia-Lara, J.; Foster, S. J.; Smythe, C.; Battaglia G.; Thomas, J. A. "A ruthenium(II) polypyridyl complex for direct imaging of DNA structure in living cells" *Nat. Chem.* **2009**, *1*, 662.

108. Matson, M.; Svensson, F. R.; Norde´n, B.; Lincoln, P. "Correlation between cellular localization and binding preference to RNA, DNA, and phospholipid membrane for luminescent ruthenium(II) complexes" *J. Phys. Chem. B* **2011**, *115*, 1706.

109. Bolhuis, A.; Hand, L.; Marshall, J. E.; Richards, A. D.; Rodger A.; Aldrich-Wright, J. "Antimicrobial activity of ruthenium-based intercalators" *Eur. J. Pharm. Sci.* **2011**, *42*, 313.

110. Dwyer, F. P.; Mellor, D. P. "Chelating Agents and Metal Chelates" Academic Press, New York, **1964**.

111. Li, F.; Feterl, M.; Warner, J. M.; Keene, F. R.; Collins, J. G. "Dinuclear polypyridylruthenium(II) complexes: flow cytometry studies of their accumulation in bacteria and the effect on the bacterial membrane" *J. Antimicrob. Chemother.* **2013**, *68*, 2825.

112. Devi, C. S.; Kumar, D. A.; Singh, S. S.; Gabra, N.; Deepika, N.; Kumar Y. P.; Satyanarayana, S. "Synthesis, interaction with DNA, cytotoxicity, cell cycle arrest and apoptotic inducing properties of ruthenium(II) molecular "light switch" complexes" *Eur. J. Med. Chem.* **2013**, *64*, 410.

113. Kumar, K. A.; Reddy, K. L.; Vidhisha, S.; Satyanarayana, S. "Synthesis, characterization and DNA binding and photocleavage studies of $[Ru(bpy)_2BDPPZ]^{2+}$, $[Ru(dmb)_2BDPPZ]_{2+}$ and $[Ru(phen)_2BDPPZ]^{2+}$complexes and their antimicrobial activity" *Appl. Organomet. Chem.* **2009**, *23*, 409.

114. Lam, P. L.; Lu, G. L.; Hon, K. M.; Lee, K. W.; Ho, C. L.; Wang, X.; Tang, J. C. O.; Lam, K. H.; Wong, R. S. M.; Kok, S. H. L.; Bian, Z. X.; Li, H.; Lee, K. K. H.; Gambari, R.; Chui, C. H.; Wong, W. Y. "Development of ruthenium(II) complexes as topical antibiotics against methicillin resistant Staphylococcus aureus" *Dalton Trans.* **2014**, *43*, 3949.

115. Aldrich-Wright, J.; Brodie, C.; Glazer, E. C.; Luedtke, N. W.; Elson-Schwaband, L.; Tor, Y. "Symmetrical dinuclear complexes with high DNA affinity based on $[Ru(dpq)_2(phen)]^{2+}$" *Chem. Commun.* **2004**, 1018.

116. Delaney, S.; Pascaly, M.; Bhattacharya, P. K.; Han, K.; Barton, J. K. "Oxidative damage by ruthenium complexes containing the dipyridophenazine ligand or its derivatives: a focus on intercalation" *Inorg. Chem.* **2002**, *41*, 1966.

117. Li, F.; Mulyana, Y.; Feterl, M.; Warner, J.; Collins, J. G.; Keene, F. R. "The antimicrobial activity of inert oligonuclear polypyridylruthenium(II) complexes against pathogenic bacteria, including MRSA" *Dalton Trans.* **2011**, *40*, 5032.

118. Kozlov, D. V.; Tyson, D. S.; Goze, C.; Ziessel, R.; Castellano, F. N. "Room temperature phosphorescence from ruthenium(II) complexes bearing conjugated pyrenylethynylene subunits" *Inorg. Chem.* **2004**, *43*, 6083.

119. Galletta, M.; Puntoriero, F.; Campagna, S.; Chiorboli, C.; Quesada, M.; Goeb, S.; Ziessel, R. "Absorption spectra, photophysical properties, and redox behavior of ruthenium(II) polypyridine complexes containing accessory dipyrromethene−BF_2 chromophores" *J. Phys. Chem. A* **2006**, *110*, 4348.

120. Balzani, V.; Juris, A. "Photochemistry and photophysics of Ru(II)-polypyridine complexes in the Bologna group. From early studies to recent developments" *Coord. Chem. Rev.* **2001**, *211*, 97.

121. Juris, A.; Balzani, V. "Ru(II) polypyridine complexes: photophysics, photochemistry, eletrochemistry, and chemiluminescence" *Coord. Chem. Rev.* **1988**, *84*, 85.

122. Alstrum-Acevedo, J. H.; Brennaman, M. K.; Meyer, T. J. "Chemical approaches to artificial photosynthesis. 2" *Inorg. Chem.* **2005**, *44*, 6802.

123. Gao, F. G.; Bard, A. J. "Solid-state organic light-emitting diodes based on tris (2, 2 '-bipyridine) ruthenium(II) complexes" *J. Am. Chem. Soc.* **2000**, *112*, 7426.

124. Strouse, G. F.; Schoonover, J. R.; Duesing, R.; Boyde, S.; Jones, W. E. Jr.; Meyer, T. J. "Influence of electronic delocalization in metal-to-ligand charge transfer excited states" *Inorg. Chem.* **1995**, *34*, 473.

125. Kober, E. M.; Caspar, J. V.; Lumpkin, R. S.; Meyer, T. J. "Application of the energy gap law to excited-state decay of osmium(II)-polypyridine complexes: calculation of relative nonradiative decay rates from emission spectral profiles" *J. Phys. Chem.* **1986**, *90*, 3722.

126. Crosby, G. A.; Perkins, W. G.; Klassen, D. M. "Luminescence from transition-metal complexes: Tris(2,2′-bipyridine)-and Tris(1,10-phenanthroline)Ruthenium(II)" *J. Chem. Phys.* **1965**, *43*, 1498.

127. Juris, A.; Campagna, S.; Balzani, V.; Gremaud, G.; Zelewsky, A. V. "Absorption spectra, luminescence properties, and electrochemical behavior of tris-heteroleptic ruthenium(II) polypyridine complexes" *Inorg. Chem.* **1988**, *27*, 3652.

128. Vlachopoulos, N.; Liska, P.; Augustynski, J.; Gratzel, M. "Very efficient visible light energy harvesting and conversion by spectral sensitization of high surface area polycrystalline titanium dioxide films" *J. Am. Chem. Soc.* **1988**, *110*, 1216.

129. Hagfeldt, A.; Gratzel, M. "Molecular photovoltaics" *Acc. Chem. Res.* **2000**, *33*, 269.

130. Hagfeldt, A.; Gratzel, M. "Light-induced redox reactions in nanocrystalline systems" *Chem. Rev.* **1995**, *95*, 49.

131. O'Regan, B.; Gratzel, M. "A low-cost, high-efficiency solar cell based on dye-sensitized colloidal TiO_2 films" *Nature* **1991**, *353*, 737.

132. Kamper, S.; Paretzki, A.; Fiedler, J.; Zalis, S.; Kaim, W. "Solar Cell Sensitizer Models $[Ru(bpy\text{-}R)_2(NCS)_2]$ Probed by Spectroelectrochemistry" *Inorg. Chem.* **2012**, *51*, 2097.

133. Zhao, H. C.; Harney, J. P.; Huang, Y. T.; Yum, J. H.; Nazeeruddin, Md. K.; Gratzel, M.; Tsai, M. K.; Rochford, J. "Evaluation of a ruthenium oxyquinolate architecture for dye-sensitized solar cells" *Inorg. Chem.* **2012**, *51*, 1.

134. Anderson, P. A.; Struose, G. F.; Treadway, J. A.; Keene, F. R.; Meyer, T. J. "Black MLCT absorbers" *Inorg. Chem.* **1994**, *33*, 3863.

135. Nazeeruddin, Md. K.; Kay, A.; Rodicio, I.; Humphry-Baker, R.; Muller, E.; Liska, P.; Vlachopuolos, N.; Gratzel, M. "Conversion of light to electricity by *cis*-X_2Bis(2, 2'-bipyridyl-4,4'-dicarboxylate) ruthenium(II) charge-transfer sensitizers ($X=Cl^-$, Br^-, I^-, CN^-, and SCN^-) on nanocrystalline titanium dioxide electrodes" *J. Am. Chem. Soc.* **1993**, *115*, 6382.

136. De Angelis, F.; Fantacci, S.; Mosconi, E.; Nazeeruddin, M. K.; Gratzel, M. "Absorption Spectra and Excited State Energy Levels of the N719 Dye on TiO_2 in Dye-Sensitized Solar Cell Models" *J. Phys. Chem. C* **2011**, *115*, 8825.

137. Ignarro, L. J.; Buga, G. M.; Wood, K. S.; Byrns, R. E.; Chaudhuri, G. "Endothelium-derived relaxing factor produced and released from artery and vein is nitric oxide" *Proc. Natl. Acad. Sci. USA* **1987**, *84*, 9265.

138. Koshland, D. E. "Molecule of the year: the DNA repair enzyme" *Science* **1992**, *258*, 1861.

139. Rose, M. J.; Mascharak, P. K. "Fiat Lux: selective delivery of high flux of nitric oxide (NO) to biological targets using photoactive metal nitrosyls" *Curr. Opin. Chem. Biol.* **2008**, *12*, 238.

140. Xu, N.; Lilly, J.; Powell, D. R.; Richter-Addo, G. B. "Synthesis, characterization, and infrared reflectance spectroelectrochemistry of organoruthenium nitrosyl porphyrins" *Organometallics* **2012**, *31*, 827.

141. Bredt, D. S.; Snyder, S. H. "Isolation of nitric oxide synthase, a calmodulin-requiring enzyme" *Proc. Natl. Acad. Sci. USA* **1990**, *87*, 682.

142. Bredt, D. S.; Hwang, P. M.; Snyder, S. H. "Localization of nitric oxide synthase indicating a neuronal role for nitric oxide" *Nature* **1990**, *347*, 768.

143. Moncada, S.; Radomski, M. W.; Palmer, R. M. J. "Endothelium-derived relaxing factor: Identification as nitric oxide and role in the control of vascular tone and platelet function" *Biochem. Pharmacol.* **1988**, *37*, 2495.

144. Marsden, P. A.; Schappert, K. T.; Chen, H. S.; Flowers, M.; Sundell, C. L.; Wilcox, I. N.; Lamas, S.; Michel, T. "Molecular cloning and characterization of human endothelial cell nitric oxide synthase" *FEBS Lett.* **1992**, *307*, 287.

145. Mayer, B.; Schmidt, K.; Humbert, P.; Bohme, E. "Biosynthesis of endothelium-derived relaxing factor: A cytosolic enzyme in porcine aortic endothelial cells Ca^{2+}-dependently

converts L-arginine into an activator of soluble guanylyl cyclise" *Biochem. Bioph. Res. Co.* **1989**, *164*, 678

146. Woodward, J. J.; Chang, M. M.; Martin, N. I.; Marletta, M. A. "The second step of the nitric oxide synthase reaction: evidence for ferric-peroxo as the active oxidant" *J. Am. Chem. Soc.* **2009**, *131*, 297.
147. Hecker, M.; Sessa, W. C.; Harris, H. J.; Anggard, E. E.; Vane, J. R. "The metabolism of L-arginine and its significance for the biosynthesis of endothelium-derived relaxing factor: cultured endothelial cells recycle L-citrulline to L-arginine" *Proc. Natl. Acad. Sci. USA* **1990**, *87*, 8612.
148. Miller, M. R.; Megson, I. L. "Recent developments in nitric oxide donor drugs" *Brit. J. Pharmacol.* **2007**, *151*, 305 and references therein.
149. Thatcher, G. R.; Nicolescu, A. C.; Bennett, B. M.; Toader, V. "Nitrates and NO release: Contemporary aspects in biological and medicinal chemistry" *Free Radical Bio. Med.* **2004**, *37*, 1122.
150. Kollau, A.; Hofer, A.; Russwurm, M.; Koesling, D.; Keung, W. M.; Schmidt, K. Brunner, F.; Mayer, B. "Contribution of aldehyde dehydrogenase to mitochondrial bioactivation of nitroglycerin: Evidence for the activation of purified soluble guanylate cyclase through direct formation of nitric oxide" *Biochem. J.* **2005**, *385*, 769.
151. Pluta, R. M.; Oldfield, E. H.; Boock, R. J. "Reversal and prevention of cerebral vasospasm by intracarotid infusions of nitric oxide donors in a primate model of subarachnoid hemorrhage" *J. Neurosurg.* **1997**, *87*, 746.
152. Richter-Addo, G. B.; Legzdins, P. "Metal nitrosyls" Oxford University Press, New York, **1992**.

153. McCleverty, J. A. "Chemistry of nitric oxide relevant to biology" *Chem. Rev.* **2004**, *104*, 403.

154. Lahiri, G. K.; Kaim, W. "Electronic structure alternatives in nitrosylruthenium complexes" *Dalton Trans.* **2010**, *39*, 4471 and references therein.

155. Ford, P. C.; Fernandez, B. O.; Lim, M. D. "Mechanisms of reductive nitrosylation in iron and copper models relevant to biological systems" *Chem. Rev.* **2005**, *105*, 2439.

156. Ford, P. C.; Lorkovic, I. M. "Mechanistic aspects of the reactions of nitric oxide with transition metal complexes" *Chem. Rev.* **2002**, *102*, 993.

157. Rath, S. P.; Koerner, R.; Olmstead, M. M.; Balch, A. L. "Reversible binding of nitric oxide and carbon–carbon bond formation in a meso-hydroxylated heme" *J. Am. Chem. Soc.* **2003**, *125*, 11798.

158. Eroy-Reveles, A. A.; Leung, Y.; Beavers, C. M.; Olmstead, M. M.; Mascharak, P. K. "Near-infrared light activated release of nitric oxide from designed photoactive manganese nitrosyls: Strategy, design, and potential as NO donors" *J. Am. Chem. Soc.* **2008**, *130*, 4447.

159. Hayton, T. W.; Legzdins, P.; Sharp, W. B. "Coordination and organometallic chemistry of metal-NO complexes" *Chem. Rev.* **2002**, *102*, 935.

160. Patra, A. K.; Afshar, R. K.; Olmstead, M. M.; Mascharak, P. K. "The first non-heme iron(III) complex with a carboxamido group that exhibits photolability of a bound NO ligand" *Angew. Chem. Int. Ed.* **2002**, *41*, 2512 and references therein.

161. Rose, M. J.; Mascharak, P. K. "Photoactive ruthenium nitrosyls: Effects of light and potential application as NO donors" *Coord. Chem. Rev.* **2008**, *252*, 2093 and references therein.

162. Patra, A. K.; Rowland, J. M.; Marlin, D. S.; Bill, E.; Olmstead, M. M.; Mascharak, P. K. "Iron nitrosyls of a pentadentate ligand containing a single carboxamide group: Syntheses, structures, electronic properties and photolability of NO" *Inorg. Chem.* **2003**, *42*, 6812.

163. Ghosh, K.; Eroy-Reveles, A. A.; Avila, B.; Holman, T. R.; Olmstead, M. M.; Mascharak, P. K. "Reactions of NO with Mn(II) and Mn(III) centers coordinated to carboxamido nitrogen: Synthesis of a manganese nitrosyl with photolabile NO" *Inorg. Chem.* **2004**, *43*, 2988.

164. Franz, K. J.; Lippard, S. J. "Nitrosyl transfer from manganese to iron in tropocoronand complexes" *Inorg. Chem.* **2000**, *39*, 3722.

165. Ghosh, K.; Eroy-Reveles, A. A.; Olmstead, M. M.; Mascharak, P. K. "Reductive nitrosylation and proton-assisted bridge splitting of a (μ-oxo)dimanganese(III) complex derived from a polypyridine ligand with one carboxamide group" *Inorg. Chem.* **2005**, *44*, 8469.

166. DeLeo, M. A.; Ford, P. C. "Photoreactions of coordinated nitrite ion. Reversible nitric oxide labilization from the chromium(III) complex [*trans*-Cr(cyclam)$(ONO)_2]^+$" *Coord. Chem. Rev.* **2000**, *208*, 47.

167. Fry, N. L.; Rose, M. J.; Rogow, D. L.; Nyitray, C.; Kaur, M.; Mascharak, P. K. "Ruthenium nitrosyls derived from tetradentate ligands containing carboxamido-N and phenolato-O donors: Syntheses, structures, photolability, and time dependent density functional theory studies" *Inorg. Chem.* **2010**, *49*, 1487.

168. Patra, A. K.; Rose, M. J.; Murphy, K. A.; Olmstead, M. M.; Mascharak, P. K. "Photolabile ruthenium nitrosyls with planar dicarboxamide tetradentate N_4 ligands:

Effects of in-plane and axial ligand strength on NO release" *Inorg. Chem.* **2004**, *43*, 4487.

169. Fry, N. L.; Heilman, B. J.; Mascharak, P. K. "Dye-tethered ruthenium nitrosyls containing planar dicarboxamide tetradentate N_4 ligands: Effects of in-plane ligand twist on NO photolability" *Inorg. Chem.* **2011**, *50*, 317.
170. Rose, M. J.; Fry, N. L.; Marlow, R.; Hinck, L.; Mascharak, P. K. "Sensitization of ruthenium nitrosyls to visible light via direct coordination of the dye resorufin: Trackable NO donors for light-triggered NO delivery to cellular targets" *J. Am. Chem. Soc.* **2008**, *130*, 8834.
171. Rose, M. J.; Olmstead, M. M.; Mascharak, P. K. "Photosensitization via dye coordination: A new strategy to synthesize metal nitrosyls that release NO under visible light" *J. Am. Chem. Soc.* **2007**, *129*, 5342.
172. Szundi, I.; Rose, M. J.; Sen, I.; Eroy-Reveles, A. A.; Mascharak, P. K.; Einarsdottir, O. "A new approach for studying fast biological reactions involving nitric oxide: Generation of NO using photolabile ruthenium and manganese NO donors" *Photochem. Photobiol.* **2006**, *82*, 1377.
173. Hoffman-Luca, C. G.; Eroy-Reveles, A. A.; Alvarenga, J.; Mascharak, P. K. "Syntheses, structures, and photochemistry of manganese nitrosyls derived from designed Schiff base ligands: Potential NO donors that can be activated by near-infrared light" *Inorg. Chem.* **2009**, *48*, 9104.
174. Patra, A. K.; Rowland, J. M.; Marlin, D. S.; Bill, E.; Olmstead, M. M.; Mascharak, P. K. "Iron nitrosyls of a pentadentate ligand containing a single carboxamide group:

Syntheses, structures, electronic properties and photolability of NO" *Inorg. Chem.* **2003**, *42*, 6812.

175. Madhani, M.; Patra, A. K.; Miller, T. W.; Eroy-Reveles, A. A.; Hobbs, A. J.; Fukuto, J. M.; Mascharak, P. K. "Biological activity of designed photolabile metal nitrosyls: Light-dependent activation of soluble guanylate cyclase and vasorelaxant properites in rat aorta" *J. Med. Chem.* **2006**, *49*, 7325.
176. Tfouni, E.; Doro, F. G.; Figueiredo, E.; Pereira, J. C. M.; Metzke, G.; Franco, D. W. "Tailoring NO donors metallopharmaceuticals: Ruthenium nitrosyl ammines and aliphatic tetraazamacrocycles" *Curr. Med. Chem.* **2010**, *17*, 3643.
177. Hoshino, M.; Laverman, L.; Ford, P. C. "Nitric oxide complexes of metalloporphyrins: An overview of some mechanistic studies" *Coord. Chem. Rev.* **1999**, *187*, 75 and references therein.
178. Vos, M. H.; Lipowski, G.; Lambry, J.-C.; Martin, J.-L.; Liebl, U. "Dynamics of nitric oxide in the active site of reduced cytochrome *c* oxidase aa_3" *Biochemistry* **2001**, *40*, 7806.
179. Antonini, A.; Brunori, M. "Hemoglobin and myoglobin in their reaction with ligands" North Holland, Amsterdam, **1971**.
180. Xu, N.; Yi, J.; Richter-Addo, G. B. "Linkage isomerization in heme-NOx compounds: Understanding NO, nitrite, and hyponitrite interactions with iron porphyrins" *Inorg. Chem.* **2010**, *49*, 6253.
181. Ford, P. C.; Laverman, L. E. "Reaction mechanisms relevant to the formation of iron and ruthenium nitric oxide complexes" *Coord. Chem. Rev.* **2005**, *249*, 391 and references therein.

182. Lim, M. D.; Lorkovic, I. M.; Ford, P. C. "NO and NO_x interactions with group 8 metalloporphyrins" *J. Inorg. Biochem.* **2005**, *99*, 151.

183. Chanda, N.; Paul, D.; Kar, S.; Mobin, S. M.; Datta, A.; Puranik, V. G.; Rao, K. K.; Lahiri, G. K. "Effect of 2-(2-pyridyl)azole-based ancillary ligands (L^{1-4}) on the electrophilicity of the nitrosyl function in $[Ru^{II}(trpy)(L^{1-4})(NO)]^{3+}$ [trpy = 2,2':6',2''-terpyridine]. Synthesis, structures, and spectroscopic, electrochemical, and kinetic aspects" *Inorg. Chem.* **2005**, *44*, 3499.

184. Chanda, N.; Mobin, S. M.; Puranik, V. G.; Datta, A.; Niemeyer, M.; Lahiri, G. K. "Stepwise synthesis of $[Ru(trpy)(L)(X)]^{n+}$ (trpy = 2,2':6',2''-terpyridine; L = 2,2'-dipyridylamine; X = Cl^-, H_2O, NO_2^-, NO^+, O_2^-). Crystal structure, spectral, electron-transfer, and photophysical aspects" *Inorg. Chem.* **2004**, *43*, 1056.

185. Chowdhury, A. D.; De, P.; Mobin, S. M.; Lahiri, G. K. "Influence of nitrosyl coordination on the binding mode of quinaldate in selective ruthenium frameworks. Electronic structure and reactivity aspects" *RSC Advances* **2012**, *2*, 3437.

186. Sauaia, M. G.; de Lima, R. G.; Tedesco, A. C.; da Silva, R. S. "Photoinduced NO release by visible light irradiation from pyrazine-bridged nitrosyl ruthenium complexes" *J. Am. Chem. Soc.* **2003**, *125*, 14718.

187. Sauaia, M. G.; de Lima, R. G.; Tedesco, A. C.; da Silva, R. S. "Nitric oxide production by visible light irradiation of aqueous solution of nitrosyl ruthenium complexes" *Inorg. Chem.* **2005**, *44*, 9946.

188. Rose, M. J.; Patra, A. K.; Alcid, E. A.; Olmstead, M. M.; Mascharak, P. K. "Ruthenium nitrosyls derived from polypyridine ligands with carboxamide or imine nitrogen donor(s): Isoelectronic complexes with different NO photolability" *Inorg. Chem.* **2007**, *46*, 2328.

189. Patra, A. K.; Mascharak, P. K. “A ruthenium nitrosyl that rapidly delivers NO to proteins in aqueous solution upon short exposure to UV light” *Inorg. Chem.* **2003**, *42*, 7363.

190. Fry, N. L.; Wei, J.; Mascharak, P. K. “Triggered dye release via photodissociation of nitric oxide from designed ruthenium nitrosyls: Turn-on fluorescence signaling of nitric oxide delivery” *Inorg. Chem.* **2011**, *50*, 9045.

191. Enriquez, C. A.; Lacroix, P. G.; Sasaki, I.; Mallet-Ladeira, S.; Farfan, N.; Barba-Barba, R. M.; Ramos–Ortiz, G.; Malfant, I. “Comparison of carbazole and fluorene donating effects on the two-photon absorption and nitric oxide photo-release capabilities in a ruthenium-nitrosyl complex” *Eur. J. Inorg. Chem.* **2018**, 531.

192. Amabilino, S.; Tasse, M.; Lacroix, P. G.; Mallet–Ladeira, S.; Pimienta, V.; Akl, J.; Sasaki, I.; Malfant, I. “Photorelease of nitric oxide (NO) on ruthenium nitrosyl complexes with phenyl substituted terpyridines” *New J. Chem.* **2017**, *41*, 7371.

193. Enriquez-Cabrera, A.; Sasaki, I.; Bukhanko, V.; Tasse, M.; Mallet-Ladeira, S.; Lacroix, P. G.; Barba-Barba, R. M.; Ramos-Ortiz, G.; Farfan, N.; Voitenko, Z.; Malfant, I. “Replacing two chlorido ligands by a bipyridine ligand in ruthenium nitrosyl complexes with NO-release capabilities: A comparative study” *Eur. J. Inorg. Chem.* **2017**, *11*, 1446.

194. Akl, J.; Sasaki, I.; Lacroix, P. G.; Hugues, V.; Vicendo, P.; Boce, M.; Mallet-Ladeira, S.; Blanchard-Desce, M.; Malfant, I. "*trans*– and *cis*–(Cl,Cl)–[Ru^{II}(FT)Cl_2(NO)](PF^6): promising candidates for NO release in the NIR region” Photochem. Photobiol. Sci. **2016**, *15*, 1484.

195. Hadadzadeh, H.; DeRosa, M. C.; Yap, G. P. A.; Rezvani, A. R.; Crutchley, R. J. “Cyclometalated ruthenium chloro and nitrosyl complexes” *Inorg. Chem.* **2002**, *41*, 6521.

196. Ghosh, K.; Kumar, S.; Kumar, R.; Singh, U. P.; Goel, N. "Oxidative cyclization of a phenolic schiff base and synthesis of a cyclometalated ruthenium nitrosyl complex: Photoinduced NO release by visible light" *Inorg. Chem.* **2010**, *49*, 7235.

197. Ignarro, L. J.; Cirino, G.; Casini, A.; Napoli, C. "Nitric oxide as a signaling molecule in the vascular system: an overview" *J. Cardiovasc. Pharmacol.* **1999**, 879.

198. Moncada, S. "Nitric oxide: discovery and impact on clinical medicine" *J. R. Soc. Med.* **1999**, *92*, 164.

199. Motterlini, R.; Otterbein, L. E. "The therapeutic potential of carbon monoxide" *Nat. Rev. Drug Discov.* **2010**, *9*, 728.

200. Gonzales, M. A.; Mascharak, P. K. "Photoactive metal carbonyl complexes as potential agents for targeted CO delivery" *J. Inorg. Biochem.* **2014**, *133*, 127.

201. Chakraborty, I.; Carrington, S. J.; Mascharak, P. K. "Design Strategies To Improve the Sensitivity of Photoactive Metal Carbonyl Complexes (photoCORMs) to Visible Light and Their Potential as CO-Donors to Biological Targets" *Acc. Chem. Res.* **2014**, *47*, 2603.

202. Motterlini R.; Clark J. E.; Foresti R.; Sarathchandra P.; Mann B. E.; Green C. J.; "Carbon monoxide-releasing molecules: characterization of biochemical and vascular activities" *Circ. Res.* **2002**, *90*, 17.

203. Gonzalez, M. A.; Carrington, S. J.; Chakraborty, I.; Olmstead, M. M.; Mascharak, P. K. "Photoactivity of Mono- and Dicarbonyl Complexes of Ruthenium(II) Bearing an N,N,S-Donor Ligand: Role of Ancillary Ligands on the Capacity of CO Photorelease" *Inorg. Chem.* **2013**, *52*, 11320.

204. Bischof, C.; Joshi, T.; Dimri, A.; Spiccia, L.; Schatzschneider, U. “Synthesis, Spectroscopic Properties, and Photoinduced CO-Release Studies of Functionalized Ruthenium(II) Polypyridyl Complexes: Versatile Building Blocks for Development of CORM−Peptide Nucleic Acid Bioconjugates” *Inorg. Chem.* **2013**, *52*, 9297.

205. Kubeil, M.; Vernooij, R. R.; Kubeil, C.; Wood, B. R.; Graham, B.; Stephan, H.; Spiccia, L. “Studies of Carbon Monoxide Release from Ruthenium(II) Bipyridine Carbonyl Complexes upon UV-Light Exposure” *Inorg. Chem.* **2017**, *56*, 5941.

206. Muntané, J.; De la Mata, M. "Nitric oxide and cancer" *World J Hepatol*, **2010**, *2*, 337.

207. Olson, S. Y.; Garbán, H. J. "Regulation of apoptosis-related genes by nitric oxide in cancer" *Nitric Oxide*, **2008**, *19*, 170.

208. Rodrigues, F. P.; Carneiroa, Z. A.; Mascharak, P. K.; Curti, C.; da Silva, R.S. "Incorporation of a ruthenium nitrosyl complex into liposomes, the nitric oxide released from these liposomes and HepG2 cell death mechanism" *Coord. Chem. Rev.*, **2016**, *306*, 701.

209. Ramos, L. C. B.; Marchesi, M. S. P.; Callejon,; Baruffi, D. M. D.; Lunardi, C. N.; Slep, L. D.; Bendhack, L. M.; da Silva, R. S. "Enhanced Antitumor Activity against Melanoma Cancer Cells by Nitric Oxide Release and Photosensitized Generation of Singlet Oxygen from Ruthenium Complexes" *Eur. J. Inorg. Chem.*, **2016,** 3592**.**

210. Akl, J.; Sasaki, I.; Lacroix, P. G.; Malfant, I.; Ladeira, S. M.; Vicendo, P.; Farfánc, N.; Santillan, R. "Comparative photo-release of nitric oxide from isomers of substituted terpyridinenitrosylruthenium(II) complexes: experimental and computational investigations" *Dalton Trans.*, **2014**, *43*, 12721.

211. Franco, L. P.; Cicillini, S. A.; Biazzotto, J. C.; Schiavon, M. A.; Mikhailovsky, A.; Burks, P.; Garcia, J.; Ford, P. C.; da Silva, R. S. "Photoreactivity of a Quantum Dot–Ruthenium Nitrosyl Conjugate" *J. Phys. Chem. A*, **2014**, *118*, 12184.

212. Ford, P. C. "Photochemical delivery of nitric oxide" *Nitric Oxide*, **2013**, *34*, 56.

213. Schatzschneider, U. "Photoactivated Biological Activity of Transition-Metal Complexes" *Eur. J. Inorg. Chem.*, **2010**, 1451.

214. Ghosh, K.; Kumar, S.; Kumar, R.; Singh, U. P.; Goel, N. "Photocleavage of Coordinated NO under Visible Light from Two Different Classes of Organometallic Ruthenium Nitrosyl Complexes: Reversible Binding of Phenolato Function" *Organometallics* **2011**, *30*, 2498.

215. Ghosh, K.; Kumar, R.; Kumar, S.; Bala, M.; Singh, U. P. "Orthometallation in bidentate Schiff base ligands via C–H activation: synthesis of ruthenium(III) organometallic complexes" *Transition Met. Chem.*, **2015**, *40*, 831.

216. Kumar, R.; Kumar, S.; Bala, M.; Ratnam, A.; Singh, U. P.; Ghosh, K. "Site-specific orthometallation via C–H bond activation and syntheses of ruthenium(III) organometallics: studies on nitric oxide (NO) reactivity and photorelease of coordinated NO" *RSC Adv.*, **2016**, *6*, 72096.

217. Kumar, R.; Anjlika, Ratnam, A.; Kumar, S.; Bala, M.; Sur, D.; Narang, S.; Singh, U. P.; Mandal, P. K.; Ghosh, K. "Organometallic ruthenium nitrosyl obtained by C-H bond activation: Photo-induced delivery of nitric oxide (NO) and NO-mediated anti-proliferation activity studies" *Eur. J. Inorg. Chem.*, **2017**, 5334.

218. Buga, G. M.; Ignarro, L. J. "Nitric Oxide and Cancer. *Nitric Oxide: Biology and Pathobiology*" **2000**, 895.

219. Ignarro, L. J. "Nitric Oxide: Biology and Pathobiology" 2nd ed.; Academic Press, San Diego, CA, **2000**, 3.

220. Carpenter, A. W.; Schoenfisch, M. H. "Nitric oxide release: Part II. Therapeutic applications" *Chem. Soc. Rev.*, **2012**, *41*, 3742.

221. Godwin, J. B.; Meyer, T. J. "Preparation of ruthenium nitrosyl complexes containing 2,2'-bipyridine and 1,10-phenanthroline" *Inorg. Chem.*, **1971**, *10*, 471.

222. Borges, S. S. S.; Davanzo, C. U.; Castellano, E. E.; Schpector, J. Z.; Silva, S. C.; Franco, D. W. "Ruthenium Nitrosyl Complexes with N-Heterocyclic Ligands" *Inorg. Chem.*, **1998**, *37*, 2670.

223. Sauaia, M. G.; Oliveira, F. S.; Tedesco, A. C.; da Silva, R. S. "Control of NO release by light irradiation from nitrosyl–ruthenium complexes containing polypyridyl ligands" *Inorg. Chim. Acta*, **2003**, *355*, 191.

224. Thangavel, S.; Paulpandi, M.; Friedrich, H. B.; Murugan, K.; Kalva, S.; Skelton, A. A. "Synthesis, characterization, antiproliferative and molecular docking study of new half sandwich Ir(III), Rh(III) and Ru(II) complexes" *J. Inorg. Biochem.*, **2016**, *159*, 50.

225. Venkatachalam, G.; Ramesh, R.; Mobin, S. M. "Synthesis, structure, catalytic transfer hydrogenation and biological activity of cyclometallated ruthenium(III)2-(arylazo)phenolate complexes" *J. Organomet. Chem.*, **2005**, *690*, 3937.

226. Simon, H. U.; Haj-Yehia, A.; Levi-Schaffer, F. "Role of reactive oxygen species

(ROS) in apoptosis induction" *Apoptosis*, **2000**, *5*, 415.

227. Brüne, B.; von Knethen, A.; Sandau, K. B. "Nitric oxide and its role in apoptosis" *Eur. J. Pharmacol.*, **1998**, *351*, 261.

228. Heigold, S.; Sers, C.; Bechtel, W.; Ivanovas, B.; Schäfer, R.; Bauer, G. "Nitric oxide mediates apoptosis induction selectively in transformed fibroblasts compared to nontransformed fibroblasts" *Carcinogenesis*, **2002**, *23*, 929.

229. Kroemer, G.; Galluzzi, L.; Brenner, C. "Mitochondrial Membrane Permeabilization in Cell Death" *Physiol. Rev.*, **2007**, *87*, 99.

230. Bertini, I.; Chevance, S.; Del Conte, R.; Lalli, D.; Turano, P. "The Anti-Apoptotic Bcl-x_L Protein, a New Piece in the Puzzle of Cytochrome C Interactome" *PLoS One*, **2011**, *6*, 18329.

231. Lin, M. T.; Beal, M. F. "Mitochondrial dysfunction and oxidative stress in neurodegenerative diseases" *Nature*, **2006**, *443*, 787.

232. Galluzzi, L.; Vitale, I.; Aaronson, S. A.; Abrams, J. M.; Adam, D.; Agostinis, P.; Alnemri, E. S.; Altucci, L.; Amelio, I.; Andrews, D. W.; Annicchiarico-Petruzzelli, M. "Molecular mechanisms of cell death: recommendations of the Nomenclature Committee on Cell Death 2018" *Cell Death Differ.*, **2018**, *25*, 486.

233. Stephenson, T. A.; Wilkinson, G. "New complexes of ruthenium (II) and (III) with triphenylphosphine, triphenylarsine, trichlorostannate, pyridine and other ligands" *J. Inorg. Nucl. Chem.* **1966**, *28*, 945.

234. Maiti, N.; Pal, S.; Chattopadhyay, S. "Reaction of 2-(Phenylazo)aniline with Na_2PdCl_4: Formation of a 2-(Phenylazo)imino Complex of Bivalent Palladium" *Inorg. Chem.*, **2001**, *40*, 2204.

235. Sheldrick, G. M. "Phase annealing in SHELX-90: direct methods for larger structures" *ActaCrystallogr., Sect. A: Found. Crystallogr.* **1990**, *28*, 467.

236. Sheldrick, G. M. "*SHELXTL – NT2000version6.12, ReferenceManual*, University of Gottingen, Pergamon, New York", **1980**.

237. Klaus, B. *Diamond, Version1.2c*, University of Bonn, Germany, **1999**.

238. Stubbe, J.; van der Donk, W. A. "Protein Radicals in Enzyme Catalysis" *Chem. Rev.* **1998**, *98*, 705.

239. Buttner, T.; Geier, J.; Frison, G.; Harmer, J.; Calle, C.; Schweiger, A.; Schonberg, H.; Grutzmacher, H. "A Stable Aminyl Radical Metal Complex" *Science* **2005**, *307*, 235.

240. Kochem, A.; Gellon, G.; Leconte, N.; Baptiste, B.; Philouze, C.; Jarjayes, O.; Orio, M.; Thomas, F. "Stable Anilinyl Radicals Coordinated to Nickel: X-ray Crystal Structure and Characterization" *Chem. Eur. J.* **2013**, *19*, 16707.

241. Maire, P.; Konigsmann, M.; Sreekanth, A.; Harmer, J.; Schweiger, A.; Grutzmacher, H. "A Tetracoordinated Rhodium Aminyl Radical Complex" *J. Am. Chem. Soc.* **2006**, *128*, 6578.

242. Konigsmann, M.; Donati, N.; Stein, D.; Schonberg, H.; Harmer, J.; Sreekanth, A.; Grutzmacher, H. "Metalloenzyme-Inspired Catalysis: Selective Oxidation of Primary

Alcohols with an Iridium–Aminyl-Radical Complex" *Angew. Chem. Int. Ed.* **2007**, *46*, 3567.

243. Rodriguez-Lugo, R. E.; de Bruin, B.; Trincado, M.; Grutzmacher, H. "A Stable Aminyl Radical Coordinated to Cobalt" *Chem. Eur. J.* **2017**, *23*, 1.

244. Kochem, A.; Gellon, G.; Jarjayes, O.; Philouze, C.; Leconte, N.; van Gastel, M.; Billa, E.; Thomas, F. "A singlet ground state for a cobalt(II)–anilinosalen radical complex" *Chem. Commun.* **2014**, *50*, 4924.

245. Mankad, N. P.; Antholine, W. E.; Szilagyi, R. K.; Peters, J. C. "Three-Coordinate Copper(I) Amido and Aminyl Radical Complexes" *J. Am. Chem. Soc.* **2009**, *131*, 3878.

246. Miyazato, Y.; Wada, T.; Muckerman, J. T.; Fujita, E.; Tanaka, K. "Generation of a Ru^{II}–Semiquinone–Anilino-Radical Complex through the Deprotonation of a Ru^{III}–Semiquinone–Anilido Complex" *Angew. Chem. Int. Ed.* **2007**, *46*, 5728.

247. Bera, S.; Maity, S.; Weyhermuller, T.; Ghosh, P. "Arylamino radical complexes of ruthenium and osmium: dual radical counter in a molecule" *Dalton Trans.* **2016**, *45*, 19428.

248. Kundu, S.; Dutta, D.; Maity, S.; Weyhermuller, T.; Ghosh, P. "Proton-Coupled Oxidation of a Diarylamine: Amido and Aminyl Radical Complexes of Ruthenium(II)" *Inorg. Chem.* **2018**, *57*, 11948.

249. De, P.; Maji, S.; Chowdhury, A. D.; Mobin, S. M.; Mondal, T. K.; Paretzki, A.; Lahiri, G. K. "Ruthenium nitrosyl complexes with 1,4,7-trithiacyclononane and 2,2'-bipyridine (bpy) or 2-phenylazopyridine (pap) coligands. Electronic structure and reactivity aspects" *Dalton Trans.* **2011**, *40*, 12527.

250. 17. Karidi, K.; Garoufis, A.; Tsipis, A.; Hadjiliadis, N.; den Dulk, H.; Reedijk, J.

"Synthesis, characterization, *in vitro* antitumor activity, DNA-binding properties and electronic structure (DFT) of the new complex *cis*-(Cl,Cl)[$Ru^{II}Cl_2(NO^+)$(terpy)]Cl" *Dalton Trans*. **2005**, 1176.

251. Ghosh, K.; Tyagi, N.; Kumar, P.; Singh U. P.; Goel, N. "Stabilization of Mn(II) and Mn(III) in mononuclear complexes derived from tridentate ligands with N_2O donors: Synthesis, crystal structure, superoxide dismutase activity and DNA interaction studies" *J. Inorg. Biochem.*, **2010**, *104*, 9.

252. Nag, S.; Butcher, R. J.; Bhattacharya, S. "N-(Aryl) picolinamide complexes of Ruthenium: Usual Coordination and Strategic Cyclometalation" *Eur. J. Inorg. Chem.* **2007**, 1251.

253. Nagaraju, K.; Pal, S. "Ortho-ruthenation of 1-naphthalenyl in 1-naphthaldehyde 4-R-benzoylhydrazones: Ruthenium(III) CNO pincer complexes" *J. Organomet. Chem.* **2013**, *745–746*, 404.

254. Dutta, J.; Richmond, M. G.; Bhattacharya, S. "Cycloruthenation of N-(Naphthyl) salicylaldimine and related ligands: utilization of the Ru-C bond in catalytic transfer hydrogenation" *Eur. J. Inorg. Chem.* **2014**, 4600.

255. Chai, H.; Liu, T.; Wang, Q.; Yu, Z. "Substituent Effect on the Catalytic Activity of Ruthenium(II) Complexes Bearing a Pyridyl-Supported Pyrazolyl-Imidazolyl Ligand for Transfer Hydrogenation of Ketones" *Organometallics* **2015**, *34*, 5278.

256. Wang, D.; Astruc, D. "The Golden Age of Transfer Hydrogenation" *Chem. Rev.* **2015**, *115*, 6621.

257. Pandiarajan, D.; Ramesh, R. "Catalytic transfer hydrogenation of ketones by ruthenium(II) cyclometallated complex containing para-chloroacetophenone thiosemicarbazone" *Inorg. Chem. Commun*. **2011**, *14*, 686.

258. Kondrashov, M.; Provost, D.; Wendt, O. F.“ Regioselectivity in C–H activation: reagent control in cyclometallation of 2-(1-naphthyl)-pyridine” *Dalton Trans*. **2016**, *45*, 525.

259. Ramesh, M.; Kumar, M. D.; Jaccob, M.; Kaleeswaran, D.; Venkatachalam, G. " Ru(III) mediated C-H bond activation of N-(naphthyl)salicylaldimine and related Schiff base ligands: Synthesis, structure, DFT study and catalytic activity" *Inorg. Chem. Commun*. **2017**, *85*, 26.

260. Kasez, H. D.; Saillant, R. B. "Hydride Complexes of the Transition Metals" *Chem. Rev*. **1972**, *72*, 231.

261. Waldie, K. M.; Ostericher, A. L.; Reineke, M. H.; Sasayama, A. F.; Kubiak, C. P. "Hydricity of Transition-Metal Hydrides: Thermodynamic Considerations for CO2 Reduction" *ACS Catal*. **2018**, *8*, 1313.

262. Paul, P.; Bhattacharya, S. "Iridium mediated N-H and C-H bond activation of N-(aryl)pyrrole-2-aldimines. Synthesis, structure and, spectral and electrochemical properties" *J. Organomet. Chem*. **2012**, *713*, 72.

263. Paul, P.; Richmond, M. G.; Bhattacharya, S. " Iridium-mediated N-H and methyl C-H bond activations in N-(2',6'-dimethylphenyl)pyrrole-2-aldimine. Synthesis, characterization and catalytic applications" *J. Organomet. Chem*. **2014**, *751*, 760.

264. Sommer, M. G.; Marinova, S.; Krafft, M. J.; Urankar, D.; Schweinfurth, D.; Bubrin, M.; Kosmrlj, J.; Sarkar, B. “Ruthenium Azocarboxamide Half-Sandwich Complexes: Influence of the Coordination Mode on the Electronic Structure and Activity in Base-Free Transfer Hydrogenation Catalysis” *Organometallics* **2016**, *35*, 2840.

265. Samanta, S.; Ghosh, P.; Goswami, S. "Recent advances on the chemistry of transition metal complexes of 2-(arylazo)pyridines and its arylamino derivatives" *Dalton Trans.* **2012**, *41*, 2213.

266. Joy, S.; Kramer, T.; Paul, N. D.; Banerjee, P.; McGrady, J. E.; Goswami, S. " Isolation and Assessment of the Molecular and Electronic Structures of Azo-Anion-Radical Complexes of Chromium and Molybdenum. Experimental and Theoretical Characterization of Complete Electron-Transfer Series" *Inorg. Chem.* **2011**, *50*, 9993.

267. Paul, N. D.; Rana, U.; Goswami, S.; Mondal, T. K.; Goswami, S. "Azo Anion Radical Complex of Rhodium as a Molecular Memory Switching Device: Isolation, Characterization, and Evaluation of Current−Voltage Characteristics" *J. Am. Chem. Soc.* **2012**, *134*, 6520.

268. Mandal, A.; Schwederski, B.; Fiedler, J.; Kaim, W.; Lahiri, G. K. "Evidence for Bidirectional Noninnocent Behavior of a Formazanate Ligand in Ruthenium Complexes" *Inorg. Chem.* **2015**, *54*, 8126.

269. Paul, N.; Samanta, S.; Goswami, S. "Redox Induced Electron Transfer in Doublet Azo-Anion Diradical Rhenium(II) Complexes. Characterization of Complete Electron Transfer Series" *Inorg. Chem.* **2010**, *49*, 2649.

270. Pramanik, S.; Dutta, S.; Roy, S.; Dinda, S.; Ghorui, T.; Mitra, A. K.; Pramanik, K.; Ganguly, S. "Luminescent closed shell nickel(II) pyridyl-azooximates and the open shell

anion radical congener: molecular and electronic structure, ligand redox behaviour and biological activity" *New J. Chem.* **2017**, *41*, 4157.

271. Joy, S.; Pal, P.; Mondal, T. K.; Talapatra, G. B.; Goswami, S. "Synthesis of Amphiphilic Azo-Anion-Radical Complexes of Chromium (III) and the Development of Ultrathin Redox-Active Surfaces by the Langmuir–Schaefer Technique" *Chem. Eur. J.* **2012**, *18*, 1761.

272. Shivakumar, M.; Pramanik, K.; Ghosh, P.; Chakravorty, A. " Isolation and Structure of the First Azo Anion Radical Complexes of Ruthenium" *Inorg. Chem.* **1998**, *37*, 5968.

273. Doslik, N.; Sixt, T.; Kaim, W. "The First Structural Characterization of an Azoaromatic Radical Anion Stabilized by Dicopper(I) Coordination" *Angew. Chem. Int. Ed.* **1998**, *37*, 2403.

274. Berman, R. S.; Kochi, J. K. "Kinetics and Mechanism of Oxygen Atom Transfer from Nitro Compounds Mediated by Nickel(0) Complexes" *Inorg. Chem.* **1980**, *19*, 248

275. Patra, A. K.; Afshar, R. K.; Rowland, J. M.; Olmstead, M. M.; Mascharak, P. K. "Thermally Induced Stoichiometric and Catalytic O-Atom Transfer by a Non-Heme Iron(III)–Nitro Complex: First Example of Reversible $\{Fe–NO\}^7 \leftrightarrow Fe^{III}$-NO2 Transformation in the Presence of Dioxygen" *Angew. Chem. Int. Ed.* **2003**, *42*, 4517.

276. O'Connor, J. M.; Bunker, K. D. "Conversion of $(\eta^5\text{-}C_5H_5)Co(PPh_3)_2$ and Nitro Compounds to Mononuclear η^1(N)-Nitrosoalkyl and Dinuclear μ-η^1(N): η^2(N,O)-Nitrosoaryl Complexes" *Organometallics* **2003**, *22*, 5268.

277. Li, X.; Incarvito, C. D.; Vogel, T.; Crabtree, R. H. " Intramolecular Oxygen Transfer from Nitro Groups to C≡C Bonds Mediated by Iridium Hydrides" *Organometallics* **2005**, *24*, 3066.

278. Agrawal, A.; Tratnyek, P. G. "Reduction of Nitro Aromatic Compounds by Zero-Valent Iron Metal" *Environ. Sci. Technol.* **1996**, *30*, 153.

279. Paul, N. D.; Rana, U.; Goswami, S.; Mondal, T. K.; Goswami, S. "Azo Anion Radical Complex of Rhodium as a Molecular Memory Switching Device: Isolation, Characterization, and Evaluation of Current−Voltage Characteristics" *J. Am. Chem. Soc*. **2012**, *134*, 6520.

280. Das, A. K.; Sarkar, B.; Duboc, C.; Strobel, S.; Fiedler, J.; Zalis, S.; Lahiri, G. K.; Kaim, W. "An Odd-Electron Complex $[Ru^{k}(NO^{m})(Q^{n})(terpy)]^{2+}$ with Two Prototypical Non-Innocent Ligands" *Angew. Chem. Int. Ed.* **2009**, *48*, 4242.

281. Ghosh, P.; Banerjee, S.; Lahiri, G. K. "Ruthenium Derivatives of in Situ Generated Redox-Active 1,2-Dinitrosobenzene and 2-Nitrosoanilido. Diverse Structural and Electronic Forms" *Inorg. Chem.* **2016**, *55*, 12832.

282. Frisch, M. J.; Trucks, G. W.; Schlegel, H. B.; Scuseria, G. E.; Robb, M. A.; Cheeseman, J. R.; Scalmani, G.; Barone, V.; Mennucci, B.; Petersson, G. A.; Nakatsuji, H.; Caricato, M.; Li, X.; Hratchian, H. P.; Izmaylov, A. F.; Bloino, J.; Zheng, G.; Sonnenberg, J. L.; Hada, M.; Ehara, M.; Toyota, K.; Fukuda, R.; Hasegawa, J.; Ishida, M.; Nakajima, T.; Honda, Y.; Kitao, O.; Nakai, H.; Vreven, T.; Montgomery, J. A. Jr., Peralta, J. E.; Ogliaro, F.; Bearpark, M.; Heyd, J. J.; Brothers, E.; Kudin, K. N.; Staroverov, V. N.; Kobayashi, R.; Normand, J.; Raghavachari, K.; Rendell, A.; Burant, J. C.; Iyengar, S. S.;

Tomasi, J.; Cossi, M.; Rega, N.; Millam, J. M.; Klene, M.; Knox, J. E.; Cross, J. B.; Bakken, V.; Adamo, C.; Jaramillo, J.; Gomperts, R.; Stratmann, R. E.; Yazyev, O.; Austin, A. J.; Cammi, R.; Pomelli, C.; Ochterski, J. W.; Martin, R. L.; Morokuma, K.; Zakrzewski, V. G.; Voth, G. A.; Salvador, P.; Dannenberg, J. J.; Dapprich, S.; Daniels, A. D.; Farkas, Ö.; Foresman, J. B.; Ortiz, J. V.; Cioslowski, J.; Fox, D. J. *Gaussian 09*, revision B.01; Gaussian, Inc.: Wallingford CT, **2010**.

283. Becke, A. D. "Density-functional thermochemistry. III. The role of exact exchange" *J. Chem. Phys*. **1993**, *98*, 5648.

284. Lee, C.; Yang, W.; Parr, R. G. "Development of the Colle-Salvetti correlation-energy formula into a functional of the electron density" *Phys. Rev. B* **1988**, *37*, 785.

285. Stephens, P. J.; Devlin, F. J.; Chabalowski, C. F.; Frisch, M. J. "Ab Initio Calculation of Vibrational Absorption and Circular Dichroism Spectra Using Density Functional Force Fields" *J. Phys. Chem.* **1994**, *98*, 11623.

286. Bachler, V.; Olbrich, G.; Neese, F.; Wieghardt, K. "Theoretical Evidence for the Singlet Diradical Character of Square Planar Nickel Complexes Containing Two o-Semiquinonato Type Ligands" *Inorg. Chem*. **2002**, *41*, 4179.

287. Chelopo, M. P.; Pawar, S. A.; Sokhela, M. K.; Govender, T.; Kruger, H. G.; Maguire, G. E.M. "Anticancer activity of ruthenium(II) arene complexes bearing 1,2,3,4-tetrahydroisoquinoline amino alcohol ligands" *Eur. J. Med. Chem.*, **2013**, *66*, 407.

288. Li, J.; Tian, Z.; Xu, Z.; Zhang, S.; Feng, Y.; Zhang, L.; Liu, Z. "Highly Potent Half-sandwich Iridium and Ruthenium Complexes as Lysosome-Targeted Imaging and Anticancer agents" *Dalton Trans.*, **2018**, *47*, 15772.

289. Pettinari, R.; Pettinari, C.; Marchetti, F.; Clavel, C. M.; Scopelliti, R.; Dyson, P. J. "Cytotoxicity of Ruthenium−Arene Complexes Containing β-Ketoamine Ligands" *Organometallics* **2013**, *32*, 309.

290. Gatti, A.; Habtemariam, A.; Romero-Canelón, I.; Song, J.; Heer, B.; Clarkson, G. J.; Rogolino, D.; Sadler, P. J.; Carcelli, M. "Half-Sandwich Arene Ruthenium(II) and Osmium(II) Thiosemicarbazone Complexes: Solution Behaviour and Antiproliferative Activity" *Organometallics* **2018**, *37*, 891.

291. Aman, F.; Hanif, M.; Siddiqui, W. A.; Ashraf, A.; Filak, L. K.; Reynisson, J.; Söhnel, T.; Jamieson, S. M. F.; Hartinger, C. G. "Anticancer Ruthenium(η^6-p-cymene) Complexes of Nonsteroidal Anti-inflammatory Drug Derivatives" *Organometallics* **2014**, *33*, 5546.

292. Nikolić, S.; Opsenica, D. M.; Filipović, V.; Dojčinović, B.; Aranđelović, S.; Radulović, S.; Grgurić-Šipka, S. "Strong in Vitro Cytotoxic Potential of New Ruthenium−Cymene Complexes" *Organometallics* **2015**, *34*, 3464.

293. Jeyalakshmi, K.; Haribabu, J.; Bhuvaneshb, N. S. P.; Karvembu, R. "Half-sandwich $RuCl_2$(η^6-p-cymene) core complexes containing sulfur donor aroylthiourea ligands: DNA and protein binding, DNA cleavage and cytotoxic studies" *Dalton Trans.*, **2016**, *45*, 12518.

294. Biancalana, L.; Batchelor, L. K.; Funaioli, T.; Zacchini, S.; Bortoluzzi, M.; Pampaloni, G.; Dyson, P. J.; Marchetti, F. "α-Diimines as Versatile, Derivatizable Ligands in Ruthenium(II) p-Cymene Anticancer Complexes" *Inorg. Chem.*, **2018**, *57*, 6669.

295. Tian, M.; Li, J.; Zhang, S.; Guo, L.; He, X.; Kong, D.; Zhang, H.; Liu, Z. "Half-sandwich ruthenium(II) complexes containing N^N-chelated imino-pyridyl ligands that are selectively toxic to cancer cells" *Chem. Commun.*, **2017**, *53*, 12810.

296. Wu, Q.; Fan, C.; Chen, T.; Liu, C.; Mei, W.; Chen, S.; Wang, B.; Chen, Y.; Zheng, W. "Microwave-assisted synthesis of arene ruthenium(II) complexes that induce S-phase arrest in cancer cells by DNA damage-mediated p53 phosphorylation" *Eur. J. Med. Chem.*, **2013**, *63*, 57.

297. Pettinari, R.; Marchetti, F.; Pettinari, C.; Petrini, A.; Scopelliti, R.; Clavel, C. M.; Dyson, P. J. "Synthesis, Structure, and Antiproliferative Activity of Ruthenium(II) Arene Complexes with N,O-Chelating Pyrazolone-Based β-Ketoamine Ligands" *Inorg. Chem.*, **2014**, *53*, 13105.

298. Tian, Z.; Li, J.; Zhang, S.; Xu, Z.; Yang, Y.; Kong, D.; Zhang, H.; Ge, X.; Zhang, J.; Liu, Z. "Lysosome-Targeted Chemotherapeutics: Half-Sandwich Ruthenium(II) Complexes That Are Selectively Toxic to Cancer Cells" *Inorg. Chem.*, **2018**, *57*, 10498.

299. Hanahan, D.; Weinberg, R. A. "Hallmarks of cancer: the next generation" *Cell*, **2011**, *144*, 646.

300. Rubbiani, R.; Can, S.; Kitanovic, I.; Alborzinia, H.; Stefanopoulou, M.; Kokoschka, M.; Monchgesang, S.; Sheldrick, W. S.; Wolfl, S.; Ott, I. "Comparative in vitro evaluation of N-heterocyclic carbene gold(I) complexes of the benzimidazolylidene type" *J. Med. Chem.*, **2011**, *54*, 8646.

301. Circu, M. L.; Aw, T. Y. "Reactive oxygen species, cellular redox systems, and apoptosis" *Free Radical Bio. Med.*, **2010**, *48*, 749.

302. Khan, N. S.; Khan, P.; Ansari, M. F.; Srivastava, S.; Hasan, G. M.; Husain, M.; Hassan, M. I. "Thienopyrimidine-Chalcone Hybrid Molecules Inhibit Fas-Activated Serine/Threonine Kinase: An Approach To Ameliorate Antiproliferation in Human Breast Cancer Cells" *Mol. Pharm.*, **2018**, *15*, 4173.

303. Bennett, M. A.; Smith, A. K. "Arene ruthenium(II) complexes formed by dehydrogenation of cyclohexadienes with ruthenium(III) trichloride" *J. Chem. Soc., Dalton Trans.*, **1974**, 233.

304. Peerzada, M. N.; Khan, P.; Ahmad, K.; Hassan, M. I.; Azam, A. "Synthesis, characterization and biological evaluation of tertiary sulfonamide derivatives of pyridyl-indole based heteroaryl chalcone as potential carbonic anhydrase IX inhibitors and anticancer agents" *Eur. J. Med. Chem.*, **2018**, *155*, 13.

305. Queen, A.; Khan, P.; Idrees, D.; Azam, A.; Hassan, M. I. "Biological evaluation of p-toluene sulphonylhydrazone as carbonic anhydrase IX inhibitors: An approach to fight hypoxia-induced tumors" *Int. J. Biol. Macromol.*, **2018**, *106*, 840.

306. Boaz, H.; Rollefson, G. "The quenching of fluorescence. Deviations from the Stern-Volmer law" *J. Am. Chem. Soc.*, **1950**, *72*, 3435.

307. Khan, P.; Rahman, S.; Queen, A.; Manzoor, S.; Naz, F.; Hasan, G. M.; Luqman, S.; Kim, J.; Islam, A.; Ahmad, F.; Hassan, M. I. "Elucidation of Dietary Polyphenolics as Potential Inhibitor of Microtubule Affinity Regulating Kinase 4: In silico and In vitro Studies" *Sci. Rep.*, **2017**, *7*, 9470.